ESPOO 2006 VTT RESEARCH NOTES 2347

Hannu Hänninen, Pertti Aaltonen, Anssi Brederholm,
Ulla Ehrnstén, Hans Gripenberg, Aki Toivonen,
Jorma Pitkänen & Iikka Virkkunen

Dissimilar metal weld joints and their performance in nuclear power plant and oil refinery conditions

VTT TIEDOTTEITA – RESEARCH NOTES 2347

Dissimilar metal weld joints and their performance in nuclear power plant and oil refinery conditions

Hannu Hänninen[2], Pertti Aaltonen[1], Anssi Brederholm[2],
Ulla Ehrnstén[1], Hans Gripenberg[2], Aki Toivonen[1],
Jorma Pitkänen[1] & Iikka Virkkunen[2]

[1] VTT Technical Research Centre of Finland
[2] Helsinki University of Technology, Finland

ISBN 951–38–6805–2 (soft back ed.)
ISSN 1235–0605 (soft back ed.)

ISBN 951–38–6806–0 (URL: http://www.vtt.fi/publications/index.jsp)
ISSN 1455–0865 (URL: http://www.vtt.fi/publications/index.jsp)

JULKAISIJA – UTGIVARE – PUBLISHER

VTT, Vuorimiehentie 3, PL 1000, 02044 VTT
puh. vaihde 020 722 111, faksi 020 722 4374

VTT, Bergsmansvägen 3, PB 1000, 02044 VTT
tel. växel 020 722 111, fax 020 722 4374

VTT Technical Research Centre of Finland, Vuorimiehentie 3, P. O. Box 1000, FI-02044 VTT, Finland
phone internat. +358 20 722 111, fax +358 20 722 4374

VTT, Otakaari 3 A, PL 1000, 02044 VTT
puh. vaihde 020 722 111, faksi 020 722 6390

VTT, Otsvängen 3 A, PB 1000, 02044 VTT
tel. växel 020 722 111, fax 020 722 6390

VTT Technical Research Centre of Finland, Otakaari 3 A, P.O. Box 1000, FI-02044 VTT, Finland
phone internat. +358 20 722 111, fax +358 20 722 6390

Technical editing Anni Kääriäinen

Valopaino Oy, Helsinki 2006

Hänninen, Hannu, Aaltonen, Pertti, Brederholm, Anssi, Ehrnstén, Ulla, Gripenberg, Hans, Toivonen, Aki, Pitkänen Jorma & Virkkunen, Iikka. Dissimilar metal weld joints and their performance in nuclear power plant and oil refinery conditions. Espoo 2006. VTT Tiedotteita – Research Notes 2347. 208 p.

Keywords nuclear power plants, refineries, steel structures, welded joints, dissimilar metals, welding, Ni-base alloys, residual stress, environment-assisted cracking, hot cracking, non-destructive testing

Abstract

The operating experience of major nuclear power plant (NPP) pressure boundary components has recently shown that dissimilar metal weld joints can jeopardize the plant availability and safety because of increased incidences of environment-assisted cracking (EAC, PWSCC) of Alloy 600 and corresponding weld metals (Alloys 182/82). Alloy 690 and associated weld metals (Alloys 152/52) are widely used for repair and replacement of the affected thick-section components. The selection of new materials relies mainly on excellent laboratory results and short-term service experience. The long-term behaviour of these materials and their performance in the plant has still to be demonstrated.

Weldability of the studied nickel-base materials is evaluated based on the results obtained for weld metals of different chromium contents. The susceptibility to hot cracking is examined as well as the PWSCC susceptibility in the reactor primary water based on the metallurgical properties of the nickel-base alloys. The microstructure and microchemistry in the multi-pass nickel-base alloy welds is very different than in the wrought and recrystallized nickel-base materials. Additionally, the thermal ageing experience of various nickel-base weld metals is discussed. Weld residual stresses and their role in PWSCC as well as surface stress improvement techniques for PWSCC mitigation are also reviewed.

Finally the application, improvements and qualification of NDE for nickel-base weld locations are evaluated concerning the probes, techniques and scanning devices. The need for representative mock-ups for technique development and qualification is discussed. The technical basis for development of inspection requirements for dissimilar metal welds and efforts to qualify inspection procedures and personnel are also emphasized.

Maintaining the structural integrity of the NPP and oil refinery main components throughout the service life in spite of the several possible ageing mechanisms related to the dissimilar metal welds is essential for plant safety and availability.

Contents

List of acronyms

ABB	Asea Brown Bowery, NPP manufacturer, now Westinghouse
AES	Auger Electron Spectroscopy
ATEM	Analytical Transmission Electron Microscopy
BMI	Bottom Mounted Instrumentation
BTR	Brittle Temperature Range
BWR	Boiling Water Reactor
BWROG	Boiling Water Reactor Owners Group
BWR-VIP	Boiling Water Reactor – Vessels and Internals Projects
°C	Degree Celsius
C(T)	Compact Tension
cc	Cubic Centimetre
CEA	Commissariat à l'Energie Atomique
CEPM	Corrosion-Enhanced Plasticity
CERT	Constant Elongation Rate Tensile test
CGR	Crack Growth Rate
cm	Centimetre
CRDM	Control Rod Drive Mechanism
CSP	Cavitation Shotless Peening
da/dt	Crack Growth Rate as Increment per Time
DDC	Ductility Dip Cracking
DMW	Dissimilar Metal Weld
DRT	Ductility Recovery Temperature
DTA	Differential Thermal Analysis
DTR	Ductility Dip Temperature Range
EBSD	Electron Backscattering Diffraction
EDF	Electricité de France
EDM	Electric Discharge Machining
EDS	Energy Dispersive Spectrometer
EFPY	Effective Full Power Year
EPR	Electrochemical Potentiokinetic Repassivation
EPRI	Electric Power Research Institute
ETH	Eidgenössische Technische Hochschule Zürich
FEA	Finite Element Analysis
FEM	Finite Element Method
FM	Filler Metal
FN	Ferrite Number
FZ	Fusion Zone
HAGB	High Angle Grain Boundary
HAZ	Heat Affected Zone

HELP	Hydrogen-Enhanced Localised Plasticity
HWC	Hydrogen Water Chemistry
Hz	Hertz
IAEA	International Atomic Energy Agency
ID	Inner Diameter
IDSCC	Interdendritic Stress Corrosion Cracking
IGA	Intergranular Attack
IGC	Intergranular Corrosion
IGSCC	Intergranular Stress Corrosion Cracking
ISI	In-Service Inspection
J	J-integral
K	Stress Intensity
K_I	Stress Intensity, Mode I
K_{ISCC}	Threshold Stress Intensity, Mode I
K_J	Stress Intensity in Terms of J-integral
LTCP	Low Temperature Crack Propagation
LLNL	Lawrence Livermore National Laboratory
LP	Laser Peening
LSP	Laser Shot Peening
L-T	Longitudinal-Transverse Direction
LTA	Low Temperature Aging
LWR	Light Water Reactor
M	Moment
MIG	Metal Inert Gas (Welding)
MISO	Measurement by Means of in-Situ Observation
MMA	Manual Metal Arc (Welding)
mV_{SHE}	Millivolt on Standard Hydrogen Scale
N-bar	Stress Corrosion Cracking Parameter
NDE	Non Destructive Examination
NFI, FFI	Types of Filler Metals
NGW	Narrow Gap Welding
Nomarski DIC	Normarski Differential Interference Contrast
NPP	Nuclear Power Plant
NWC	Normal Water Chemistry
OD	Outer Diameter
p	Pressure
PD	Potential Drop
PDAS	Primary Dendrite Arm Spacing
ppb	Parts Per Billion
ppm	Parts Per Million
PWR	Pressurised Water Reactor

PWHT	Post-Weld Heat Treatment
PWSCC	Primary Water Stress Corrosion Cracking
Q	Activation Energy
R	Load Ratio
RPV	Reactor Pressure Vessel
RUB	Reverse U-Bend (Specimen)
S	Siemens
SMAW	Shielded Metal Arc Welding
SCC	Stress Corrosion Cracking
SCRI	Stress Corrosion Cracking Resistance Index
SEM	Scanning Electron Microscope
SEN(B)	Single Edge Notch Bend (Specimen)
SSRT	Slow Strain Rate Test
STF	Strain-to-Fracture
T	Temperature
t	Time
TCL	Total Crack Length
TD	Trans-Dendritic
Tekes	Finnish Funding Agency for Technology and Innovation
TEM	Transmission Electron Microscope
TIG	Tungsten Inert Gas Welding
TMI	Three Mile Island (NPP)
TOFDT	Time of Flight Diffraction Technique
T-S	Transverse-Thickness Direction
TV	Television
TVO	Teollisuuden Voima Oy
US	United States
UT	Ultrasonic Technique
VTT	VTT Technical Research Centre of Finland
VVER	Name of Russian Type Reactor
WJP	Water Jet Peening
WIL	Weld Inlay
WM	Weld Metal
WOL	Weld Overlay
XRD	X-ray Diffraction
λ	Wavelength
σ	Stress
$\varnothing$	Diameter

1. Introduction

The project Dissimilar Metal Welding (ERIPARI) deals with issues concerning nickel-base alloy dissimilar metal welds. Dissimilar metal welds are used in nuclear power plants and in oil refineries at locations where two different types of materials, e.g., carbon steel and stainless steel are joined.

The nickel-base alloy dissimilar metal welds are typically made of Alloy 182 and Alloy 82. Recently, Alloy 52 has started to be used both in new constructions as well as in repair welding. The trend towards alloys with higher amounts of chromium is driven by the observed cracking in Alloy 182, and recently also in Alloy 82. One driving force towards what are today believed to be more resistant alloys is also the challenges and costs related to non-destructive examination of dissimilar metal welds.

Although all the parameters affecting cracking susceptibility of nickel-base weld metals are not yet known, weld repairs increase the susceptibility, e.g. by increasing the residual stresses. Weld defects, such as hot cracks, are probably also playing a key role in crack initiation. Thus, several parameters are important when evaluating the manufacturing and performance of nickel-base alloy dissimilar metal welds. The main issues are dealt with in this literature review.

2. Materials used in LWRs

The main construction materials of light water reactors (LWR) are low alloy steels, stainless steels and nickel-base alloys (base materials as well as weld metals). In the following, a brief description of the main construction materials is given.

2.1 Pressure vessels and nozzles

The reactor pressure vessel (RPV) of a pressurised water reactor (PWR) or a boiling water reactor (BWR), i.e., of a light water reactor (LWR), is made of low alloy steel. The inside surface is clad with stainless steel to prevent general corrosion. Pressure vessel steels employed in modern LWRs all over the world are SA-508 Class 2 (German Type 22 NiMoCr 3 7), SA-508 Class 3 (German Type 20 MnMoNi 5 5) and SA 533 Grade B Class 1. In Russian VVER 440 reactors the RPV steel has been 12Х2МФА (equal to 15Х2МФА), which are also used for the forged nozzle rings joining piping to the pressure vessel. The pressure vessels in Russian VVER 1000 reactors are made of 15Х2МФА type steel.

A nuclear power plant (NPP) RPV has several nozzles, as shown in Figure 1. There are several aspects to consider when deciding on the design and materials for the joints. Some key parameters are weldability, coefficients of thermal expansion (especially differences between them for the materials concerned), stress corrosion cracking susceptibility, manufacturing details and influence of heat treatments.

The main pipe line material is stainless steel (with the exception of the German design using cladded pipes). This results in a dissimilar metal weld at the intersection between the pressure vessel and the main pipe lines. Similar joints exist in steam generators and pressurizers. To facilitate assembly welding between the RPV and the stainless steel piping a transition piece, i.e. a “safe end”, is used. The majority of the transition pieces are either made of stainless steel or nickel-base alloy (Alloy 600). The transition piece is welded to the RPV in the shop, and the assembly weld in the field is made between the transition piece and the piping. In the literature and spoken language ‘cracking in the safe end’ is used when referring to cracking in the RPV-safe end dissimilar metal weld.

a)

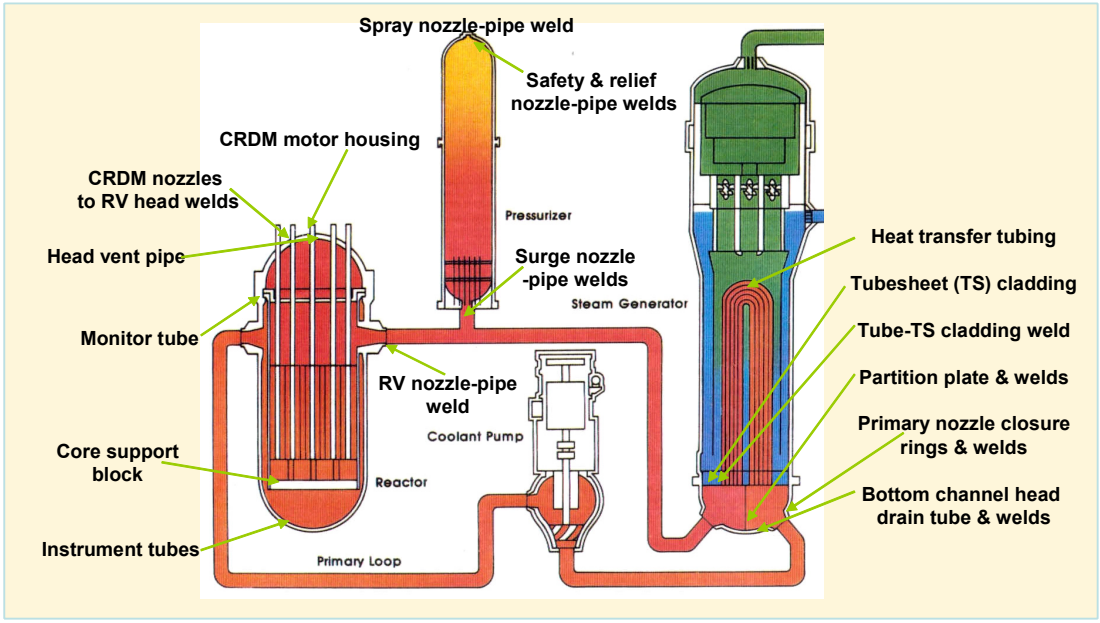

b)

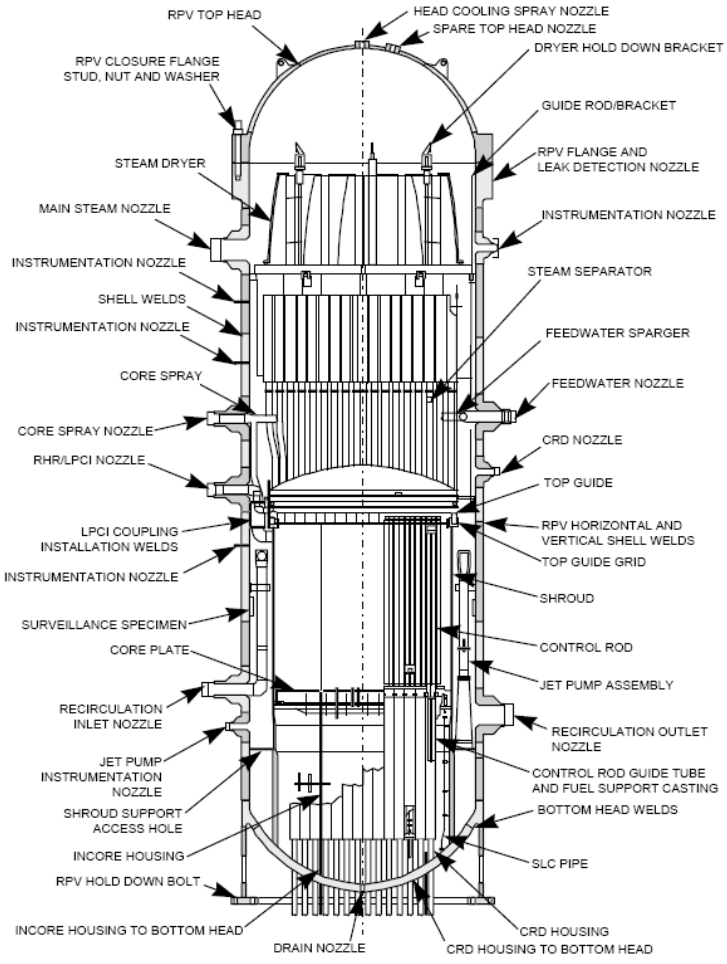

Figure 1. a) Regions in the PWR primary water system where PWSCC of nickel-base alloys have been observed. b) An example of BWR RPV showing locations of different nozzles and attachments (Shah & MacDonald 1993).

2.2 PWR piping materials

The materials used for the PWR main coolant loop piping include carbon steel piping clad with austenitic stainless steel, austenitic stainless steel piping (both in the cast and wrought forms), Alloys 600 and 690, as well as various weld and buttering materials. The austenitic stainless steels used for cladding and piping are either stabilised or non-stabilised stainless steel.

2.2.1 Clad carbon steel main coolant loop piping

US Plants: The main coolant piping, fitting, and nozzle material of the Babcock & Wilcox and Combustion Engineering plants is wrought ferritic steel clad with austenitic stainless steel. The inside surface of the piping adjacent to penetrations is, however, clad with Alloy 182. Cladding provides corrosion resistance to carbon steel piping. The cladding is normally deposited by welding or installed by roll bonding.

German plants: The main coolant piping, fitting, and nozzle material of the German PWR plants is fine-grained, low-alloy steel, clad with stabilized austenitic stainless steel. The types of low-alloy steels commonly used are SA-508 Class 2 (German Type 22 NiMoCr 3 7), and SA-508 Class 3 (German Type 20 MnMoNi 5 5). The cladding material is niobium-stabilized austenitic stainless steel. To ensure corrosion resistance, the composition of the upper 2 mm of the cladding weld deposit is specified as: $C \leq 0.045$, $Nb \leq 0.9$ and $Nb/C \geq 12.0\%$. Straight pipes and elbows are clad individually and then butt welded together.

Typical cladding operations are:

- elbows cladded automatically by longitudinal strip submerged arc welding (SAW) with subsequent post-weld heat treatment, PWHT (1. layer)
- straight pipes cladded by automatic helicoidal strip shielded metal arc welding, SMAW (1. layer)
- nozzles cladded by manual or automatic tungsten inert gas (TIG) welding process with subsequent PWHT (2 or 3 layers)
- butt-weld areas cladded by manual (2 or 3 layers) or automatic (1 to 2 layers) strip SAW with subsequent PWHT.

The material is preheated for all cladding operations for both automatic and manual welding. No machining of the cladding is necessary for ultrasonic examination. The surface roughness of the as-welded cladding is smooth enough for ultrasonic examina-

tion from the outside. The clad components are post-weld heat treated in the temperature range of 580–600°C.

2.2.2 Stainless steel main coolant loop piping

US plants: The main coolant piping, fitting, and nozzle materials of the Westinghouse plants include both wrought and cast stainless steels. The cast stainless steel components include statically cast fittings, present in all the Westinghouse plants, and centrifugally cast straight piping, present in some plants. The cast stainless steel materials include Grades CF8, CF8A, and CF8M. The compositions of Grades CF8 and CF8M are similar to those of wrought Type 304 and Type 316 stainless steel grades, respectively. The straight stainless steel pipes used in the Westinghouse plants are seamless. The stainless steel welds such as those in the Westinghouse main coolant piping are fabricated using either shielded metal arc or gas tungsten arc welding process. Type 308 stainless steel is generally used as the weld filler material. The ferrite content in the welds varies over a wide range: measurements of the delta ferrite content of about 1450 production stainless steel pipe welds showed that the ferrite content ranged from about 3.0 to 17.5 FN (ferrite number) (IAEA-TECDOC-1361, 2003).

French plants: Main coolant pipe lines are made of AISI 316L stainless steel and centrifugally cast stainless steel; the elbows are made of cast stainless steel (CF8 or CF8M), except for three old plants, where the elbows are made of two stainless steel shells with longitudinal welds. The connections with the major large components are made with the safe end and stainless steel dissimilar metal welds. For some younger plants the cold leg is made in one piece without any welds and with included forged nozzles.

Russian VVER 440 plants: All piping of the primary circuits of the Russian design VVER 440 reactors is made of titanium-stabilised austenitic stainless steels. The main coolant piping is made of seamless rolled pipes (diameter 560 × 34 mm) of Ti-stabilised Grade 08Ch18N12T stainless steel.

2.3 BWR piping materials

Piping material used in BWRs does not vary much between the different plant vendors. In USA and in Germany as well as in ABB designed plants, ferritic low-alloy steel pipe materials have been used for the steam and condensate lines, but the reactor water recirculation lines have been made of wrought austenitic stainless steels.

2.4 Dissimilar metal welds in PWRs and BWRs

Depending on the piping material, the connection to the RPV consists of dissimilar (ferritic/austenitic) or similar (ferritic/ferritic) materials as is the case in the German plants. The design of a US BWR nozzle-to-safe end joint is shown in Figure 2, as an example of a typical dissimilar metal weld.

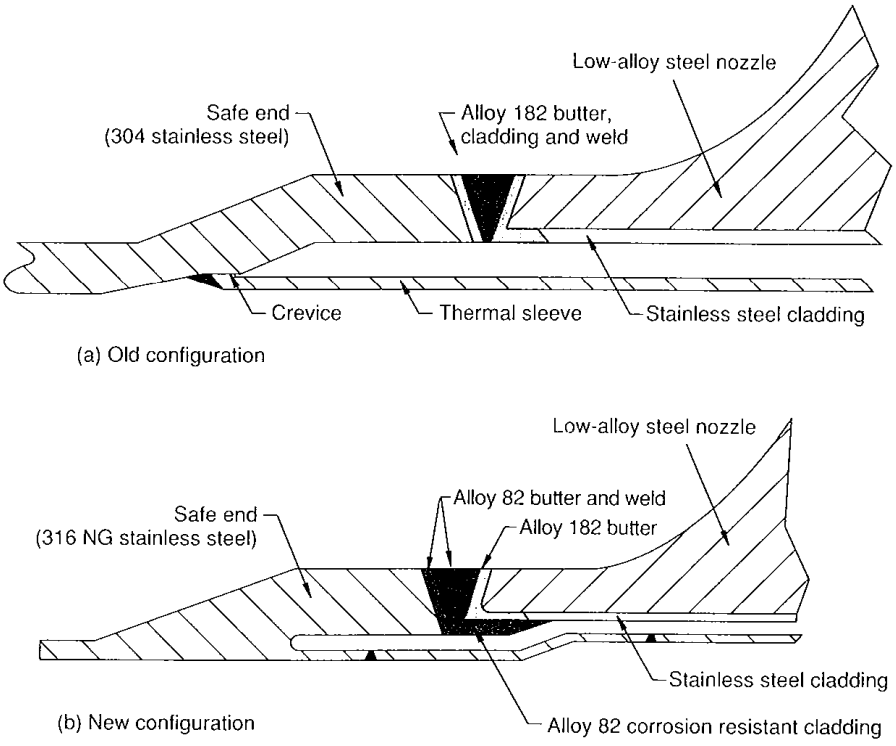

Figure 2. Cross-section of a recirculation system inlet nozzle and safe end in a US BWR. The old and new configurations differ in the materials and the construction of the thermal sleeve (Shah & MacDonald 1993).

Dissimilar metal welds are typically made in two steps. First, two (in some cases three) thin layers of buttering material are applied to the end of the ferritic steel vessel nozzles to form a buttering. The typical thickness of the buttering is 5 to 8 mm. The material for the first layer is over-alloyed with Cr and Ni, in order to compensate for dilution by the base metal. The buttering is then post-weld heat treated at a temperature which is specific to the type of low-alloy steel, for a time determined by the thickness of the ferritic steel component. For example, the post-weld heat treatment temperature for SA 508 Cl. 3 steel nozzle is about 580°C. The safe ends are then welded to the nozzles using the same filler material as for the second buttering layer, and this weld is not heat treated. In the case where the safe end is made of stainless steel, welding after the vessel post-weld heat treatment is important to avoid sensitisation of the safe end.

USA: US plants constructed prior to 1968 received PWHT following attachment of austenitic stainless steel brackets of internal components and nozzles with attached austenitic stainless steel safe ends. This resulted in furnace-sensitised material, highly sensitive to SCC. After 1970, the fabrication requirements were changed and PWHT was completed before the austenitic stainless steel components were attached. Since as-received (mill-annealed) Alloy 600 and Alloy 182 weld metal are generally equivalent or even worse to furnace-sensitised material, Alloy 600 components were not restricted to receive PWHT. In a majority of BWR plants, the vessel PWHT was performed prior to the completion of attachment welds, except buttering welds using Alloy 182 (Alloy 600) weld material.

Westinghouse plants have various safe end and buttering designs, Figure 3. The most common design includes a forged Type 316 stainless steel safe end welded to the nozzle with a NiCrFe alloy (Alloy 82/182) buttering material and a full-penetration weld of the same material. In another design, austenitic stainless steel buttering is weld-deposited on the nozzle end but no safe end is used. The least common design includes a NiCrFe alloy buttering on the nozzle end welded to a forged stainless steel safe end with a stainless steel full-penetration weld.

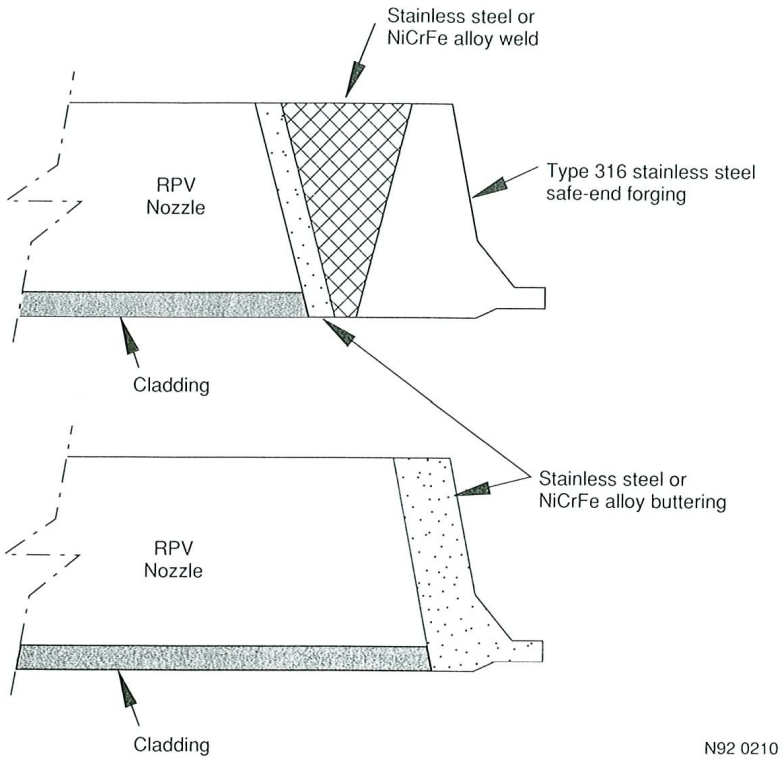

Figure 3. Variations of the Westinghouse main coolant piping to RPV safe end construction (Shah & MacDonald 1993).

Stainless steel safe ends are used between the cast stainless steel primary coolant pump nozzles and the carbon steel cold leg piping in the Babcock & Wilcox and Combustion Engineering plants. The safe ends are first welded to the stainless steel pump casing, and an Alloy 600 layer (buttering) is applied to the ends of the cold leg piping. Then, in the field an Alloy 600 weld is made between each safe end and the buttered end of each ferritic steel pipe. All field welds are post-weld heat treated.

In the Combustion Engineering plants, Alloy 82/182 is used both as buttering and filler materials for dissimilar metal welds at the reactor coolant pump nozzles and at the branch connections. Stainless steel safe ends are employed between the main coolant piping branch nozzles and stainless steel branch lines. In one Combustion Engineering plant with isolation valves on the main coolant loop, safe ends are used between the valve and the piping.

France: In the French plants, the safe ends are always shop welded. The buttering, the weld and the cladding are made of either AISI 308 or AISI 309 type stainless steels, with the exception of the last 3 plants, where the reactor pressure vessel dissimilar metal welds utilize Alloy 82. In the latest design, i.e., in the EPR plants, the construction and manufacturing of dissimilar metal joints between the RPV, steam generators and pressurizers are done in a totally different manner than earlier.

Germany: The typical layout of a Siemens-designed BWR is shown in Figure 4. The piping is made of carbon steel cladded with stainless steel. The weld between the RPV and the main coolant piping is, thus, not a dissimilar metal weld, as seen in the right hand upper corner of Figure 4. Dissimilar metal welds exist between the piping and the stainless steel nozzles. These utilize a buttering of Alloy 182 (or Alloy 82) and a weld of Alloy 182 (or Alloy 82). A typical dissimilar metal weld fabrication employed in later German NPPs has buttering at the inside surface and the root pass of the weld joint (including at least one cover layer) utilizing stainless steel filler material. This design results in an inner surface totally free of Ni-base alloy, which makes inspection of the weld root easier during in-service ultrasonic examination.

Russia: In VVER 440 plants the dissimilar metal welds between the RPV forging ring (12Х2МФА / 15Х2МФА steel) and the reactor coolant lines (08Х18Н10Т steel) are welded with a buttering where the first layer on RPV steel is made with 25Cr/12.5Ni or 16Cr/25Ni/6Mo electrodes and subsequent layers by 19Cr/10Ni/1Mo/1Nb or 18Cr/11Ni/3Mo/V electrodes. The weld joint is then made by 18Cr/11Ni/3Mo/V electrode. No nickel-base alloys are used for the dissimilar metal joints in the VVER plants.

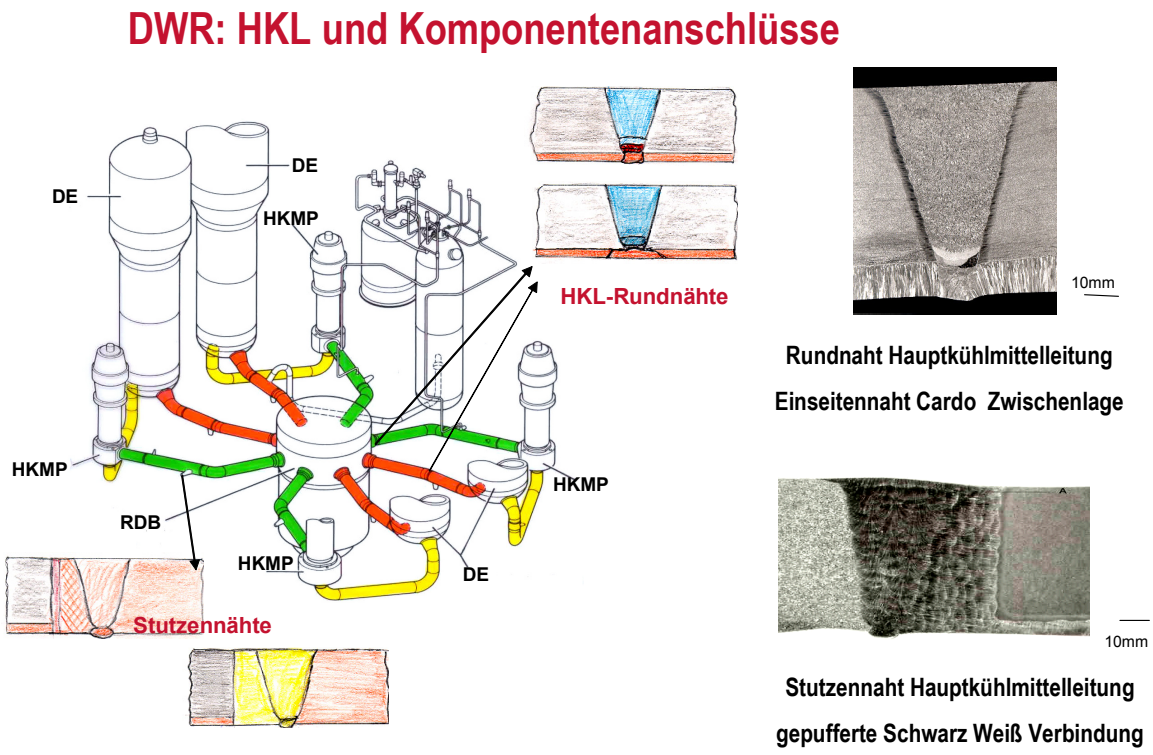

Figure 4. Layout of Siemens BWR design showing the design of the welds between the RPV and the carbon steel piping, and between the main piping and stainless steel nozzles (Kilian 2005).

2.5 Dissimilar metal welds in oil refineries

Dissimilar metal welds (DMW) have been used with success in oil refinery applications. In high temperature applications in oil refineries, dissimilar metal welds made with nickel-base alloy filler metals provide extended service lives as compared to welds made with stainless steel filler metals. Although considerable oil refinery experience exists, it is difficult to find published information on pressure boundary welds made with nickel-base filler metals in hot hydrogen and/or H_2S services. Pressure boundary welds made with nickel-base alloy filler metals have been used in hot hydrogen and/or hydrogen sulphide (H_2S) service in a number of refinery piping applications. Clad piping has been in similar service at more severe conditions for more than 15 years. As an example Alloy 625 (ERNiCrMo-3) weld filler metal has shown excellent resistance to corrosion and mechanical degradation under hydrogen / hydrogen sulfide (H/H_2S) conditions.

Over the years, failures of solid stainless steel piping have occurred as a result of polythionic acid SCC from the inside of the pipes, and both internal and external chloride SCC has taken place. As a result of these failures, piping in the other units of the refineries has been replaced with clad piping. Other examples of clad piping use

include vacuum transfer lines, crude oil tower overhead lines, and both hot and cold service hydroprocessing reactor effluent lines (Penuela et al. 1999). Results of mechanical testing and metallurgical analyses after years in operation show that no significant loss in mechanical properties has occurred.

One-sided full penetration nickel-alloy welds are commonly used to join stainless steel piping to weld overlaid Cr-Mo steel nozzles of hydroprocessing reactors operating in hot, high pressure hydrogen service. The 1¼ % Cr – ½ % Mo piping with type AISI 321 cladding has been used as a replacement for solid stainless steel piping because of its immunity to SCC in chloride and polythionate containing acids. In the construction of clad piping systems, carbon or low alloy steel base materials serve as the pressure boundary, while the stainless steel cladding is the corrosion allowance.

A DMW of AISI 321 stainless steel clad 1¼ % Cr – ½ % Mo piping that had operated without problems for 5 years was selected for analysis to determine the effects of operating conditions, listed in Table 1, on the properties of butt-weld joints.

Table 1. Operating conditions for stainless steel clad piping and DMW in oil refinery (Penuela et al. 1999).

	Design values	Operating values
Pressure [bar]	38	34.5
Temperature [°C]	371	371
Hydrogen partial pressure [bar]	25.5	24.1
H_2S content [mole-%]	34	6

Base metal, weld metal, and heat-affected zone (HAZ) hardness were determined to be normal. Microhardness surveys were made transverse to a weld just below the cap, above the root, and through the wall thickness from outside diameter to inside diameter. Tensile properties of the weld and base metal were essentially unchanged from new material properties, Table 2. Charpy impact testing across the weld showed excellent toughness retention. No evidence of intergranular fracture was observed in the DMW or HAZ of the AISI 321 stainless steel cladding.

Table 2. Results of mechanical testing (Penuela et al. 1999).

	Ex-Service Weld Metal	Ex-Service Base Metal	SA-387 Gr. 11 Cl. 2 Specification
Tensile strength [ksi]	88.1	90.8	75 to 100
Yield strength [ksi]	–	62	45 min.
Elongation [% in 2"]	–	30	22
Charpy impact toughness [ft-lbs @-20F]	50, 47, 47	not tested	–

Notes: 1. All impact specimens of the weld metals showed 100% shear fracture, 8 mm × 10 mm.
2. Tensile test of base metal with clad removed.

The results of the base metal and the weld metal characterization after five years operation are summarized as follows (Penuela et al. 1999):

- No corrosion or sulphidation of the ERNiCrMo-3 weld metal was detected. Chemical analysis of the weld root exposed to the inside of the pipe showed the following composition: 0.04% C, 19.4% Cr, 49% Ni, 3.92% Mo and Fe bal.
- Bonding of AISI 321 stainless steel cladding to 1¼% Cr – ½% Mo base material was intact; no evidence of disbonding was observed.
- Base metal, weld metal and HAZ hardness are normal. Microhardness surveys were made across the weld just below the cap and just above the root. Another survey was taken through the wall thickness from OD to ID.
- Tensile properties of the weld and the base metals were essentially unchanged from new material properties.
- Charpy impact testing across the weld showed excellent toughness retention.

The DMWs most commonly used to join clad piping components in high temperature refining applications utilize nickel-base alloy filler metals. The filler metal used has been, e.g., an Alloy 625 filler metal utilizing GTA welding with ERNiCrMo-3 (SFA 5.14 F43) wire for the root and cap, and SMA welding with ENiCrMo-3 covered electrodes (SFA 5.11 F43) for filler and cap passes.

The key to filler metal selection in sulphidizing environments is to select a filler metal with a level of chromium sufficient to resist high temperature sulphidation. As in the AISI 300 series stainless steels, chromium increases the sulphidation resistance of nickel-base alloy filler metals. Nickel-base alloy filler metals commonly used in these environments contain a minimum of about 16 to 18% Cr, and show good resistance to sulphidation up to 500°C and even above. The operating temperatures of most

hydroprocessing units are well below the temperature where high temperature nickel sulphide eutectic formation is a concern. Filler metal selection is determined by the cladding and base materials, as well as the weld root chemistry, taking into account the dilution effects required for corrosion resistance under the service conditions. For example, when Alloy 625 (UNS N06625) filler metal was used, a distinguishing feature of nickel-base alloy filler metals was their coefficient of thermal expansion. Nickel-base alloy filler metals such as Alloy 625 have coefficients of thermal expansion close to those of ferritic materials, such as carbon and Cr-Mo steels, so differential thermal expansion and thermal fatigue issues can usually be minimized in the design of clad pipe girth welds (Dobis & Chakravarti 1997).

The piping girth welds are usually preheated and post-weld heat treated in accordance with ASME B31.3 code requirements, as outlined below:

- Preheat and interpass: 204°C
- PWHT: 745°C for 2 hours
- Heating rate: 150°C/h from 315°C to 745°C
- Cooling rate: 40°C/h from 745°C to 650°C and 150°C/h from 650°C to 315°C
- Joint geometry: 37 ½ degree bevel, single side V-groove
- Root gap: 1.6 mm to 3.2 mm.

It has also been noted that, during the qualification of the welding procedures, it was necessary to reduce the cooling rate to 40°C/h between 745°C and 650°C, to minimize weld hardness.

2.6 References

Dobis, J. D. & Chakravarti, B. 1997. Materials Performance, Vol. 36, No. 7, pp. 29–35.

IAEA. 2003. Assessment and Management of Ageing of Major Nuclear Power Plant Components Important to Safety; Primary Piping in PWRs. IAEA-TECDOC-1361.

Kilian, R. 2005. Personal communication.

Penuela, L. E. et al. 1999. Analysis of Dissimilar Welds Exposed to High Temperature H_2/H_2S Conditions in a Hydrodesulfurizing Unit. Corrosion/99, Paper No. 383. Houston TX, NACE.

Shah, V. & MacDonald, P. (Eds.). 1993. Aging and Life Extension of Major Light Water Reactor Components. Elsevier, the Netherlands. ISBN 0 444 89448 9. 941 p.

3. Properties and welding of nickel-base Inconel materials

The Ni-base Inconel materials are widely used in nuclear power plants and in the chemical industry. Inconel materials have high chromium and nickel content (Cr > 15% and Ni > 50%). The austenitic iron- and nickel-base alloys have good mechanical properties and corrosion resistance (Lee & Jeng 2001, Jeng et al. 2005).

High-quality joints are readily produced in nickel-base alloys by common welding processes, such as shielded metal arc welding (SMAW), gas tungsten arc welding (GTAW), gas metal arc welding (GMAW) and submerged arc welding (SAW). The choice of welding process is based on (1) thickness of metal to be joined, (2) design of the product, (3) design of the joint, (4) position in which the joint is to be made, (5) need for jigs or fixtures, (6) service conditions and corrosive environments to which the joint will be exposed, and (7) special shop or field construction conditions (Kiser, Special Metals Welding Products Company, 2006).

Welding procedures for nickel-base alloys are similar to those used for stainless steels. The thermal expansion characteristics of the alloys are approximate to those of carbon steels, and essentially the same warping or distortion can be expected during welding. All weld beads should have slightly convex contours. Flat or concave beads should be avoided. Preheating is not required. If the base metal is cold (2°C or less) an area of about 300 mm surrounding the weld location should be warmed to 16–21°C to prevent the formation of condensate. Postweld thermal treatment may be required for precipitation hardening. Postweld stress relief may be necessary to meet specification requirements or to avoid stress-corrosion cracking (SCC) (Kiser, Special Metals Welding Products Company, 2006).

3.1 Nickel-base Inconel materials

Alloy 690 is a high-chromium nickel-base alloy that is used today in the petrochemical and nuclear industries. Alloy 690 has a significantly higher Cr content; the Cr content is 30% as compared to 16% of Alloy 600. This helps to prevent Cr-depletion by carbide precipitation on grain boundaries. Moreover, higher Cr enhances resistance to corrosion. With 60% Ni, Alloy 690 is SCC resistant to sodium hydroxide and chloride. Furthermore, under simulated steam generator conditions in laboratory environments, Alloy 690 is highly resistant to IGSCC (Wu & Tsai 1999, Crum & Nagashima 1997, Aoh & Yang 2003). Table 3 shows the chemical compositions of Ni-base Inconel 600 and 690 materials (Staehle & Gorman 2003).

Table 3. Chemical compositions of Ni-base Inconel 600 and 690 materials (Staehle & Gorman 2003).

	Alloy 600 (EPRI Guidelines) [%]	**Alloy 690 (EPRI Guidelines) [%]**
C	0,025-0,05	0,015-0,025
Mn	< 1,00	0,50
P	0,015	0,015
S	< 0,010	0,003
Si	< 0,50	0,50
Cr	15,0-17,0	28,5-31,0
Ni	> 72,0	Bal (> 58,0)
Mo	-	0,2
Fe	6,0-10,0	9,0-11,0
Cu	< 0,50	0,10
Co	0,015	0,014
Al	-	0,40
Ti	-	0,40
Others	-	N: 0,050 B: 0,005 Nb: 0,1

Since their development over 20 years ago, Ni-Cr-Fe filler metal 82 and welding electrode 182 have been extensively utilized for welding nickel-base alloys, especially Alloy 600, and for dissimilar combinations of materials including pressure vessel steels joined to stainless steels. In the 1990s filler metal 52 and welding electrode 152 have been either selected or considered as a prime candidate material for joining Alloy 690 materials of pressurized water reactors (PWRs), where primary water stress corrosion cracking (PWSCC) and intergranular stress corrosion cracking (IGSCC) have been encountered. Welding consumables are available for TIG, MIG, MMA, and SAW (Wu & Tsai 1999, Crum & Nagashima 1997, Aoh & Yang 2003, Hood & Lin 1995). Table 4 lists the chemical compositions and Table 5 the mechanical properties of Inconel filler materials and weld metals (Inconel filler metal specifications 2003, Boursier et al. 2004).

Table 4. Chemical compositions of Inconel filler materials (Inconel filler metal specifications 2003).

	Inconel 182 [%]	Inconel 82 [%]	Inconel 52 [%]	Inconel 152 [%]	Inconel 52M [%]
C	< 0,1	< 0,1	< 0,04	< 0,05	< 0,04
Si	< 1	< 0,5	< 0,5	< 0,75	< 0,5
Mn	5-9,5	2,5-3,5	1	< 5	<1
P	< 0,03	< 0,03	< 0,03	< 0,03	< 0,03
S	< 0,015	< 0,015	< 0,015	< 0,015	< 0,015
Cr	13-17	18-22	28-31,5	28-31,5	28-31,5
Ni	> 59	< 67	Ni+Co remainder	Ni+Co remainder	Ni remainder
Mo	-	-	< 0,5	< 0,5	< 0,5
Nb	1-2,5	2-3	Nb+Ta < 0,1	Nb+Ta 1-2,5	0,5-1
Ti	< 1	< 0,75	< 1	< 0,5	< 1
Fe	< 10	< 3	7-11	7-12	7-11
Al	-	-	< 1,1 (Al+Ti <1,5)	< 0,5	< 1,1 (Al+Ti <1,5)
Cu	< 0,5	< 0,5	< 0,3	< 0,5	< 0,3
Co	< 0,1 when specified	< 0,12 when specified	-	-	< 0,12
Zr	-	-	-	-	< 0,02
B	-	-	-	-	< 0,005
Ta	< 0,3 when specified	-	-	-	-
	Others < 0,5	Others < 0,5	Others < 0,5	Others < 0,5	Others < 0,5

Table 5. Mechanical properties of Inconel filler materials (Boursier et al. 2004).

Parameter	Alloy 182	Alloy 82	Alloy 152	Alloy 52	Alloy 52M**
$R_{p0.2}$ (20ºC) [MPa]	> 250 / *375**	> 250 / *396*	> 250 / *431*	*300*	445
R_m (20ºC) [MPa]	> 550 / *641*	> 550 / *610*	> 586-750/ *674*	*539*	645
A (20ºC) [%]	> 30 / *41*	> 30 / *33*	> 30 / *37*	*42*	35
$R_{p0.2}$ (350ºC) [MPa]	> 190 / *342*	>190 / *316*	> 190 / *359*	*248*	320
R_m (350ºC) [MPa]	*576*	*547*	> 435 / *548*	*460*	480
A (350ºC) [%]	*46*	*48*	*37*	*48*	37

* Values in italic are measured values presented in (Boursier et al. 2004).
** Typical values of Alloy 52M (Kiser 2006). The other values are according to RCC-M.

In Table 6 a classification of impurities and trace elements in nickel-base superalloys is presented (Holt & Wallace 1976). In this table the deleterious elements are classified as residual gases (H, N, O, etc.), non-metallic impurities (S, P), and metallic or metalloid impurities (Pb, Bi, As, Sb, etc.). Beneficial trace elements are classified as refining agents (Ca, Mg, Ce, etc.) or parts-per-million alloying additions (B, Zr, Hf).

Table 6. Classification of impurities and trace elements in nickel-base superalloys (Holt & Wallace 1976).

TYPE	EXAMPLES
A. Detrimental elements	
1. Residual gases	H, N, O, Ar, He
2. Non-metallic impurities	S, P
3. Metallic or metalloid impurities	Pb, Bi, As, Sb, Se, Ag, Cu, Tl, Te
B. Beneficial elements	
1. Refining agents	Ca, Mg, Ce, La
2. Minor and ppm alloying additions	B, Zr, Hf, Mg, C
3. Alloying additions up to 1.5%	Zr, Hf

These alloying elements and impurities may interact with each other or with major alloying ingredients in the melt to form non-metallic inclusions such as carbides, borides, sulphides, and oxides or complexes of them. These phases may be removed from the melt during refining or they may be retained in the solidified alloy and hence influence cast alloy properties. The detrimental trace elements invariably cause grain boundary embrittlement and additions of beneficial trace elements are often made to counteract the embrittlement (Holt & Wallace 1976). The following is a summary of the current philosophy regarding the weldability of Ni-base superalloys:

- Sulphur content should be kept to as low a value as possible since it is a tramp element and imparts no discernable benefit to the weldability or other properties of the alloys. Strong sulphide formers such as Mg, Zr, Ti, and Mn should be used to combine with the element and reduce its effect to a low level, especially on grain boundaries.
- Phosphorus normally should be given the same consideration as S. Removal of the element is difficult during melting and low P materials need to be used during melting stages.
- Boron content should be kept to as low as possible.
- Suitable Mg and rare earth metal additions can be used, ensuring that other properties are not adversely affected.
- Cooling rates from the preweld solution treatment temperature need to considered and carefully controlled to reduce non-equilibrium segregation.
- In wrought products it may be possible to change the character of the grain boundaries through grain boundary engineering (Richards & Chaturvedi 2000).

3.2 Solidification of Ni-base alloys and their microstructures

The dissimilar metal welding process provides a means of integrating the advantages of constituent materials, and hence enables designers to achieve practical, low-cost solutions to engineering requirements. The dilution of the two different base metals causes a non-identical composition within the fusion zones, which may degrade the properties of the weldment in some cases (Jeng et al. 2005).

The Cr and Ni contents of a nickel-base alloy play an essential role in determining the corrosion resistance of the material. It has been shown previously that the IGSCC and SCC effects of a nickel-base alloy can be suppressed effectively by specifying either a 30 wt.-% Cr content or a 60 wt.-% Ni content. Furthermore, Cr has a high affinity with C and readily forms carbides. The heat generated during the welding process causes the Cr to interact readily with carbon to form carbides such as $M_{23}C_6$ and M_7C_3, which then precipitate on the grain boundaries. This reaction may result in Cr-depletion within the first-pass welding layer or in the heat affected zone (HAZ), which causes degradation of the corrosion resistance. The problem of Cr-depletion can be avoided by either increasing the Cr content of the alloy, or by introducing high affinity elements such as Ti and Nb to stabilize carbon (Lee et al. 2004).

The role of carbon in influencing the mechanical properties of Ni-base superalloys is mainly via carbide formation of primary and secondary carbides. The primary carbides, such as MC form either in the melt or at high temperatures after primary solidification. The MC carbide can occur as discrete precipitates at grain boundaries or on other defects within the grain, showing no preference for location. The M component is often Nb or Ti, though substitution of Mo and W is also possible (Richards & Chaturvedi 2000).

Secondary carbides form during the heat treatment and are often of the $M_{23}C_6$ type, with a distinct preference for forming at the grain boundaries. The M component is typically Cr, with the possible substitution of Mo and W. M_6C carbides, being similar to the $M_{23}C_6$ carbide, also form during heat treatment in some superalloys (Richards & Chaturvedi 2000).

When fabricating steam generator tubing, control of the metallurgical condition of the material is of utmost importance. As Alloys 600 and 690 are concerned, probably the most influential separate factor determining the final properties of the tubing is the carbon content. Since the solubility of carbon is fairly low in these materials, chromium carbides form readily during the annealing cycle and may also remain undissolved if the temperature is not kept high enough. In general, the presence of undissolved carbides during annealing has a pronounced effect on the resulting microstructure and consequently also on the material properties (Nordberg 1985).

The solubility of carbon in Alloy 690 as a function of the temperature has been estimated as:

$$log\ (\%C) = 4{,}771 \times 10^{-3} T(°C) - 6{,}819 \quad (1)$$

and a corresponding formula for Alloy 600 has been fitted to the solubility data published by Scarberry et al. (1976):

$$log\ (\%C) = 3{,}265 \times 10^{-3} T(°C) - 4{,}766. \quad (2)$$

A comparison of the solubility, e.g. at 1050°C, shows that Alloy 690 dissolves only 0,016% C, whereas the corresponding amount of C for Alloy 600 is 0,046% C. Thus, the solubility of C is much lower in Alloy 690 than in Alloy 600 (Nordberg 1985).

Yamanaka and Yonezawa (1989) presented the results of electron microscopy studies of Alloy 690. Specimens containing from 0.004 to 0.07 wt.-%C were solution treated at 1350°C and water quenched, or solution treated and aged at temperatures from 800 to 1200°C and then water quenched. The carbon solubility equation for Alloy 690 and revised equation for Alloy 600 were (Yamanaka & Yonezawa 1989, Gold et al. 1990):

$$Alloy\ 690:\ log\ (\%C) = 3{,}14 - 6397 / T(K) \quad (3)$$

$$Alloy\ 600:\ log\ (\%C) = 2{,}90 - 5834 / T(K) \quad (4)$$

Lee and Jeng (2001) studied characteristics of dissimilar metal welding of nickel-base Alloy 690 and SUS 304L stainless steel using two alternative Inconel filler metals, namely, 82 (I-82) and 52 (I-52). Gas tungsten arc welding with identical parameters and procedures was used to carry out single V-groove butt welding with six passes in four layers on nickel-base Alloy 690 and 304L stainless steel. The chemical compositions of the base and filler metals are presented in Table 7 (Lee & Jeng 2001).

Table 7. Compositions of Alloy 690 and 304L base metals, and I-52 and I-82 filler metals (in wt.-%) (Lee & Jeng 2001).

Material	C	Si	Mn	P	S	Cr	Ni	Al	Cu	Nb	Ti	Fe
690	0.02	0.35	0.29	0.007	0.001	29.70	60.65	…	0.02	…	0.20	8.76
304L	0.03	1.00	2.00	0.045	0.003	18.00	8.00	…	…	…	…	Bal.
I-52	0.03	0.15	0.24	0.003	0.001	28.83	60.65	0.71	0.01	…	0.51	8.86
I-82	0.04	0.09	0.92	0.007	0.001	19.76	73.38	0.05	0.07	0.27	0.44	0.94

The microstructure of Alloy 690 base metal is shown in Figure 5a. The structure is single phase austenitic with annealing twins formed at heat treatment. Many precipitates are dispersed in the matrix and along the grain boundaries. The principal precipitates are TiN and $Cr_{23}C_6$. The TiN precipitates can be seen as tiny rectangles within the grains, and appear golden under an optical microscope. $Cr_{23}C_6$ is distributed at the grain boundaries. The microstructure of 304L can be seen in Figure 5b. This image shows an austenitic phase with twins and δ-ferrite (Lee & Jeng 2001).

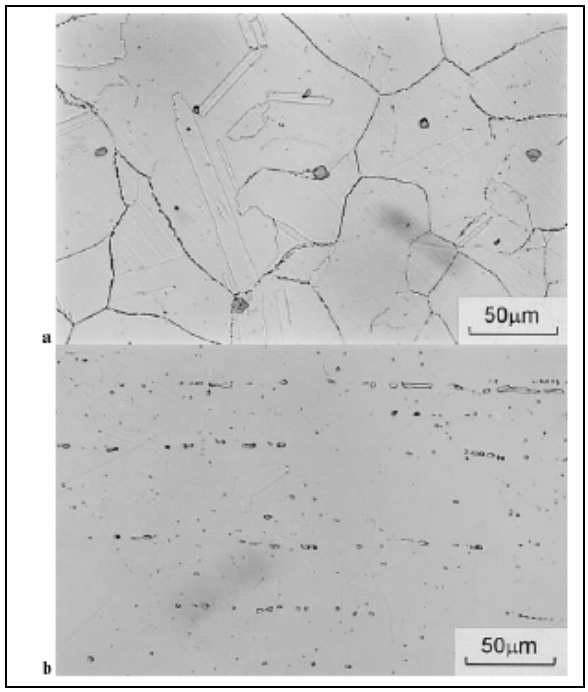

Figure 5. Microstructures of Alloy 690 (a) and 304L (b) (Lee & Jeng 2001).

Figure 6 presents microstructures of the HAZ in Alloy 690 and 304L. In the HAZ of Alloy 690, the grain size varies with heat distribution. Moving from the fusion line to Alloy 690 base metal, first the grain growth zone is evident, then the fine grain zone, and finally the base metal. The HAZ microstructure in 304L shows the distribution of δ-ferrite phase, influenced by the welding heat.

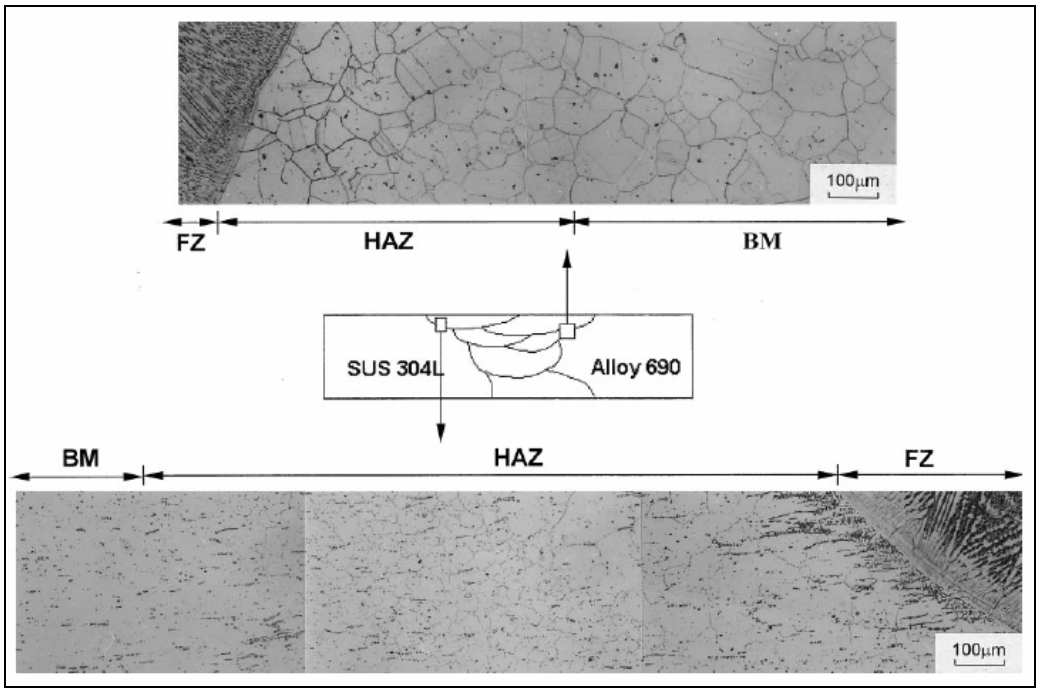

Figure 6. Microstructures of the HAZ in Alloy 690 and 304L (Lee & Jeng 2001).

Figure 7 presents subgrain microstructures of I-52 weldment. In the I-52 fusion zone, epitaxial growth from the HAZ occurs spontaneously. The subgrain structures close to the two base metals are different owing to the base metal dilution effects. Between Alloy 690 and I-52, the compositional difference is slight. The subgrain structure is mainly cellular dendritic and grain boundaries extend from the HAZ to the fusion zone. The compositional difference between I-52 and 304L is great and the subgrain structure is columnar dendritic. In the root fusion zone, the microstructures close to the two base metals are cellular dendritic and columnar dendritic, but the central microstructure is equiaxed dendritic (Lee & Jeng 2001).

Figure 8 presents subgrain microstructures of I-82 weldment. Epitaxial growth also occurs spontaneously in I-82. In the cap (crown) fusion zone, the central microstructure is equiaxed dendritic, but close to the two base metals it is columnar dendritic. The microstructure is not influenced by any dilution effect. The microstructure of the root fusion zone is similar to that of I-52. The interdendritic region in the root fusion zone is larger than in the cap fusion zone. The quantity of precipitates in I-82 is greater than in I-52. In I-82 the precipitates (also the faceted particles) are composed mainly of nickel, niobium, chromium, and titanium (Lee & Jeng 2001).

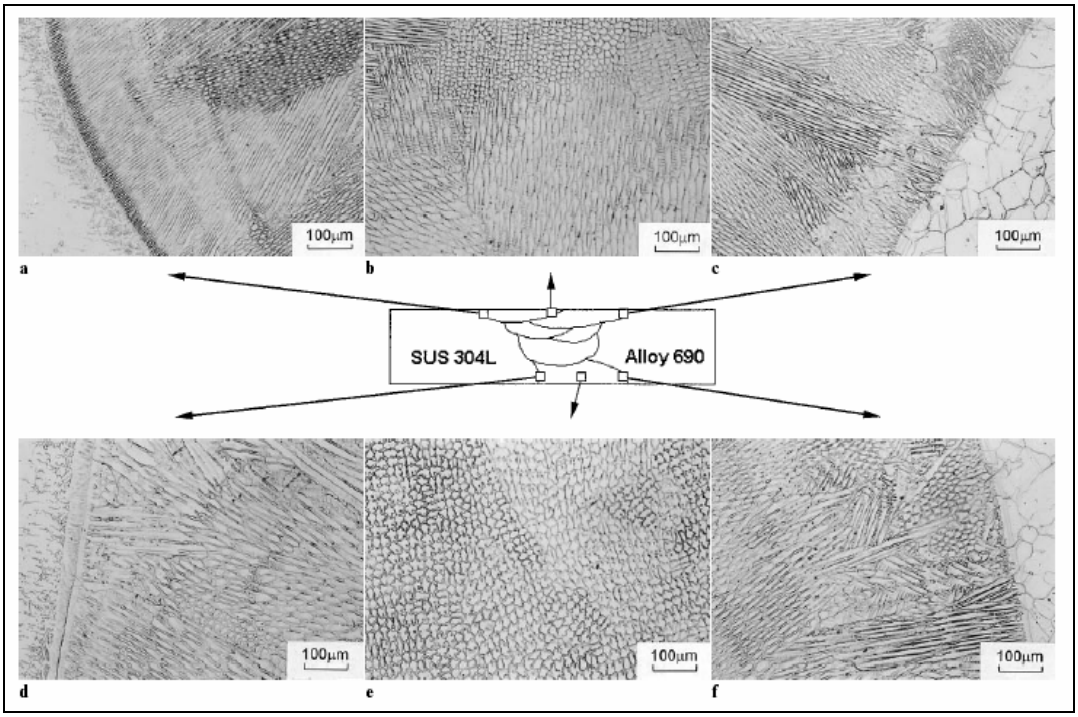

Figure 7. Subgrain microstructures of I-52 weldment: (a) crown welded face near 304L, (b) crown welded face near centreline, (c) crown welded face near Alloy 690, (d) root welded face near 304L, (e) root welded face near centreline, and (f) root welded face near Alloy 690 (Lee & Jeng 2001).

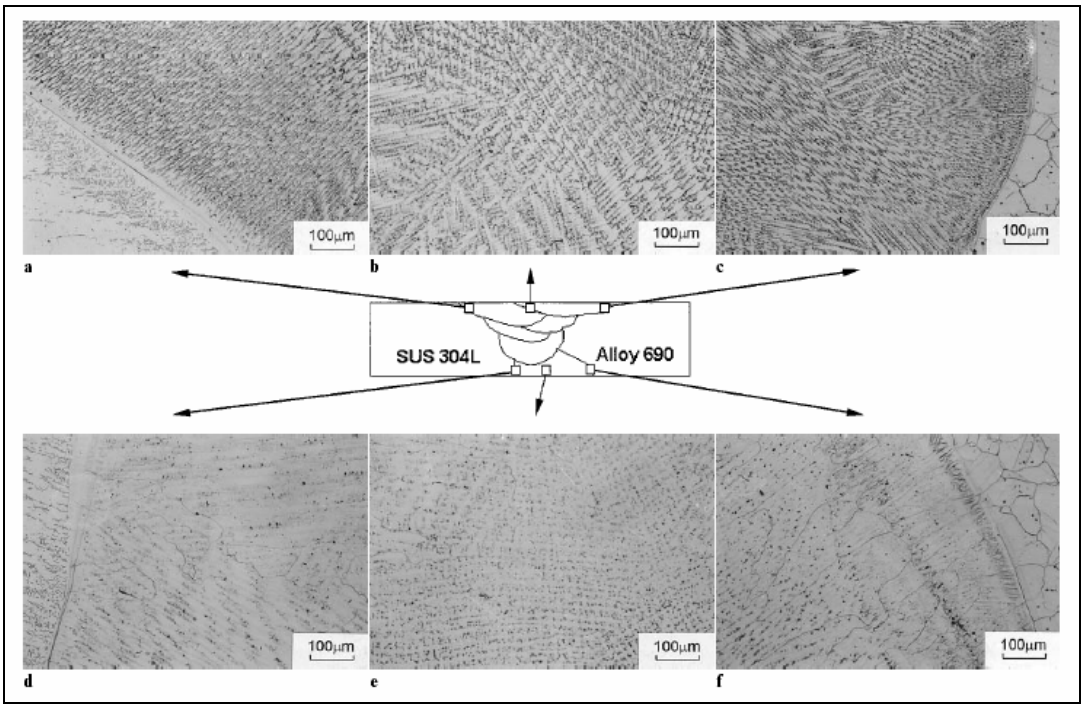

Figure 8. Subgrain microstructures of I-82 weldment: (a) crown welded face near 304L, (b) crown welded face near centreline, (c) crown welded face near Alloy 690, (d) root welded face near 304L, (e) root welded face near centreline, and (f) root welded face near Alloy 690 (Lee & Jeng 2001).

The constitutional cooling rate is different between the two filler metals owing to the composition difference. I-82 has a greater constitutional cooling rate than I-52. The different constitutional cooling rates induce variation in the microstructure. The greater the constitutional cooling rate, the greater the tendency for the subgrain structure to change from cellular dendrites to columnar dendrites. Therefore, the microstructure in the I-52 fusion zone tends to be a mixture of cellular dendrites and columnar dendrites, whereas that of I-82 tends to be mainly columnar dendritic. Comparison of dendritic density shows greater density in I-82 than in I-52. The greater constitutional cooling rate produces smaller grains and denser dendrites, improving the mechanical properties. During the solidification period, niobium segregates to the interdendritic regions, and niobium-rich precipitates occur. Meanwhile, because of the influence of residual stresses produced by welding, cracks occur along and between closely-located niobium-rich precipitates. Hence, the addition of niobium to I-82 may cause hot cracking. However, niobium causes finer grains, denser dendrites, and niobium-rich precipitates, which improve mechanical properties (Lee & Jeng 2001).

The dilution and composition differences between the filler metal and base metal also affect the fusion zone microstructure. In I-52 weldment, the compositions of the filler metal and Alloy 690 are very similar. The grains evidently grow from the HAZ to the fusion zone. However, in the I-82 fusion zone, only the region with high dilution shows grain growth. Grain growth can also be seen on the 304L side of both weldments. These

observations demonstrate that lower compositional difference between the base metal and filler metal, or higher dilution, assist grain growth in the HAZ to the fusion zone (Lee & Jeng 2001).

Metallographic investigation of Alloy 82 welds showed three distinct microstructures. Figure 9 presents SEM images of different subgrain structures observed in an Alloy 82 weldment. Recrystallized grains were observed in limited regions between weld beads (Figure 9a). Cellular dendritic grains were of similar size scale to recrystallized grains, as shown in Figure 9b. The solidification grain boundaries were more readily distinguished under Nomarski DIC illumination than polarized light. The majority of the weld structure consisted of columnar dendritic grains, as shown in Figure 9c (Young et al. 2003).

Briant and Hall (1987) investigated microstructural effects on intergranular corrosion (IGC) in the nickel-base weld metals of Alloy 182 and Alloy 82. The unwelded Alloy 182 and 82 filler metal samples were heat treated at 1200°C for 3 h in argon and then water quenched. This solution annealing heat treatment dissolves most precipitates formed during processing. The samples were then aged at 600, 650 and 700°C for 0.5 to 100 h (Briant & Hall 1987).

Welds were prepared by welding many layers of weld metal on plates of Inconel 600 or AISI 304. The welds were not solution annealed. However, they were exposed to two aging treatments intended to represent the thermal ageing they would undergo in nuclear applications. The first ageing treatment consisted of an anneal at 620°C for 24 h followed by air cooling. This heat treatment represents the stress relief heat treatment of safe ends welded to pressure vessel. The second heat treatment was a low temperature ageing (LTA) treatment at 400°C for 200 h followed by air cooling, intended to produce the same microstructural changes that would occur during long time service at reactor operating temperatures (Briant & Hall 1987).

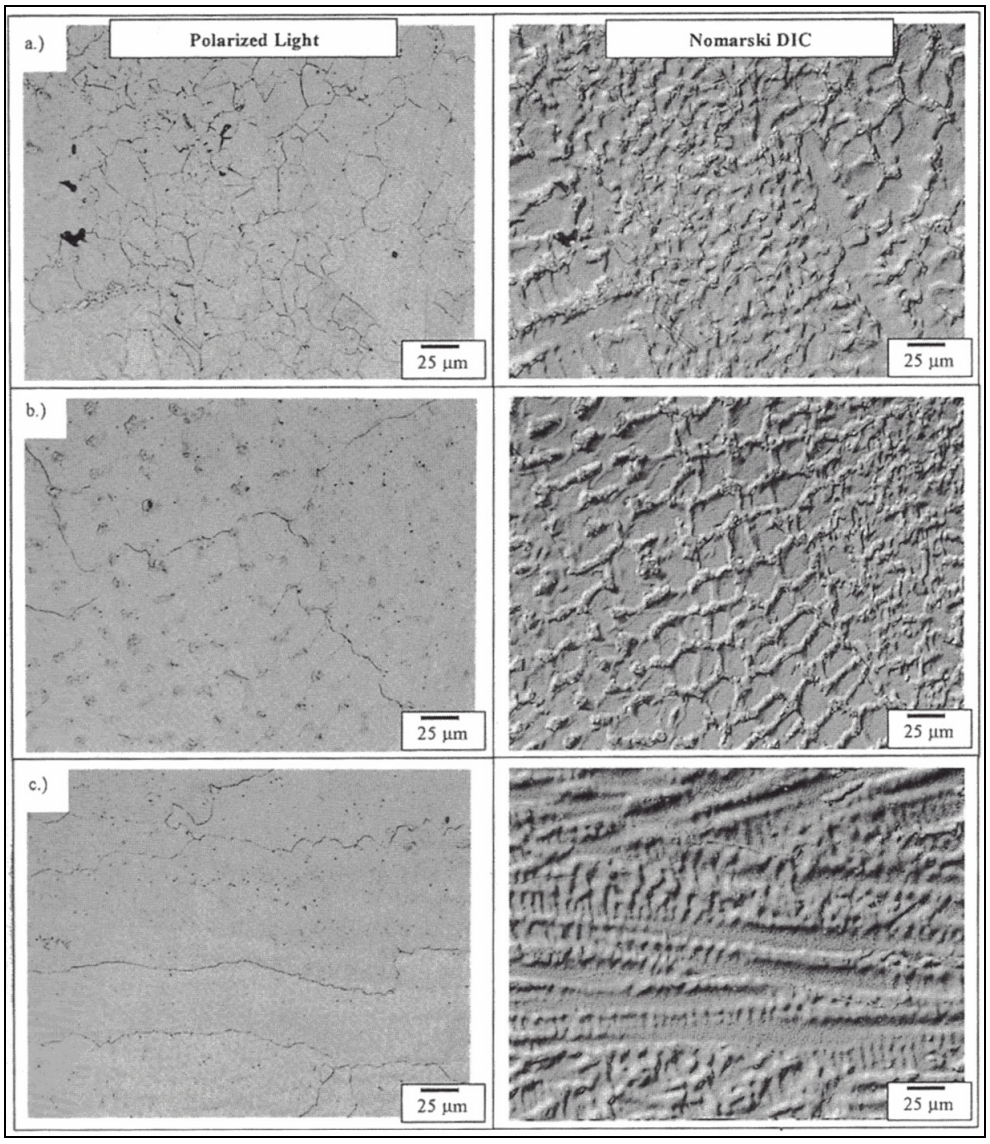

Figure 9. SEM images of different subgrain structures observed in Alloy 82 weldment: (a) recrystallized grains, (b) cellular dendritic grains, (c) columnar dendritic grains (Young et al. 2003).

The IGC susceptibility was evaluated with the 25% nitric acid test. Samples were electropolished prior to testing and then placed in the boiling solution for 48 h. After testing, the extent of corrosion was evaluated by weight loss measurement and then scanning electron microscopy (SEM). Auger electron spectroscopy (AES) was used to examine the impurity segregation to grain boundaries during ageing. Alloy 182 corroded significantly more than Alloy 82 after various thermal ageing treatments. Carbide precipitation depletes chromium at the grain boundaries to lower levels than in Alloy 82, since Alloy 182 has a higher carbon content and lower chromium content. The thermal treatments caused precipitation of $M_{23}C_6$ along the grain boundaries in Alloy 82. In Alloy 182, the same treatments caused grain boundary precipitation of $M_{23}C_6$, M_7C_3 and TiC, as well as matrix precipitation of γ' (Ni_3Ti). Phosphorous segregates to grain boundaries

during the ageing treatments, but it does not appear to have a large effect on the corrosion resistance. Some welds of Alloy 82 were found to be susceptible to IGC after thermal ageing, which was attributed to carbon pick-up during welding (Briant & Hall 1987).

Lee et al. (2004) studied the effects of Ti addition on the weldability, microstructure and mechanical properties of a dissimilar metal weldment of Alloy 690 and SUS 304L. Shielded metal arc welding (SMAW) was employed to butt-weld of two plates with three welding layers, where each layer was deposited in a single pass. To investigate the effects of Ti addition, the flux coatings of the electrodes used in the welding process were modified by varying additions of either a Ti–Fe compound or Ti powder. The compositions of the electrodes prepared for the investigation were based on the Inconel Welding Electrode 152 series. Oxford filler metal 52 of diameter 3.2 mm was chosen as the core wire. A series of welding electrodes were prepared by coating the core wire with a flux containing various additions of either Ti powder or a Ti–Fe compound. A total of three welding layers were utilized, each layer being deposited in a single pass. Table 8 presents the compositions of the base metals and welding electrodes used (Lee et al. 2004).

Table 8. The compositions of base metals and welding electrodes (in wt.-%) (Lee et al. 2004).

	Ni	Cr	Fe	Mn	Nb	Ti	Mo	C	Si	Cu	Al	S	P
Alloy 690	60.65	29.70	8.76	0.29	-	0.20	-	0.022	0.35	0.02	-	0.001	0,007
SUS 304L	8.00	18.00	Bal	2.00	-	-	-	0.030	1.00	-	-	0.003	0.045
Oxford Filler Metal 52	60.00	29.30	8.80	0.40	0.02	0.500	0.100	0.030	0.17	0.060	0.61	0.010	-
Inconel Welding Electrodes 152	52.80	30.00	10.40	3.42	1.87	0.112	0.071	0.032	0.42	<0.005	0.14	0.008	0.009
Without extra addition[a] S009	51.20	29.60	11.70	3.99	1.82	0.099	0.072	0.048	0.47	0.061	0.06	0.009	0.019
Ti-Fe compound[b]													
STF013	51.90	28.50	12.00	3.88	1.90	0.132	0.073	0.048	0.52	0.062	0.06	0.008	0.019
STF027	51.50	28.30	12.40	3.78	1.96	0.271	0.077	0.047	0.64	0.062	0.06	0.008	0.018
Ti-powder[c]													
ST017	53.50	26.82	11.86	3.96	1.82	0.176	-	0.039	0.61	-	0.06	0.004	0.013
ST041	53.00	26.92	11.83	3.94	1.92	0.410	-	0.040	0.78	-	0.05	0.003	0.013
ST091	53.17	27.01	12.64	3.61	1.45	0.910	0.057	0.050	0.93	0.010	0.05	-	-

[a] Without extra Ti addition in the flux. the Ti content comes from the filler metal
[b] Adding Ti-Fe compound in the flux to change the Ti content
[c] Adding Ti-powder in the flux to change the Ti content

Figure 10 presents the macrostructure of S009 weldment (without extra Ti addition). It can be seen that the resulting structure is mainly dendritic when the Ti content of the electrode is not modified. As shown in Figure 11, when the level of Ti addition is increased with the Ti-Fe compound addition, the microstructure changes from a columnar dendritic and equiaxed dendritic structure to an equiaxed dendritic structure. However, as shown in Figure 12 the fusion zone (FZ) microstructure with Ti powder addition does not change significantly, but remains as a predominantly columnar dendritic structure (Lee et al. 2004).

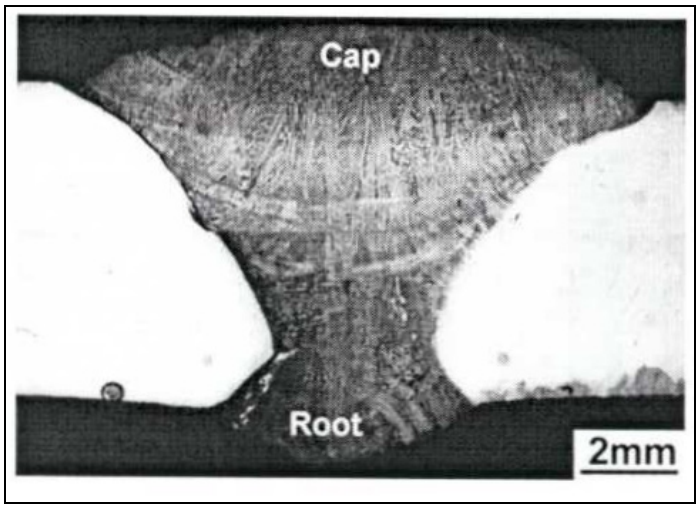

Figure 10. The macrostructure of S009 weldment (Lee et al. 2004).

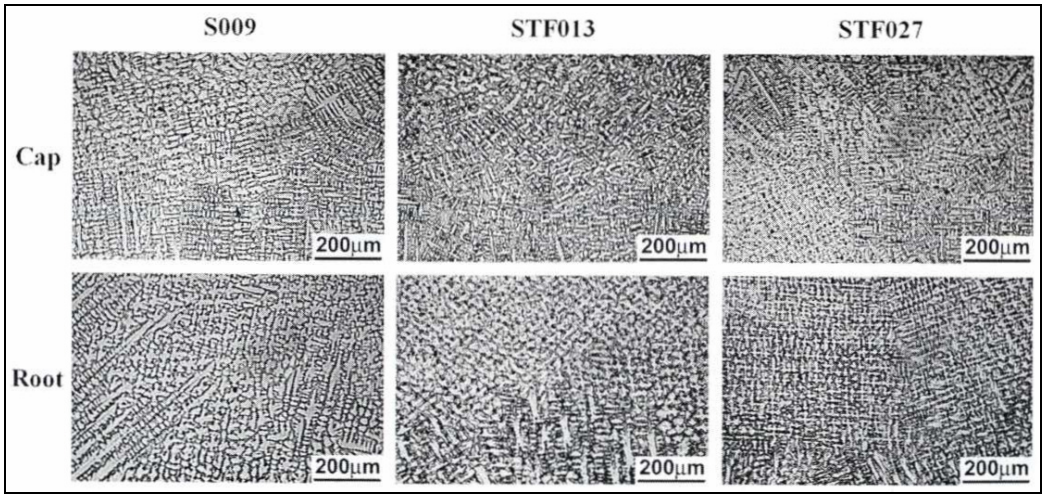

Figure 11. The microstructure of the central fusion zone with Ti–Fe compound additive (Lee et al. 2004).

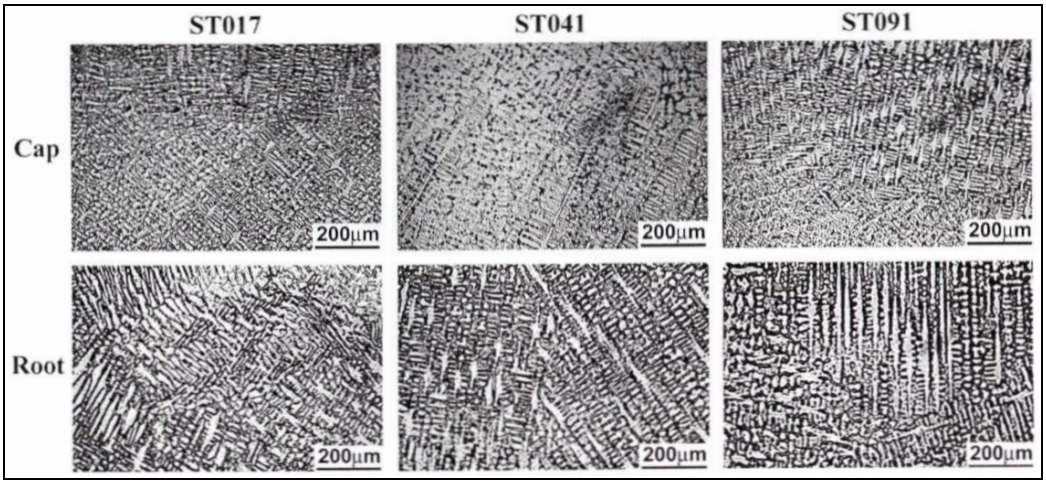

Figure 12. The microstructure of the central fusion zone with Ti powder additive (Lee et al. 2004).

The results show that when a Ti–Fe compound additive is added, the microstructure tends to change from columnar dendritic to equiaxed dendritic as the level of Ti addition increases. Moreover, the primary dendrite arm spacing (PDAS) shortens with increasing Ti content, particularly with electrodes with Ti powder additive. Observations of the interdendritic phases revealed the presence of irregular Nb-rich phases, Al-Ti oxides and Al-Ti-Nb-rich particles. Al–Ti oxides tended to dominate in this region with increasing Ti addition (Lee et al. 2004).

Jeng et al. (2005) studied the effects of Nb addition on the microstructure and corrosion properties of Alloy 690–SUS 304L weldments. Four different electrodes were used, each with a different Nb content, namely Nb1 (0.1 wt.-%), 152 (1.03 wt.-%), Nb2 (2.49 wt.-%), and Nb3 (3.35 wt.-%). The compositions of these electrodes are presented in Table 9 (Jeng et al. 2005).

Table 9. Compositions of Alloy 690, SUS 304L and coated welding electrodes (in wt.-%) (Jeng et al. 2005).

	Ni	Cr	Fe	Mn	Nb	Mo	Ti	Al	Si	Cu	P	S	C
Alloy 690	60.65	29.70	8.76	0.29	-		0.20	-	0.35	0.02	0.007	0.001	0.02
SUS 304L	8.00	18.00	Bal.	2.00	-		-	-	1.00	-	0.045	0.003	0.03
I-52	60.39	28.91	8.89	0.25	-		0.51	0.64	0.16	0.01	0.003	0.001	0.03
I-152	Bal.	28.0–31.5	7.0–12.0	≤5.0	1.0–2.5	≤0.50	≤0.50	≤0.50	≤0.25	≤0.50	≤0.30	≤0.015	-
Nb1	59.07	28.25	10.19	1.47	0.10	0.27	0.12	0.11	0.17	0.03	0.01	0.006	-
152	59.07	27.53	10.24	1.44	1.03	0.34	0.10	0.14	0.17	0.08	0.02	0.005	-
Nb2	58.06	26.80	10.60	1.46	2.49	0.25	0.12	0.12	0.19	0.06	0.01	0.007	-
Nb3	58.05	26.22	10.86	1.21	3.35	0.39	0.14	0.10	0.18	0.05	0.02	0.006	-

A total of three welding layers were used, with each layer being deposited in one single pass of the electrode. Figure 13 shows the macrostructure of Nb2 (2.49 wt.-%) weldment. In the fusion zone, the microstructure is primarily dendritic. In general, the dendrites tend to follow the direction of the maximum temperature gradient during the solidification process, and hence grow in a direction perpendicular to the solid/liquid interface. This implies that the dendrites associated with each pass will demonstrate different growth orientations, e.g., in the root (1st pass) dendritic growth initiates from the base metal at the fusion zone boundary and then proceeds toward the center of the weld, while in the cap, most of the dendrites initiate at the fusion zone boundary of the previous pass (2nd pass), and then grow vertically (Jeng et al. 2005).

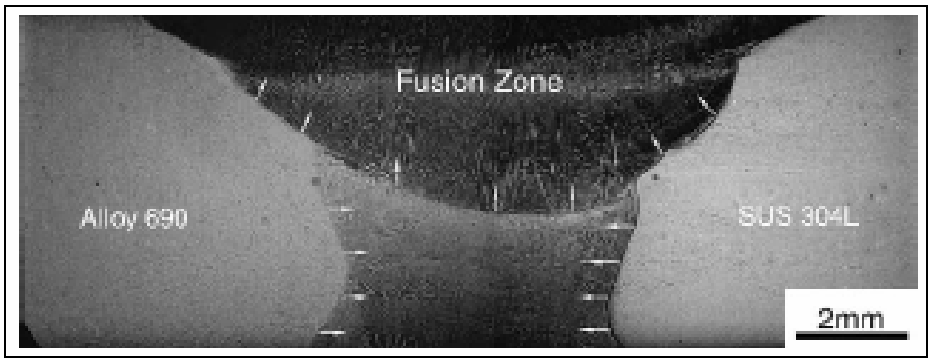

Figure 13. The macrostructure of Nb2 (2.49 wt.-%) weldment (Jeng et al. 2005).

In the low Nb weldment (0.1 wt.-%), the matrix of the fusion zone is composed primarily of a solid solution of Ni, Cr, Fe, and trace elements of Si and C, as shown in Figure 14(a). The cap region of this weldment contains spherical particles and an eutectic-like phase. Among them, the spherical particles are located principally in the interdendritic regions. EDS-analysis reveals that these particles are basically composed of Al, Ti and O, as shown in Figure 14 (b), and hence it is assumed that they are Al–Ti oxides. The eutectic-like phase exists primarily at the grain boundaries. Its composition resembles that of the matrix, but the local EDS analyses reveal a notable presence of C and O shown in Figure 14 (c) and Figure 14 (d) (Jeng et al. 2005).

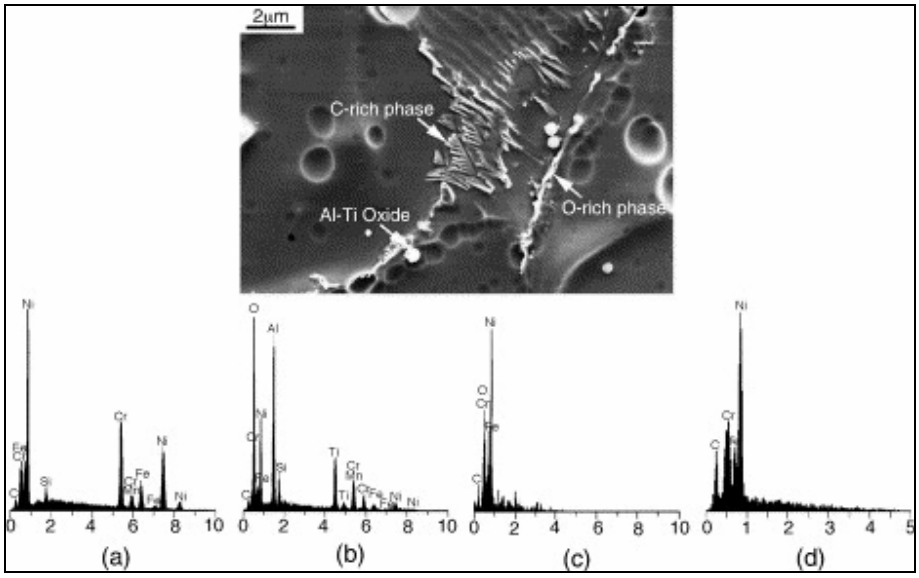

Figure 14. Analysis in the cap of Nb1: (a) matrix, (b) Al–Ti oxide, (c) O-rich phase, and (d) C-rich phase (Jeng et al. 2005).

The composition of the root region of the weldment shown in Figure 15, is affected by the dilution of the base metals. It was determined that the Fe content of the root region was higher than that of the cap, but that the Ni content was lower, as shown in Figure 15(a). In Figure 15, there existed a significant presence of Al–Ti oxide in the

interdendritic regions and at the grain boundaries of the cap. However, the high Cr and C contents of these particles suggest that they are actually Cr-carbides as shown in Figure 15(b) and Figure 15(c). Specifically, these particles may be further classified as either Cr-carbides, or as Cr-carbides rich in O (Jeng et al. 2005).

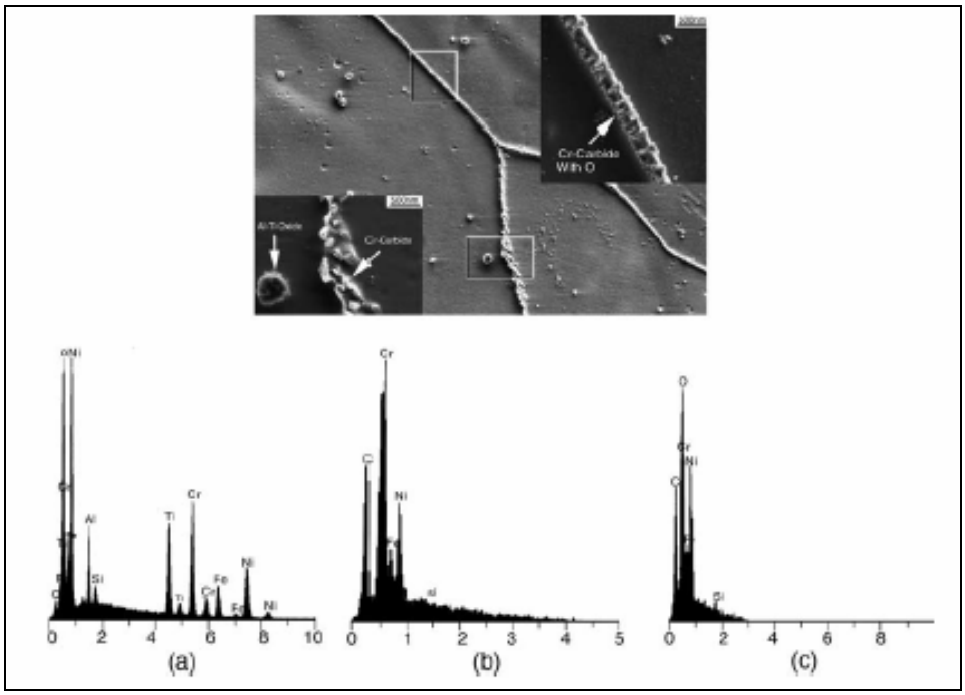

Figure 15. Analysis in the root of Nb1: (a) Al–Ti oxide, (b) Cr-carbide, and (c) Cr-carbide with O (Jeng et al. 2005).

Figure 16 shows the results of TEM observations. It clearly shows that the grain boundary contains a mixture of block and rectangular carbides. Based on selected area diffraction patterns, the rectangular carbides were identified as Cr_7C_3 (Jeng et al. 2005).

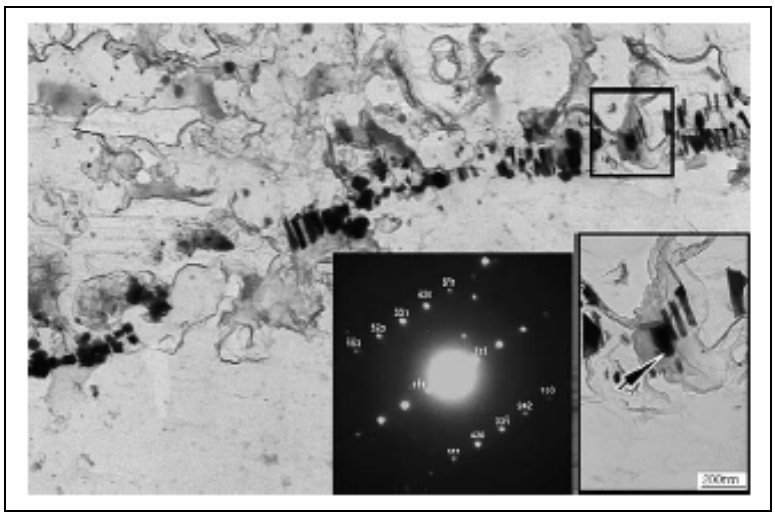

Figure 16. TEM analysis in the root of Nb1 (Jeng et al. 2005).

In the high Nb weldment (3.35 wt.-%), the matrix of the fusion zone is comprised primarily of Ni, Cr and Fe, with trace elements of Si and Nb, as shown in Figure 17. It shows the significant presence of an interdendritic phase within the cap region of the weldment, which consists principally of Nb–Si and Nb-rich phases. A random distribution of spherical Al–Ti oxides is also observed. The Nb–Si phase, with Nb content of up to 30 wt.-%, resembles an eutectic-like phase. Of the two Nb phases observed in the cap region, it is noted that the Nb-rich phase with Nb content of up to 78 wt.-% is significantly less evident than the Nb–Si phase (Jeng et al. 2005).

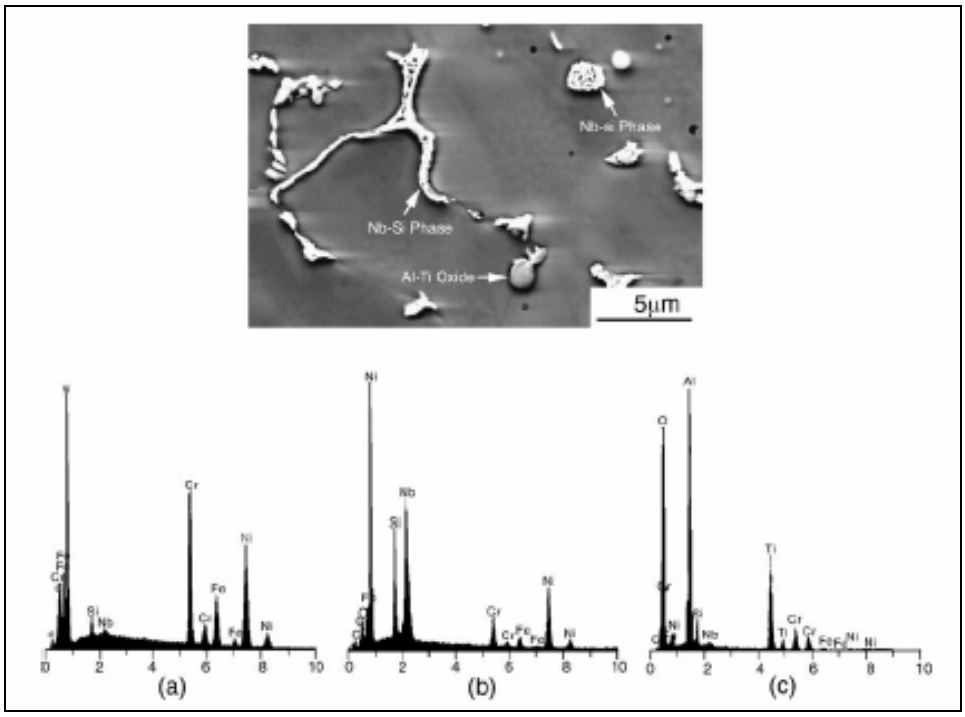

Figure 17. Analysis in the cap of Nb3: (a) matrix, (b) Nb–Si phase, and (c) Al-Ti oxide (Jeng et al. 2005).

The presence of interdendritic phase in the root region is less pronounced than within the cap, see Figure 18. Analysis reveals the presence of, not only Al–Ti oxides, but also Nb-Si phase and Nb-rich phase. It was observed that the root region contains greater presence of Nb-rich phase than Nb–Si phase (Jeng et al. 2005).

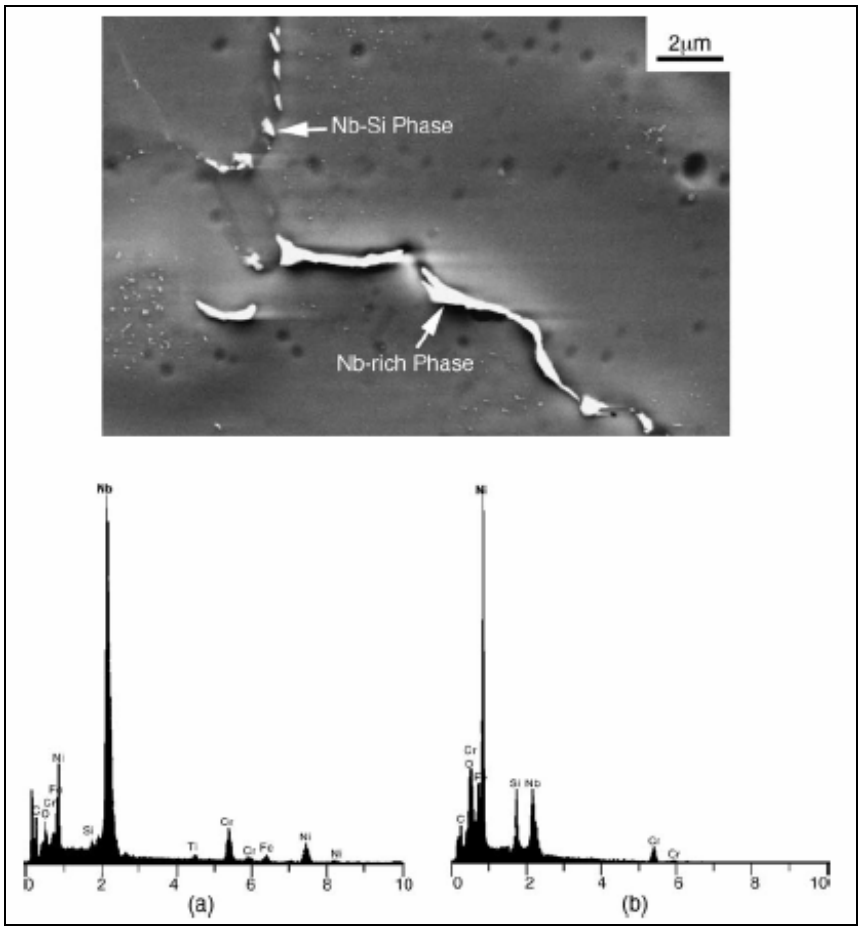

Figure 18. Analysis in the root of Nb3: (a) Nb-rich phase, and (b) Nb–Si phase (Jeng et al. 2005).

Peng et al. (2003) investigated the microchemistry of the dendrite boundaries of Alloy 182 by using Auger Electron Spectroscopy (AES) analysis. The weldment had been prepared by SMAW and a post-weld heat treatment was made at 620°C for 24.5 h. Interdendritic (ID) fracture surfaces of hydrogen-charged specimens of Alloy 182 showed that the distribution of chromium was heterogeneous and both depletion and enrichment of chromium was observed in the precipitate-free zones. The majority of the precipitates at the dendrite boundaries are small (≤ 1 μm) chromium carbides. Precipitation of niobium carbides, sulphides, etc., was found as well. The analyses also showed extensive segregation of phosphorous at the dendrite boundaries (Peng et al. 2003).

The quantitative AES analyses on the ID facets and TD surfaces showed that chromium depletion was about 4 to 10 at.-% at the dendrite boundaries. The segregation of phosphorous at the dendrite boundaries was around 3 to 5 at.-%. The thickness of the layer showing phosphorous enrichment and chromium depletion was about 10 nm. The study implied that the depletion of chromium at dendrite boundaries of Alloy 182 may be one cause of the high susceptibility to IDSCC in high-temperature water conditions (Peng et al. 2003).

The weld microstructures related to in-service SCC of nickel-base alloy weld metals in LWRs are presented in Chapter 5.

3.3 Hot cracking

The restrained contraction of a weld during cooling sets up tensile stresses in the joint, and may even cause the most serious of weld defects – cracks. Cracking may occur in the weld metal, in the heat-affected zone, or in both of these regions. Hot cracking is either of the gross type, which is visible to the naked eye and termed macrocracking, or is only visible under a microscope, in which case it is termed microcracking or microfissuring (Lancaster 1999). Hot cracks are categorized based on their location called solidification cracking when found in the solidified weld, liquation cracking when found in the base material's heat affected zone (HAZ), and ductility dip cracking when found in the weld or HAZ. Regardless of classification, all hot cracking

- appears during weld solidification
- follows grain boundaries or subgrain boundaries in the weld metal
- occurs when a thin layer of liquid exists at the boundaries of solid grains
- is not usually generated with a sharp point (most begin with more rounded shape)
- develops a surface that may be coloured by oxidation (although unexposed and non-oxidized cracks exhibit a metal colour) (Wu & Tsai 1999).

3.3.1 Solidification cracking

There are two necessary preconditions for the occurrence of cracking during the weld thermal cycle: the metal must lack ductility, and the tensile stress developed as a result of contraction must exceed the corresponding fracture stress. Solidification cracking may take place in two ways. The first, which may affect both castings and fusion welds, relates to the alloy constitution. On cooling in a liquid alloy below its liquidus temperature, solid crystals are nucleated and grow until they join together and form a coherent, although not completely solidified, mass. At this temperature the alloy first acquires some mechanical strength. At first it is brittle, but on further cooling to the nil-ductility temperature (NDT), ductility appears and rises sharply as the temperature is further reduced, as shown in Figure 19 (Lancaster 1999).

The interval between the coherence and nil-ductility temperature is known as brittle temperature range (BTR), and in general it is found that alloys possessing a wide brittle temperature range are sensitive to weld cracking, whereas those having a narrow brittle temperature range are not.

The second mode of solidification cracking, which occurs in the region of the solidus, is believed to be due to the presence of continuous intergranular liquid films. The liquid may be an eutectic, as in certain crack-sensitive aluminium alloys, or it may be formed by an impurity such as sulphur in steel. In the cases where cracking is promoted by impurities, a film only forms if the liquid is capable of wetting the grain boundaries; i.e. if its surface energy relative to that of the grain boundaries is low. Sulphur and phosphorus tend to widen the freezing range of steels tremendously. Since they have a rather strong tendency to segregate at grain boundaries and to form low-melting-point compounds, they can cause severe solidification cracking, even at relatively low concentrations. S and P can also cause solidification cracking in nickel-base alloys and ferritic stainless steels (Lancaster 1999, Kou 2003). The distinguishing feature of such a liquation crack is the presence of remains of the liquid films on the fracture surface. Morphologies may be dendritic, but this is not always the case. Ductility dip cracks do not display liquid films (Robinson & Scott 1980). The higher the degree of restraint, the more likely it is that any given alloy will crack. The degree of restraint is a function of the type of the joint, the rigidity of the structure, the amount of gap between the abutting edges, the plate thickness, and the relative thickness of plate and weld metal. Maximum restraint is obtained when two rigidly clamped thick plates are joined by a weld of small cross-section. Minimum restraint occurs in a weld of relatively large cross-section between two close-butting thin sheets (Figure 20) (Lancaster 1999, Kou 2003).

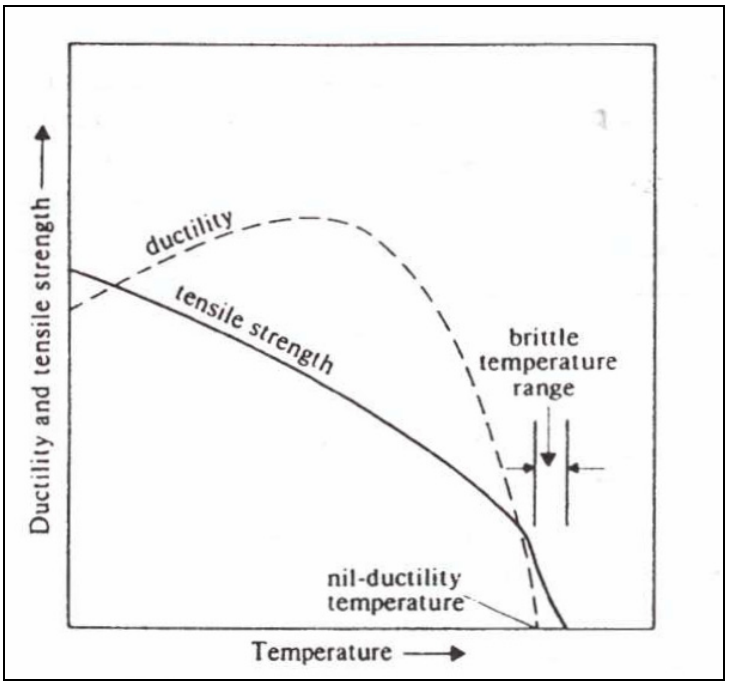

Figure 19. Mechanical properties of metals as function of temperature (Lancaster 1999).

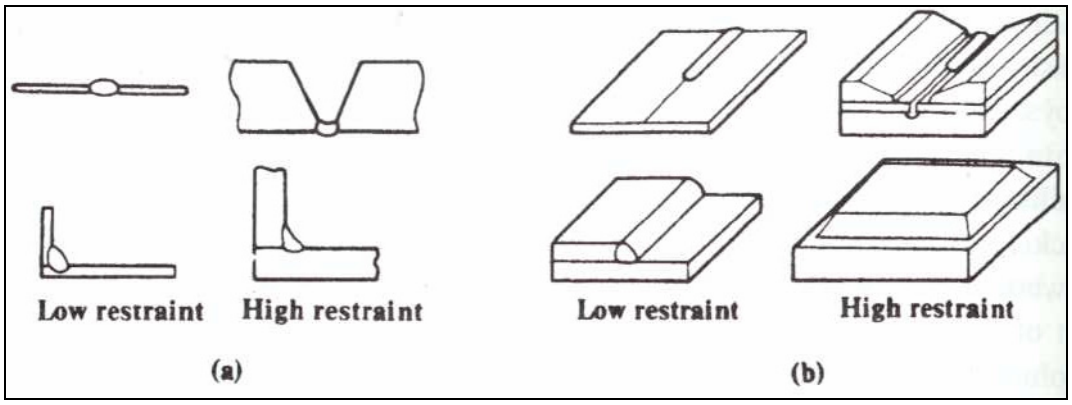

Figure 20. (a) Restraint dependent on dimensions of weld and plate. (b) Restraint dependent on rigidity of joint or set-up (Lancaster 1999).

Tests for assessing the susceptibility to solidification cracking usually require that the weld is made under conditions where sufficient restraint is present to ensure cracking. The susceptibility of the weld metal is then assessed by measuring the crack length, the crack area, or the number of cracks. This measurement may be made on the as-welded surface, on longitudinal sections, on transverse sections or by radiography. There are several test methods to investigate solidification cracking. The most common tests are Varestraint (also Trans-Varestraint) test, Houldcroft test, MISO (measurement by means of *in situ* observation), hot tensile test and flat tensile test (Lancaster 1999, CEN ISO/TR 17641-3:2005).

3.3.2 Ductility dip cracking

Ductility dip cracking (DDC) is a solid-state phenomenon leading to a situation where a number of alloys may be embrittled within a specific temperature range. Such materials include austenitic stainless steels, Ni-base alloys, Cu-base alloys, and titanium alloys. These normally ductile materials can exhibit a loss of ductility over a temperature range below the solidus temperature. DDC is often associated with the welding of heavy sections commonly encountered in critical high-pressure steam, nuclear, and power generation applications. Although a study by Honeycombe et al. (1970) demonstrated that microcracking in fully austenitic weld metal is unlikely to have a detrimental effect on mechanical or fatigue properties, DDC can have serious consequences in critical applications where defect tolerance is low and repair is both difficult and costly (Collins et al. 2002, Nissley et al. 2002, Collins & Lippold 2003).

Ductility dip cracking susceptibility is quantified by the ductility dip temperature range (DTR) and the threshold strain (E_{min}) for cracking. The schematic picture in Figure 21 shows the expected ductility as well as the ductility dip.

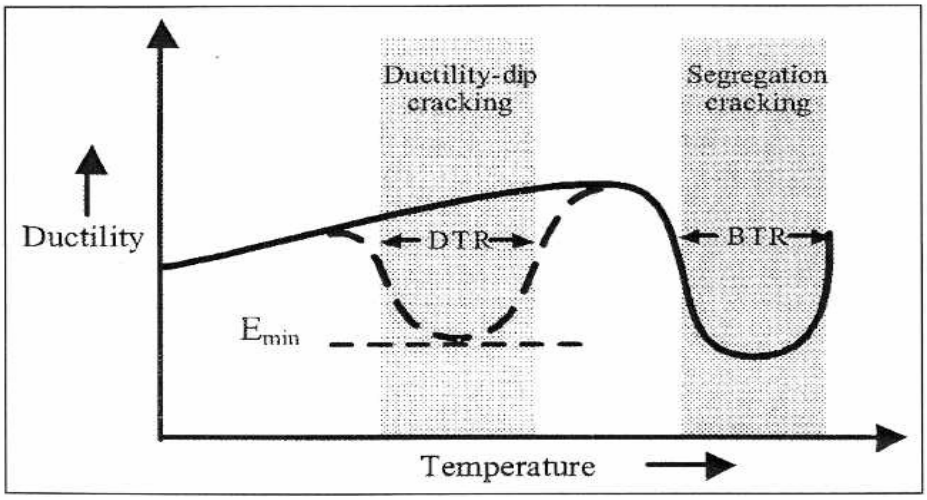

Figure 21. Schematic presentation of elevated temperature cracking susceptibility (Nissley et al. 2002).

The DTR is defined as the temperature range over which ductility dip cracks can occur, and E_{min} is the threshold strain required for cracking to occur. It is not clear exactly when the ductility dip cracks occur, but it appears that they can occur during both heating and cooling stages of the weld thermal cycle. A number of factors have been reported to contribute to the development of DDC, including: specific alloy, impurity and interstitial element content; solute, impurity and interstitial element segregation; grain growth; grain boundary sliding; grain boundary precipitation; grain boundary orientation relative to the applied strain; and multipass welding operations. The DDC mechanism is not well understood, and neither are the relative effects of each factor reported to contribute to the overall mechanism. Furthermore, preventive methods to avoid DDC have proven elusive (Collins et al. 2002, Nissley et al. 2002, Collins & Lippold 2003).

Tests for DDC have had difficulties with repeatability due to the number of variables that affect cracking. Several different testing techniques have been used to test for DDC, including laboratory test welds, the transverse-Varestraint test, the hot ductility and hot tensile tests, the MISO technique, the double and triple-bead Varestraint test and spot-on-spot (double spot) Varestraint test. While each of these tests has advantages and dis-advantages, none have emerged as an ideal test for DDC (Nissley et al. 2002).

3.3.3 Cracking susceptibility of nickel-base alloys Inconel 600 and 690 and weld metals Inconel 82, Inconel 182, Inconel 52 and Inconel 152

In the study by Aoh and Yang (2003) the weldability and cracking susceptibility of Inconel 600 were studied using Varestraint and hot ductility tests with a two-pass TIG welding experiment (filler materials were Inconel 62 and 82). Results of the study showed that a higher welding current resulted in grain coarsening in the heat affected

zone (HAZ). Higher heat input resulted in migration of precipitated particles to grain boundaries. In Figure 22 the effect of heat input on total crack length (TCL) is presented (Aoh & Yang 2003).

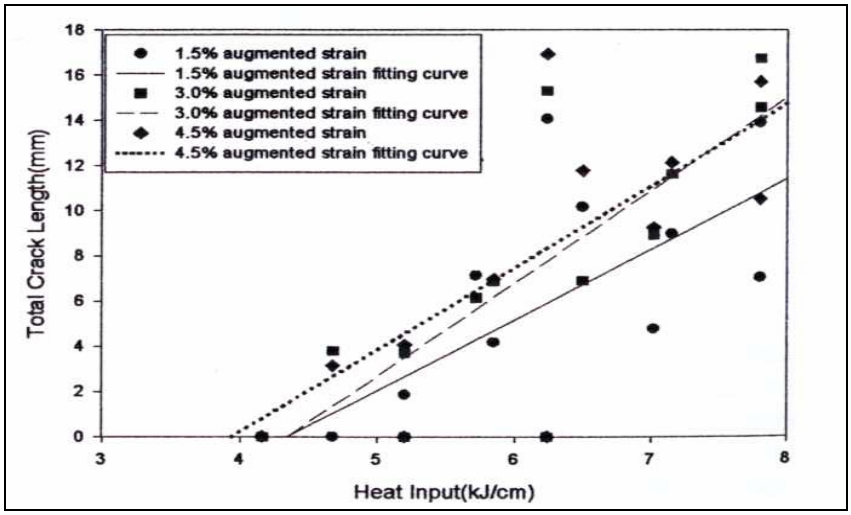

Figure 22. The effect of heat input on total crack length (TCL) accumulated from the weld pool periphery (Aoh & Yang 2003).

The results of the hot ductility tests revealed that a higher heat input (12 kJ/cm) resulted in a delayed ductility recovery of the HAZ upon cooling, which implied a wider crack susceptible region and brittle temperature range. Welding current exhibited a pronounced effect on the total crack length in the Varestraint test. Greater cracking susceptibility was observed at higher welding current, even if the heat input remained at the same level, as shown in Figure 23 (Aoh & Yang 2003). Figure 24 presents a transverse section of a crack found in the Varestraint specimen (Aoh & Yang 2003).

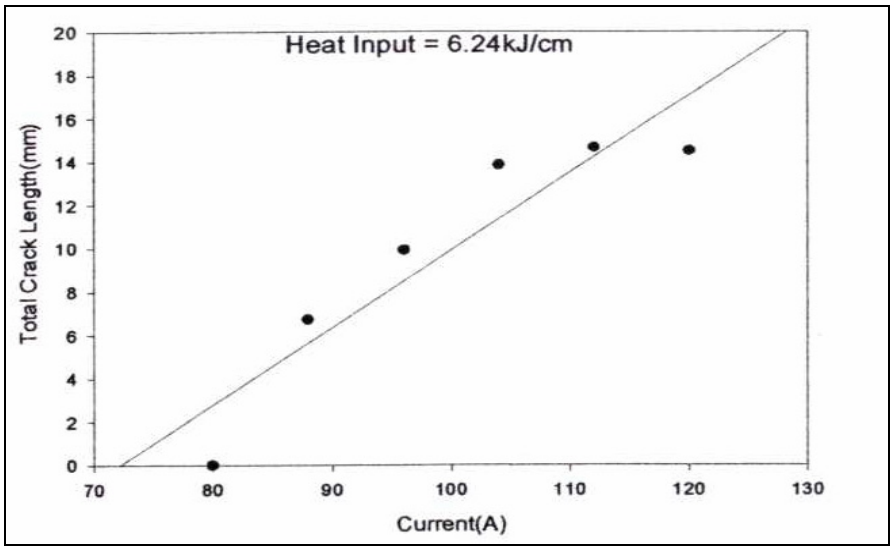

Figure 23. Relationship between current and total crack length under same heat input 6.24 kJ/cm (Aoh & Yang 2003).

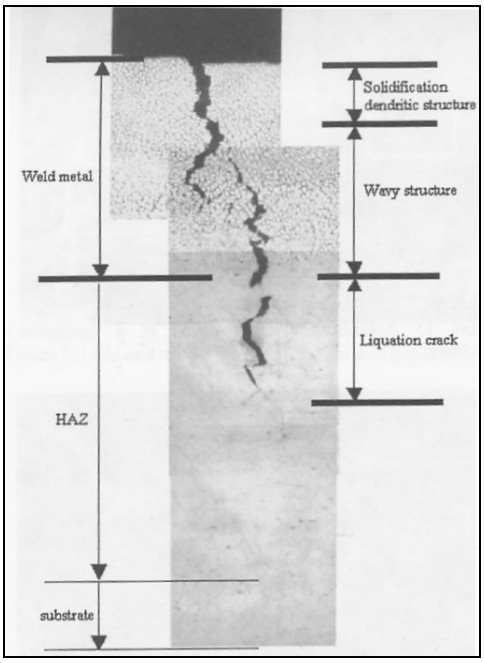

Figure 24. Transverse section of a crack found in Varestraint specimen propagating into HAZ (Aoh & Yang 2003).

Several studies have been made to investigate the hot cracking susceptibility of filler materials Inconel 82, Inconel 182, Inconel 52 and Inconel 152 and base material Inconel 690 (Hood & Lin 1995, Wu & Tsai 1999, Collins & Lippold 2003).

Hood and Lin (1995) studied the hot cracking susceptibility of Inconel filler materials (82, 182, 52 and 152) using the Varestraint test and the spot-Varestraint test. An investigation of the repair weldability of filler material 52 was also made using the Gleeble thermo-mechanical simulation technique. The results of the Varestraint tests of four filler materials with nickel-base Alloy 690 are presented in Figure 25 (Hood & Lin 1995).

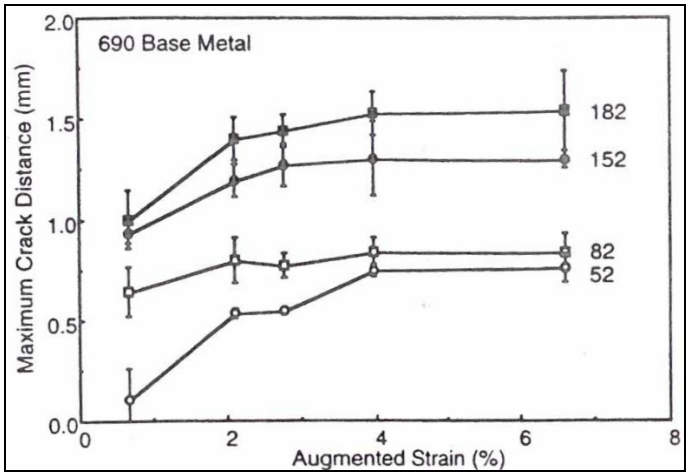

Figure 25. Results of the Varestraint test of four filler materials with nickel-base Alloy 690 (Hood & Lin 1995).

The results showed that the cracking resistance of these four filler materials deposited on Alloy 690 and carbon steel A285 is similar or better than that of 1¼Cr-½Mo and Alloy 690-AISI 316L combinations. Filler material 52 exhibited the best resistance to both weld solidification cracking and weld metal liquation cracking, followed by Alloys 82, 152 and 182. The AISI 316LN/52 combination exhibited better resistance than the Alloy 690/52 one. The repair weldability study of Alloy 52 weld metal made by Gleeble™ suggested that the resistance to weld metal liquation cracking was not reduced after ten weld repair simulations made to peak temperatures of 900°C and 1300°C (Hood & Lin 1995).

Wu and Tsai (1999) investigated the hot cracking susceptibility of filler materials 82 and 52 with Alloy 690 by Varestraint tests. Differential thermal analysis (DTA) was made to determine the bulk solidification temperature range (ΔT) between each material's liquidus (T_L) and solidus (T_S) temperatures. ΔT values were as follows: Alloy 690 ΔT = 12°C, Alloy 52 ΔT = 13°C and Alloy 82 ΔT = 44°C. These data give an indication of supersolidus cracking, which is usually divided into solidification and liquation cracking. Since the molten metal suffers contraction stress during solidification, a large ΔT implies a large region of coexisting liquid and solid states. Accordingly, residual stress is significant and crack susceptibility is proportionally increased. It may be expected that hot cracking susceptibility for the tested materials follows the order: Alloy 82 > Alloy 52 > Alloy 690 (Wu & Tsai 1999).

In Varestraint tests five samples of filler materials 82 and 52 were tested at each of three strain levels 3%, 4% and 5%. Figure 26 presents total crack length (TCL) plotted against augmented strain for both filler materials (Wu & Tsai 1999).

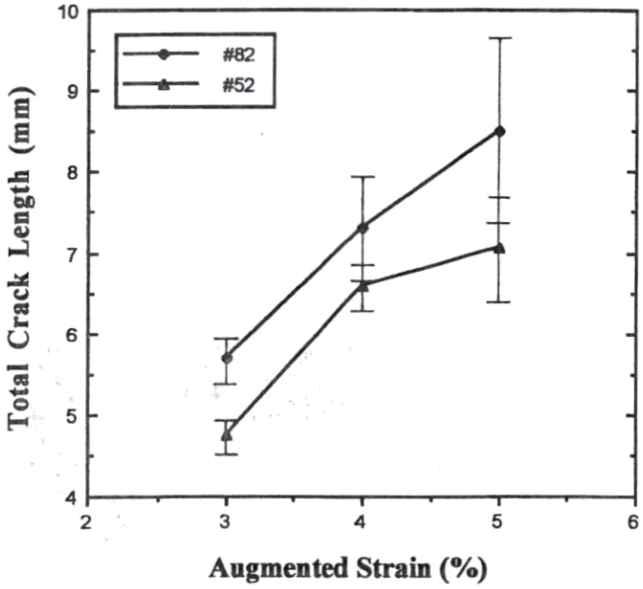

Figure 26. Results of Varestraint tests of filler materials 82 and 52 (Wu & Tsai 1999).

Alloy 82 has a greater TCL than Alloy 52 while the TCL values for both alloys increase with strain. Solidification cracks and ductility dip cracks were found in the fusion zone. The solidification crack is closer to the fusion line than the ductility dip crack. Liquation cracks and ductility dip cracks were found in the HAZ. However, to accurately distinguish all the crack types is difficult. Therefore, grouping the cracks by the location in the fusion line zone or HAZ is easier and more accurate. In Figure 27 the TCL is plotted vs. strain for weld metal (WM) and HAZ (Wu & Tsai 1999).

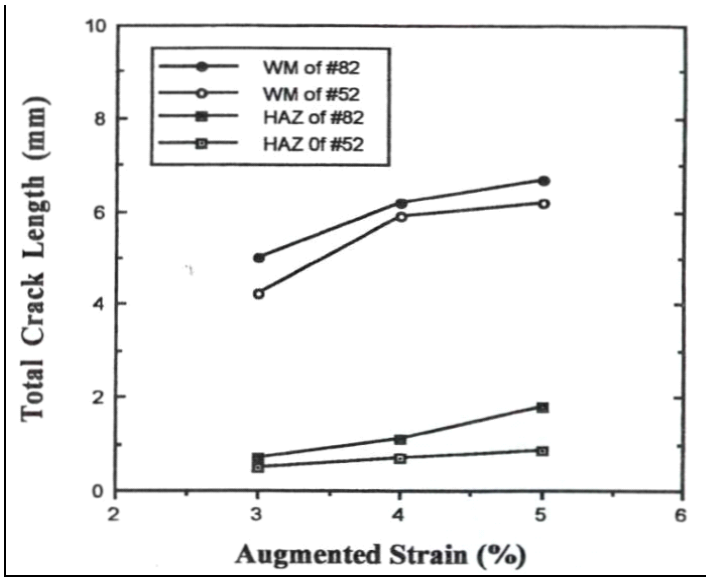

Figure 27. Results of Varestraint tests where TCL is plotted vs. strain for weld metal (WM) and HAZ (Wu & Tsai 1999).

The weld metal contains more TCL than the HAZ for both filler materials. Alloy 82 contains the greatest TCL in both regions. In summary, the preceding results show that hot cracking susceptibility in Alloy 82 is consistently greater than that of Alloy 52 during Varestraint testing. Compared to DTA data, the ΔT of Alloy 82 is higher than that of Alloy 52. This means that Alloy 82 will consist of more low strength material during cooling. This will result in hot cracking during welding. Moreover, hot cracking is found to be more prevalent in Alloy 82. Most cracks follow grain or subgrain boundaries and fracture is intergranular. In EDS-analyses several elements were present in the crack tips: Si, Al, Ca, and Ti for Alloy 52, and Si, Nb, and Ca for Alloy 82 (Wu & Tsai 1999).

Kikel and Parker (1998) investigated the susceptibility of five materials to DDC. Materials tested were filler metal 52 (FM 52), filler metal 82 (FM 82), filler metal 625 (FM 625), Alloy 600, and Alloy 690. Test specimens were 16 mm thick. Figure 28 shows a schematic of the transverse-Varestraint and spot-on-spot Varestraint testing configuration. The spot-on-spot Varestraint testing technique is an effective test method to produce HAZ DDC and to rank the materials tested relative to HAZ DDC susceptibility. The transverse-Varestraint test produces fusion zone DDC (Kikel & Parker 1998).

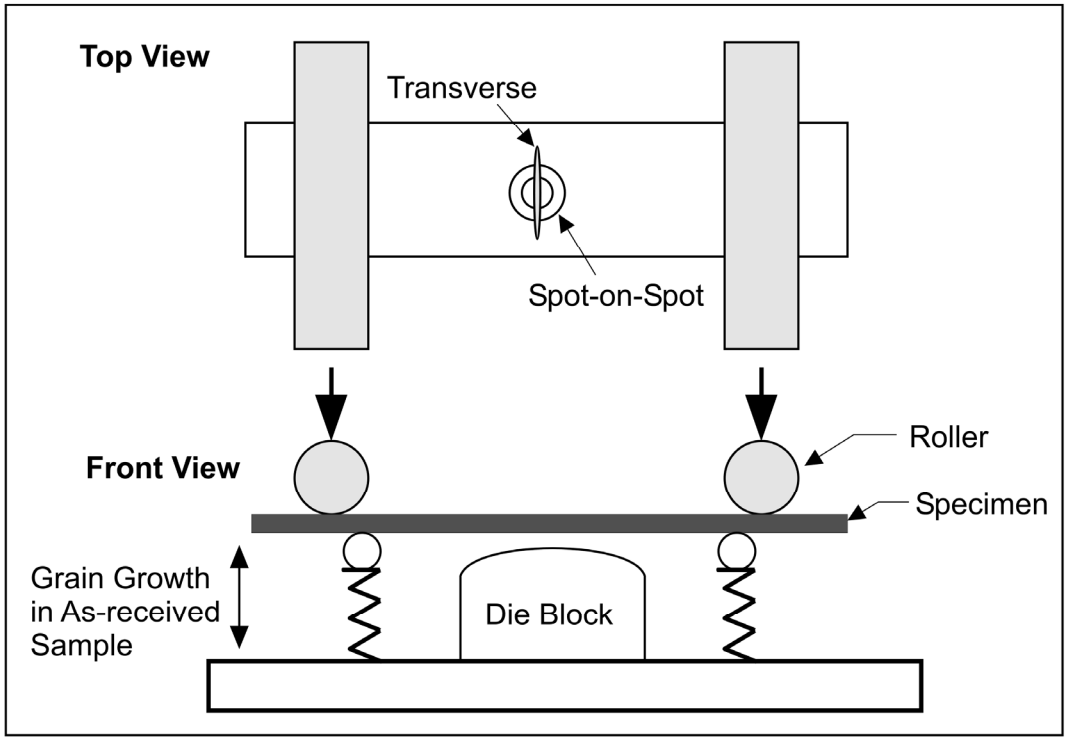

Figure 28. Schematic of the transverse-Varestraint and spot-on-spot Varestraint testing configuration (Kikel & Parker 1998).

The transverse-Varestraint tests were conducted at augmented strain levels of 4, 5 and 7%. The spot-on-spot Varestraint tests were conducted at augmented strain levels of 5, 7 and 10%, respectively. While DDC occurred in all the weld and base metals tested, there was no fusion zone DDC produced in Alloy 600. The transverse-Varestraint test successfully produced fusion zone DDC, but provided limited separation of the test materials due to variable grain boundary orientation with respect to applied strain. Of the materials tested, wrought Alloy 600 was the least susceptible to both fusion zone and HAZ DDC. This is attributed to its fine grain size in the wrought condition. Alloy 690 and FM 52 exhibit high DDC susceptibility as compared to other materials tested in this study. Large straight grain boundaries are particularly susceptible to DDC. Improved DDC resistance occurs with materials with grain boundary precipitates or second phases, which limit grain boundary migration and grain growth. Rotating a weld deposit 90° relative to the applied strain reduced the apparent grain size of a weld deposit and significantly improved DDC resistance of FM 82 (Kikel & Parker 1998).

Cola and Teter (1998) studied the effect of chemical composition on the DDC behaviour of a Ni-base filler metal 52 (FM 52). After FM 52 was deposited onto a steel substrate and then machined into plates, the transverse-Varestraint tests, spot-on-spot Varestraint tests and Gleeble hot-ductility tests were conducted. Figure 29 presents an on-cooling hot-ductility curve for FM 52. Note the ductility dip between 800°C and 1000°C (Cola & Teter 1998).

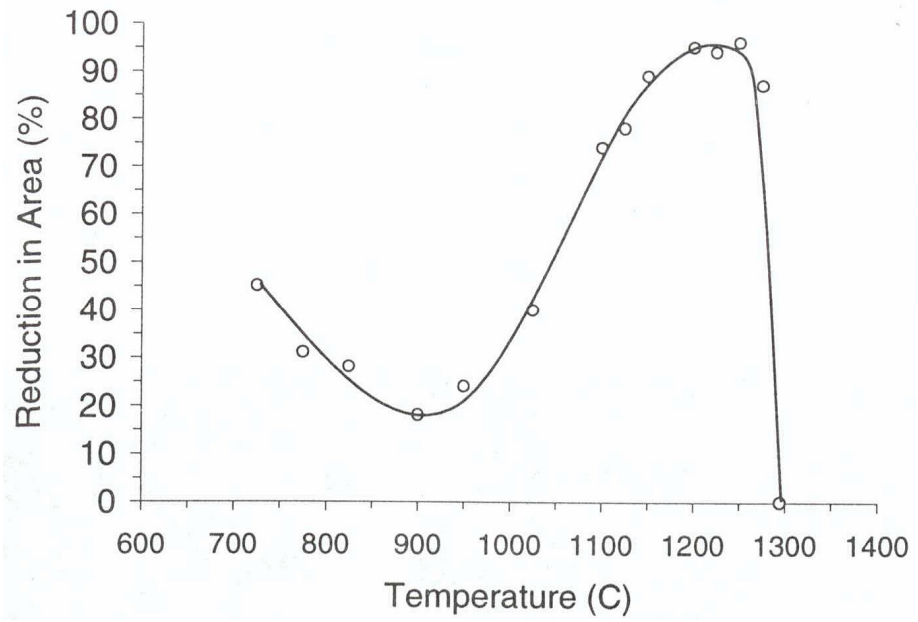

Figure 29. On-cooling hot-ductility curve for FM 52 (Cola & Teter 1998).

Figure 30 presents a SEM image of the fusion zone microstructure from a transverse-Varestraint test specimen. The weld metal build-up, the fusion zone and the weld metal HAZ microstructures were comprised of an austenitic, cellular solidification structure, migrated grain boundaries and intercellular particles (arrows) (Cola & Teter 1998).

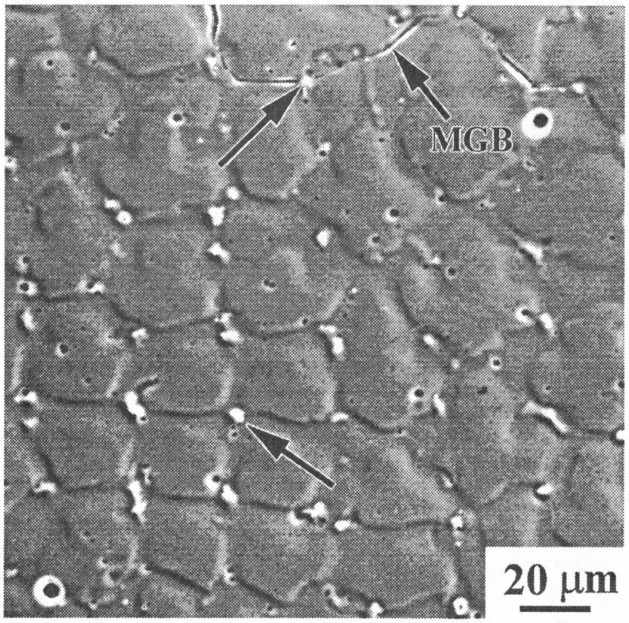

Figure 30. SEM image of the fusion zone microstructure from a transverse-Varestraint test specimen (Cola & Teter 1998).

In Figure 31 a TEM image of a high-angle grain boundary (HAGB) decorated with $M_{23}C_6$-type particles is presented (Cola & Teter 1998).

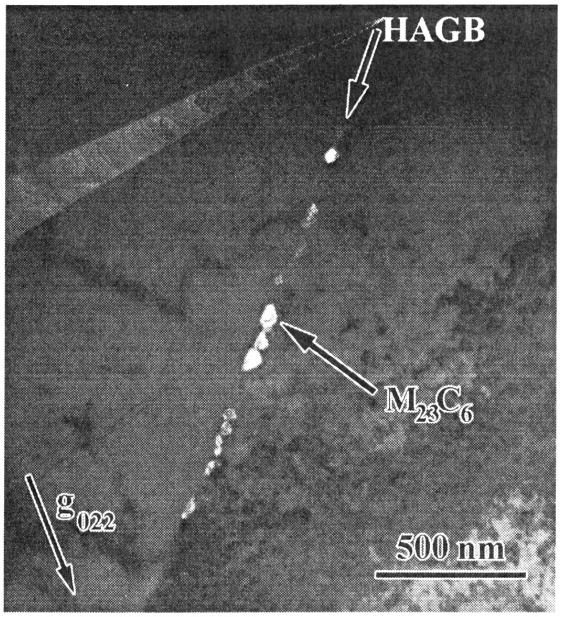

Figure 31. TEM image of a high-angle grain boundary (HAGB) decorated with $M_{23}C_6$-type particles ranging from 10 to 200 nm (Cola & Teter 1998).

Auger electron spectroscopy of a pre-strained Gleeble specimen fractured in situ revealed internal ductility-dip cracks decorated with magnesium aluminate ($MgAl_2O_4$) spinel particles (1000 nm). These particles may act as stress concentrators, which provide nucleation sites for microvoids. The microvoids will coalesce into microcracks before linking and forming ductility-dip cracks. In this study no evidence was found supporting the role of elemental segregation in the formation of ductility-dip cracks (Cola & Teter 1998).

Davé et al. (2004) investigated grain boundary character in Alloy 690 and ductility-dip cracking susceptibility. In this study, as-received wrought Alloy 690 was compared to Alloy 690 that was strain annealed to achieve a different configuration of special grain boundaries. Hot-ductility tests were performed using a Gleeble™ thermo-mechanical simulator. The as-received wrought Alloy 690 mill product was subjected to the following strain-annealing sequence:

- reduction in thickness 25% every cycle (four passes unidirectional rolling)
- anneal at 1000°C for 1 h every cycle
- four cycles for total reduction of about 67%.

The on-heating and on-cooling hot ductility data for the as-received Alloy 690 are shown in Figure 32 and for strain annealed Alloy 690 in Figure 33, respectively (Davé et al. 2004).

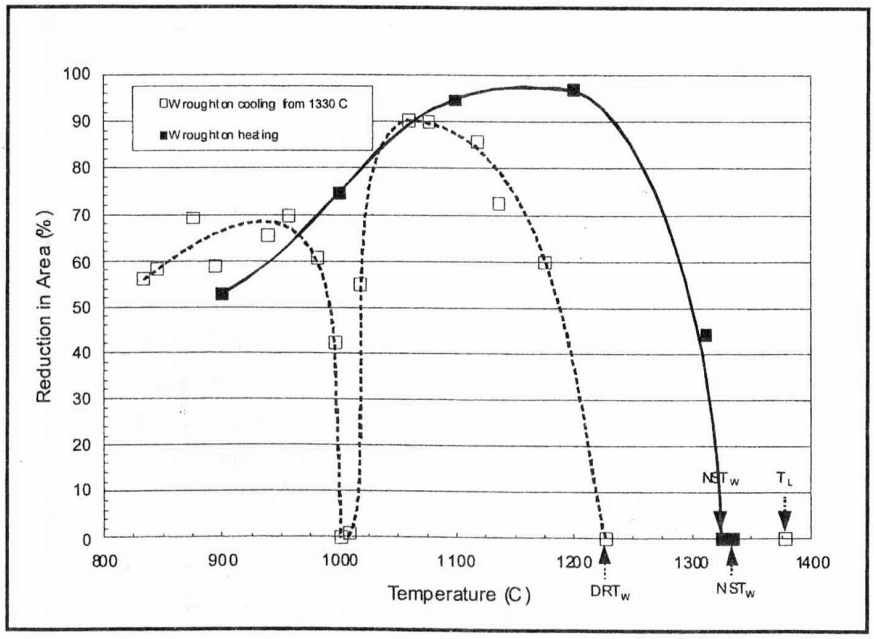

Figure 32. Hot-ductility curves for as-received Alloy 690 (Davé et al. 2004).

The on-cooling curve has a pronounced ductility-dip at approximately 1000°C (950 to 1050°C) at which the reduction in area falls to almost zero. The ductility-dip for the as-received material is very severe, with a minimum value of less than 2% reduction of area. The implications of this dip for weldability are that a joint under extreme constraint can exhibit cracking on cooling through the susceptible temperature range following welding (Davé et al. 2004).

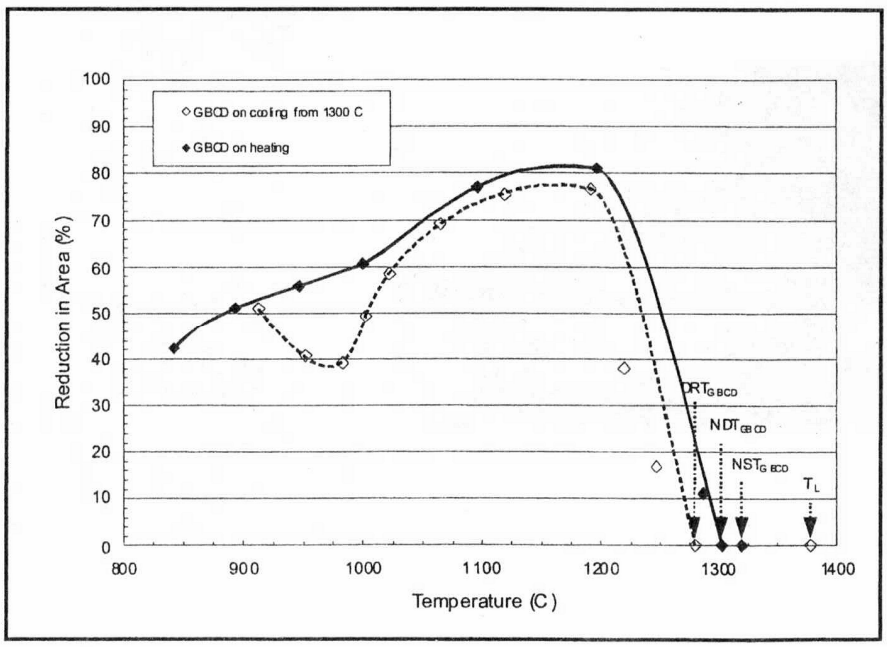

Figure 33. Hot-ductility curves for strain-annealed Alloy 690 (Davé et al. 2004).

It is possible to alter the grain boundary character distribution in Alloy 690 through strain annealing. The processed material has a slightly elevated fraction of special grain boundaries, but more significantly, there are regions in which the random grain boundary network was effectively disrupted. Furthermore, combination of a higher minimum ductility located at a lower temperature together with a higher ductility recovery temperature DRT will result in increased material resistance to ductility-dip cracking. All these factors are expected to improve the resistance of the Alloy 690 HAZ to ductility-dip cracking on cooling from welding, and thereby improve weldability in a given mechanical restraint condition (Davé et al. 2004).

Nishimoto et al. (2004) investigated the microcracking behaviour in TIG-welded multi-pass Inconel 690 weld metal by the spot- and transverse-Varestraint tests using three different filler metals corresponding to Inconel 52 by varying the contents of impurity elements such as P and S. Figure 34 presents a schematic illustration of the Varestraint test procedure used (Nishimoto et al. 2004).

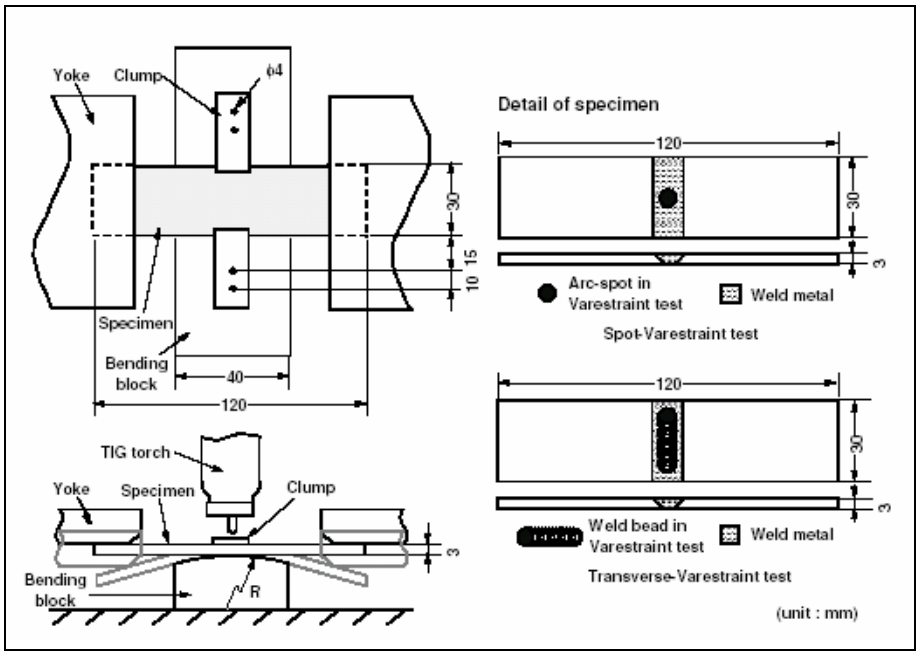

Figure 34. Schematic illustration of used Varestraint test procedure (Nishimoto et al. 2004).

Based on the fact that impurity elements such as P and S in a filler metal influence the microcracking in reheated weld metal, the reduction of impurity element contents in weld metal is one of the most efficient methods for preventing the microcracks in multi-pass welding. However, it is not easy to reduce the content of P and S in a filler metal to extremely low values for practical applications. In the present study, the effect of La addition, which has high affinity to P and S, to filler metal on microcracking susceptibility was investigated. Table 10 presents the chemical compositions of the base material and filler metals used (Nishimoto et al. 2004).

Table 10. Chemical compositions of the base material and filler metals studied (Nishimoto et al. 2004).

	C	Si	Mn	Ni	Cr	Co	Mo	Ti	Al	Fe	P*	S*	B*	La
Base material	0,02	0,12	0,26	Bal.	29,55	0,03	0,02	0,11	0,09	9,61	90*	20'	<10*	-
Filler metal FF1	0,02	0,28	0,25	Bal.	29,15	0,024	0,039	0,17	0,092	11,05	50*	16*	<1*	-
Filler metal FF3	0,008	0,078	0,076	Bal.	29,55	0,0004	0,0046	0,36	0,21	10,59	9*	37*	12*	-
Filler metal FF5	0,015	0,086	0,076	Bal.	29,68	0,015	0,0039	0,39	0,21	10,97	20*	1*	24'	-
Filler metal NF1	0,01	0,22	0,25	Bal.	29,9	0,02	0,02	0,1	0,1	10,3	60*	10*	<10*	0,01

* : ppm

The results of the study showed that the microcracking susceptibility decreased with decreasing impurity element content. The morphology of the crack surfaces indicated the characteristic structure of a ductility-dip crack. The ductility-dip cracks occurred in the temperature range of 1450–1550 K. The hot ductility of the reheated weld metal dropped at temperatures above 1400 K, and that of the alloy containing the low amount of impurity elements was much higher than that having the high impurity element content. The ductility-dip cracking in reheated weld metal was mainly caused by the embrittlement of grain boundaries due to the imbalance between intergranular strength and intragranular strength at high temperatures.

In Figure 35 macro- and schematic pictures of the cracks in spot-Varestraint testing are presented. Filler materials contain different amounts of S and P (Nishimoto et al. 2004).

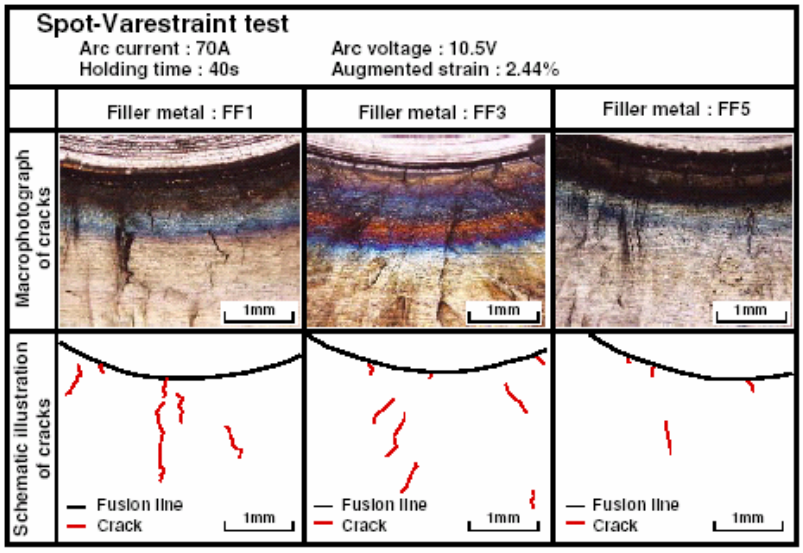

Figure 35. Macro- and schematic pictures of the cracks in spot-Varestraint testing (Nishimoto et al. 2004).

The microcracking susceptibilities of ductility-dip, liquation and solidification cracking were much improved by adding 0.01–0.02 mass-% La to the weld metal. However, excessive La addition to the weld metal led to liquation and solidification cracking in the weld metal. The ductility-dip cracking susceptibility was improved by the

amelioration of hot ductility of reheated weld metal. The excessive La addition resulted in the formation of Ni-La intermetallic compound, and therefore, liquation and solidification cracks can occur in the weld metal attributed to the enlargement of brittle temperature range (BTR) and/or the occurrence of local liquation during the reheating process. In Figure 36 are presented macro- and schematic pictures of the cracks in spot-Varestraint testing using La-added weld metal (Nishimoto et al. 2004).

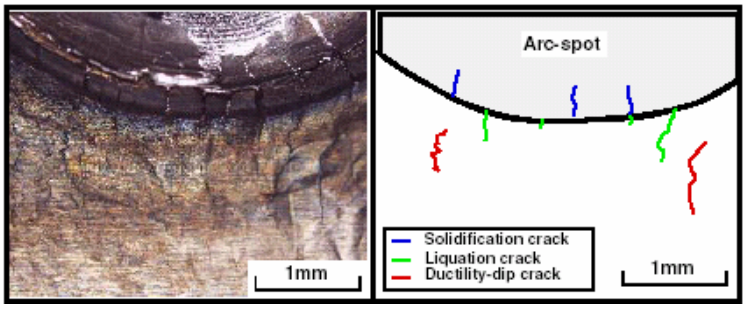

Figure 36. Macro- and schematic pictures of the cracks in spot-Varestraint testing using La-added weld metal (Nishimoto et al. 2004).

The microcracking susceptibility in multipass weld metal was investigated using La-added filler metal. Figure 37 presents macro- and microstructures of cross-section of multipass weld metal using commercial filler metal FF1 without La-addition (Nishimoto et al. 2004).

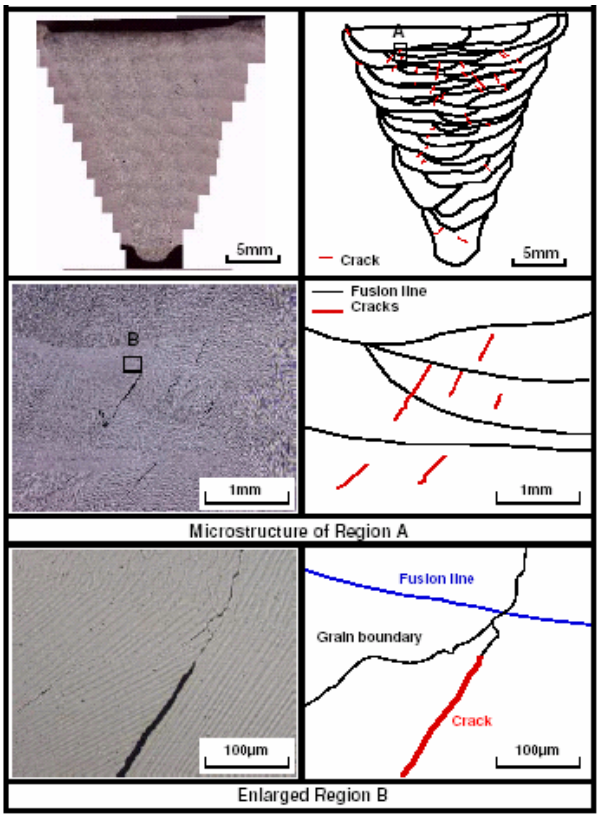

Figure 37. Macro- and microstructures of cross-section of multipass weld metal using commercial filler metal FF1 without La addition (Nishimoto et al. 2004).

Figure 38 shows the macrostructure of across-section of multipass weld made using the newly developed filler metal NF1 (see Figure 38) with La-addition (Nishimoto et al. 2004).

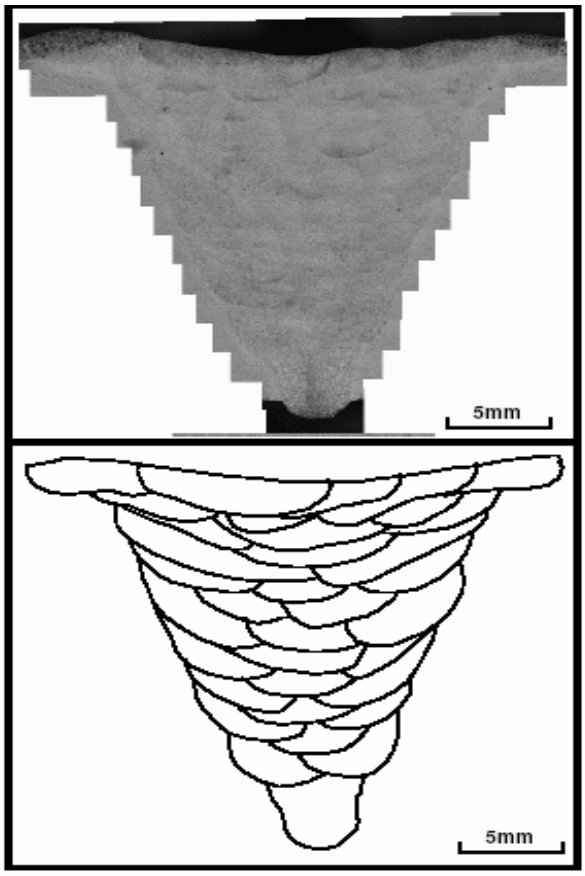

Figure 38. Macrostructure of cross-section of multipass weld metal using newly developed filler metal NF1 with La addition (Nishimoto et al. 2004).

Microcracks in multipass Inconel 690 weld metal were completely prevented by using La-added filler metal (Figure 38). It could be concluded that the microcracking susceptibility in multipass welding of Inconel 690 was improved drastically by La addition to the filler metal (Nishimoto et al. 2004).

In recent years a Gleeble-based test technique, termed strain-to-fracture (STF) has been developed by Nissley and Lippold (2002), and was employed to evaluate strain-to-fracture in ductility-dip cracking (STF DDC) susceptibility curves for filler materials 82 and 52. Figure 39 presents the STF test sample (Lippold et al. 2004).

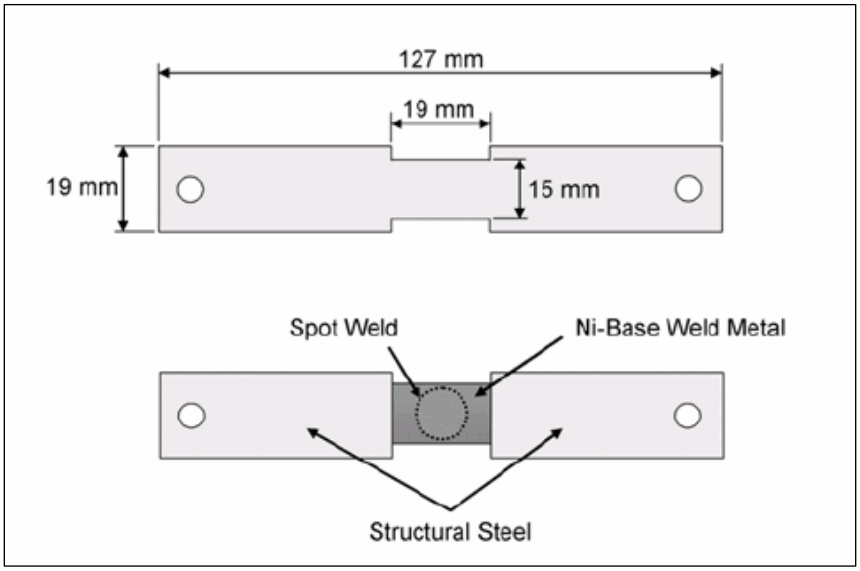

Figure 39. Strain-to-fracture (STF) test sample (Lippold et al. 2004).

In the study, three filler material heats of Alloy 82 (82-A, 82-B and 82-C) and one heat of Alloy 52 were investigated by the STF test. In Figure 40, the DDC behaviour of the filler material 82 heats is presented (Collins & Lippold 2003, Nissley et al. 2002).

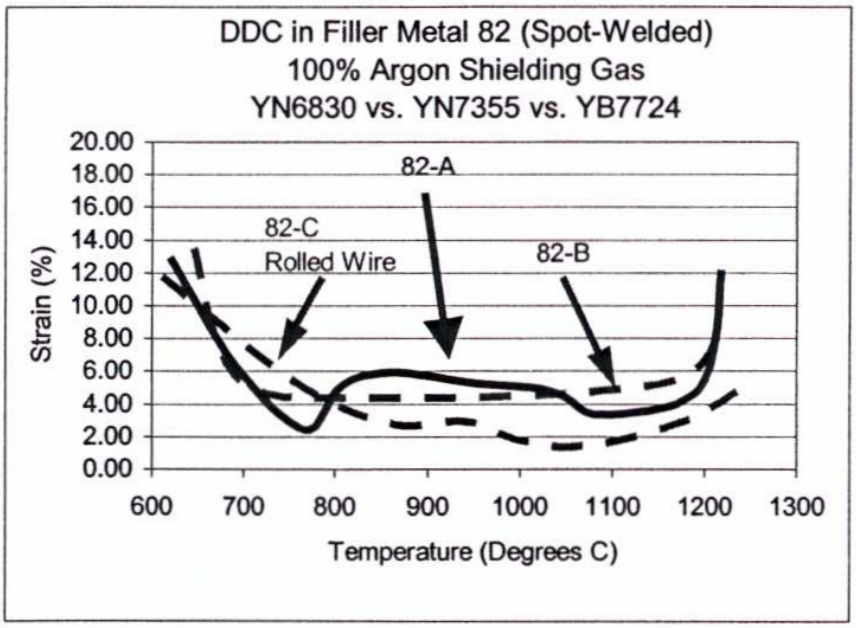

Figure 40. DDC behaviour of filler material 82 heats (Collins & Lippold 2003, Nissley et al. 2002).

The threshold strains for 82-A, 82-B and 82-C are 2.5%, 4% and 1.5%, respectively. At a strain level of 10%, the DTR for all three heats of Alloy 82 is approximately 650–1200ºC. 82-A exhibits two rather distinct ductility dips at approximately 750ºC and

1100ºC within the 650–1200ºC ductility-dip trough, while 82-B displays a more consistent threshold strain level of 4% throughout the entire ductility-dip trough. The rolled wire heat, 82-C, exhibits a threshold strain of 1.5% over a rather narrow temperature range of 1000–1100ºC, while a strain of 2% causes cracking in the 850–1150ºC range (Collins & Lippold 2003, Nissley et al. 2002, Lippold et al. 2004).

In Figure 41 the DDC behaviour of filler material 52 is compared with that of 82-A and 82-B (Collins & Lippold 2003, Nissley et al. 2002).

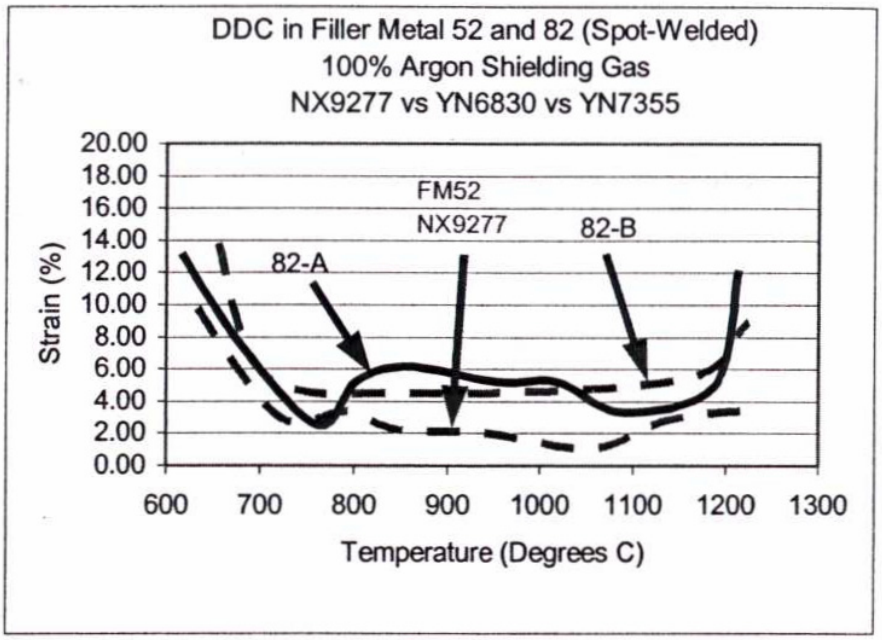

Figure 41. DDC behaviour of filler material 52 with 82-A and 82-B (Collins & Lippold 2003, Nissley et al. 2002).

The threshold strain for Alloys 52, 82-A and 82-B are 1%, 2.5% and 4%, respectively. Figure 41 depicts DTR of approximately 650–1200ºC for filler material 52. For filler material 52, the threshold strain of 1% occurs between 1000–1100ºC, while the strain necessary to cause cracking in the 700–1000–1200ºC temperature ranges is varying between 2% and 3%. In conclusion, the filler material 52 is more susceptible to DDC than the filler material 82 (Collins & Lippold 2003).

Additions of hydrogen in shielding gas and sulphur into the weld were also evaluated in this study, with filler metal 82. Hydrogen was added by using a 95Ar-5H_2 shielding gas, while sulphur was added to a 1/16-in. diameter hole drilled into the middle of the STF sample gauge section. The powder was sealed into the filler metal portion of the sample by placing a small piece of 0.045-in. welding wire into the drilled hole on top of the sulphur. A low heat input, rapid spot weld was then performed to further seal in the sulphur prior to proceeding with the full spot weld cycle. Figure 42 and Figure 43

present the respective effects of hydrogen and sulphur additions for filler material 82 (Collins & Lippold 2003).

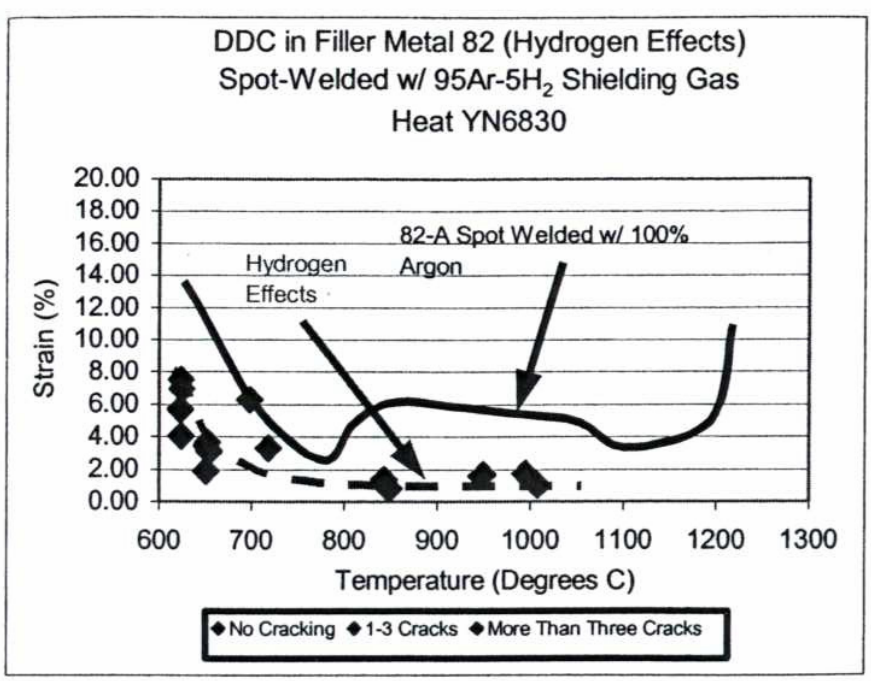

Figure 42. Effect of hydrogen on STF DDC behaviour of Alloy 82 (Collins & Lippold 2003).

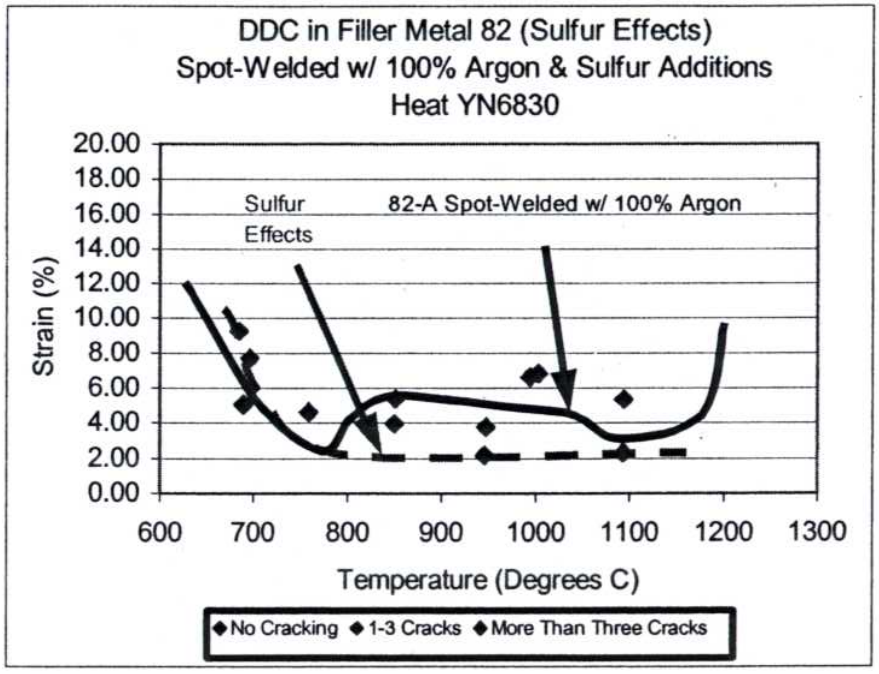

Figure 43. Effect of sulphur on STF DDC behaviour of Alloy 82 (Collins & Lippold 2003).

As shown in Figure 42, a dramatic negative effect on DDC susceptibility occurs with hydrogen additions to the weld, especially in the 850 to 1000°C temperature range of the ductility dip trough. The threshold strain to cause DDC in Alloy 82 was nearly 6% in the 850 to 1000°C temperature range, but additions of hydrogen to the shielding gas dropped the threshold strain to 1%. Furthermore, significant cracking was encountered in each hydrogen-containing sample in this particular temperature range, whereas a gradual change from minor cracking (1–3 cracks) at 6% threshold strain, to significant cracking (>3 cracks) at 8% threshold strain, was observed in Alloy 82 when no hydrogen was added to the spot weld.

Additions of sulphur also revealed negative effects on DDC susceptibility for Alloy 82, though not quite as dramatic as hydrogen additions. As seen in Figure 43, sulphur additions dropped the threshold strain in the 800 to 1000°C temperature range from 6%, to approximately 2% (Collins & Lippold 2003).

Young et al. (2003) studied factors affecting the hydrogen embrittlement resistance of Ni-Cr-Mn-Nb welds. Multipass, automatic TIG welding was used in this investigation using EN82H filler metal. Inconel Alloy 600 was used as the base plate to minimize dilution of the EN82H filler wire. For hydrogen uptake measurements, bead-on-plate welds were fabricated with different shielding gas compositions (95Ar-5H_2, 97Ar-3H_2, 99Ar-1H_2, and 75He-25Ar). The as-welded hydrogen concentration dissolved in the weld metal decreases from 12.5 wt. ppm in the 95Ar-5H_2 weld to 3,5 wt. ppm in the 75He-25Ar weld. Shielding gas mixtures with ≥1% hydrogen additions can result in hydrogen concentrations greater than 5 wt. ppm in the weld metal which reduce ductility via hydrogen embrittlement. Even though nickel-base alloys are more resistant to hydrogen embrittlement than many ferritic, bainitic, or martensitic steels, this study shows that 95Ar-5H_2 shielding gas can embrittle EN82H welds. Moreover, the relatively slow diffusivity of hydrogen in nickel limits the beneficial effects of hydrogen outgassing during post-weld heat treatment, so hydrogen embrittlement or delayed cracking in service must still be considered (Young et al. 2003).

Tensile test data shows that as the internal hydrogen concentration increases, the elongation, reduction in area, and the ultimate tensile strength decrease. Tensile test data plotted vs. hydrogen concentration are summarized in Figure 44 (Young et al. 2003).

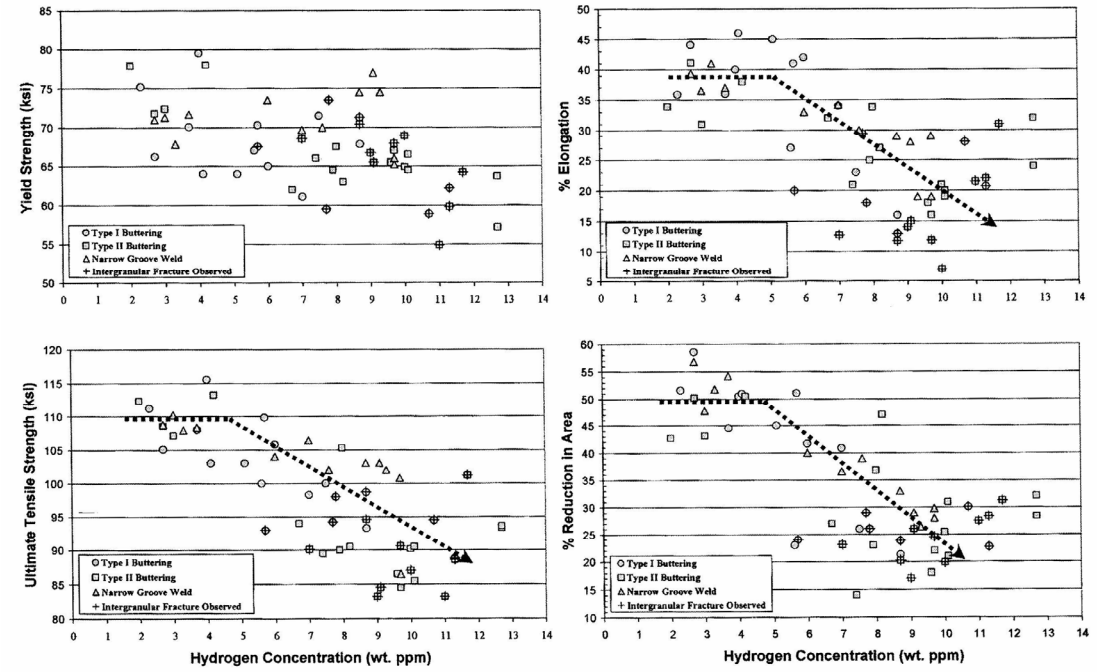

Figure 44. Summary of tensile test data for Alloy EN82H as a function of hydrogen concentration (Young et al. 2003).

Thermal desorption spectra for the narrow groove weld of EN82H and Alloy X-750 AH are shown in Figure 45. Data are plotted as the relative intensity of the hydrogen outgassing signal vs. temperature. The area under the curve is a measure of the hydrogen concentration (Young et al. 2003).

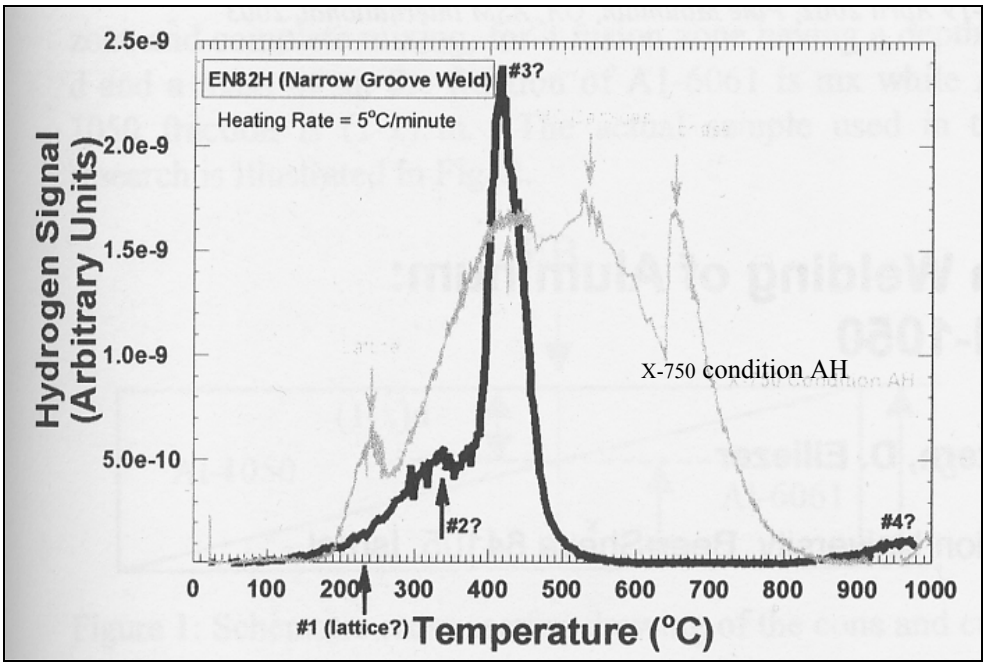

Figure 45. Thermal desorption spectra for the narrow groove weld of EN82H and Alloy X-750 AH (Young et al. 2003).

Thermal desorption spectrum for the narrow groove weld of EN82H shows hydrogen release from possibly four trapping states with peak centres near 230, 330, 420 and 970°C. These multiple hydrogen trapping states suggest that hydrogen/microstructure interactions can affect the hydrogen embrittlement resistance even up to high temperatures (Young et al. 2003).

Since the narrow groove weld is highly constrained, residual stresses and strains may contribute to the variability in the mechanical properties. The magnitude of the residual plastic strains were investigated via Electron Backscatter Diffraction (EBSD) and were determined to range from 0% in recrystallised regions up to ~20% near the root of the narrow groove weld. Residual stresses and plastic strains likely contribute to the observed variability in the hydrogen embrittlement resistance (Young et al. 2003).

Recrystallisation was observed in the upper temperature range (1050–1200°C) of the DTR, and it coincided with the ductility recovery (Collins et al. 2002, Collins & Lippold 2003, Nissley et al. 2002). In Figure 46 a SEM image of migrated grain boundaries in the STF samples is presented. In Figure 47 examples of migrated weld metal boundaries in FM-52 heat NX9277 are schematically presented (Lippold et al. 2004).

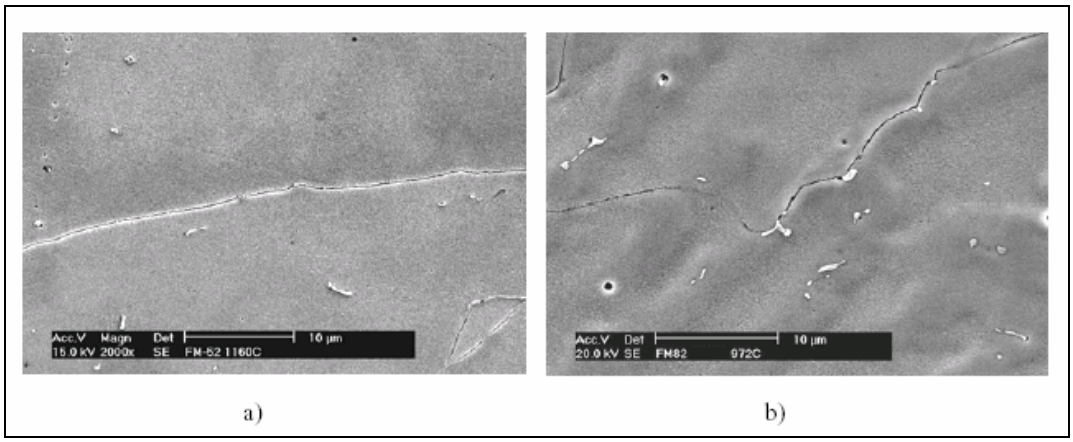

Figure 46. SEM images of migrated grain boundaries in the STF samples. In (a) straight migrated grain boundary in FM-52 heat NX9277 (STF sample deformed 2.9% at 1160°C) and (b) grain boundary pinning caused by the frequent medium size eutectic (NbTi)C precipitates in FM-82 heat YN6830 (STF sample deformed 7.5% at 972°C) (Lippold et al. 2004).

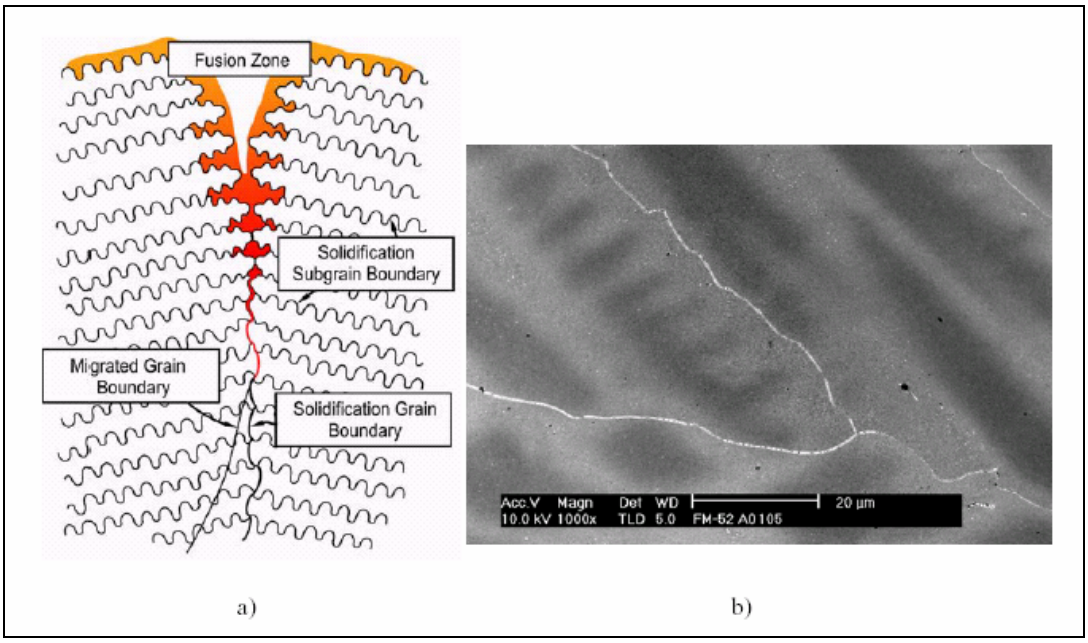

Figure 47. Weld metal boundaries in austenitic weld metal. In (a) schematic illustration and (b) migrated grain boundaries in FM-52 weld metal, which pulled away from the segregation patterns revealed by the etching (Lippold et al. 2004).

The ductility-dip cracking susceptibility of nickel-base filler metals is a strong function of grain boundary tortuosity, and boundary composition and precipitate distribution. FM-52 weld deposits are very susceptible to DDC, because the migrated grain boundaries in these welds are extremely straight (non-tortuous), allowing large strain build-up at grain boundary triple points. FM-82 weld deposits exhibit more tortuous migrated grain boundaries which provide a mechanical locking effect opposing the grain boundary sliding. Strain is distributed more evenly along these boundaries and higher applied strains are required to promote crack initiation. The formation of Nb-rich carbides via an eutectic reaction at the end of solidification is primarily responsible for the increased boundary tortuosity in FM-82 relative to FM-52, in which no such reaction occurs (Lippold et al. 2004).

The nature of grain boundary precipitation reactions in the solid state and elevated temperature impurity segregation to the grain boundaries also influence susceptibility to ductility-dip cracking. Both hydrogen in shielding gas and sulphur additions to FM-82 have been shown to increase susceptibility. Precipitate type, size and distribution presumably also influence susceptibility, but these factors are not so easily quantified and are much more complex, particularly in multipass welds, where multiple thermal cycles may generate a range of precipitate types and sizes. Clearly, there is still much to be understood about the ductility-dip cracking mechanism. The precise control of thermal and mechanical history of the weld metal that can be achieved using the strain-to-fracture test coupled with detailed characterization allows the importance of these

factors to be better quantified. This will eventually lead to the development of nickel-base filler materials that are resistant to ductility-dip cracking (Lippold et al. 2004).

Inconel filler material 52M is a new 30% chromium alloy. Inconel 52M is used for TIG and MIG welding of Inconel 690. Like Inconel 52 and Inconel 152, Inconel 52M is designed to resist primary water intergranular stress corrosion cracking. In addition, Inconel 52M provides significantly improved resistance to ductility-dip cracking or cold cracking during fabrication. Clean weld deposits are produced that tend to be free of inclusions, oxides and porosity, mainly as a consequence of the controlled low levels of aluminium and titanium. Inconel 52M is used in the fabrication and repair of nuclear components and it exhibits a good resistance to root-cracking (Inconel filler metal specifications 2003). In the study made by EPRI, Welding Services Inc. and Special Metals-Welding Products Company, weldability and non-destructive testing of Inconel 52MS (S indicates special processing to promote cleaner welds) was investigated using an orbital TIG welded weld overlay mock-up, Figure 48 (Findlan et al. 2005, Amador et al. 2005).

Figure 48. Inconel 52MS structural weld overlay (Findlan et al. 2005).

The presence of oxide floaters has been troublesome for applications welded downhill or full orbital on piping components made in the horizontal position. In Figure 49a oxide floaters in Alloy 690 welded with Alloy 52 are shown (Findlan et al. 2005, Amador et al. 2005). In Figure 49b is presented a detailed example of oxide floaters.

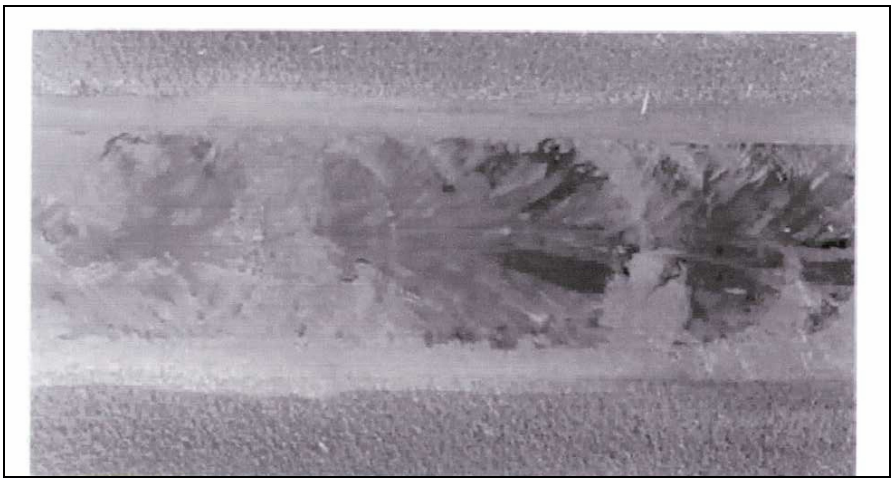

Figure 49a. Oxide floaters in Alloy 690 welded with Alloy 52 (Findlan et al. 2005).

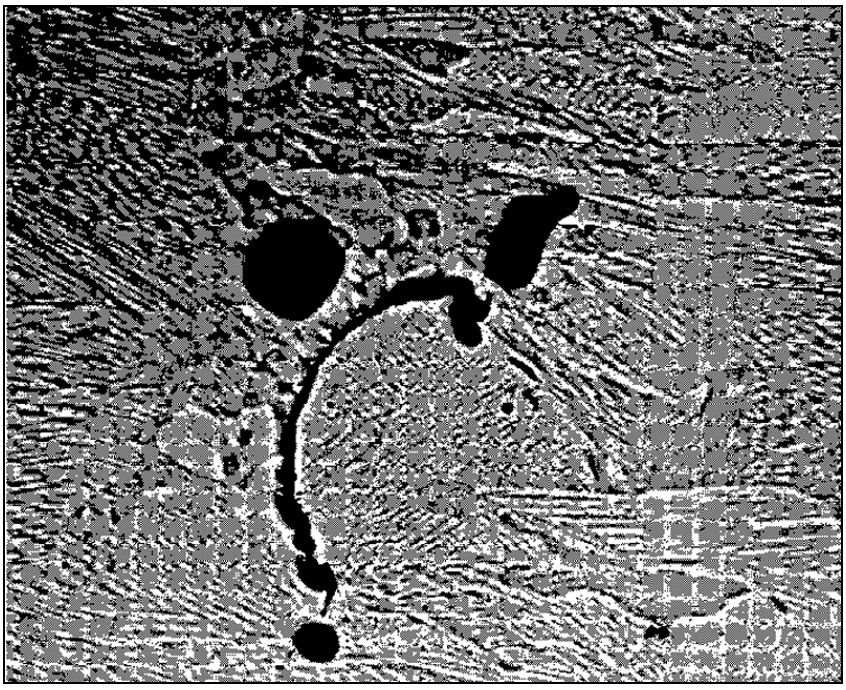

Figure 49b. Detailed example of oxide floaters. Magnification is 53x.

Inconel 52M does not rely on aluminium and titanium as primary deoxidizers, and this metallurgical difference was considered a potential contributor to the reduction in the oxides/contaminants whose entrapment leads to "lack of bond" ultrasonic testing (UT) indications. UT indications found were due to finely dispersed porosity that was likely related to welding conditions designed for ultra low dilution. There was no evidence of oxide floaters, hot cracking or DDC. The result of this study was that the weldability and welder appeal of Inconel 52 MS was excellent (Findlan et al. 2005, Amador et al. 2005).

3.4 Hot cracking tests

Many different tests have been developed over the years, some of which are specific to individual groups of materials, some to specific welding processes and some to individual pieces or test equipment in one or more laboratories. The complexities of the actual cracking mechanisms combined with the diversity of individual tests means that standardization is difficult, and true international standardization is particularly challenging (Farrar 2005).

Here are listed some hot cracking tests that are described, e.g. in Farrar (2005), Lippold (2005), and Heuser (2005). If the method is standardized, the standard is shown in brackets.

- Self restraint T-joint-test (CEN ISO/TR 17641-2)
- Weld metal tensile test (CEN ISO/TR 17641-2)
- Longitudinal bend test (CEN ISO/TR 17641-2)
- Hot tensile test (CEN ISO/TR 17641-3)
- Varestraint- and Transvarestraint test (CEN ISO/TR 17641-3)
- Flat tensile test, e.g. PVR (Programmable Deformation Cracking) test (CEN ISO/TR 17641-3)
- Cylinder sample test (DIN 50129)
- Ring segment test
- HDR (Hot Deformation Rate) test
- CPT (Cast Pin Tear) test
- Spot Varestraint test
- STF (Strain-To-Fracture) test.

Despite the large number of available weldability test techniques, only a few are applicable to thin material, particularly in thicknesses less than 3 mm (Lippold et al. 1996). The Sigmajig test, developed by G. M. Goodwin in 1986, is a hot cracking test commonly used for sheet metal. The test uses a pre-applied load during welding and determines the threshold stress above which centreline cracks initiate. The Sigmajig test, if utilized properly, can be an effective tool to both discriminate and rank susceptibility to weld metal solidification cracking due to alloy-to-alloy and heat-to-heat variations in composition (Feng et al. 1997).

Chapter 3.5 introduces in detail the Varestraint test that is the most commonly used hot cracking test.

3.5 The Varestraint Test

The Varestraint Test (**VA**riable **RESTRAINT**) was originally developed to evaluate the relative hot-cracking sensitivity of base materials. It has proven to also be useful in the studies of

- the hot-cracking sensitivity of filler materials
- the effect of specific alloying elements on hot-cracking sensitivity
- the establishment of the basic mechanisms of hot-cracking.

The Varestraint testing procedure utilizes a small, laboratory scale specimen supported as a cantilever beam, as shown schematically in Figure 50 (Savage & Lundin 1966).

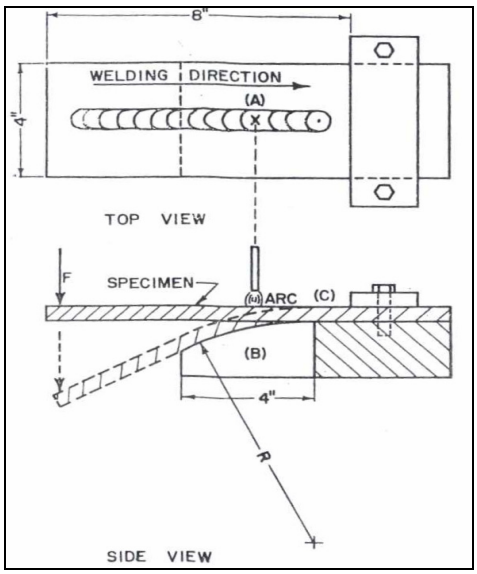

Figure 50. Simplified sketch of the operation of the Varestraint testing device (Savage & Lundin 1966).

A weld is deposited from left to right, as indicated, using whatever combination of process, joint geometry, and welding parameters of interest. As the arc passes the point marked by A in Figure 50, a pneumatically or hydraulically actuated loading yoke suddenly bends the specimen downwards to conform to the radius of curvature of the top surface of the removable die bloc, B. Meanwhile, the arc continues steadily onwards, until it is interrupted in the run-off area at C (Savage & Lundin 1966).

From the geometry of the system, the nominal value of the suddenly applied, augmented tangential strain in the outer fibre of the test specimen can be calculated as follows:

$$\varepsilon_t = t/2R \tag{5}$$

where

ε_t = augmented tangential strain
t = specimen thickness
R = radius of curvature of the die block.

By substituting the die block with the appropriate radius of curvature, any desired augmented strain can be applied to the weldments at any predetermined instant during weld deposition (Savage & Lundin 1966).

The last part of the standard CEN ISO/TR 17641: Destructive tests on welds in metallic materials – hot cracking tests for weldments – Arc welding processes – parts 1–3 was published in March 2005. In part 3 (CEN ISO/TR 17641-3:2005), an outline to the test methods and procedures for carrying out externally loaded tests to assess susceptibility to hot cracking is presented. It is primarily intended for austenitic stainless steels, nickel, nickel-base and nickel-copper alloys, weldments and welding consumables. However, the principles can also be extended to other materials such as aluminium alloys and high strength steels, by agreement between contracting parties.

The standard gives general recommendations on the specimen size and test procedures. Specimen size is not fixed, but is dependent on the material available for testing, the nature of the test and the loading capacity of the machine. However, the most common form of specimen is a simple flat bar with the following dimensions:

- length 80–300 mm
- width 40–100 mm
- thickness depending on the material being tested and the loading capacity of the machine.

Performance of the tests in their standard form involves the production of a TIG melt run on the parent material or on previously-deposited weld metal. Welding parameters can be chosen to suit particular applications, but the standard conditions are:

- low heat input: 12.5 V, 85 A, 18 cm/min travel speed
- high heat input: 13.5 V, 220 A, 11 cm/min travel speed.

In completion of each test, the specimen should be visually examined for cracks at a magnification of 25x. The total length of all visible cracks is determined and plotted as a function of the bending strain. In Figure 51 an example of the calculation of the total crack length in Alloy 182 weld metal is presented (ongoing project DISSIMILAR METAL WELDS, 2005).

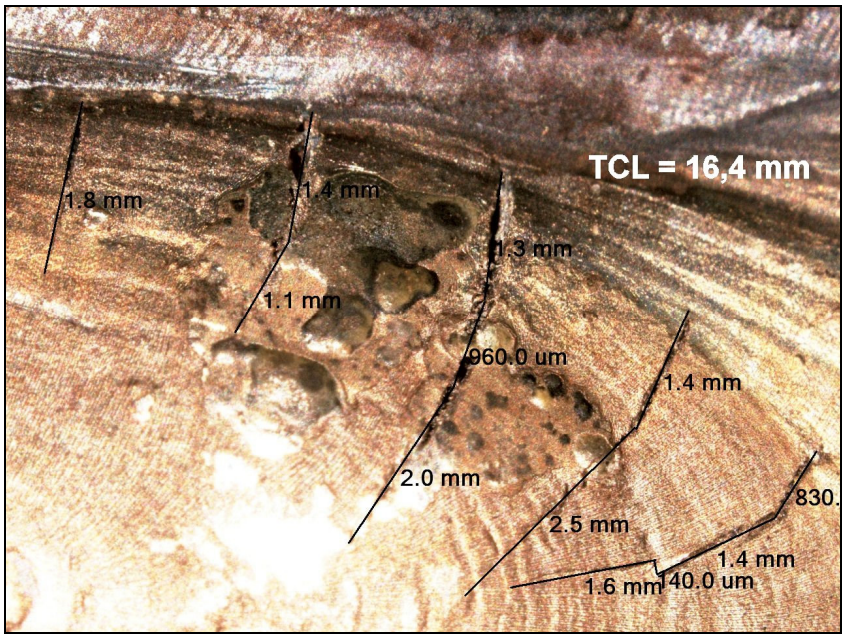

Figure 51. Example of the calculation of the total crack length (TCL) in Alloy 182 weld metal (ongoing project DISSIMILAR METAL WELDS, 2005).

The relative position of the crack length vs. surface strain curve enables the assessment of susceptibility to hot cracking (CEN ISO/TR 17641-3:2005). Figure 26 shows a typical presentation of the results of the Varestraint test (Wu & Tsai 1999).

3.6 References

Amador, P., Smith, R., Kiser, S., Findlan, S. & McGehee, A. 2005. Beneficial Application of FM52M on Dissimilar Metal Weldments. 2005 EPRI International PWSCC of Alloy 600 Conference, 7–10 March 2005, Santa Ana Pueblo, New Mexico, USA. 18 p.

Aoh, J. & Yang, C. 2003. Cracking Susceptibility Study of Inconel 600 Alloy Using Varestraint and Hot Ductility Test. 6th International Trends in Welding Research Proceedings. ASM International, Pine Mountain, GA, USA. Pp. 597–602.

Boursier, J., Valliant, F. & Yrieix, B. 2004. A Review of PWSCC Behaviour of Nickel Weld Metals Containing 15 to 30% Chromium. Proceedings of ASME/JSME Pressure Vessels and Piping Conference, San Diego, California, USA, 25 – 29 July 2004. Ed. Tahara, T. PVP Vol. 490. Pp. 109–121.

Briant, C. L. & Hall, E. L. 1987. The Microstructural Causes of Intergranular Corrosion of Alloys 82 and 182. Corrosion, Vol. 43, pp. 539–548.

CEN ISO/TR 17641-3. 2005. Destructive Tests on Welds in Metallic Materials. Hot Cracking Tests for Weldments. Arc Welding Processes. Part 3: Externally Loaded Test. 17 p.

Cola, M. J. & Teter, D. F. 1998. Optical and Analytical Electron Microscopy of Ductility Dip Cracking in Ni-Base Filler Metal 52 – Initial Studies. 5th International Trends in Welding Research Proceedings, 1–5 June 1998. ASM International, Pine Mountain, GA, USA. Pp. 781–786.

Collins, M. & Lippold, J. 2003. An Investigation of Ductility Dip Cracking in Nickel-Based Filler Materials – Parts I–III. Welding Research, pp. 288–295.

Collins, M., Lippold, J. & Kikel, J. 2002. Quantifying Ductility Dip Cracking Susceptibility in Nickel-Base Weld Metals Using the Strain to Fracture Test. 6th International Trends in Welding Research Proceedings, 15–19 April 2002. ASM International, Pine Mountain, GA, USA. Pp. 586–590.

Crum, J. R. & Nagashima, T. 1997. Review of Alloy 690 Steam Generator Studies. Proceedings of the Eight International Symposium on Environmental Degradation of Materials in Nuclear Power Systems – Water Reactors. Amelia Island, Florida, USA, 10–14 August 1997. Pp. 127–137.

Davé, V. R., Cola, M. J., Kumar, L., Schwartz, A. J. & Hussen, G. N. A. 2004. Grain Boundary Character in Alloy 690 and Ductility-Dip Cracking Susceptibility. Welding Journal, Vol. 83, No. 1, 1-S–5-S.

Farrar, J. 2005. Hot Cracking Tests – The Route to International Standardization. In: Böllinghaus, T. and Herold, H. (Eds.). Hot Cracking Phenomena in Welds. Springer, Germany. ISBN 3-540-22332-0. Pp. 291–304.

Feng, Z., Zacharia, T. & David, S. A. 1997. Thermal Stress Development in a Nickel-Based Superalloy During Weldability Test. Welding Journal, Vol. 76, No. 11, pp. 81–92.

Findlan, S., Newton, B. & Kiser, S. 2005. Successful Structural Weld Metal Build-Ups on P-3 Gr-3 Pipe Coupon Made with INCONEL® Filler Metal 52M. 2005 EPRI International PWSCC of Alloy 600 Conference. 7–10 March 2005, Santa Ana Pueblo, New Mexico, USA. 15 p.

Gold, R., Harrod, D., Aspden, R. & Baum, A. 1990. Alloy 690 for Steam Generator Tubing Applications. Research Project S408-6; Background Report. Westinghouse Electric Corporation, Pittsburgh, Pennsylvania, USA. Pp. 2-1–2-8.

Heuser, H. 2005. Value of Different Hot Cracking Tests for the Manufacturer of Filler Metals. In: Böllinghaus, T. and Herold, H. (Eds.). Hot Cracking Phenomena in Welds. Springer, Germany. ISBN 3-540-22332-0. Pp. 305–327.

Holt, R. & Wallace, W. 1976. Impurities and Trace Elements in Nickel-Base Superalloys. International Metals Reviews, Vol. 21, No. 3, pp. 1–24.

Hood, B. & Lin, W. 1995. Weldability Testing of Inconel Filler Materials. Proceedings of the Seventh International Symposium on Environmental Degradation of Materials in Nuclear Power Systems – Water Reactors. Breckenridge, Colorado, USA, 7–10 August 1995. Pp. 69–79.

Inconel filler metal specifications. 2003. http://www.specialmetalswelding.com/.

Jeng, S. L., Lee, H. T., Rehbach, W. P., Kuo, T. Y., Weirich, T. E. & Mayer, J. P. 2005. Effects of Nb on the Microstructure and Corrosive Property in the Alloy 690–SUS 304L Weldments. Materials Science and Engineering A, Vol. 397, No. 1–2, pp. 229–238.

Kikel, J. M. & Parker, D. M. 1998. Ductility Dip Cracking Susceptibility of Filler Metal 52 and Alloy 690. 5th International Trends in Welding Research, Proceedings. ASM International, Pine Mountain, GA, USA. Pp. 757–762.

Kiser, S. 2006. Special Metals Welding Products Company. Personal communication.

Kou, S. 2003. Welding Metallurgy. Second edition. Wiley-Interscience. 461 p.

Lancaster, J. 1999. Metallurgy of Welding. Sixth edition. Abington Publishing. 446 p.

Lee, H. T. & Jeng, S. L. 2001. Characteristics of Dissimilar Welding of Alloy 690 to 304L Stainless Steel. Science and Technology of Welding and Joining, Vol. 6, No. 4, pp. 225–234.

Lee, H. T., Jeng, S. L., Yen, C. H. & Kuo, T. Y. 2004. Dissimilar Welding of Nickel-Based Alloy 690 to SUS 304L with Ti Addition. Journal of Nuclear Materials, Vol. 335, No. 1, pp. 59–69.

Lippold, J. 2005. Recent Developments in Weldability Testing. In: Böllinghaus, T. and Herold, H. (Eds.). Hot Cracking Phenomena in Welds. Springer, Germany. ISBN 3-540-22332-0. Pp. 271–290.

Lippold, J. C., Shademan, S. S. & Baeslack III, W. A. 1996. The Effect of Specimen Strength and Thickness on Cracking Susceptibility during the Sigmajig Weldability Test. Welding Journal, Vol. 75, No. 3, pp. 81–92.

Lippold, J., Ramirez, A. & Sowards, J. 2004. New Insight into the Mechanism of Ductility Dip Cracking in Nickel-Based Weld Metals. IIW Doc. No. IX-2123-04. 15 p.

Nishimoto, K., Saida, K. & Okauchi, H. 2004. Microcracking Susceptibility in Multi-Pass Weld Metal of Inconel 690 Alloy. IIW Doc. No. IX-2097-04. 15 p.

Nissley, N., Collins, M., Guaytima, G. & Lippold, J. 2002. Development of the Strain to Fracture Test for Evaluating Ductility Dip Cracking in Austenitic Stainless Steels and Ni-base Alloys. Welding in the World, Vol. 46, No. 7/8, pp. 32–40.

Nordberg, P. 1985. The Influence of Composition and Heat Treatment on Microstructure and Material Properties of SANICRO 69 (Alloy 690). AB Sandvik Steel Report presented at EPRI Workshop on Thermally Treated Alloy 690 for Tubes in Nuclear Steam Generators. Pittsburgh, PA, USA, 26–28 June 1985. 20 p.

Peng, Q. J., Yamauchi, H. & Shoji, T. 2003. Investigation of Dendrite-Boundary Microchemistry in Alloy 182 using Auger Electron Spectroscopy Analysis. Metallurgical and Materials Transactions, Vol. 34A, pp. 1891–1899.

Richards, N. & Chaturvedi, M. 2000. Effect of Minor Elements on Weldability of Ni-Base Superalloys. International Metals Reviews, Vol. 45, No. 3, pp. 109–129.

Robinson, J. & Scott, M. 1980. Liquation Cracking During the Welding of Austenitic Stainless Steels and Nickel Alloys. Phil. Trans. R. Soc. Lond., Vol. A 295, pp. 105–117.

Savage, W. & Lundin, C. 1966. Application of the Varestraint Technique to the Study of Weldability. Welding Research Supplement, November, pp. 497–503.

Scarberry, R., Pearman, S. & Crum, J. 1976. Precipitation Reactions in Inconel 600 and Their Effect on Corrosion Behavior. Corrosion, Vol. 32, No. 10, pp. 401–406.

Staehle, R-.W. & Gorman, J. A. 2003. Quantitative Assessment of Submodes of Stress Corrosion Cracking on the Secondary Side of Steam Generator Tubing in Pressurized Water Reactors. Corrosion, Vol. 59, No. 11, pp. 931–994.

Wu, W. & Tsai, C. 1999. Hot Cracking Susceptibility of Fillers 52 and 82 in Alloy 690. Metallurgical and Materials Transactions, Vol. 30A, pp. 417–426.

Yamanaka, K. & Yonezawa, T. 1989. Optimum Time and Temperature of TT Alloy 690. Electric Power Research Institute, Alloy 690 Workshop. New Orleans, USA, 12–14 April 1989. 18 p.

Young, G., Bettige, N., Lewis, N., Penik, M., Kikel, J., Silvia, A. & McDonald, C. 2003. Factors Affecting the Hydrogen Embrittlement Resistance of Ni-Cr-Mn-Nb Welds. 6th International Trends in Welding Research, Proceedings. ASM International, Pine Mountain, GA, USA. Pp. 666–671.

4. Residual stress distributions of dissimilar metal welds

Assessment of the structural integrity of critical components and structures in nuclear power plants is of vital importance for safe operation. When assessing the structural integrity of a component, both the loading and the load-carrying capacity are determined. The residual stresses are included in the analysis on either the loading or the capacity side, depending on the design strategy.

Since residual stresses with various magnitudes and distributions are present in virtually all structurally engineered components, there is a demand for accurate assessment of the residual stress state, especially in critical components. The residual stress state present in a structure is the result of the manufacturing history and the elastic properties of the structure. The former referring to the mechanical and thermal processes executed during the whole production sequence and the latter to the elastic behaviour of the structure. Because the elastic properties influence the severity and distribution of the residual stresses, it follows that a structure comprised of several materials, i.e., a composite, will experience the development of the residual stresses in a completely different way than one made of a single material.

Depending on the importance of the residual stresses, different approaches have been introduced for the assessment of the structural integrity. In structures where the effect of the residual stresses on the performance is limited or small, the assessment of the residual stresses is of less importance. On the other hand, in the structures where the integrity of the structure is of vital importance for the reliability, a thorough and accurate assessment of the residual stress state is of primary concern. Industry branches related to energy production are typically manufacturing and managing structures, which are strongly regulated by national or international technical guidelines, standards and design codes to ensure reliable operation.

4.1 Definition of residual stresses

Residual stresses are defined as static mechanical stresses that are present in a thermodynamically (and mechanically) closed system of equilibrium. In a more general way, residual stresses are mechanical stresses that exist in a component without any external applied mechanical or thermal loads. A direct consequence of the definition is that all internal forces and moments resulting from the residual stresses of a system are in mechanical equilibrium. This can be expressed in mathematical form:

$$\int \sigma dA = 0 \ and \int dM = 0, \tag{6}$$

where σ is the stress with respect to an arbitrary cross-section and M is the moment (bending moment) with respect to an arbitrary axis within the system. The size of the system under observation determines the type of the residual stresses that are assessable.

Another consequence of the above-mentioned definition is that the internal stresses induced by thermal transients are outside the scope of the residual stresses, as they do not represent closed systems. Such transients are typical for uneven cooling during heat treatments and thermal in-service loads. However, the thermal transients can induce residual stresses, when the yield strength is exceeded locally and plastic flow occurs.

4.1.1 Origin of residual stresses

Stresses that exist in a body without external loads are not only referred to as residual stresses, but also as internal stresses, initial stresses, inherent stresses and locked-in stresses, according to Masubuchi (1993). From a systematic point of view, it can be shown that formation of the residual stresses always involves interaction between the mechanical, thermal and metallurgical states of the material, according to Kloos and Kaiser (1991). Figure 52 shows the bi-directional interactions between any two of the three states.

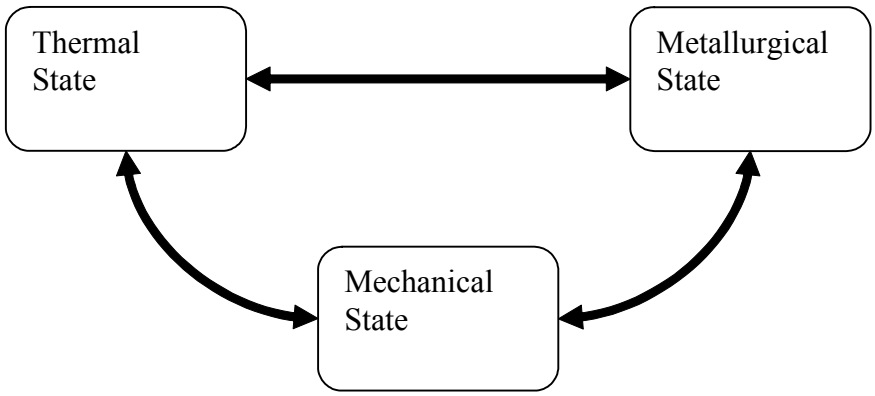

Figure 52. Illustration of the bi-directional interactions between mechanical, thermal and metallurgical states.

According to Kloos (1979), all causes of residual stresses can be classified into three main groups: material, manufacturing and service. The residual stresses related to material characteristics are caused by inhomogeneous macroscopic or microscopic structures; the former being composite structures, such as cladding or dissimilar metal weld, and the latter multiphase structures, inclusions or defects in the crystalline structure. Manufacturing of structural components inevitably includes processes that

cause residual stresses to develop. The processes include thermal transients and/or mechanical forming that cause plastic flow. The former creates localized material flow exceeding the elastic limit, which induces residual stresses in casting, welding, coating and heat treatments. The latter creates localized plastic flow by inhomogeneous deformation due to mechanical loading, as in machining and cold forming. The residual stresses related to service are caused by

- mechanical loading that is irregular and partly exceeding the elastic limit leading to local and permanent deformation
- thermal loading from processes leading to plastic deformation
- chemical processes, such as corrosion, oxidation and hydrogen diffusion leading to crystal distortions.

Manufacturing of steel structures contains various thermal and mechanical processes, which all influence the internal equilibrium of the elastic strains within the material. The processes range from hot rolling, where the influence on the residual stress state is minimal due to the high processing temperature, to cold rolling, where the influence on the residual stress state is large due to the low temperature. Following the production of primary steel products, the residual stress state pertinent to the production processes is further altered, and in various processes completely changed. Because of the manufacturing processes involved in construction, e.g. of pipelines or pressure vessels, the residual stress state is altered at least on a local level. Manufacturing processes, such as bending, form the plates to a desired shape, altering the residual stress distribution of the original steel. However, when assembling the plates to the final structure by welding the residual stress state is severely modified within the weldments as well as in their proximity. This example shows the importance of knowing the whole production history, including all process sequences and parameters, because all thermo-mechanical processes influence and determine the final residual stress state of the structure both on global and local level.

4.1.2 Residual stresses: types I, II, and III

Depending on what method or physical quantity is used in the measurement of the residual stress state, different information regarding the residual stresses is acquired. As the use of the diffraction methods, both X-ray and neutron, started to increase in residual stress measurement, a relevant classification system of the residual stresses was needed, because the definition was incapable of dealing with fluctuations in the residual stress state within the system of observation. Macherauch et al. (1973) introduced a multi-phase and grain heterogenic material model that has been generally adopted as the state-of-the-art for residual stress analysis by diffraction methods. The model represents

an idealised residual stress state and divides the residual stresses into three types, depending on the domain size used for the observation.

Residual stresses of type I range over a larger domain, such as several grains and, are approximately homogeneous. The forces and the moments associated with the residual stresses of type I are in equilibrium throughout the whole component at any cross-section. Thus, infringement of the equilibrium of force and bending moment, i.e. by drilling or machining, always leads to macroscopic dimensional changes.

Residual stresses of type II range over a smaller domain, such as one grain, and are also approximately homogeneous. The forces and the moments associated with the residual stresses of type II are in equilibrium over a smaller material volume of the component. Infringement of the system of equilibrium may lead to macroscopic dimensional changes.

Residual stresses of type III range over the smallest domain, such as a sub-grain size of several atomic distances, and are inhomogeneous. The forces and the moments associated with the residual stresses of type III are in equilibrium over a fraction of the grain size. No macroscopic dimensional changes are induced by infringement of the system of equilibrium.

In general, the residual stresses of type I are referred to as macro-stresses and the types II and III are referred to as micro-stresses, respectively. Based on the above-mentioned classification of the residual stresses, the "true local residual stress" is obtained by summing up the three types. This classification also clarifies the differences between the residual stresses measured with diffraction methods (physical) and methods based on strain gauge techniques (mechanical). The diffraction methods respond to all three types and the strain gauge techniques to only type I. Thus, diffraction methods acquire information about the micro-stresses, which is not obtainable with the strain-gauge based methods.

4.2 Welding residual stresses

Manufacturing of welded structures in nuclear power plants is carried out with traditional methods for which there is considerable welding experience. The methods are shielded metal arc welding (SMAW), tungsten inert gas welding (TIG) or submerged arc welding (SAW). However, metal inert gas (MIG) welding is generally not used due to a higher risk for lack of fusion. Manufacturing of cladded structures is a time consuming process, and therefore it is mostly done with SAW. Other methods have also been used, though less frequently. Butt-welding of pipes, on the other hand, is made with tungsten inert gas welding (TIG).

Regardless of the welding method used, the material properties of the welds and the structural materials affect the formation and distribution of residual stresses. The resulting residual stress state in a welded component is determined by welding-related parameters and geometrical constraints. The former refers to the local shrinkage, quench and phase transformations resulting from the localised thermal cycle. The latter is dealt with through the unbalance in material properties of dissimilar metal welds, but the constraining effect of the surrounding structure is beyond the scope of this report.

The components of primary interest in nuclear power plants often have a bimetallic or dissimilar metal structure, where the mechanical properties of the joined materials are different, and thus add to the formation of welding residual stresses. The materials used in the weldments for which residual stresses have been assessed are structural steels cladded with austenitic stainless steels of pressure vessel components, and butt-welded, thick-walled austenitic stainless steel pipes of primary water systems.

Welding residual stresses have been measured and analysed for a large variety of industrial applications, ranging from steel processing to energy production. In many cases a brief analysis is enough, but the applications in the nuclear industry often require extensive and accurate determination of the residual stress state in and around weldments.

4.2.1 Three residual stress components pertinent to welding

Typical for all fusion welding processes is that the resulting residual stresses are induced and determined by the localized heating inherent to the welding processes. It is generally accepted that the post-weld residual stress state is composed of residual stress components resulting from three characteristic sub-processes in welding: shrinkage, quench and phase transformation. Christian et al. (1978) have published a detailed study of the formation of welding residual stresses based on these three sub-processes. Below is outlined the important features of each sub-process.

When studying the formation of residual stresses due to shrinkage, the presumption is that the cooling rate through the wall thickness of the weld is homogeneous. During welding the surrounding metal is also heated due to the conduction of heat, but to a lower temperature than the weld. After the deposition of the weld metal, the temperature of the weld starts to decrease. However, due to heat conduction the temperature of the surrounding metal continues to rise until equilibrium is reached and then the temperature starts to decrease. Thus, the surrounding metal expands before it starts to shrink. Because the maximum temperature reached is higher in the weld metal than in the surrounding metal, the yield point of the weld metal is lower. Due to the difference

in temperature and yield point the shrinkage is non-uniform and tensile residual stresses are formed. These shrinkage residual stresses are present in the weld, which reached the highest temperature, in both the longitudinal and transverse direction. The magnitude of both stresses is decreasing with increasing distance from the weld.

Nevertheless, the cooling process associated with the actual welding is heterogeneous through the thickness of the weld section. This requires an additional residual stress component that accounts for the so-called quenching effect. Due to the uneven cooling in the thickness direction, the surface of the weld metal and heat-affected zone cools faster than the sub-surface section of the weld. Thus, thermal stresses of different magnitude are introduced in the thickness direction. Upon completion of the cooling process to room temperature, quenching residual stresses are formed when the above-mentioned thermal stresses have exceeded the equivalent high temperature yield point, causing the metal to be deformed plastically. The magnitude and distribution of these stresses is determined by the temperature from which cooling starts, the cooling rate, the high temperature yield point, and the thickness of the weld section. When observing the quenching residual stresses alone in a weld cross-section, a compressive residual stress distribution is formed in the surface layers of the weld.

The third component in the formation of the post-welding residual stress state is the residual stresses induced from phase transformations. For instance, when cooling or quenching steels, the phase transformation of γ to α can take place and induce residual stresses due to the associated volume change. When a phase transformation occurs in some section of a weld, the residual stresses are compressive in the middle and tensile on the boundaries of the section. The starting temperature of the phase transformation is the deciding factor for the magnitude of these stresses. It must be sufficiently low to override the stresses caused by plastic deformation.

In actual welded structures, the residual stress state of the weld is the sum of the residual stresses created by these three processes. The residual stress distribution due to the sub-processes and the combined total residual stress distribution are presented in Figure 53. Therefore it is obvious that the sign, absolute value and distribution of the post-weld residual stresses in the surface layers and the middle section of the weld metal, the HAZ and the surrounding metal all depend upon which of the three processes is dominating in each case, respectively.

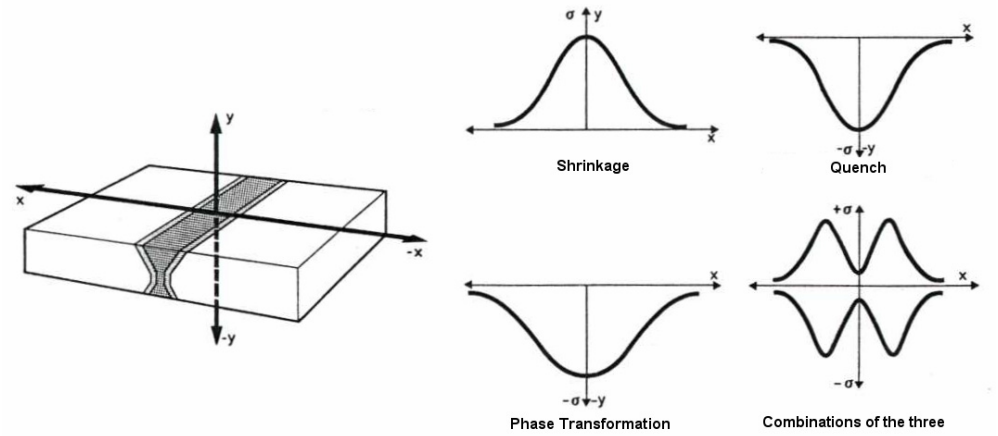

Figure 53. The sub-processes forming the residual stresses as a result of welding (Christian et al. 1978).

4.2.2 The effect of the material properties in dissimilar metal welds

When welding dissimilar materials, the resulting residual stress state is further influenced by the mismatch in adjoining material properties in comparison to welding materials of the same type. By virtue of the imbalance in mechanical and thermal properties of the adjoining materials, a complex intrinsic stress state is induced. This residual stress component is added to those related to the welding procedure.

The mechanical properties that govern the formation of residual stresses are primarily the modulus of elasticity and the strain hardening coefficient. In the case of a work hardening material the residual stresses are completely different than in a work softening material. Thus, a mismatch in strain hardening capabilities in adjoining materials, with otherwise similar elastic properties, induces local plastic deformation in the weaker material. To illustrate the difference in physical properties of alloys used in nuclear power plants, a summary of pressure vessel and piping materials and welding filler materials with their coefficients of thermal expansion and thermal conductivity is presented in Table 11.

Because the materials are locally heated and cooled during welding, temperature transients are inherent to the process. When the temperature dependence of the thermo-mechanical properties is taken into account, it is obvious that the uneven thermal load and thermal transients add to the formation of residual stresses.

By virtue of the above-mentioned differences in thermo-mechanical properties of the adjoining materials and their temperature dependence, it is obvious that the resulting residual stress state in a dissimilar metal weld is more complex than that of a regular weld. Therefore, the availability of numerical computing through finite element modelling (FEM) of the weldments is a powerful and suitable tool to predict the residual stresses in NPP structures.

Table 11. Near room temperature values of thermal properties for some alloys typical in primary circuit structures of nuclear power plants.

Material	Thermal property		Source
	Coefficient of thermal expansion ($\times 10^{-6}$/°C) at 20…300°C	Coefficient of thermal conductivity (W/m°C) at 100°C	
Carbon steel	13.5	45.0	Sandvik 1996
A508	13.08 13.6	 44	RCC-M KTA 3201.2
A533	13.08 13.6	 44	RCC-M KTA 3201.2
304L	17.7	16.0	Sandvik 1996
316L	17.5	16.0	ASM 2002
309	16.6 *	15.6 *	ASM 2002
Alloy 600	14.4	15.8	ASM 2002
Alloy 690	14.5	14.0	ASM 2002
Alloy 82	14.1	11.7 **	Special Metals Welding Products Co.
Alloy 52	14.6	12.1 **	Special Metals Welding Products Co.
Alloy 182	14.9	14.9 **	Special Metals Welding Products Co.
Alloy 152	14.7	12.1 **	Special Metals Welding Products Co.
*) Value of equivalent alloy **) Estimate at RT of equivalent alloy			

4.2.3 Welding residual stress distributions

In the fabrication of structures like pressure vessels and pipes, cast and forged plates and rings are joined by welding, and thus residual stresses develop. The magnitude and distribution of the residual stresses are determined by key factors related to the heat input during welding, weld sequence, weld starts and stops, cooling between passes, surrounding joint geometry, fit-up strains required to match up parts, base/weld metal mechanical properties, local weld repairs, post-weld heat treatment, and any post-weld mechanical processes such as grinding and machining.

The most important factors are related to welding energy and geometrical constraints. Most pipes are typically butt-welded from one side, but some structures are welded from both sides. Hence, the heat input used in the fabrication may be different, but more important is the difference in the geometrical constraint for the two procedures. A difference in wall thickness of the pipes in an abutment (end-to-end) joint adds to the geometrical constraints, when welding through a stiffness mismatch, which influences the though-wall residual stress distribution. Additionally, the radius-to-thickness ratio (R/t) also influences the geometrical constraint.

The magnitude and distribution of the residual stresses have not been studied extensively for many structures where it is presumed that those stresses do not play a significant role in any potential mode of failure. However, a considerable amount of experimental and analytical work performed on residual stresses of butt welds in stainless steel piping has shown that, in general, near-yield level tensile residual stresses are developed at the weld centreline on the inside surface. This is especially detrimental in nuclear power plant pressure vessels and piping, where different types of stress corrosion cracking represent a typical mode of failure.

4.2.4 Measured welding residual stresses

Measurement of welding residual stresses is an elaborate task, due to the fact that not only the surface stress is of interest, but also the stress inside the material, and moreover, the stress distribution just beneath the surface. Through the years several methods have been developed for measuring the spatial residual stress distribution. Typical for most methods is that elastic energy is released by complete or partial sectioning of the specimen. Even the non-destructive neutron diffraction method requires sectioning to access the target of measurement.

An early example of measured welding residual stress distributions in austenitic stainless steel pipings is presented by Shack (1984). The butt-welded piping under study was not subjected to any kind of stress improvement procedures prior to measurement. The through-wall residual stresses in large diameter AISI 304 stainless steel piping were determined by the layer removal method, which is based on strain gauge techniques. The axial residual stresses at various distances from the weld fusion line are presented in Figure 54. The main difference in the results obtained for large diameter piping compared to smaller diameter weldments was the position where the residual stresses became compressive. The stresses became compressive at a short distance into the wall, whereas the residual stresses in smaller-diameter piping can remain tensile all the way through the wall.

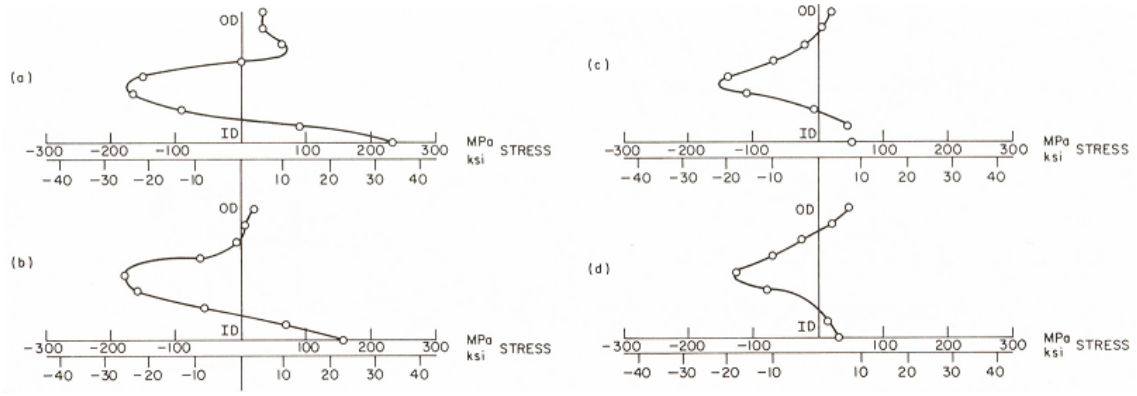

Figure 54. Through-wall distribution of axial residual stresses in the piping from a 24-in. weldment: (a) 3 mm, (b) 8 mm, (c) 15 mm and (d) 20 mm from the weld fusion line (Shack 1984).

Another example of the measured surface and through-wall axial and hoop residual stresses of an orbital TIG-welded austenitic stainless steel has been reported by Faure and Leggatt (1996). The studied weldment was representative of primary water pipes in a pressurized water reactor. The pipe material used, AFNOR Z3 CN 20-09 M, is equivalent to ASME CF8M. The measurements were carried out by two mechanical methods: the layer removal and hole drilling technique. The former included measurement of strain from partition of the block and sequential layer removal, and the latter used an abrasive jet for drilling. The measured residual stresses for both methods are shown in Figure 55. The layer removal results are shown with continuous and broken lines and the hole drilling results with round markings, referred to as centre hole measurements, close to the inside and outside surfaces. It can be concluded from the measurements that the general trend for large pipes is that the hoop and axial stresses are tensile near the outside surface, whereas near the inside surface the stresses are compressive except for the axial direction at the weld centreline (Faure & Leggatt 1996).

As a result of the tedious machining process inherent to the layer removal methods, other measurement methods, such as the ring core method, have been developed. In the ring core method, where an annular groove is machined around the strain gauge rosette, the amount of machining is drastically reduced as compared to the layer removal method. The ring core method was developed by Wolf and Böhm (1971) for residual stress measurements in large generator axles. In an extensive study by Engelhard et al. (2000) for optimizing the residual welding stresses, residual stresses have been measured with the ring core method in several narrow gap welded AISI 347 pipings. For comparison, the surface stresses around the welds were also measured by X-ray diffraction (XRD). An example of the measured residual stress distributions is shown in Figure 56. The stresses were measured with the ring core method as a function of depth (distance from surface) and with XRD as a function of the distance from the weld centre line. The measurements show tensile stresses dominating the weld while compressive stresses are present in the base material surrounding the weld.

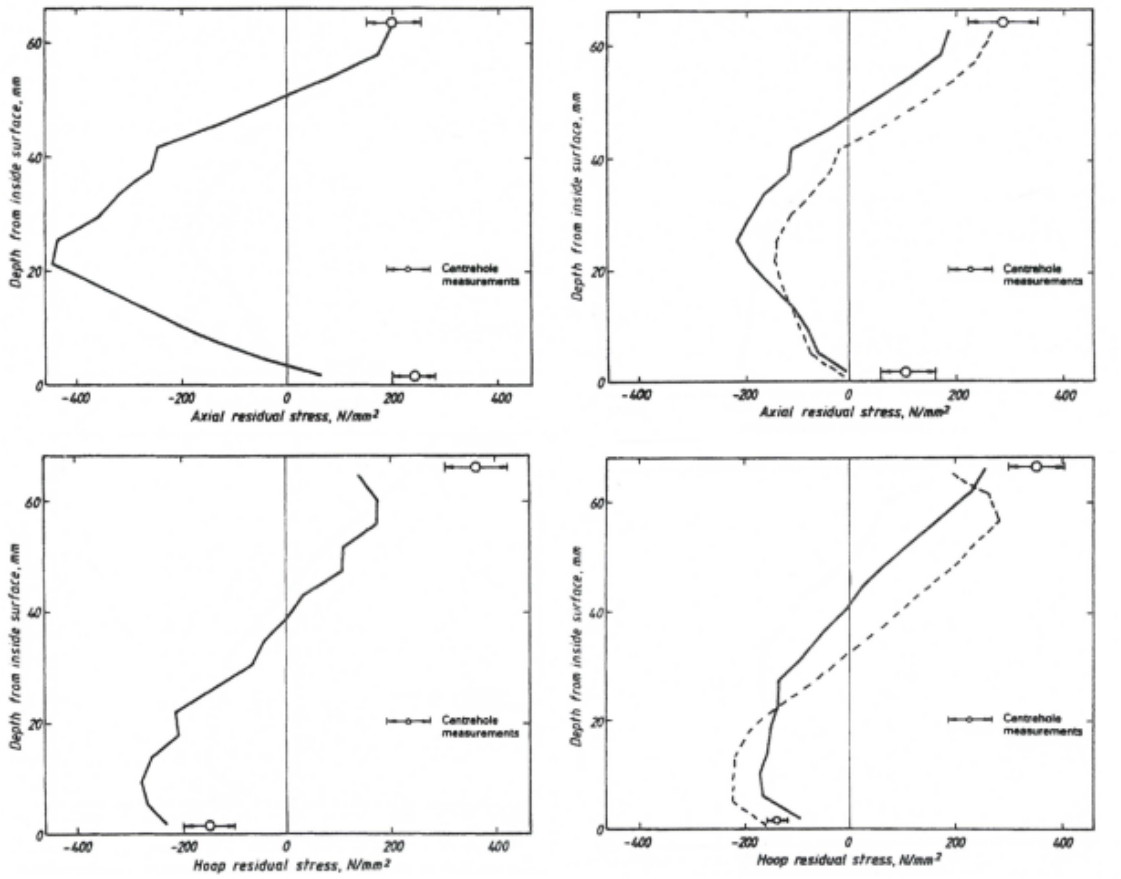

Figure 55. The surface and through-wall residual stresses in an aged cast austenitic-ferritic steel pipe at the TIG weld centreline in the left and symmetrically 20 mm on both sides of the weld fusion line in the right column (Faure & Leggatt 1996). The axial stresses are in the upper and the hoop stresses in the lower row.

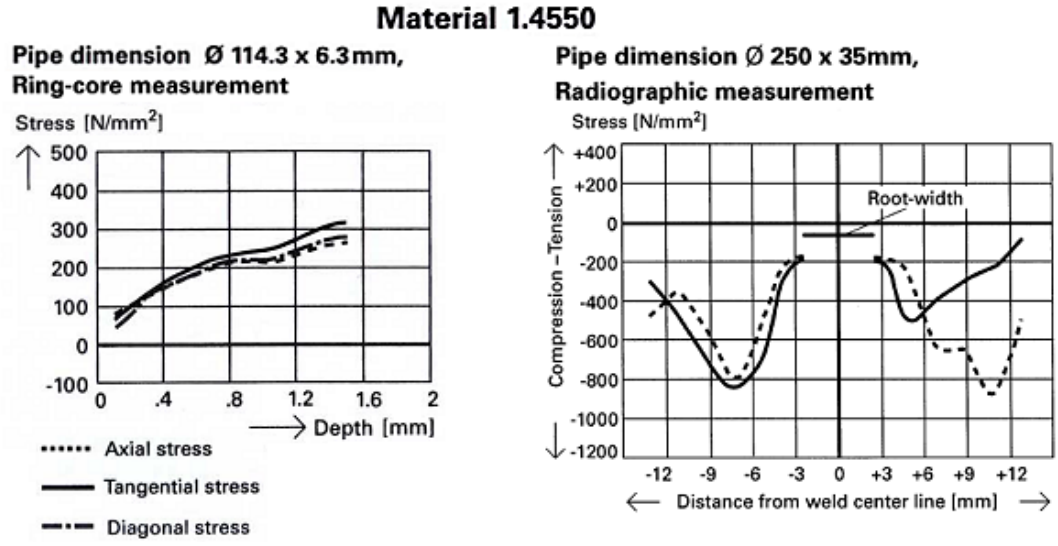

Figure 56. Residual stress distributions in NG welded AISI 347 piping as measured by ring core and XRD methods (Engelhard et al. 2000).

4.3 Handling stresses in the design process

A structure is loaded by the actual or true stress state. For the purpose of efficient handling in the design process, the actual stress can be classified into two broad categories: operational stresses and stresses related to fabrication. The former type of stresses refers to operation of the structure and is generally accounted for in the design process by numerical calculations or by following some design code. The latter refers to the residual stresses, which are induced into the structure during fabrication. Depending on the mode of failure to be assessed, the relative importance between the operational and residual stresses varies, and the assessment is carried out accordingly.

The actual stresses are a sum of the welding residual stresses, thermal stresses and the pressure, mass, and fit-up stresses as determined by the particular geometric and functional details of the individual structure. Peak welding residual stresses are known to vary with the details of weld metal deposition rate, and particularly with the structural size and shape, such as pipe diameter and wall thickness.

4.3.1 Operational stresses

The magnitude and direction of the operational stresses are structure-dependent and readily assessed, but are usually relatively low in components such as a reactor pressure vessel. If the operational stresses are dynamic, spectral or thermal, the design stresses are even lower to ensure an adequate safety margin. The main contributors to operating stresses are mechanical, such as normal, bending, torque, gravity, pressure, thermal, and seismic loads. In the design of thick-walled structures, typical for pressure vessels, the pressure load results in membrane stresses, whereas the other loads result also in bending stresses.

Details for calculating the stresses due to the variety of loads are provided in the design codes, but the rules are not provided for all types of loadings. Rules are usually provided for calculating stresses due to pressure, dead weight, thermal expansion and shock loading, such as earthquake. In addition, restrictions or limits on the allowable stress due to these loadings are provided. The designer is generally not allowed to ignore any applied load, but guidelines on how to deal with stresses caused by vibration, through-wall temperature gradients, or gradients through the cross-section of the pipe are out of the scope. In codes where no rules are provided, these effects are usually judged unimportant, as in the case of ANSI B31.1 power piping stress analysis.

4.3.2 Residual stresses

In addition to the residual stresses formed during fabrication, additional stresses, referred to as fit-up stresses, are introduced in the assembly of the components to larger structures. These residual stresses are due to differences in the elastic properties and discrepancies in the dimensions of the components that are, e.g., welded together.

Residual stresses due to welding, field fit-up, and cold work in manufacturing have traditionally not been included in the code-type stress analyses. The code calculations are aimed at protection against bursting or collapse of the piping systems, ensuring elastic cycling and shakedown of piping systems, and protection against failure by fatigue.

Residual stresses caused by the shrinkage of the weld are present in all pipe welds and HAZ's, but they are significantly smaller in small pipes than in large pipes, due to the greater quenching effect of the greater mass of large pipes. However, residual stresses are appropriately ignored in most piping design applications because of plastic shakedown, since the plasticity of metals limits the peak stresses that can persist in service.

The actual loading of a structure is the sum of the above-discussed operational and residual stresses. The actual or total load causes straining of certain sections in the structure to a level that is ensured by the design codes to be well below the critical level of the onset of irreversible deformation or damage. Thus, a critical strain (stress) level has to be exceeded for damage to take place. The most important contributing factor in the event of damage is an unanticipated and rare pile-up of the actual stresses in certain sections of the structure.

4.4 Assessing the actual stresses

The requirement to assess the residual stresses in austenitic stainless steel piping relates back to the early reports of an increased number of IGSCC incidents in boiling water reactor (BWR) piping in the end of the 1970's (Danko 1984). Cracking had been observed in the heat affected zones (HAZs) of girth welds in power plant piping made of AISI 304 stainless steel. These reports represent the beginning of vast research efforts in mitigating SCC of BWR piping systems. In 1979 a group of BWR utilities in the US and the Electric Power Research Institute (EPRI) started a national research and development program to solve the problem: the Boiling Water Reactor Owners Group (BWROG) Intergranular Stress Corrosion Cracking (IGSCC) Research Program. In 1981 the program reached an international level, when BWR utility owners in Sweden, Finland, Switzerland, Italy, Spain, Taiwan and India joined the program (Danko 1984).

The work on assessing and modifying the welding residual stresses was based on the observations that three factors required for IGSCC must be present simultaneously for cracking to occur. These factors are (i) a corrosive environment, (ii) a material susceptible to cracking and (iii) a tensile state of stress. Reports showed that, for several pipe sizes used in BWR piping, conventional welding generally produces a zone of tensile residual stresses in regions where IGSCC had been observed (Rybicki 1984).

Throughout the years the residual stresses in these butt-welded austenitic stainless steel pipings have been both analytically and numerically assessed. In addition, a large amount of work has been carried out to measure the residual stresses in actual welded piping, and several methods for inducing compressive residual stresses at the ID of the weldments in the piping have been investigated and developed. The residual stress measurements have primarily been executed on butt-welded austenitic stainless steel piping containing similar alloys on both sides of the weld. In the assessment of residual stresses in dissimilar metal welds, more efforts have been dedicated to theoretical studies than to actual measurements.

Two different approaches can be observed in the assessment of the actual stress state for structural components. The operational stresses have traditionally been dealt with in terms of analytical solutions, and design rules and the welding residual stresses have been assessed through generic residual stress models, which have been established by testing. With the enormous computing power available today, the numerical solutions to very complicated nonlinear problems in multidiscipline calculation can be obtained with reasonable effort. Thus, finite element analysis (FEA) is a tool that provides the means for predicting both the operational and the welding residual stresses. However, the results obtained must be critically evaluated, even if they usually seem to be “correct” at first glance. In fact, the results of the analyses depend strongly on the material model used, and the data provided for thermal and mechanical material properties.

The fundamental reason for assessing the actual stresses is the need for reliable calculation of crack growth rates, which is required to determine the remaining time of safe operation for the evaluated component. To illustrate this, an example of the assessment of welding residual and operational stresses by FEA in comparison to generic strength of materials analysis has been made by Dominion Engineering Inc. (Broussard et al. 2005). The analysed structure, shown in Figure 57, represents a butt-welded stainless steel piping to a low alloy steel pressurizer surge line nozzle, made using Alloy 82/182 filler metal and Alloy 182 buttering. An overview of the procedure for determination of crack growth rates in weldments is presented in Figure 58, which illustrates the option of the two approaches in the stress analysis step. The chart also points out the various tasks to be solved inside each step.

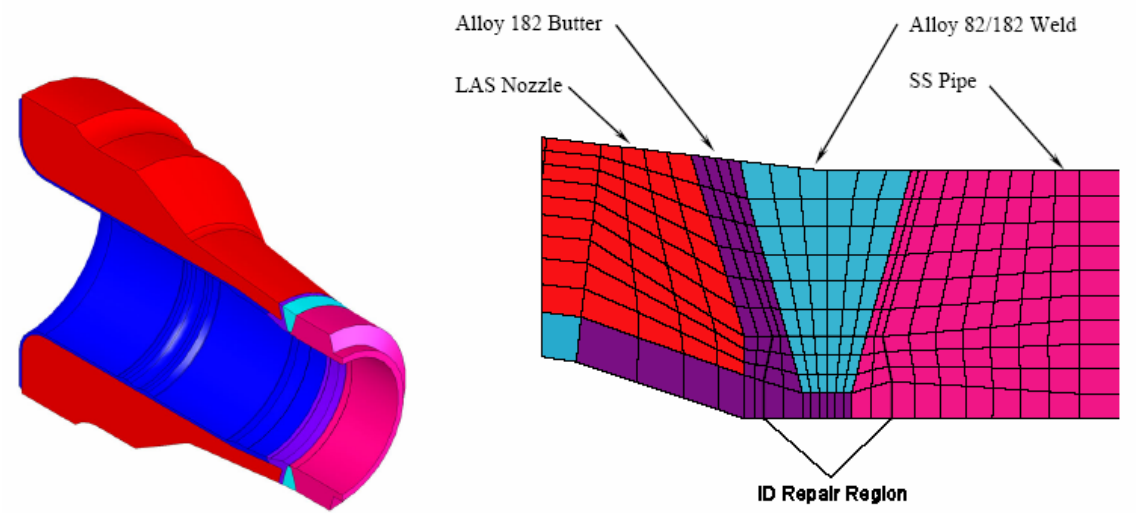

Figure 57. The finite element model of a typical weldment joining the pressurizer surge line nozzle to stainless steel piping (Broussard et al. 2005).

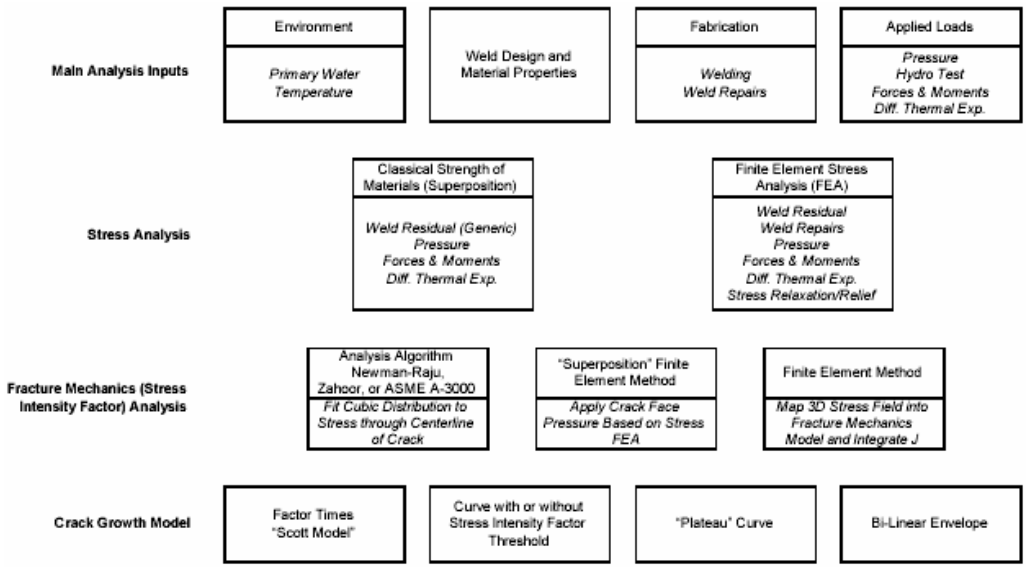

Figure 58. The flowchart of the analysis procedure for assessing crack growth rates in weldments (Broussard et al. 2005).

The study showed that there are clear differences between the conventional and numerical approach in the capability of quantifying welding residual stresses. To illustrate the difference in induced residual stresses between a complete 360º circumferential butt-weld, and a local weld repair, two FE analyses were carried out. The complete and the shorter partial-length circumferential welds are referred to as 360º and partial-length repairs, respectively.

In the as-designed weldments without repairs the generic welding residual stress model is conservative. However, both 360º and partial-length weld repairs from the inner diameter (ID) surface significantly increase the ID surface stresses, which may exceed

the stresses estimated by the generic model. In the case of partial-length outer diameter (OD) weld repairs, the through-wall stress distributions are similar to the partial-length ID ones. The high stresses created by partial-length repairs are limited to the repaired area, and local cracks limited to the repaired area can be anticipated. The welding residual stress study is summed up by the conclusion that the generic welding residual stress model underestimates the residual stresses estimated by FEA in repairs at the ID and in partial-length repairs at the OD surface. A comparison of the as-designed axial residual stress distribution to the ID and OD partial-length weld repair stress distributions are presented in Figure 59. In analyzing the differential thermal expansion stresses, the results can be overly conservative if the differential thermal expansion stresses are added by linear superposition. This can be avoided by FEA including actual material elastic-plastic properties to assess the actual stress levels. It can be concluded that the study illustrates the risk of using generic models, which have been established by testing for as-designed cases, when assessing the residual stresses of weld repairs in butt welding of piping (Broussard et al. 2005).

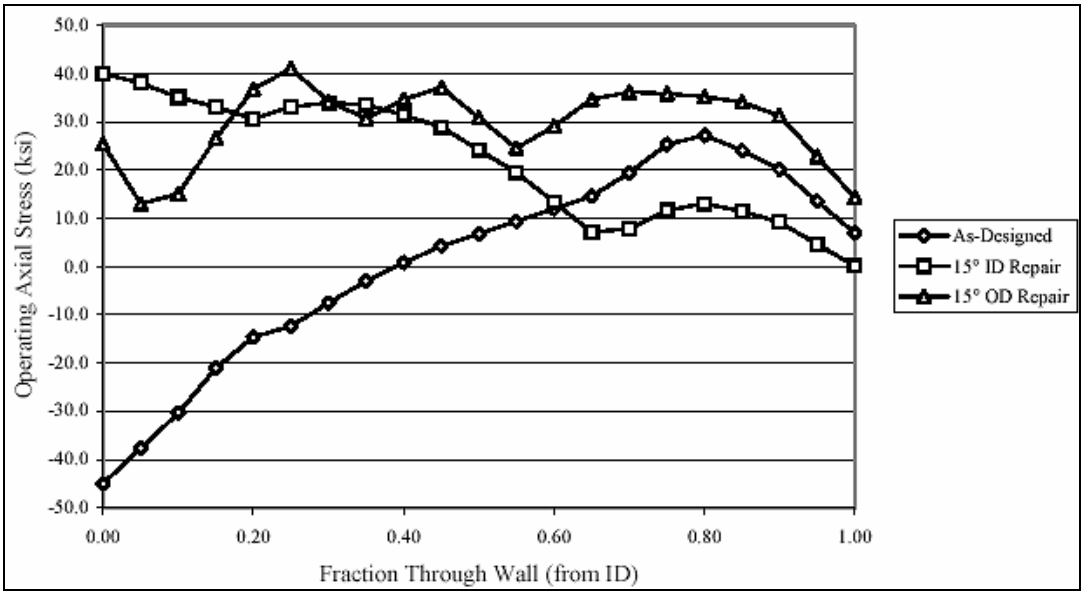

Figure 59. The axial residual stress distributions through the wall thickness after partial-length inner and outer diameter weld repairs compared to the as-designed case (Broussard et al. 2005).

4.5 Procedures for altering the residual stresses

The main processes used for altering the residual stresses caused by welding are based on mechanical or thermal processes. The aim of the treatment can be to reduce the overall tensile stress state or to create compressive stresses at a predefined site, such as the inner surface of a welded pipe. Processes primarily used in design, fabrication and installation to achieve this are, for example, solution annealing of stainless steels prior

to fabrication, limiting the amount of cold work after solution annealing heat treatment, and providing strict tolerances on all the welds in the field to minimize the fit-up stresses. However, to reduce the residual stresses in many welded structures, different post-weld heat treatments are required.

Several methods have been tested and developed for removing or redistributing tensile residual stresses through the years, and new ones are being investigated. Modifying the welding parameters and sequence is a widely used theme along with heat sink and mechanical methods. Danko (1990) has published a review of methods for altering the residual stresses in austenitic stainless steel piping. The common denominator in all methods is local plastic deformation, which alters the surrounding residual stress state. Heat sink welding (HSW), last pass heat sink welding (LPHSW), induction heating stress improvement (IHSI) and mechanical stress improvement process (MSIP) are four processes qualified for BWRs. Welding modifications, such as weld overlay (WOL) and weld inlay (WIL) have been studied and used successfully. However, the most effective method to reduce the stresses at a weld is to use narrow gap welding (NGW). This technique reduces residual stresses and allows welding using lower heat input, which reduces sensitization levels as well.

4.5.1 Welding methods

The local and transient feature of the high temperature field associated with any fusion welding procedure has made welding a suitable method for inducing plastic strain, which thereby modifies the residual stress state. For enhancing the temperature gradient, local cooling can be applied.

The heat sink welding (HSW) method relies on spraying a cooling medium, such as water or CO_2, on the inside welding surface during application of the outermost welding layers. Prior to this HSW, several welding layers have been applied without cooling in order to provide the structural strength of the pipe. The cooling creates compressive residual stresses on the pipe inside surface and partially through the wall. A slight modification of the HSW is LPHSW, where the cooling medium is not introduced until the last pass or deposition of the crown weld. In addition, high heat input is used in the last pass to enhance the temperature gradient across the wall thickness.

HSW has found only limited application in the repairs of IGSCC welds, due to the requirement for cooling water in the pipe. In addition, when the LPHSW was qualified for use, other residual stress mitigation methods were already available, which restricted its implementation (Danko 1990).

The use of WOL has become a short term repair method of AISI 316 welds that had experienced IGSCC. In the WOL process, a wider weld layer is built up on the outside diameter of the pipe, to restore the load carrying capacity of the underlying flawed pipe or weld. This overlay is applied without removal of the flawed material, which means that the system can remain water-filled (Danko 1990). Thus, the water present in the piping can work as a heat sink. As a result of the pipe shrinkage, favourable compressive residual stresses are introduced. However, exceptions to this conclusion have been found in large diameter thick-walled pipes. Results from residual stress measurements of WOL on AISI 304 piping have shown that compressive stresses develop at the inner surface (Yen et al. 1996). A serious disadvantage with the utilization of wide weld overlay, is the fact that the non-destructive testing of the weldments is then partly obstructed. The application of WOL has also been investigated for Alloy 52 (Newton 2005).

As a result of the extensive research work carried out on repair and mitigation techniques for dissimilar metal butt welds related to safe ends in NPPs, a large variety of procedures have been evaluated (Waskey 2005). In the pursuit of improving weld repairs, attempts have been carried out to repair welds from the inside by a procedure referred to as weld inlay (WIL). The driving force behind WIL is the need to prevent Alloy 182 from being in contact with the reactor coolant water. This is achieved by a WIL of the more corrosion resistant Alloy 52. A schematic drawing of the position of the WIL in the repair of a safe end is shown in Figure 60. The application of WIL has found use for both preventive reasons and repair, and is recommended for larger diameter piping. However, no quantitative measurements regarding the residual stresses were reported. A detailed overview of the beneficial and the unfavourable features associated with a selected range of mitigation methods for IGSCC was presented by Waskey (2005), and is shown here in Figure 61.

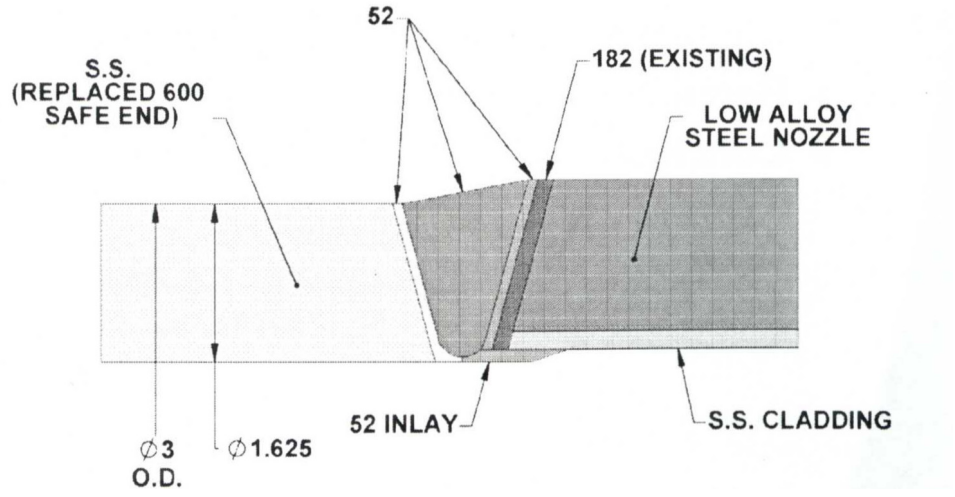

Figure 60. A schematic representation of WIL in a safe-end replacement (Waskey 2005).

	Pros	Cons
MSIP	• Places ID in compression • No pipe entry • Can be both mitigation and remediation technique • Can be performed in flooded condition • Can be life of plant repair • Offers shortest schedule	• Cannot be used if flaw is above predescribed length • Requires OD spatial envelope • Requires regulatory approval for DM welds • Not a repair option • Requires subsequent outage inspection to verify no flaw growth • Accurate profile required prior to MSIP to design device • Leaves flaw in place • Leaves flaw exposed to RCS water
Preventative Overlay	• Puts ID surface in compression • Can be wet or dry • Short schedule • Can provide life of plant repair • No subsequent outage flaw growth verification by UT	• Mitigation technique, i.e. no flaws • No Code rules – requires regulatory approval • Requires spatial envelope
Structural Overlay	• Can be wet or dry • Addresses compressive plus new structural boundary • Is both a mitigation and remediation technique	• Leaves flaw in place • Requires spatial envelope • Is more expensive and schedule intensive on larger diameter pipes • Requires subsequent outage inspections to show flaw has not grown into outer 25% of wall • No Code rules – requires regulatory approval
Inlay	• Permanently removes Alloy 182 from RCS interface • Represents lowest possible future inspection requirements • No OD spatial envelope needed • Lower dose • Shortest on component schedule for large pipes • Can remove flaw or optionally imbed a flaw • No regulatory approval required – unless flaw removal uses Ambient Temperature Temperbead welding	• Breach system – FME Concerns • Drain down requirement • Component accessibility challenges
Safe End Replacement (Spool Piece)	• Best for small pipes • Highest confidence for life of plant repair • No regulatory approval required	• Limited to smaller pipes based on cost and schedule • Requires drain down • FME concerns • Higher dose – location dependent

Figure 61. A list of the pros and cons for some selected IGSCC mitigation methods in comparison to safe-end replacement (Waskey 2005).

4.5.2 Induction heating methods

The induction heating stress improvement (IHSI) method was conceived and developed in Japan (Danko 1990). Applying local induction heating to the outside surface of the pipe weldment causes the surface temperature to rise. However, to achieve a great enough temperature gradient across the wall thickness, cooling of the inside surface is included in the IHSI. Typically, the surface is heated and kept at 500 to 550ºC by restricting the inside surface temperature to 100ºC by flowing water. In terms of the manner of cooling the inside surface, the method can be considered as a type of heat sink welding method. Small plastic strains are induced by the temperature gradient achieved across the wall thickness, and the residual stresses are altered. With this procedure initial tensile stresses at the inner surface can be modified to become compressive, as shown for the IHSI treated AISI 304 stainless steel pipe weldment, Figure 62.

The IHSI was first implemented in Japan in 1980, when an AISI 304 stainless steel piping was replaced. Since then it has been widely used in NPPs, and even in a number of new plants under construction (Danko 1990).

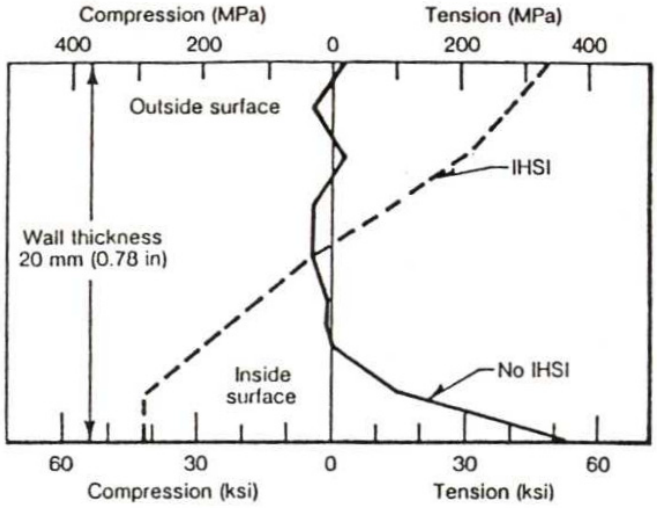

Figure 62. Residual stress distributions across the wall after application of IHSI to an AISI 304 piping weldment compared to the untreated case (Danko 1990).

4.5.3 Narrow gap welding

The development of narrow gap welding (NGW) has proven to be a powerful welding method for butt-weld applications in construction and repairing related to nuclear power plants (Lambs & Guigon 1998). The method has been successfully used in primary water circuit structures, such as safe ends and steam generators. The main advantages of the method lie in the improved quality of the welds, which is a result of lower volume of weld material, shorter welding times, lower ionisation radiation exposure, uniform root shape and improved material properties. All these features are obtained when the size of the groove is reduced. In many engineering cases the groove has had a bevel angle of 37½˚, but that has been reduced drastically in NGW, even down to 3˚ in some cases. Due to the change of the bevel angle, the total weld metal volume is reduced. The reduction in volume of the weld, welding time and energy consumption is accentuated with increased wall thickness, because of the dependence of power on the bevel angle.

Depending on the required productivity, NGW is primarily used in combination with two methods. When the primary objective of the welding procedure is a high deposition rate, submerged arc welding (SAW) is used, but when the most important concern is the high quality of the weld, gas tungsten arc welding (GTAW) is the choice (equivalent to tungsten inert gas or TIG welding). As a consequence of the above mentioned modifications to the groove dimensions, accurate control of the welding torch and parameters is required (Lambs & Guigon 1998). Therefore, NGW is in most cases automated.

The advantages following the reduction in the weld volume lead to less weld metal being applied and less opportunity for weld-related problems. Another fact is that, due

to the smaller volume of the weld metal, less weld metal shrinkage follows, and less distortion occurs. Thus, the narrow gap has a positive effect on the residual stresses as compared to the wider gaps. However, only limited information is available on the reduction of the residual stress state by NGW. Another indirect benefit of the narrow groove is that more stringent requirements are imposed on the fabrication of the groove, which in the end pays off as fewer ultrasonic geometric reflectors at the root of the weld (Lambs & Guigon 1998).

When comparing the NGW to the other stress improvement methods, which represent procedures carried out after the welding, it is obvious that NGW has a clear advantage, since no additional procedures are required. However, application of NGW alone does not seem to reliably provide a compressive residual stress at the weld root. Tests carried out on optimised NGW together with additional cover beads, such as in WOL, have clearly shown that compressive stresses are induced at the weld root and quite deep below the material surface, Figure 63 (Engelhard et al. 2000). That study also showed that the magnitude of the compressive stress at the weld root was increasing as the width of the applied cover beads increased.

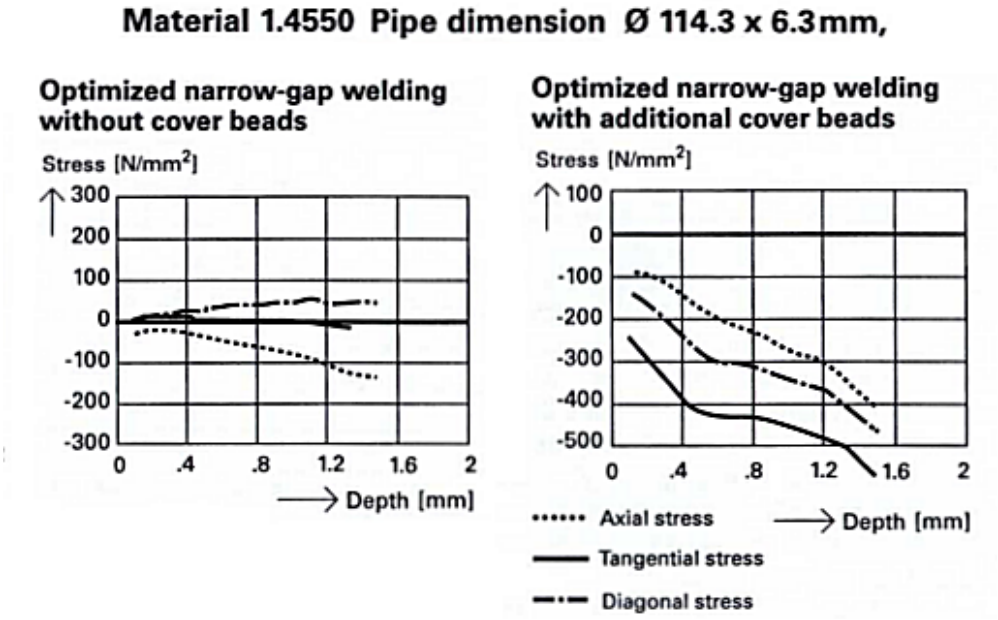

Figure 63. The influence of the variations in NGW process on the residual stresses at the weld root as measured by ring core method (Engelhard et al. 2000).

The improved mechanical properties of the welds obtained by NGW in comparison to traditional welding are, however, readily destroyed when repairing NG welds. Minimizing the deterioration of the mechanical properties during the repair of NG welds is a technically demanding task, and at the same time, the favourable residual stress state associated with NGW is also altered.

4.5.4 Mechanical stress improvement process

In the pursuit to mitigate stress corrosion cracking in operating reactor vessel head control rod drive mechanism CRDM penetrations, the mechanical stress improvement process (MSIP) has been patented and developed by AEA Technology Engineering Services, Inc. (Badlani & Damico 2005). The method relies on introducing small plastic strains to redistribute or remove the detrimental tensile residual stresses from the critical weld regions. Typical applications involve a slight circumferential contraction on one side of the pipe weldment. A variant involving axial contraction for application to the CRDM penetrations of the pressurised water reactor (PWR) reactor vessel head has also been developed. Figure 64 shows the principle of the MSIP.

The MSIP uses a mechanical tool, such as a clamping system, that is tightened circumferentially around the pipe in the direct vicinity of the weld during welding. Applying the load creates a concave contour at the weld location, and results in a corresponding reduction in the pipe circumference. After the removal of the clamping system, the weldment remains in axial compression through about half of the wall, and is protected by a layer of compressive hoop stress that extends almost through the whole wall. The most important factors that have promoted the use of MSIP are that the application is straight-forward and fast, there is no need for accurate control of the process parameters, and no requirement for cooling media, as required in HSW and IHSI (Engelhard et al. 2000).

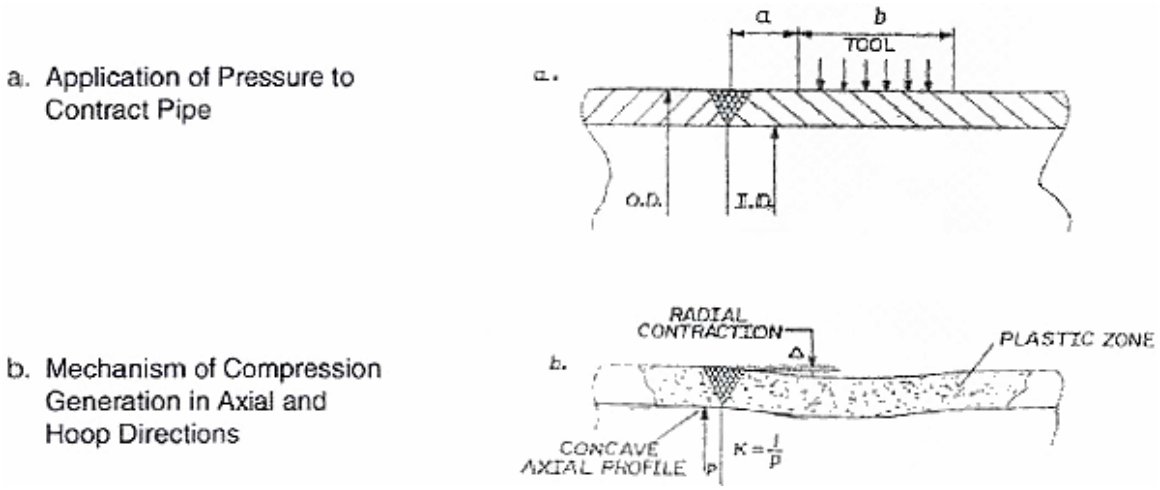

Figure 64. The principle of MSIP for stress improvement, showing the position, where for instance a hydraulically operated mechanical clamp is applied to contract the pipe on one side of the weld (Badlani & Damico 2005).

4.5.5 Laser peening

Laser shock peening (LSP) or simple laser peening (LP) is a surface treatment method which has evolved from the conventional shot peening process, and many variations of the LP concept has been developed through the years. The method has been used commercially in the aeronautics industry, with the first application being for GE aircraft engines in 1997 (Demma 2005). The method uses a pulsed high energy laser beam to generate shock waves that induce plastic deformation in the near surface regions of the target material. As a result large compressive residual stresses are formed in a layer, typically over 1 mm deep. The peening intensity is more exactly controlled in LP than in conventional shot peening, where an indication of the intensity is determined according to the Almen type gage. Additionally, LP results in a smoother surface finish.

In the early development of LP, the energy output of the laser pulse reached tens of Joules. In these applications, it was found that restricting the free expansion of the laser generated plasma by a transparent protective coating, such as paint or tape, enhanced the amplitude of the stress waves, which in turn improved the compressive stress layer (Montross et al. 2002). However, the requirement for a surface coating and drainage of the vessel prevented the utilisation of the technique in NPPs. This restriction pushed the development towards laser peening systems where the pulse energy is low, around 100 mJ, and no protective layer is required. In this system, the high peak power required to create a compressive layer is obtained through short pulse lengths in the ns range (Sano 2005). Toshiba has developed such a laser peening procedure without the protective layer, which has been implemented for the first time in Japanese NPPs in 1999 for mitigating SCC (Sano 2005). A schematic presentation of the basics of LP without a protective layer is shown in Figure 65, along with the residual stress depth profiles in un-peened and laser peened AISI 304 plates. Another important feature of the developed process is the reduction of the laser light wavelength from infrared (λ = 1.06 μm) to green (λ = 532 nm), which has a much lower absorption in water. This means that the process works in water, which enables treatment of inner surfaces of the pressure vessel without drainage of the water. The developed system uses a laser peening unit attached to a robot, which can be operated inside the pressure vessel to reach the desired structures with very high accuracy.

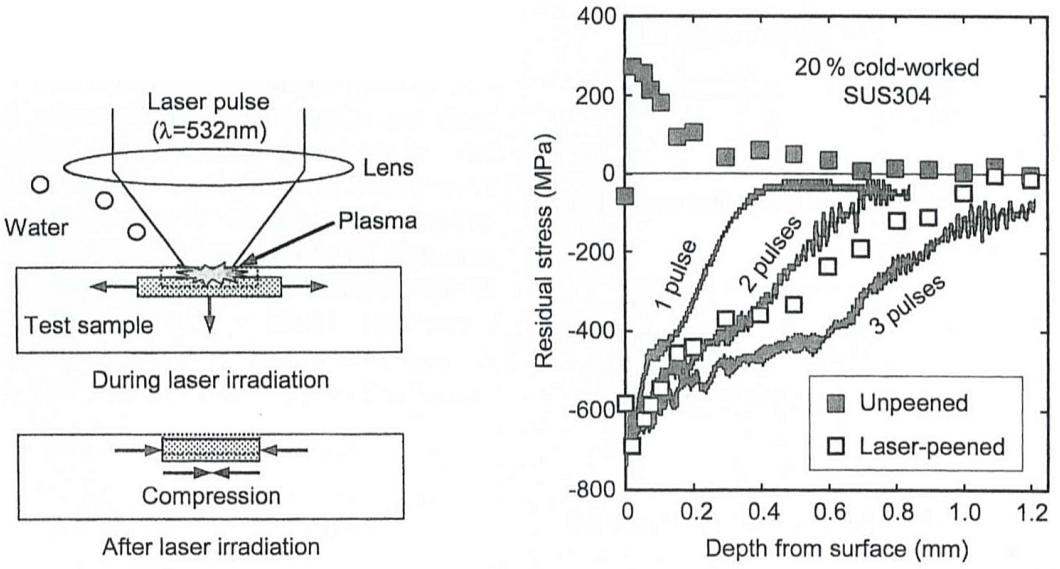

Figure 65. A schematic presentation of laser peening without protective layer and an example of the residual stress depth profiles in un-peened and laser peened AISI 304 plates (Sano 2005).

Laser peening, currently under development at Lawrence Livermore National Laboratory (LLNL), induces compressive residual stresses on the surface of the weld. The concept of LP with a protective layer is presented in Figure 66 along with the compressive residual stress distribution resulting from laser peening. In the US design of nuclear waste containers, SCC due to residual stresses at or near the closure weld of Alloy 22 is currently thought to be a likely waste package failure mechanism. To rule out SCC, stress mitigation techniques such as laser peening and induction annealing will be used for the dual lid closure welds in the spent-fuel nuclear waste canisters.

All but the closure weld will be solution annealed with a slow cooling rate to increase the depth of the compressive residual stresses on the outer surface. The importance of knowing the residual stresses induced by LP in Alloy 22 welds has resulted in both numerical and actual measurement studies. DeWald et al. (2004) have been studying the effect of LP parameters and number of peening layers on the residual stress state in Alloy 22 welds with both crack compliance and contour methods. All tested combinations resulted in compressive stresses, even though there were variations in the number of layers and processing time. Thus, it is important to find the acceptance criteria such that peening can be carried out economically (Wong 2001, DeWald et al. 2004).

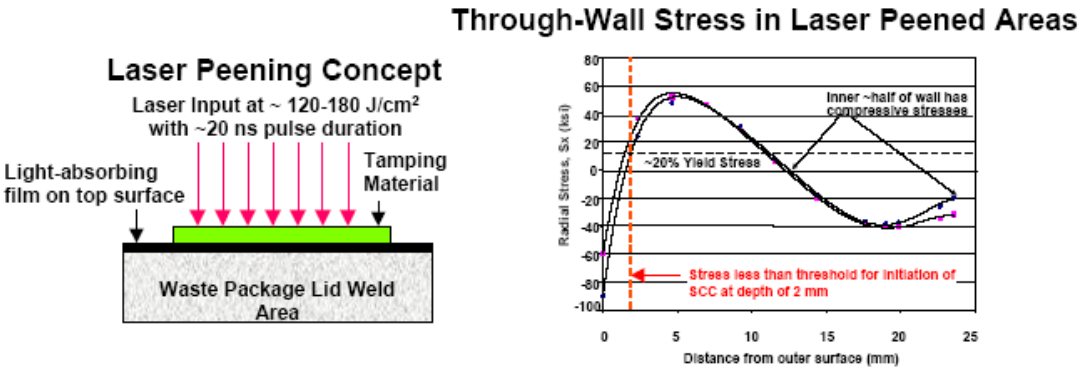

Figure 66. The concept of LP with a light-absorbing protective layer and an example of the obtained compressive residual stress profile (Wong 2001).

4.5.6 Water jet peening

Another method based on the peening principle has originally been developed by Mitsubishi Heavy Industries and Hitachi Ltd for mitigating IGSCC (Elder & Taniguchi 2005). The water jet peening (WJP), cavitation shotless peening (CSP) or simply cavitation peening (CP) is a procedure based on a high pressure jet flow peening of the material surface (Payne & Levesque 2005). The method uses only water with no foreign materials as shots, and there is no heat input. The power of the method is actually in the collapse of the cavitation that creates the high impact pressure, around 1000 MPa, which in turn causes the material surface to deform plastically. As the plastically deformed material is constrained elastically compressive residual stresses are induced in the surface layers. The typical features of the WJP process are presented in Figure 67.

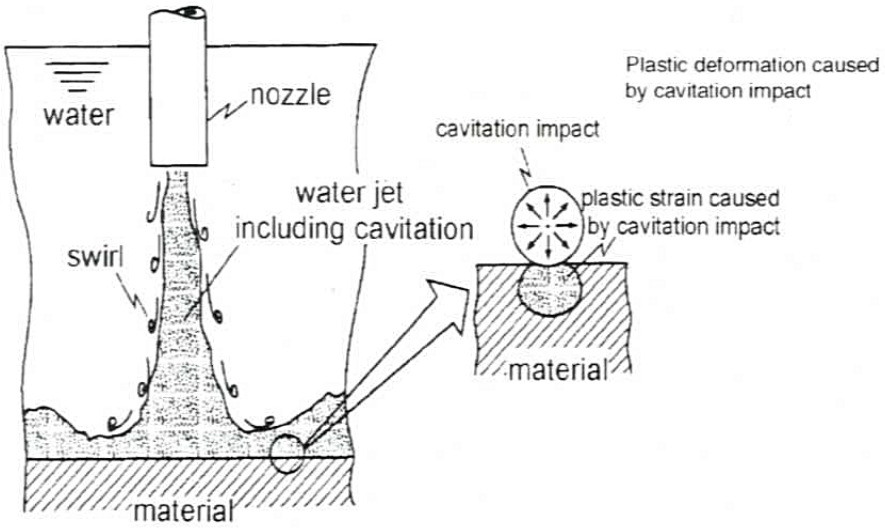

Figure 67. A schematic presentation of the WJP process (Elder & Taniguchi 2005).

WJP has been used in Japan for BWR internals, such as core shroud welds and bottom mounted instrument (BMI) nozzles for the purpose of IGSCC mitigation (Elder & Taniguchi 2005). Another example of materials and welds treated with WJP are nickel-base alloys Inconel 600 and 182. Depending on the process parameters, the induced stress stays compressive up to 400 μm beyond the material surface. As a result of the good results obtained by the WJP method Hitachi has developed technology and equipment for other BWR internals. An example of residual stress distributions obtained with LP and WJP processes is presented in Figure 68.

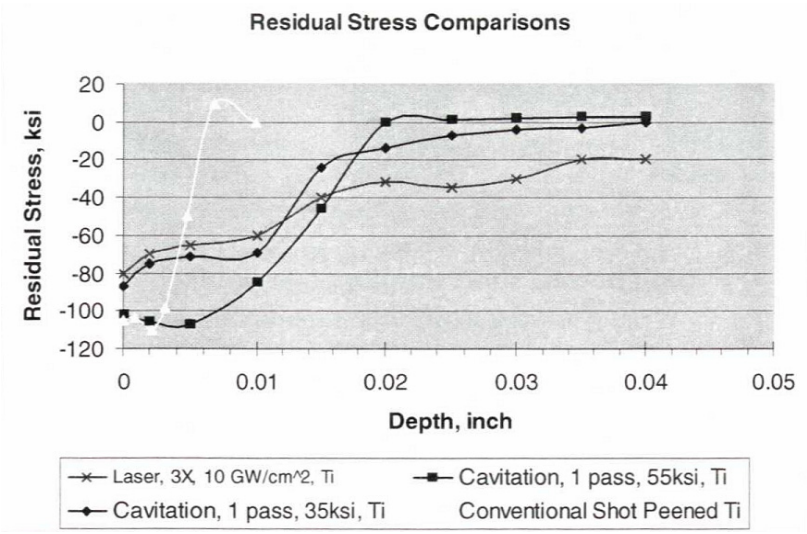

Figure 68. The compressive residual stress distributions obtained by LP and WJP in comparison to conventional shot peening (Payne & Levesque 2005).

4.6 Strain measurement by EBSD

Scanning electron microscopes (SEM) equipped with sophisticated data acquisition and analysing systems based on Electron Backscatter Diffraction (EBSD) enable improved materials characterization, in terms of microstructure, crystallography and micro-chemistry. The acquisition system contains a digital camera for recording the small angle diffraction lines, commonly referred to as Kikuchi lines. The lines are simply intensity maxima created by the constructive interference of the backscattered electrons. The analysing software processes the obtained data and solves for the crystallographic structure satisfying the obtained diffraction line pattern.

In recent years, development trends in EBSD have turned towards analyses of residual plastic strain in wrought alloys. This can be achieved in two ways: by measuring the quality of the diffraction pattern or by determining the rotation of the diffraction pattern (Young et al. 2003). The latter method has proven to be more reliable for quantitative analysis of residual plastic strain than the previous one.

Young et al. (2003) studied the residual strains in highly constrained, multipass dissimilar metal GTAW welds using EBSD. The specimen was fabricated of Alloy 82 (I and II) weld butter layers on a low carbon steel plate. Finally, the dissimilar metal weldment was completed by narrow-gap (NG) welding of Alloy 82 to an Alloy 690 plate. The configuration of the welded specimen is shown in Figure 69, and the results of the study are shown in Figure 70. The EBSD parameter studied was the average intra-grain misorientation over all grains for a given region, i.e. the "amis" value. The study showed that the "amis" value quantifies the extent to which dislocation sub-cells rotate the internal lattice orientation with respect to the neighbouring sub-cells, and hence the electron diffraction pattern. It was shown that a linear relationship describes the correlation between the plastic strain and "amis" parameter.

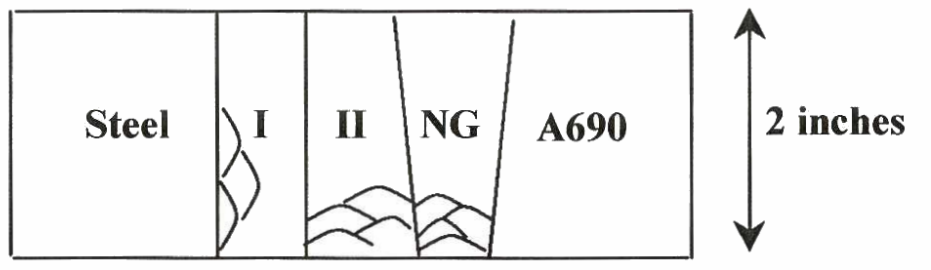

Figure 69. Schematic drawing of the weldment investigated by EBSD. The joint consisted of two types of Alloy 82 buttering (I and II) and a narrow-gap weld (NG) for joining a low carbon steel plate to an Alloy 690 plate (Young et al. 2003).

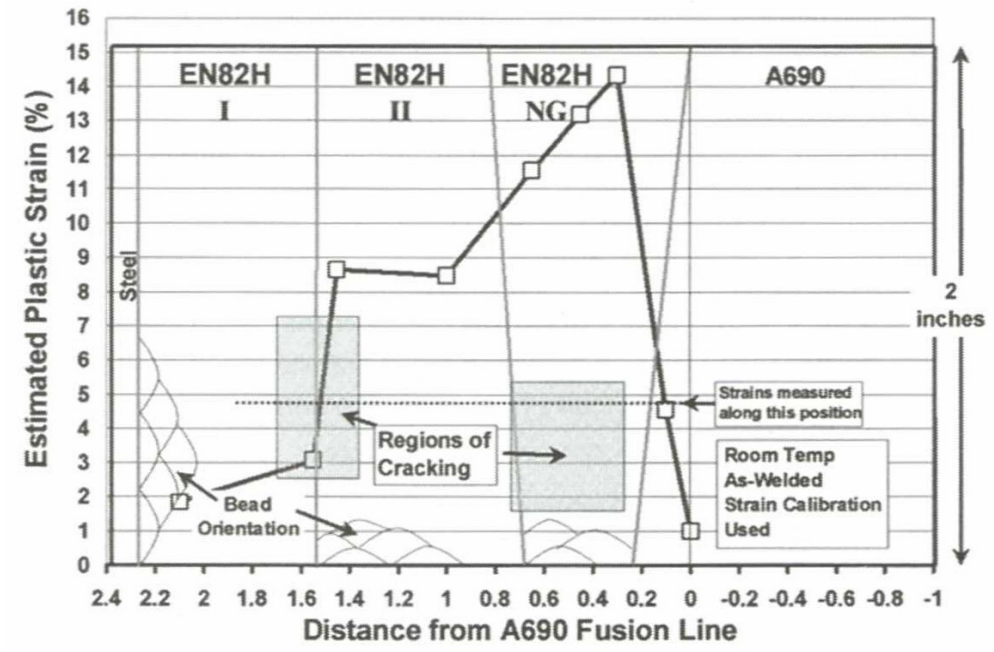

Figure 70. Graph of plastic strain superimposed on the cross-section of the studied weldment showing the correlation between regions of observed weld cracking and plastic strain determined by EBSD (Young et al. 2003).

Furthermore, the correlation between the “amis” parameter and plastic strain was shown to be insensitive to weld orientation in the range of 1 to 20% uniaxial tensile strain at temperatures of 20˚C and 540˚C. However, at a temperature of 980˚C, where recrystallisation occurs, the correlation was poor.

Another study of strain measurement in Alloy 182/Alloy 600 weldments by EBSD has been reported by Morra et al. (2005). The study is related to an ongoing international EAC round robin program, where the capabilities of EBSD for mapping of plastic strain were demonstrated in addition to the general characterisation of the weld microstructure, such as phase distributions and segregation.

4.7 Relaxation of residual stresses

In the assessment of the residual stress distributions, the possible relaxation of the residual stresses by post processing of the welds or during service operation has to be taken into account. It is a generally known fact that there are three primary sources for residual stress redistribution or relaxation.

The first source of residual stress relaxation is related to irradiation effects, which have been studied for several stainless steels and nickel-base alloys. The results showed that exposure to a high neutron fluence level corresponding to over ten effective full power years (EFPY) causes the residual stress to relax by 30% (Danko 1990).

The second source of residual stress relaxation is due to thermal effects. It is well known that prolonged holding or operating times at elevated temperatures causes residual stresses to relax. At the BWR operating temperature of 288°C the relaxation of residual stresses is small and further relatively small compared to irradiation related relaxation. Even though the operating temperature of a PWR is around 50°C higher than that of a BWR, the thermal relaxation effect remains small. Relaxation of the residual stresses requires higher temperatures, where the yield strength drops below the residual stress and plastic flow occurs. A controlled reduction in the magnitude of the residual stresses is obtained when applying a post-weld heat treatment to the structure. The time and temperature are primarily determined by the alloys.

In the third case, a static or dynamic mechanical load is applied to cause local plastic yielding, which redistributes the residual stresses. Lopez Martinez et al. (1997) have studied the effect of static and spectrum loading on the residual stresses in weldments. As the place of the highest tensile residual stress, i.e. the weld toe is close to the yield point of the metal, a tensile load causes the weld toe stress to exceed the yield point and local plastic deformation takes place. To compensate for the reduction in load carrying

capacity of the weld toe, the surrounding stress field changes to accommodate the load increase. As the applied load is removed, the residual stress distribution has been altered and the highest tensile stresses have been reduced.

4.8 Numerical modelling of residual stresses in dissimilar metal welds

The residual stresses in the dissimilar metal welds appear to be the dominating source of loads driving PWSCC, and thus have a decisive role in crack growth. Unfortunately, the direct measurement of residual stresses is difficult. Consequently strong effort has been made to estimate the residual stresses by numerical modelling, primarily using finite element method (FEM).

To correctly predict the residual stresses of the dissimilar metal weld, an elastic-plastic analysis of the whole manufacturing history, i.e. all manufacturing operations contributing significantly to the final residual stresses, has to be carried out. Namely, the analysis should include the welding operations, post-weld heat treatments and possible repair operations done. The analysis is, thus, very demanding and the results are difficult to verify.

Numerical analyses of the residual stresses in dissimilar metal welds have been recently reported by Fricke et al. (2001), Hunt et al. (2003), Rudland et al. (2003), Broussard and Gross (2003), Broussard et al. (2005) and Wilkowski et al. (2005).

Fricke et al. (2001) report development of a FE-model and code for analyzing residual stresses of an austenitic butt weld with different welding procedures. Interestingly, this analysis also included comparison to published experimental results on residual stresses (Figure 71) and axial shrinkage. Furthermore, the analysis included the effect of estimated operational cycles and showed the reduction of residual stresses caused by them (Figure 72). The development of computing capacity has been significant in recent years, and some of the compromises made in the analysis in order to obtain reasonable computing times (for example, the choice of a low order element) is no longer necessary. Consequently, although this analysis is less than 5 years old, it is already outdated in some respects.

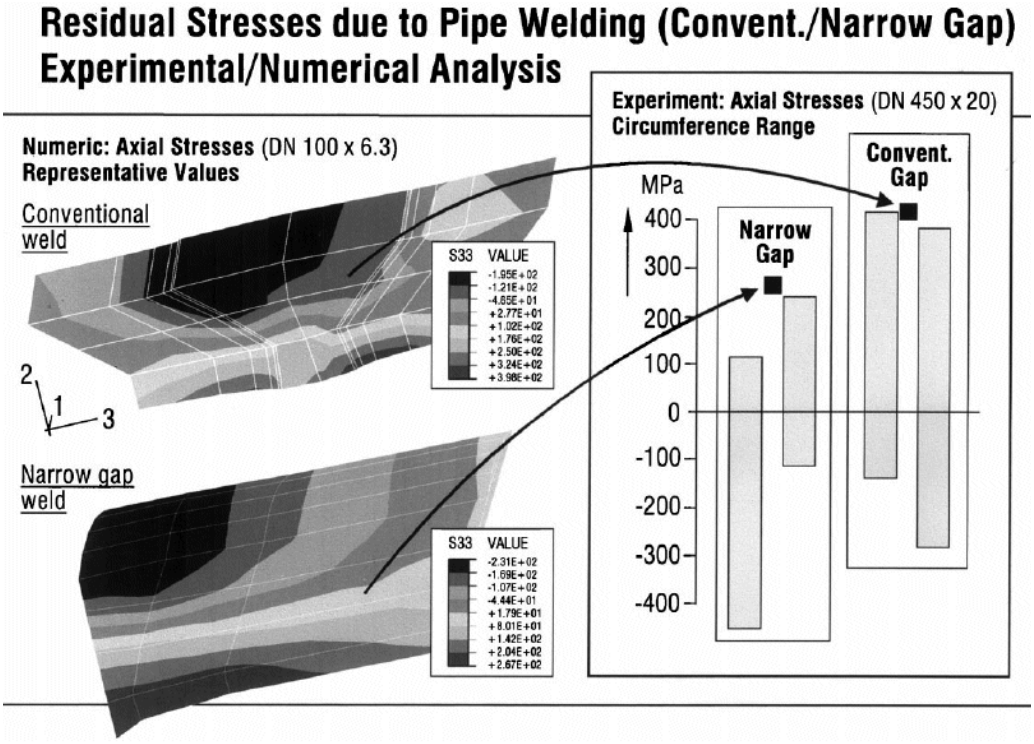

Figure 71. Residual stresses calculated by FEA as compared to experimental measurements (Fricke et al. 2001).

Hunt et al. (2003) explored the possibility of reducing dissimilar metal weld residual stresses by OD weld overlay. The target case was the PWSCC cracks discovered in RPV inlet and outlet nozzles to primary coolant pipe butt welds at the V.C. Summer and Ringhals PWR plants. The FEM analysis included thermal and stress analyses for each weld pass, in a manner similar to that reported by Broussard et al. (2003). The result of this analysis was that the as-designed dissimilar metal weld contains reasonable tensile residual hoop stresses at ID (62 MPa) while in-service. A partial-arc ID repair weld increases the stresses up to 496 MPa. By applying a weld overlay to outside of the nozzle, the in-service stresses decreased to –160 MPa and 138 MPa, respectively.

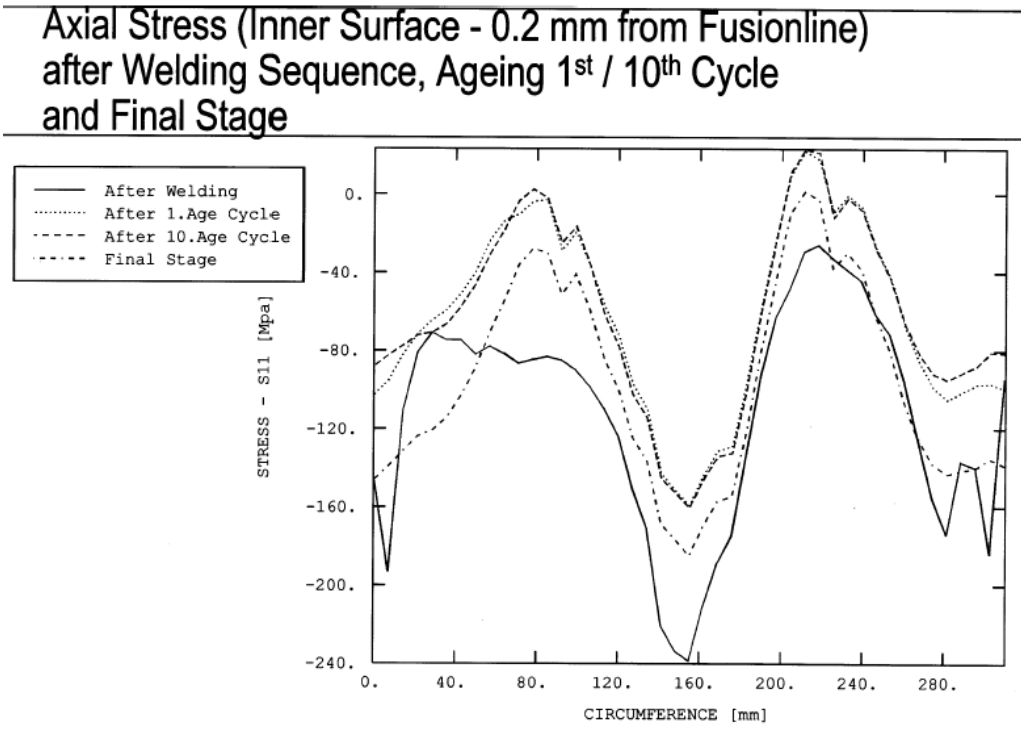

Figure 72. The effect of operational aging cycles on residual stresses (Fricke et al. 2001).

Rudland et al. (2003) analyzed the J-groove weld in a CRDM. They noted that the as-welded stress states depend primarily on the weld size and strength level of the tube material. Hoop stresses increase with increasing weld size, whereas in the longitudinal direction the stresses decrease with the increasing weld size.

Broussard et al. (2003, 2005) noted that, for large crack sizes the residual stresses are mostly relieved and the K-level is mostly caused by the pressure load. It was concluded, that the stress intensities calculated without taking stress relaxation into account can be overly conservative, and using FEA to calculate the J-integral was recommended instead. The J-based FE-analysis for structures containing residual stresses is, however, very laborious.

Wilkowski et al. (2005) summarized several recent efforts, including modelling of residual stresses in dissimilar metal welds, and this analysis reflects the current state-of-the-art in this application. Figure 73 shows the residual stress distributions predicted for a dissimilar metal butt weld. Figure 74 shows the residual stresses predicted in the CRDM J-groove weld configuration.

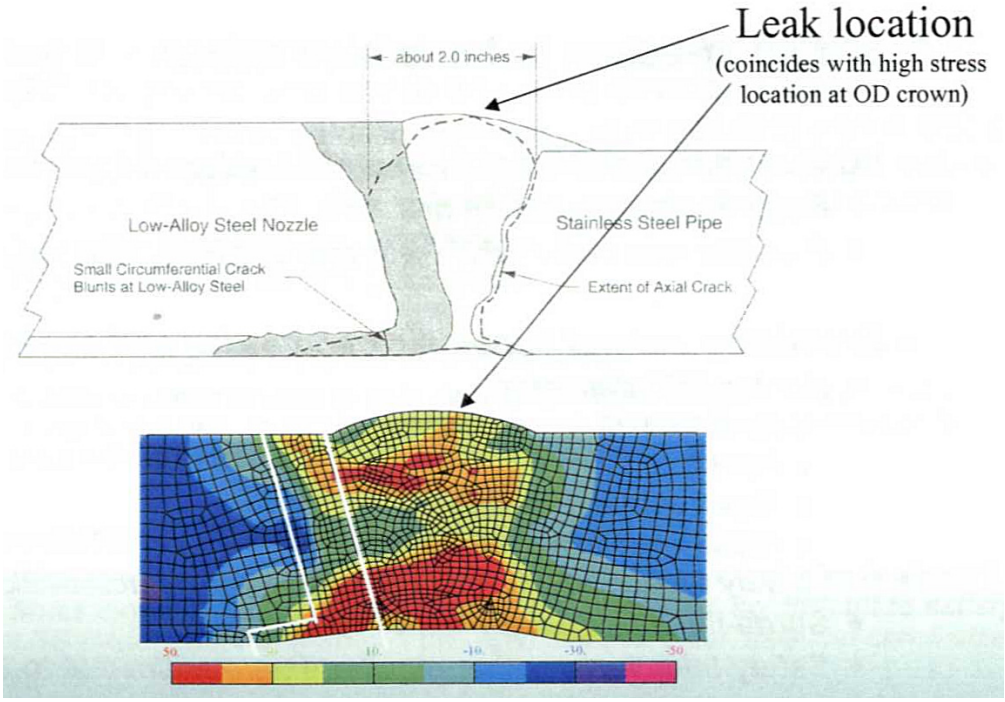

Figure 73. Residual stress distributions in a dissimilar metal butt weld reported by Wilkowski et al. (2005).

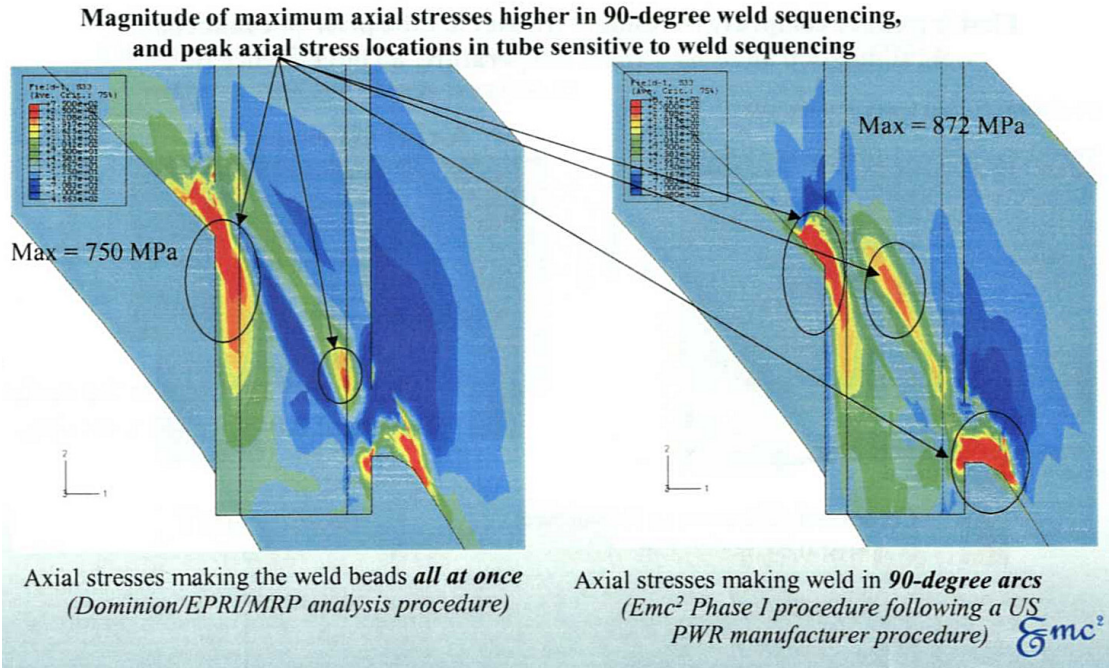

Figure 74. Residual stresses in the CRDM J-groove weld configuration reported by Wilkowski et al. (2005).

In summary, the recently published analyses show high residual stresses in the dissimilar metal weld material, as expected, and emphasize the significance of residual

stresses as a driving force of the PWSCC failures reported. Weld repair is also shown to increase the residual stresses. The analyses differ in choice of material model used (e.g., monotonic stress-strain curves, cyclic stress-strain curves and elastic-perfectly plastic behaviour were reported) and the amount of manufacturing details included in the analysis (weld beads, heat treatments and shrink fit).

4.9 References

ANSI B31.1 Code for Pressure Piping.

ASM. 2002. Thermal Properties of Metals – ASM Ready Reference. Edited by Cverna, F. ASM International, 2002. Metals Park, Ohio, USA. 560 p.

Badlani, M. & Damico, T. 2005. The Applicability of MSIP™ for Mitigating PWSCC in Pressurizer Nozzle to Safe-End Welds. EPRI International PWSCC of Alloy 600 Conference. Hyatt Regency Tamaya Resort, Santa Ana Pueblo, New Mexico, USA, 7–10 March 2005. 25 p.

Broussard, J. & Gross, D. 2003. Welding Residual and Operating Stress Analysis RPV Top and Bottom Head Nozzles. Vessel Head Penetration Inspection. Cracking and Repair Conference, Gaithersburg, USA. To be published.

Broussard, J. E., White, G. A. & Hunt, E. S. 2005. Finite-Element Analysis of Welding Residual Stresses in Piping Butt Weldments and Their Effect on Crack Tip Stress Intensity Factors. EPRI International PWSCC of Alloy 600 Conference. Hyatt Regency Tamaya Resort, Santa Ana Pueblo, New Mexico, USA, 7–10 March 2005. 33 p.

Christian, H., Elfinger, F. X. & Schüller, H. J. 1978. Eigenspannungen in Schweiß-nähten und ihre Auswirkungen. VDI-Berichte, Nr. 313, pp. 237–244.

Danko, J. C. 1984. Overview of the Boiling Water Reactor Owners Group Research and Development Program. Proceedings of Second Seminar on Countermeasures for Pipe Cracking in BWRs. EPRI NP-3684-SR, Vol. 1: Problem Resolution, Ch. 1, pp. 1–11.

Danko, J. C. 1990. A Review of Weld Residual Stresses in Austenitic Stainless Steel Pipes. Recent Trends in Welding Science and Technology. Proceedings of 2nd International Conference, Gatlinburg, TN, 14–18 May 1989. Pp. 113–118.

Demma, A. 2005. Laser Peening: A Surface Stress Improvement Technique for Alloy 600 PWSCC Mitigation. EPRI International PWSCC of Alloy 600 Conference. Hyatt Regency Tamaya Resort, Santa Ana Pueblo, New Mexico, USA, 7–10 March 2005. 18 p.

DeWald, A. T., Rankin, J. E., Hill, M. R., Lee, M. J. & Chen, H.-L. 2004. Assessment of Tensile Residual Stress Mitigation in Alloy 22 Welds Due to Laser Peening. Journal of Engineering Materials and Technology, Vol. 126, pp. 465–473.

Elder, G. G. & Taniguchi M. 2005 Mitigation of PWSCC on Reactor Vessel Bottom Mounted Nozzles by Waterjet Peening. EPRI International PWSCC of Alloy 600 Conference. Hyatt Regency Tamaya Resort, Santa Ana Pueblo, New Mexico, USA, 7–10 March 2005. 16 p.

Engelhard, G., Habip, L. M., Pellkofer, D., Schmidt, J. & Weber, H. 2000. Optimization of Residual Welding Stresses in Austenitic Steel Piping: Proof Testing and Numerical Simulations of Welding and Postwelding Processes. Nuclear Engineering and Design, Vol. 198, pp. 141–151.

Faure, F. & Leggatt, R. H. 1996. Residual Stresses in Austenitic Stainless Steel Primary Coolant Pipes and Welds of Pressurized Water Reactors. International Journal of Pressure Vessel and Piping, Vol. 65, pp. 265–275.

Fricke, S., Keim, E. & Schmidt, J. 2001. Numerical Weld Modeling – A Method for Calculating Weld-Induced Residual Stresses. Nuclear Engineering and Design, Vol. 206, pp. 139–150.

Hunt, S., Broussard, J., Ahnert, S., O'Regan, P. & Covill, D. 2003. Weld Overlay to Reduce Tensile Stresses in Alloy 82/182 Butt Welds. Vessel Head Penetration Inspection, Cracking and Repair Conference, Gaithersburg, USA. To be published.

Kloos, K. H. 1979. Eigenspannungen, Definition und Entstehungsursachen. Zeitschrift für Werkstofftechnik, Vol. 10, pp. 293–302.

Kloos, K. H. & Kaiser, B. 1991. Residual Stresses Induced by Manufacturing. In: Hauk, V., Hougardy, H. & Macherauch, E. (Eds.). Residual Stresses Measurement, Calculation, Evaluation. DGM Informationsgesellschaft mbH, Oberursel. Pp. 205–226.

KTA 3201.2. 1998. Components of the Reactor Coolant Pressure Boundary of Light Water Reactors Part 2: Design and Analysis. Nuclear Safety Standards Commission KTA. 162 p.

Lambs, R. & Guigon, J.-P. 1998. Narrow Gap Repair Welding in Nuclear Power Plants. Welding and Metal Fabrication, October, pp. 21–22.

Lopez Martinez, L., Lin, R., Wang. D. & Blom. A. F. 1997. Investigation of Residual Stresses in As-Welded and TIG-Dressed Specimens Subjected to Static/Spectrum Loading. Welded High-Strength Steel Structures, Proceedings, First North European Engineering and Science Conference (NESCO 1). Stockholm, Sweden, 8–9 October 1997. Pp. 377–390.

Macherauch, E., Wohlfahrt, H. & Wolfstieg, U. 1973. Zur zweckmässigen Definition von Eigenspannungen. Härterei-Technische Mitteilungen, Vol. 28, pp. 201–211.

Masubuchi, K. 1993. Residual Stresses and Distortion. Metals Handbook. 10th ed. Vol. 6, Welding, Brazing, and Soldering. ASM. Pp. 1094–1102.

Montross, C. S., Wei, T., Ye, L., Clark, G. & Mai, Y.-W. 2002. Laser Shock Processing and its Effects on Microstructure and Properties of Metal Alloys: A Review. International Journal of Fatigue, Vol. 24, pp. 1021–1036.

Morra, M., Othon, M., Andersen, P., Nelson, L. & Peluso, L. 2005. Alloy 182/Alloy 600 Weldment Characterization Measuring SCC Growth Rates in Alloy 182. ICG-EAC 2005 Conference. Antwerp, Belgium, 10–15 April. 60 p. Personal communication.

Newton, B. 2005. Advances in Design and Implementation of Alloy 52 Structural Weld Overlay Repair Welding. EPRI International PWSCC of Alloy 600 Conference. Hyatt Regency Tamaya Resort, Santa Ana Pueblo, New Mexico, USA, 7–10 March. 15 p.

Payne, R. & Levesque, S. 2005 Application of Surface Stress Improvement for the Mitigation of Alloy 600 PWSCC. EPRI International PWSCC of Alloy 600 Conference. Hyatt Regency Tamaya Resort, Santa Ana Pueblo, New Mexico, USA, 7–10 March. 22 p.

RCC-M. 2000. Design and Construction Rules for Mechanical Components of PWR Nuclear Islands Section I – Sub-section Z: Technical Appendices. French Association for Design, Construction and In-Service Inspection Rules for Nuclear Island Components AFCEN. 40 p.

Rudland, D., Wilkowski, G., Wang, Y.-Y. & Norris, W. 2003. Analysis of Weld Residual Stresses and Circumferential Through-Wall Crack K-solutions for CRDM Nozzles. Vessel Head Penetration Inspection, Cracking and Repair Conference, Gaithersburg, USA. To be published.

Rybicki, E. F. 1984. Analytical Considerations for Stress Related Remedies. Proceedings of Second Seminar on Countermeasures for Pipe Cracking in BWRs. EPRI NP-3684-SR, Vol. 2: Remedy Development, Ch. 7. Pp. 1–15.

Sano, Y. 2005. Laser Peening: An Innovative Tool to Enhance Structural Integrity Against Fatigue and Stress Corrosion. Proceedings of the 2nd International Symposium on Mechanical Science Based on Nanotechnology. Sendai International Center, Sendai, Japan, 21–22 February. Pp. 81–84.

Shack, W. J. 1984. Measurement of Throughwall Residual Stresses in Large-Diameter Piping Butt Weldments Using Strain-Gauge Techniques. Proceedings of Second

Seminar on Countermeasures for Pipe Cracking in BWRs. EPRI NP-3684-SR, Vol. 2: Remedy Development, Ch. 8. Pp. 1–22.

Waskey, D. 2005. Assessment of Repair/Remediation/Mitigation Techniques for Dissimilar Metal Butt Welds. EPRI International PWSCC of Alloy 600 Conference. Hyatt Regency Tamaya Resort, Santa Ana Pueblo, New Mexico, USA, 7–10 March. 19 p.

Wilkowski, G., Rudland, D., Cheng, W., Chen, Y., Wang, Y., Scott, P. & Brust, F. 2005. Summary of NRC Funded Efforts Involving Alloy 600 Base Material and Weldments for Piping and CRDM Applications. EPRI International PWSCC of Alloy 600 Conference. Hyatt Regency Tamaya Resort, Santa Ana Pueblo, New Mexico, USA. 7–10 March. 36 p.

Wolf, H. & Böhm, W. 1971. Das Ring-Kern-Verfahren zur Messung von Eigenspannungen und seine Anwendung bei Turbinen und Generatorwellen. Archiv für das Eisenhüttenwesen, Vol. 42, No. 3, pp. 195–200.

Wong, F. M. G. 2001. Strategies and Demonstration Activities for Stress Mitigation Techniques to Minimize the Potential of SCC in Closure Welds of Nuclear Waste Containers. Presentations in Helsinki University of Technology. 49 p.

Yen, H.-J., Lin, M. C.-C. & Chen, L.-J. 1996. Residual Stress Measurement in 304 Stainless Steel Weld Overlay Pipes. Journal of Engineering Materials and Technology, Vol. 118, pp. 135–142.

Young. G. A., Lewis, N., Battige, C. K. Somers, R. A. & Penik, M. A. 2003. Quantification of Residual Plastic Strains in Ni-Cr-Mn-Nb GTAW Welds via Electron Backscatter Diffraction. Proceedings of 6th International Trends in Welding Research Conference. Pine Mountain, GA, USA, 15–19 April 2002. ASM International. Pp. 912–917.

5. Field experiences in PWRs

In general, intergranular stress corrosion cracking is not a major concern in stainless steel piping in PWRs. However, SCC is a concern for control rod drive mechanism (CRDM), instrument penetrations and pipe connections made of Alloy 600 and/or Ni-base weld metals, e.g., Alloy 182. The most susceptible degradation sites are the inside surfaces, where Alloy 600 or Ni-base weld metals can be directly in contact with primary water or steam. The failure mechanism has been classified as low potential primary water SCC (PWSCC) (IAEA-TECDOC-1361, 2003). PWSCC of nickel-base alloys is considered to be the most severe ageing issue in PWRs.

The first field failures in nickel-base alloys in PWRs were connected to cracking in Alloy 600/Inconel 182 joints, with initiation either in Alloy 600 material or by welding defects. Until 1994, stress corrosion cracking of Alloy 600 in the dissimilar metal welds was associated with areas of high stresses and heavy cold work adjacent to welds that had not been stress relieved. Sometimes a crack initiated in Alloy 600 had propagated into Alloy 182 weld metal. Up to then, cracking had not been observed to initiate in the weld metal. However, both Alloys 182 and 82 were observed to be susceptible to SCC in laboratory tests (Andresen 1987). Later, the SCC susceptibility of these weld metals was also verified by cracking cases in the operating power plants (Rao et al. 2002, Shah & MacDonald 1993). SCC has occurred in control rod drive mechanisms and thermo-couple nozzles made of Alloy 600. Initiation in these cases has taken place in the J-groove welds of Alloy 182.

In 1993, a pressurizer relief nozzle (Ø ~100 mm) leak was detected at Palisades (PWR, commercial start in 1971). The circumferential crack was about 90 mm long and was attributed to PWSCC in the Alloy 82/182 nozzle weld. Metallographic investigations indicated repairs at the inner surface of the weld. This is, to the authors' knowledge, the only case of circumferential cracking in safe ends reported publicly so far. All other reported safe end cracks have been axial.

Numerous cases of cracking in thermal sleeves in PWR pressurizers have occurred. In 1989 Calvert Cliffs 2 identified 20 leaking sleeves, which were repaired by the pad repair technique. In 1994 Calvert Cliffs 1 identified 2 leaking sleeves and performed nickel-plating of 120 sleeves as a remedy. A similar remedy was adopted at St. Lucie 1 after finding one leaking sleeve in 1997. In 2000, ANO-2 identified 12 leaking sleeves, of which 12 were plugged (Meeden 2005). Recently evidence of leakage around eight sleeves was observed during the Hot Shutdown Walk Down, one of which was a plugged nozzle (NRC Current Event Notification Report 2005).

After the detection of a leak in a vessel head penetration at the Bugey 3 plant (PWR, commercial start in 1979) in 1991, an extensive pressure vessel head exchange and material investigation programme was set in progress in France. Non-destructive examinations were performed, including both vessel head and vessel bottom penetrations. Welds of 11 vessel heads (754 welds) were inspected by dye penetrant method and vessel bottom penetrations of 14 plants were also inspected by eddy current and ultrasonic methods along with visual inspections using TV (Alloy 600) (Le Hong et al. 2001). No PWSCC cracks were detected; only a few weld defects were found after operation times between 60 000–140 000 h. The pressure vessel head exchange program has proceeded and at the end of 2001, 42 vessel heads out of 54 had been replaced. All the original vessel heads with Alloy 600 will be changed to heads with Alloy 690. Dissimilar metal welds in the replacement heads are made using Inconel 152 (Amzallag et al. 2002).

NDE of dissimilar metal welds in steam generators has been performed in France. At the end of 2001, 42 divider plates of the hot branch and 26 divider plates of the cold branch were inspected by dye penetrant method (Alloys 182 and 600). No cracks were observed after 88 000 h of operation (Amzallag et al. 2002). One case of crack initiation in Alloy 182 was encountered in France. The root cause for this cracking at a steam generator tube sheet was hammering of the surface by a loose part.

Cracking in reactor pressure vessel head penetrations has been detected in a large number of PWRs worldwide. The initiation occurs in Alloy 600, and crack growth frequently proceeds into the Alloy 182 weld metal. Cracking in Alloy 600 material is considered to be the most severe ageing issue in PWRs (Valliant et al. 2002). In April 2003, the first incidence of cracking in a bottom mounted nozzle was detected at South Texas, Unit 1. Two nozzles were observed to be leaking during visual inspection. Boat samples vere removed from both nozzles, but unfortunately one was lost. Based on the destructive investigation of the boat sample, initiation is assumed to have occurred at the severely cold deformed inner surface of Alloy 600 penetration. Crack growth proceeded into Alloy 182 J-weld until leak. A schematic picture showing the postulated crack path is shown in Figure 75 (Hongqing et al. 2005a).

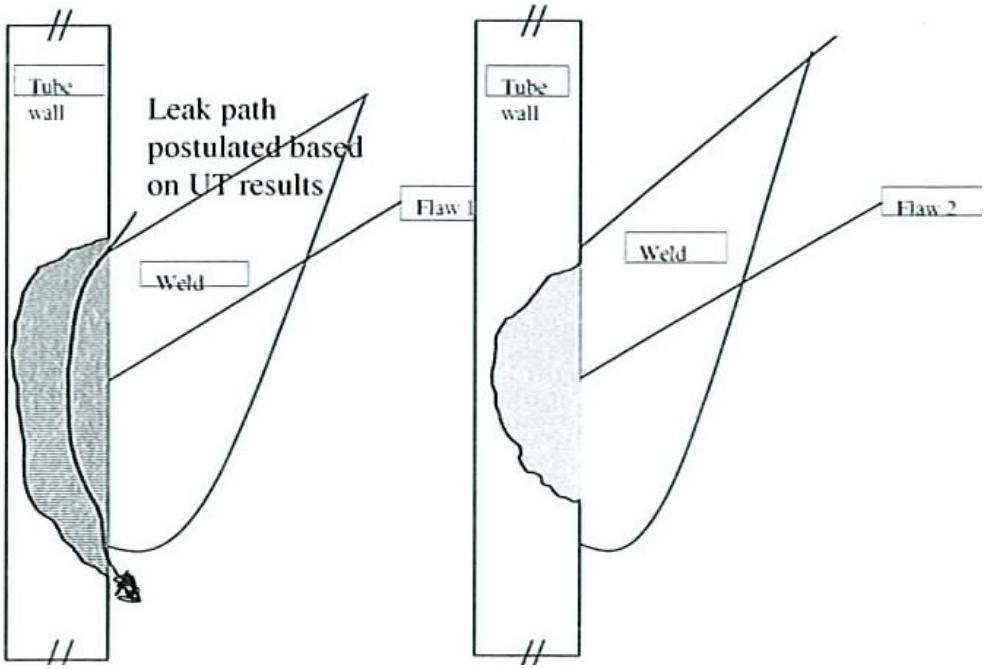

Figure 75. Schematic picture of the postulated leak path in the bottom penetration nozzle of South Texas Unit 1 (Hongqing et al. 2005a).

Cracking in the Control Rod Drive Mechanism (CRDM) nozzles and seal welds at Oconee Nuclear Station was first noted in Unit 1, when small amounts of boron residue were found on the top of the reactor pressure vessel (RPV) head during a refueling outage inspection in November 2000. Similar problems were found in Unit 3 during a planned maintenance outage in February 2001, and in Unit 2 in May 2001, during a refueling outage. Subsequent examinations of the CRDM nozzles with boron residue showed through-wall axial cracking in these nozzles, and through-wall circumferential cracking above the weld in two of the nozzles in Unit 3, and in one nozzle in Unit 2.

Since April 2001, the NRC staff has held a series of public meetings with the industry at NRC Headquarters to discuss Circumferential Cracking of CRDM Nozzles (NRC Information Notice 2001-05, 2001).

The most severe case of RPV head penetration cracking in PWRs observed so far is the Davis Besse case. In February 2002, severe corrosion of the reactor head steel was observed at Davis Besse (commercial start of operation in 1978). Investigations revealed axial indications in these nozzles. Crack initiation had occurred in the Alloy 600 penetration tube, and the crack continued into the Alloy 182 weld metal, resulting in a leak in one nozzle. The leaking nozzle caused corrosion of the RPV steel down to the stainless steel cladding within an area of ~106 cm^2, see Figure 76. Cracking continued into the stainless steel cladding to an extent depending on the local thickness of the cladding, and seemed to stop at a level leaving a ligament with a thickness of ~3.5 mm (NRC Operational Experience, Hongqing et al. 2005b). The incident has resulted in intense investigations concerning the failure as well as extensive inspections of RPV heads.

Figure 76. Picture of the corroded Reactor Vessel Head at Davis Besse (NRC Operational Experience).

The failure observed at V.C. Summer in October 2000 (PWR, commercial start in 1982) was the first incident with stress corrosion cracking in Alloy 82 weld metal in PWR conditions, although crack initiation had occurred in the Alloy 182 root weld (Pathania et al. 2002, Rao et al. 2002). During a containment inspection, plant personnel at the V.C. Summer NPP observed a boric acid deposit on the floor. Further inspection revealed that the deposit originated from a leak in the safe end weld on the hot leg side. The safe end is schematically shown in Figure 77. The safe end consisted of an Alloy 182 butter, which had been stress relieved together with the cladded pressure vessel (SA 508 + AISI 304 clad) in the shop, and a GTAW Alloy 82 field weld. The operating temperature of the weld was 326°C. Review of the weld fabrication history indicated multiple weld repairs at the location of the crack. Metallographic investigations of a spool piece indicated multiple crack initiation locations on the inner surface of the Alloy 182 butter, with evidence of microfissures. Clear evidence of cold work (microstructural indications as well as increased hardness values) of the inner surface was obtained. Both axial and circumferential cracking had occurred in the weld metal. The axial crack penetrated into Alloy 82 weld metal, but it was considered to have initiated in the Alloy 182 buttering. The crack also extended into the stainless steel safe-end nozzle, but not into the pressure vessel steel where only slight material corrosion was observed. The residual stress measurements confirmed significant tensile stresses in the axial and hoop directions. Taking the operating conditions into account (T and p), it was evaluated that the hoop stresses likely exceeded the axial stresses during operation. It was concluded that the crack initiated in the Alloy 182 buttering, and that hot cracking could have

easily contributed to the propagation of cracking through the Alloy 82 weld metal in the presence of residual stresses caused by weld repair. A spool piece was used to replace the affected weld, and was joined using narrow gap welding with Inconel 152 and 52 weld metals, as shown in Figure 78.

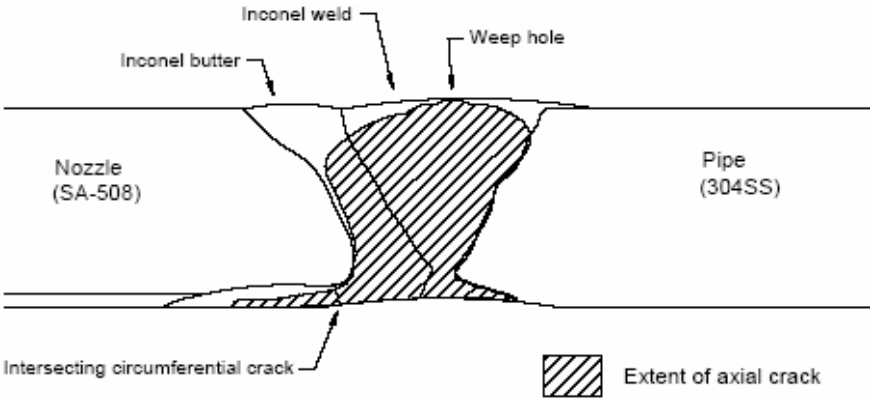

Figure 77. Schematic presentation of the failed safe end at V.C. Summer showing also the profile of the crack causing leakage through a weep hole (Pathania et al. 2002).

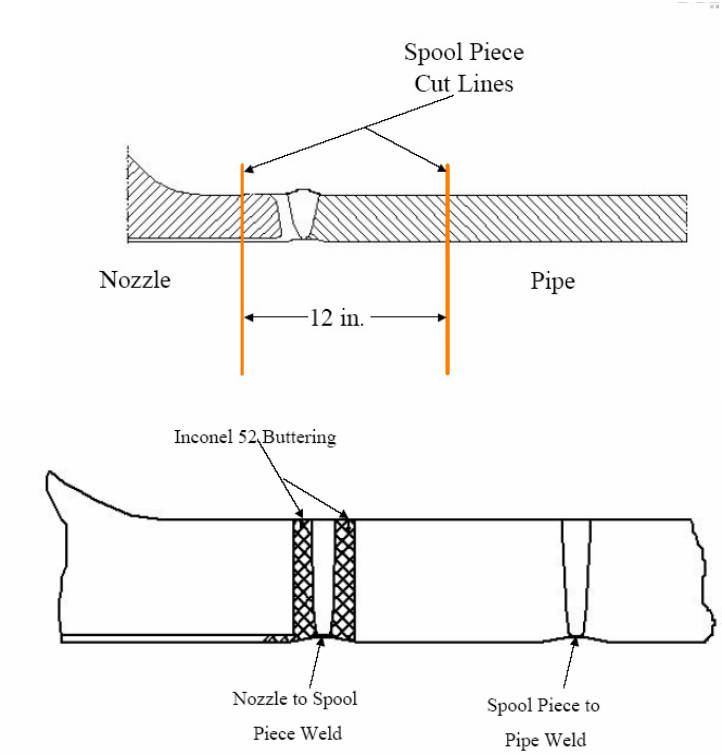

Figure 78. Schematic presentation of the repair of the safe end performed at V.C. Summer (SCE&G 2001).

During the refuelling at Ringhals 3 and 4 in 2000 (PWR, commercial start Unit 3 in 1982 and Unit 4 in 1983), indications were observed at four locations in the reactor pressure vessel nozzle to safe end weld. 4 defects were detected in Unit 4, and six boat samples from those four areas were removed and investigated both for failure analysis

purposes, and later, in more detail by performing crack-tip investigations. The appearance of the safe end is shown in Figure 79. Jenssen et al. (2001) reported the results from the failure analysis of the Alloy 182 weld metal cracks in the Ringhals 4 safe end. The objectives were to establish the fracture morphology and, if possible, the root cause for cracking. The examination revealed that cracks were present in all four boat sample locations, and that they were all confined to the weld metal made of Alloy 182. Cracking extended in the axial direction of the safe end. There was no evidence of cracks extending into the RPV-steel or the stainless steel safe end. All cracking was interdendritic and significantly branched. The conclusion from the failure investigation at that time was that these observations strongly suggested that crack propagation was mainly caused by interdendritic stress corrosion cracking (IDSCC). In addition, crack-like defects and isolated areas on the fracture surfaces suggested the presence of possible hot cracking, formed during fabrication. The reason for crack initiation could not be established based on the boat samples examined. However, increased stress levels due to repair welding, cold work from grinding, and defects produced during fabrication, e.g. hot cracks, may alone or in combination have contributed to crack initiation. However, contrary to Unit 4, where repairs were documented, Unit 3 had no documented repairs, which indicates that repair is not the only prerequisite for cracking, even if repairs obviously increase the susceptibility (Demma et al. 2005). Repairs were made using Alloy 52M weld overlay on the inside of the safe end.

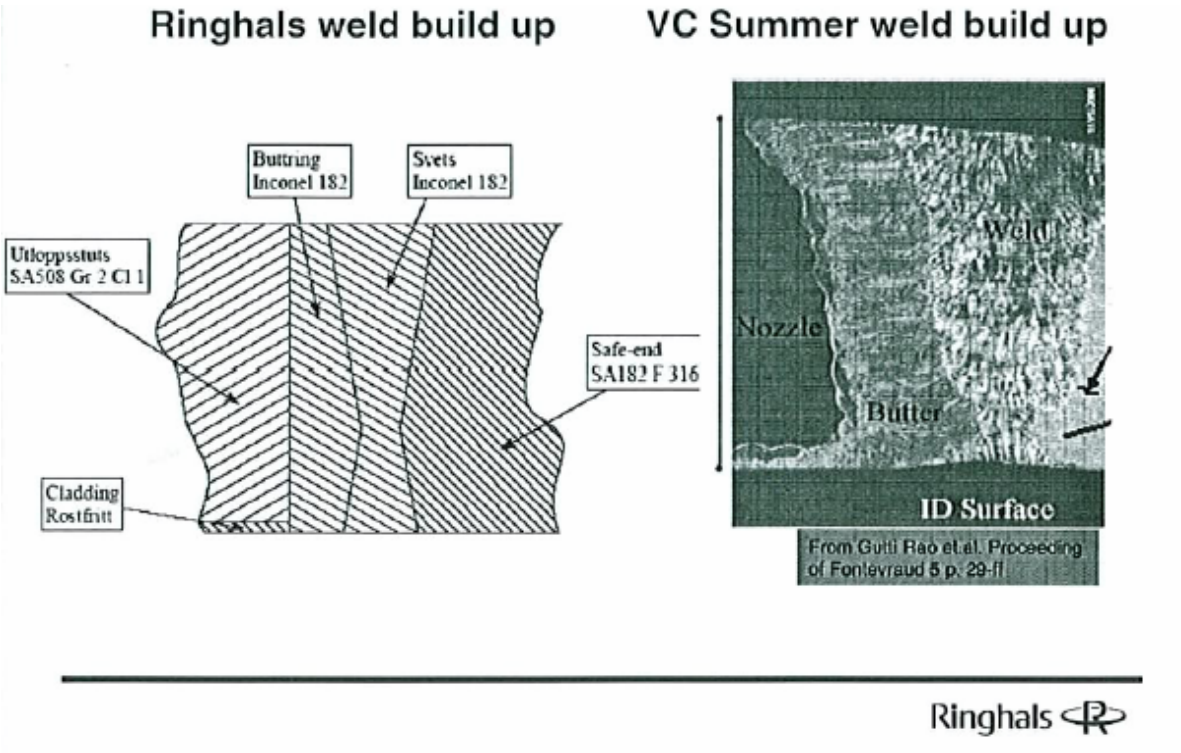

Figure 79. Schematic picture showing the construction of the Ringhals and V.C. Summer safe ends (Demma et al. 2005).

Later, Thomas et al. (2003) reported the results of the microstructural characterization of the weld cracks from Ringhals 4 safe end. The cracks in Alloy 182 safe end nozzle welds were characterized by scanning electron microscopy (SEM) and analytical transmission electron microscopy (ATEM). The goal was to investigate the causes of service failures in the weld repair regions. Backscattered electron images and SEM/EDS X-ray maps showed that the cracking occurred along non-segregated high-angle crystallographic boundaries in the weld metal, and that the grain interiors contained cellular dendritic structures with local regions of coincident Mn segregation and Nb-carbide precipitation. Even though the appearance of the fracture surfaces is interdendritic the cracks did not appear to follow dendrite boundaries. High-resolution analyses in a field-emission-gun TEM confirmed the lack of any significant segregation or precipitation on the grain boundaries leading the cracking. Oxide corrosion products found throughout the cracks indicated penetration by high-temperature water, and the crack microstructures were consistent with the previous observations of the stress corrosion cracks in Alloy 600 steam-generator tubing. The lack of compositional changes or low melting phases on the grain boundaries where cracks propagated, makes it unlikely that solidification hot cracking was the root cause for the degradation. Although a stress corrosion cracking mechanism was clearly supported, the role of the weld hot cracks could not be excluded without additional knowledge of hot crack characteristics in this material.

In September 2003 a through-wall flaw was observed in a pressurizer relief nozzle safe end weld in Tsuruga NPP, Unit-2 (PWR, commercial start in 06/86). NDE using an ultrasonic inspection technique revealed several linear indications in the safe end welds of the relief nozzle and the safety nozzle. The cracking in the safe end (∅ ~190×30 mm) was confined to the weld made of Alloy 132 (with properties similar to Alloy 182), Figure 80. The cracking was interdendritic or intergranular. The safety nozzle had been subjected to repair welding from the outside. NDE-investigations had been performed on the joint with the leak in 1999 without any observed indications. (NRC Current Event Notification Report 2005, NRC Information Notice 2004.)

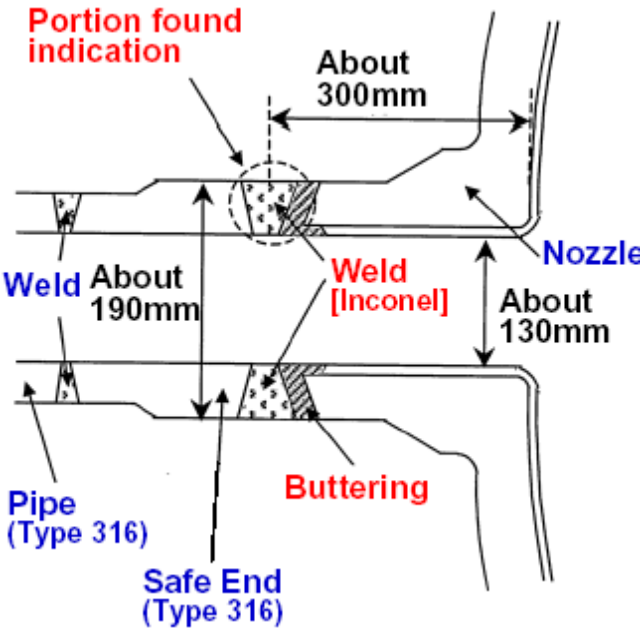

Figure 80. Schematic picture of the indication at Tsuruga 2 (NRC Current Event Notification Report).

In October 2003, an axial indication was detected in a surge line safe end weld at TMI-1 (PWR, commercial start in 1974). The surge line nozzle is made of Alloy 82/182 and is connected to the steam generator hot leg, the operating temperature of which is 317°C. The location with the indication had been subject to repair during manufacturing. Repair was performed using a weld overlay technique with Alloy 52.

During the refuelling outage of Ringhals 2 in 2004, boron deposits were found on the outer parts of the dome of the steam generators (SG). Investigations revealed cracking in the J-groove weld made of Alloy 82 filler material, on both the hot and cold sides of the SG (~320 and ~290°C, respectively). Based on the investigations performed, it was concluded that the cracks had grown by stress corrosion cracking mechanism, initiating at the inner surface and penetrating also into the butter made of Alloy 82. The weld contained root defects and microfissures, although the role of these could not be verified. The location of the cracks, at 12 o'clock, coincides with the probable starting and ending position of welding and with the maximum stress. Additional affecting factors can be thermal fluctuations. No crack growth into the low alloy steel was indicated based on the UT-inspection. Alloy 82 was used for repair. (Efsing et al. 2005.)

According to Pathania et al. (2002), there have been no field failure reports to date of the cracking in high-Cr Alloys 152 or 52. Also, only a very limited number of laboratory studies have been performed up to date.

5.1 References

Amzallag, C., Boursier, J., Pages, C. & Gimond, C. 2002. Stress Corrosion Life Experience of 182 and 82 Welds in French PWRs. Proceedings of Fontevraud 5, Contribution of Material Investigation to the Resolution of Problems Encountered in Pressurized Water Reactors. SFEN. Fontevraud, France, 23–27 September 2002. Pp. 69–80.

Andresen, P. 1987. Effect of Dissolved Oxygen, Solution Conductivity and Stress Intensity on the Interdendritic Stress Corrosion Cracking of Alloy 182 Weld Metal. Proceedings of Corrosion/87. San Francisco, California, USA, 9–13 March 1987. Paper No. 85. 12 p.

Demma, A., McIlree, A. & Herrera, M. 2005. Low Temperature Crack Propagation Evaluation in Pressurized Water Reactor Service. 12th International Conference on Environmental Degradation of Materials in Nuclear Power Systems – Water Reactors. Snowbird, Utah, USA, 15–19 August 2005. TMS. To be published.

Efsing, P., Forsgren, B. & Kilian, R. 2005. Root Cause Failure Anaysis of Defected J-Groove Welds in Steam Generator Drainage Nozzles. Proceedings of the 12th International Symposium on Environmental Degradation of Materials in Nuclear Power Systems – Water Reactors. Snowbird, Utah, 15–19 August 2005. TMS. To be published.

Hongqing, X., Fyfitch, S., Hyres, J., McIlree, A. & Cattant, F. 2005a. Laboratory Investigations of the Alloy 600 Bottom Mounted Instrumentation Nozzle Samples and Weld Boat Sample from South Texas Unit 1. International PWSCC of Alloy 600 Conference and Exhibit Show. New Mexico, USA, 7–10 March 2005.

Hongqing, X., Fyfitch, S. & Hyres, J. 2005b. Laboratory Investigations of the Stainless Steel Cladding of the Davis-Besse Reactor Vessel Head. International PWSCC of Alloy 600 Conference and Exhibit Show. New Mexico, USA, 7–10 March 2005.

IAEA-TECDOC-1361. 2003. Assessment and Management of Ageing of Major Nuclear Power Plant Components Important to Safety; Primary Piping in PWRs.

Jenssen, A., Norrgård, K., Lagerström, J., Embring, G. & Tice D. R. 2001. Assessment of Cracking in Dissimilar Metal Welds. Proceedings of the 10th International Conference on Environmental Degradation of Materials in Nuclear Power Systems – Water Reactors. Lake Tahoe, Nevada, USA, 5–9 August 2001. CDROM.

Le Hong, S., Boursier, J-M., Amzallag, C. & Daret, J. 2001. Measurements of Stress Corrosion Cracking Growth Rates in Weld Alloy 182 in Primary Water of PWR.

Proceedings of the 10th International Conference on Environmental Degradation of Materials in Nuclear Power Systems – Water Reactors. Lake Tahoe, Nevada, USA, 5–9 August 2001. CDROM.

Meeden, R. 2005. Pre-emptive Pressurizer Heater Sleeve Repairs at PVNGS. International PWSCC of Alloy 600 Conference and Exhibit Show. New Mexico, USA, 7–10 March 2005.

NRC Information Notice 2001-05. 2001. Through-wall Circumferential Cracking of Reactor Pressure Head Penetration Nozzles at Oconee Nuclear Station, Unit 3. http://www.nrc.gov/reading-rm/doc-collections/gen-comm/info-notices/2001/in01005.html.

NRC Information Notice. 2004. http://www.nrc.gov/reading-rm/doc-collections/gen-comm/ info-notices/2004/in200411.pdf.

NRC Current Event Notification Report for March 16. 2005. http://www.nrc.gov/reading-rm/doc-collections/event-status/event/en.html.

NRC Operational Experience. Davis-Besse Reactor Vessel Head Degradation. http://www.nrc.gov/reactors/operating/ops-experience/vessel-head-degradation.html.

Pathania, R., Mc Ilree, A. & Hickling, J. 2002. Overview of Primary Cracking in Alloys 182/82 in PWRs. Proceedings of Fontevraud 5, Contribution of Material Investigation to the Resolution of Problems Encountered in Pressurized Water Reactors. SFEN. Fontevraud, France, 23–27 September 2002. Pp. 13–27.

Rao, G., Moffatt, G. & McIlree, A. 2002. Metallurgical Investigation of Cracking in the Reactor Vessel Alpha Loop Hot Leg Nozzle to Pipe Weld and the V. C. Summer Station. Proceedings of Fontevraud 5, Contribution of Material Investigation to the Resolution of Problems Encountered in Pressurized Water Reactors. SFEN. Fontevraud, France, 23–27 September 2002. Pp. 29–41.

Rao, G., Jacko, R. & McIlree, A. 2002. An Assessment of the CRDM Alloy 600 Reactor Vessel Head Penetration PWSCC Remedial Techniques. Proceedings of Fontevraud 5, Contribution of Material Investigation to the Resolution of Problems Encountered in Pressurized Water Reactors. SFEN. Fontevraud, France, 23–27 September 2002. Pp. 93–105.

Shah, V. & MacDonald, P. (Eds.). 1993. Aging and Life Extension of Major Light Water Reactor Components. Elsevier, the Netherlands. ISBN 0 444 89448 9. 941 p.

SCE&G. 2001. V.C. Summer Nuclear Station. Alpha Hot Leg Evaluation and Repair. Presentation at the V.C. Summer Nuclear Station. Jenkinsville, SC, January 18, 2001. http://www.nrc.gov/reactors/operating/ops-experience/pressure-boundary-integrity/weld-issues/weld-files/ml011090370.pdf.

Thomas, L., Vetrano, J., Bruemmer, S., Efsing, P., Forssgren, B., Embring, G. & Gott, K. 2003. High-Resolution Analytical Electron Microscopy Characterization of Environmentally Assisted Cracks in Alloy 182 Weldments. Proceedings of 11th International Conference of Environmental Degradation of Materials in Nuclear Systems – Water Reactors. Stevenson, WA, USA, 10–14 August 2003. CDROM.

Valliant, F., Moulart, P., Boursier, J. M., Amzallag, C. & Daret, J. 2002. Crack Growth Rates in Thick Materials of Alloy 600 and Weld Metals of Alloy 182 in Laboratory Primary Water. Comparison with Field Experience. Proceedings of Fontevraud 5, Contribution of Material Investigation to the Resolution of Problems Encountered in Pressurized Water Reactors. SFEN. Fontevraud, France, September 23–27, 2002. Pp. 107–116.

6. Field experiences in BWRs

Pipes have cracked in the heat-affected zones of welds in primary system piping in BWRs since mid-1960. These cracks have occurred mainly in Type 304 stainless steel, which was the steel used in most operating BWRs at that time. The major problem was recognized to be intergranular stress corrosion cracking (IGSCC) of austenitic stainless steel components that were made susceptible to this failure mechanism by being sensitized, either by post-weld heat treatment or by sensitization of the narrow heat-affected zone near the welds. In the late 1960s safe ends that were attached to the vessels during fabrication and were highly sensitized by subsequent furnace heat treatment were found to be susceptible to IGSCC, see Figure 81. Most of the furnace-sensitized safe ends in older plants have been removed or clad with a protective material. Cracks reported before 1975 primarily occurred in 4-inch-diameter recirculation loop bypass lines and 10-inch-diameter core spray lines. Cracking is most often detected during in-service inspections using ultrasonic test techniques. Some piping cracks have been discovered as a result of primary coolant leaks.

The first case of intergranular cracking in a safe-end made of Alloy 600 was observed in 1978 in Duane Arnold (BWR; commercial start 1974). The crack had initiated in the HAZ of the Alloy 600 and penetrated into the Alloy 182 weld metal, causing a leak (Pasupathi et al. 1980). Subsequently several similar cracks have been found in BWR's. Pilgrim Station (BWR, commercial start in 1972) was shut down in 1984 for replacement of primary recirculation piping systems and further ISI activities. Following piping removal, a dye penetrant test conducted on the exposed ID surfaces of the reactor vessel nozzle welds disclosed a number of axially-oriented crack indications in Inconel 182 weld butter, which joins the 28-inch diameter piping safe end to reactor vessel nozzle in the "B" loop. No evidence of cracking was observed in the "A" loop nozzle weld. Metallurgical evaluation of boat samples and surface replicas of the cracks was conducted by General Electric for the licensee to determine the nature of the indications. Metallographic results confirmed the cracking to be IGSCC. Axial cracking of a similar nature was also found in three of the 10 Inconel 182 weld butters joining the 12-inch-diameter jet pump inlet riser safe ends to the reactor vessel nozzles (NRC Information Notice 84-41, 1984). In 1999, crack-like indications were detected in two inlet nozzle to safe end welds of Duane Arnold (BWR, commercial start in 1975). The nozzles had dissimilar metal welds between Alloy 600 and low alloy carbon steel. The indications were on the safe end side of the weld, and are therefore concluded by the authors of this report to be circumferential. The indications were 44–65% of the wall thickness. One crack had initiated at the root weld and the other close to the weld in the safe end material. Repair of the flawed nozzle welds was planned to be done using overlay welding with Alloy 52 material. (NRC Weekly Information Report 1999.)

EVENT	YEAR OF DETECTION
Stainless Steel Fuel Cladding IGSCC	Late 1950s and Early 1960s
IGSCC of 304 During Construction	Late 1960s
IGSCC of Furnace Sensitized Type 304 During Operation	Late 1960s
IGSCC of Welded Small Diameter Stainless Steel Piping	Mid 1970s
IGSCC of Large Diameter 304 Piping	Late 1970s
IGSCC of Alloy X750 Jet Pump Beam	Late 1970s
IGSCC of Alloy 182/600 in Nozzles	Late 1970s
Crevice-induced Cracking of Type 304L/316L	Mid 1980s
Localized Cold Work Initiates IGSCC in Resistant Material	1980s
Accelerating Occurrence of IGSCC of BWR Internals	Late 1970s
Core Spray Spargers	
Shroud Head Bolts (Alloy 600)	
Access Hole Covers (Alloy 182/600)	
Nozzle Butters	
Control Blades	
SRM/IRM Dry Tube Cracking	
Jet Pump Beam Bolts	
Cracking of Low Carbon (304L/316L) and Stabilized Stainless Steels (347/321/348) in Vessel Locations	Late 1980s - present
Core Spray Jumpers	
Creviced Safe Ends	
Shrouds (304L and 347)	
Top Guide (304, 304L, 347)	
Core Support Plate (347)	
Cracking of Internal Core Spray Piping	1990 – present

Figure 81. SCC incidents in US BWR's (Horn et al. 2002).

Information concerning cracking in BWR internals was very limited until the late 1990's, due in large part to the limited amount of performed inspections (Horn et al. 2002). The first instances of SCC in un-creviced attachment welds in USA were found in welds that attached hold-down brackets to the reactor vessel head to restrain the dryer assembly. SCC was then discovered in Alloy 182 welds in the shroud support structure of an older BWR-2 during core shroud replacement activities in late 1999. Extensive cracking has since been found in the weld build-up pad on the vessel wall (designated the H9 weld), as well as in other Alloy 182 welds, and adjacent Alloy 600 material in the lower Alloy 600 conical section itself. The cracking of greatest interest was found on the inside weld (the lower bottom side) of the H9 weld, where nearly 300 individual cracks were found.

According to Horn et al. (2002), the first inspections of the recirculation piping of boiling water reactors (BWR) that revealed stress corrosion cracking in Alloy 182 butter-welds took place around 1984. The cracks were mainly axial in nature and the maximum crack depth was 70% of the wall thickness. In some locations the cracking had taken place along the weld fusion line circumferentially. Metallographic investigations performed on boat samples revealed that the cracking was interdendritic. The cracking was confined to Alloy 182 and did not extend into the low alloy steel of the nozzles or into Alloy 82 root weld. The cracking did propagate into the stainless steel safe end, but the initiation had taken place in Alloy 182 weld metal.

Later, cracking has been observed in other locations, even in places where the cracking is associated with weld residual stresses alone, e.g., in welds that attach hold-down brackets to the reactor vessel head to restrain the steam dryer assembly.

In 1985, a 21 mm long indication was observed in a Swedish BWR, in the weld between the feedwater nozzle and the safe end. The indication was concluded to not be surface-breaking. A boat sample was removed for destructive analysis, based on which it was evaluated to be a hot crack. It was repaired in 1989 from the inside using automatic TIG-welding and Sanicro 72 filler material, which has a composition similar to that of Alloy 82 (< 0.03% C, 20% Cr, 3.0% Mn, 2.6 % Nb, < 1% Fe, Ni balance). The repair included excavation of the indication, local welding with Sanicro 72 after which a thin layer of the same material was welded around the whole weld. (Pers Anderson 1990.)

During the outage at Forsmark 1 (BWR, commercial start in 12/80) in 1997, an axial indication was observed at the safe end (determined by TOFDT). The Alloy 600 safe end was buttered with Alloy 182 and welded with Alloy 182. The axial indication was located in the weld metal, and was 10 mm long and 2 mm deep. The wall thickness was 22 mm. The exact location as well as the cracking mechanism was to be investigated from a boat sample, but the sample removal failed. The defect was machined using EDM in several cycles alternated with NDE from the outside. An indication was still observed after removal of 17 mm, which was the maximum amount that could be removed without excessively compromising the structural integrity of the weld. The weld was repaired using Alloy 82. (Pers Anderson 1990.)

In March 1989, a circumferential NDE indication was observed at the feedwater nozzle (∅ ~350×28 mm) to safe end weld in River Bend Station Unit 1 (BWR, commercial start in 1985). The indication was left and re-examined during the two following outages (March 1990 and September 1991). Crack growth was reported each time, and the safe end was replaced in 1992. Destructive examinations of the indication revealed a crack that was 23 mm deep (84% of wall thickness) and about 226 mm long (Bowerman et al. 1999). NDE (UT) had indicated a much smaller depth, of 12.1 mm (43% of wall thickness). The crack had initiated at a lack of fusion defect at the fusion line between the low alloy steel and the Inconel 182 butter weld and grown by a stress corrosion cracking mechanism into the Inconel 182 weld. The depth of the welding defect was about 1.6 mm. The safe end was repaired by replacement, but details on, e.g. the weld filler material used, are not available in the open literature.

6.1 References

Bowerman, B., Czajkowski, C., Roberts, T. & Neal, C. 1999. Metallurgical Evaluation of a Feedwater Nozzle to Safe End Weld. Materials Characterization, Vol. 43, pp. 347–347.

Horn, R., Andresen, P. & Hickling, J. 2002. BWR Alloy 182 Stress Corrosion Cracking Experience. Proceedings of Fontevraud 5, Contribution of Material Investigation to the Resolution of Problems Encountered in Pressurized Water Reactors. SFEN. Fontevraud, France, 23–27 September 2002. Pp. 55–67.

NRC Information Notice 84-41. 1984. IGSCC in BWR Plants. June 1, 1984. http://www.nrc.gov/vreading-rm/doc-collections/gen-comm/info-notices/1984/in84041.pdf.

NRC Weekly Information Report – Week Ending November 19, 1999. SECY-99-271. http://www.nrc.gov/reading-rm/doc-collections/commission/secys/1999/secy1999-271/1999-271scy.html.

Pasupathi, V., Perrin, J., Farmelo, D., Smith, G. & Weiss, S. 1980. Investigation of Inconel Safe-end Failure in Duane Arnold. Trans. ANS, 34, pp. 232–233.

Pers Anderson, E. 1990. Mission Impossible: Repairing a Crack in a Feedwater Nozzle Safe End Weld. Nuclear Engineering International, Vol. 35, No. 436, November, pp. 38–39.

7. Effects of composition and microstructure on SCC susceptibility

The cracking susceptibility of nickel-base alloys in high-temperature water is considered to be mainly a function of the chromium content, with increasing resistance with increasing chromium content. Investigations on welding, metallography and SCC have not yet been able to conclusively identify all compositional parameters which would guarantee the best overall behaviour. On the contrary, there seems to be batch differences, which are not completely understood. Furthermore, development of weld filler materials is an ongoing process, which may result in increased uncertainties when comparing results from laboratory testing performed at different times and to field performance. These factors emphasize the importance of performing welding qualification tests on the same batch as that to be used in the production. It this context it must be remembered that the nominal composition of the filler electrode material is not the same as the final composition of the weld metal due to changes occurring during welding.

In oxidising BWR environment the correlation between a higher chromium content and SCC resistance is understandable, when dissolution enhanced by chromium depletion is considered to affect the cracking. Briant and Hall (1987) investigated weld metals made of Alloy 182 and Alloy 82 and report differences in the precipitation structure as well as in the amount of chromium depletion and segregation; all factors which may play a role in the cracking susceptibility. Thermal ageing of Alloy 182 weld metals resulted in stronger grain boundary chromium depletion and concurrent higher susceptibility to grain boundary corrosion (measured with nitric acid testing) than those of Alloy 82. The reason for the higher chromium depletion is considered to be the difference in the chemical compositions; Alloy 182 has a higher carbon and iron content, but a lower chromium content. In nickel, iron increases and chromium decreases carbon activity, i.e., carbon activity is higher in Alloy 182 than in Alloy 82, resulting in stronger chromium depletion in Alloy 182. Phosphorous segregation to the grain boundaries was also observed, but it was not considered to be crucial based on the results, i.e., lack of correlation between amount of grain boundary P-concentration and intergranular corrosion susceptibility. TEM-investigations of the precipitation structure are not fully conclusive, yet. Alloy 182 has been reported to contain mainly Ti-carbides in the grain matrix in as-welded condition and additionally γ' after ageing (620°C/24h) (Briant & Hall 1987), or mainly Nb-carbides (Brummer & Thomas 2005). According to the results presented in Briant & Hall, Alloy 82 contained Nb- and Ti-carbides in grain matrices in as-welded condition and ageing did not cause precipitation of γ'. Both alloys were reported to contain $M_{23}C_6$ carbides at grain boundaries (Briant & Hall 1987).

Although TEM-investigations on the microstructure of different weld metals and from crack-tip specimens so far have not been able to fully resolve the different micro-structural features causing cracking, or more important, resistance to cracking, chromium content has been shown beneficial for the PWSCC resistance of nickel-base alloys both in BWR- and PWR-environment.

For Alloy 600 a correlation between carbide precipitate structure and stress corrosion cracking susceptibility has been observed and verified in numerous investigations. Grain boundary carbide decoration has a beneficial impact on SCC resistance. Taking the similarities in the chemical composition into account, the correlation can be considered valid also for the weld metals. However, no such correlation between grain boundary carbides and stress corrosion cracking susceptibility has been observed for Alloy 182 (Amzallag et al. 2002).

BWR vendors use a Stress Corrosion Cracking Resistance Index, SCRI, which includes the chromium level as well as the earlier used N-bar. The N-bar takes the amounts of niobium, titanium and carbon into account with the underlying logic that an increasing level of the carbide forming elements, Nb and Ti, and/or a lower amount of carbon result in less chromium carbides and less chromium depletion on dendrite boundaries and decreased stress corrosion cracking susceptibility in oxidising environments. The equations for the N-bar and the SCRI-parameter are given in Equations 7 and 8. Alloy 182 is considered susceptible, if the N-bar is lower than 12 and SCRI is less than 30 (Horn et al. 2002).

$$N\text{-}bar = 0.13 \times (Nb+Ti)/2 \times C \quad (7)$$

$$SCRI = Cr + (Nb + Ta) \times 5 + Ti \times 10 - 116.5 \times C \quad (8)$$

Crack initiation studies on Alloy 182 and Alloy 82 (Pathania et al. 2002) in simulated PWR environment using reverse U-bend specimens showed higher susceptibility to stress corrosion crack initiation in heats with higher carbon and silicon. Silicon increases the fluidity of the molten pool resulting in greater penetration during welding, but causes also a risk for solidification cracking as well as increases the risk for burn-through of the weld metal. According to (Findlan et al. 2005), silicon in Inconel 52M should be kept in the range of 0.04 to 0.05%, with the suitable limit depending on the welding process.

Impurities like phosphorous and sulphur are kept at minimum in the weld metals to avoid segregation and risk for hot cracking. For the stainless steel base metals to be welded, the sulphur content should not be driven too low, because sulphur increases the fluidity of the molten pool. Extremely low sulphur content may require higher heat

input in welding than a reasonable S-content. An S-content of 0.002% S is considered to be too low, while 0.007% S is reasonable.

The influence of crack growth orientation in relation to the weld metal structure is large. Numerous laboratory investigations have shown, that the CGR of Alloy 182 in PWR primary water in laboratory experiments is about 5–10 times faster (Pathania et al. 2002) along the dendrites than transverse to the dendrites. Recent investigations have further revealed that the cracks in operating plants grow along certain, high angle, or random dendrite boundaries.

7.1 Effect of heat treatment and ageing

Stress relief heat treatments of dissimilar metal weld joints are usually performed at ~600°C. Ni-base weld metals of stress-relieved joints are less susceptible in PWR primary water to SCC initiation due to a decrease of surface residual stresses although it does not improve the intrinsic PWSCC susceptibility of Alloy 182 (NRC Current Event Notification Report 2005). However, if the joint contains stainless steel, stress relief heat treatment can nucleate chromium carbides, which may result in low temperature sensitisation during long term operation. Therefore, all stainless steels which are to be stress relief heat treated should have a low carbon content of ≤0.02% C.

Because nickel-base weld metals containing 30% chromium have a chemical composition close to the stoechiometric composition of Ni_2Cr, an ordering transformation of the initial solid solution can occur during the long term operation at elevated temperatures. This microstructural transformation results in hardening and embrittlement, which can have large influence on the operating properties. However, this transformation becomes unlikely for alloys with iron contents above 8%. (Boursier et al. 2004.)

Investigations of changes in hardness, Charpy-V toughness and resistivity properties after 30 000 and 60 000 h at 325–450°C of Alloy 152 SMAW weld metals has shown a high resistance to thermal ageing of weld metals with a chromium content above 30%. Assuming an activation energy of 125 kJ/mol, the lack of thermal ageing after 30 000 h at 400°C and 60 000 h at 360°C has qualified Alloy 152 for operation at 325°C for up to 500 000 h. Ageing investigations are ongoing, and further experiments will be performed (Boursier et al. 2004).

7.2 Effect of cold deformation

Cold deformation due to grinding, weld shrinkage etc. has a detrimental influence on the SCC susceptibility in PWR primary water. An increase in the CGR by a factor of 2 due to 10% CW was observed in PWR environment in both as-welded and stress-relieved weld metals (Rao et al. 2002). Lathe turned Alloy 600 surfaces show about one order of magnitude shorter times to failure compared to electrolytically polished surfaces under the same experimental stress corrosion test conditions (Amzallag et al. 2002). This was proposed to be possible also for Alloy 182 weld metals.

7.3 References

Amzallag, C., Boursier, J., Pages, C. & Gimond, C. 2002. Stress Corrosion Life Experience of 182 and 82 Welds in French PWRs. Proceedings of Fontevraud 5, Contribution of Material Investigation to the Resolution of Problems Encountered in Pressurized Water Reactors. SFEN. Fontevraud, France, 23–27 September 2002. Pp. 69–80.

Boursier, J., Valliant, F. & Yrieix, B. 2004. Weldability, Thermal Ageing and PWSCC Behaviour of Nickel Weld Metals Containing 15 to 30% Chromium. ASME/JSME Pressure Vessels and Piping Conference. San Diego, California, USA, 25–29 July 2004. Ed. T. Tahara, PVP Vol. 490. Pp. 109–121.

Briant, C. & Hall, E. 1987. The Microstructural Causes of Intergranular Corrosion of Alloys 82 and 182. Corrosion – NACE, Vol. 43, September, pp. 539–548.

Brummer, S. & Thomas, L. 2005. High-Resolution Analytical Electron Microscopy Characterization of Environment-Assisted Cracks in Alloy 182 Weldments. International PWSCC of Alloy 600 Conference and Exhibit Show. New Mexico, USA, 7–10 March 2005.

Findlan, S., Newton, B. & Kiser, S. 2005. Successful Structural Weld Metal Build-Ups on P-3 Gr-3 Pipe Coupon Made with INCONEL® Filler Metal 52M. 2005 EPRI International PWSCC of Alloy 600 Conference. 7–10 March 2005, Santa Ana Pueblo, New Mexico, USA. 15 p.

Horn, R., Andresen, P. & Hickling, J. 2002. BWR Alloy 182 Stress Corrosion Cracking Experience. Proceedings of Fontevraud 5, Contribution of Material Investigation to the Resolution of Problems Encountered in Pressurized Water Reactors. SFEN. Fontevraud, France, 23–27 September 2002. Pp. 55–67.

NRC Current Event Notification Report for March 16, 2005. http://www.nrc.gov/reading-rm/doc-collections/event-status/event/en.html.

Pathania, R., McIlree, A. & Hickling, J. 2002. Overview of Primary Cracking in Alloys 182/82 in PWRs. Proceedings of Fontevraud 5, Contribution of Material Investigation to the Resolution of Problems Encountered in Pressurized Water Reactors. SFEN. Fontevraud, France, 23–27 September 2002. Pp. 13–27.

Rao, G., Jacko, R. & McIlree, A. 2002. An Assessment of the CRDM Alloy 600 Reactor Vessel Head Penetration PWSCC Remedial Techniques. Proceedings of Fontevraud 5, Contribution of Material Investigation to the Resolution of Problems Encountered in Pressurized Water Reactors. SFEN. Fontevraud, France, 23–27 September 2002. Pp. 93–105.

8. Laboratory investigations

Extensive laboratory investigations on the SCC susceptibility of nickel-base materials and weld metals have been performed, and in several countries this is one of the most important areas of investigations at the moment. These investigations focus both on crack initiation as well as on crack growth rate measurements. The investigations can be parametrical studies, where the influence of some environmental parameter (temperature, hydrogen concentration, impurity level, etc.) is studied or where different materials (e.g., Inconel 182, 82, 52) are compared in similar environments, or the investigations can be focused on production of data for crack growth rate or life-time prediction.

Consequently, the susceptibility of materials to stress corrosion cracking is investigated using several testing methods, such as slow strain rate tests (SSRT), constant elongation rate tests (CERT), reversed U-bend (RUB) tests, compact tension (C(T)) specimens with different types of loading etc. An accelerated test has recently been developed for nickel-base weld metals, i.e., the doped steam test. This test is performed using four-point bending specimens in high pressure (21 MPa) hydrogen containing steam at 400ºC with added impurities (chloride, fluoride, sulphate and nitrate sodium salts) (Kilian 2005). The test has proven successful when comparing nickel-base alloys having high chromium contents, which are highly resistant to cracking, where differences may be difficult to determine quantitatively.

8.1 Laboratory investigations in PWR environment

8.1.1 Crack growth rate studies

Laboratory results on stress corrosion crack growth rates show a high range of values even under nominally similar test conditions. Plant experience in France indicates a better performance of Inconel 182 weldments compared to the results of laboratory investigations (Amzallag et al. 2002). The reasons for this difference are not yet fully clarified. Residual stresses built up in the welded billets used for the laboratory investigations have been proposed as one major reason. Valliant et al. (2002) pointed out the importance of evaluating the influence of cyclic loading on crack initiation and propagation in weld metals, and many of the differences observed in the SCC CGRs in different programmes may be due to subtle differences in the loading mode used.

After the observation of cracking at Bugey 3 in France, EDF started a large programme in order to assess CGRs in Alloy 600 and Alloy 182. The results indicate a similar influence of the main parameters, i.e., T, K and degree of cold work on the crack growth

rates of Alloy 600 and Alloy 182. However, there is one major difference between Alloy 600 and Alloy 182, i.e., the influence of the orientation of the crack with respect to the dendrites, which is one of the major parameters for the CGR in Alloy 182 weld metal (Rao et al. 2002).

According to Vaillant et al. (2002) and Le Hong et al. (2001), the crack growth rate vs. stress intensity factor dependency can be presented in the following form:

$$da/dt = \alpha \boldsymbol{x} (K\text{-}K_{ISCC})^n \quad (9)$$

Vaillant et al. (2002) and Le Hong et al. (2001) suggested that for Inconel 182 in PWR primary water between 290–350°C, the value for the threshold stress intensity factor K_{ISCC} is around 9 MPa√m and the exponent n is 0.1, which indicates that there is effectively a plateau in the crack growth rate. The threshold stress intensity factor was not specifically determined from the crack growth rate data, but it was observed that the value used for Alloy 600 fits reasonably well to the data when the relation presented above was applied.

The above-mentioned tests were performed in several laboratories. Specimens were tested in as-welded and stress-relieved conditions. Stress-relieving was performed by annealing at 610°C for 6 h. The test environment was de-mineralized water with the following water chemistry:

- 2 ppm lithium added as lithia (Li_2O)
- 1000 ppm boron added as boric acid
- 25–50 cc/kg dissolved hydrogen.

The crack growth rates were measured at 290°C, 310°C, 320°C, 350°C and 360°C. The crack growth rate test results are summarized in Figure 82. The crack growth rate increases significantly with temperature for each tested weld metal condition. The effect of the stress intensity factor K_I was evaluated in the range from 15 to 65 MPa√m. Above 15 MPa√m, the stress intensity factor has a limited influence on the crack growth rate. The scatter of the results seems to increase with decreasing temperature.

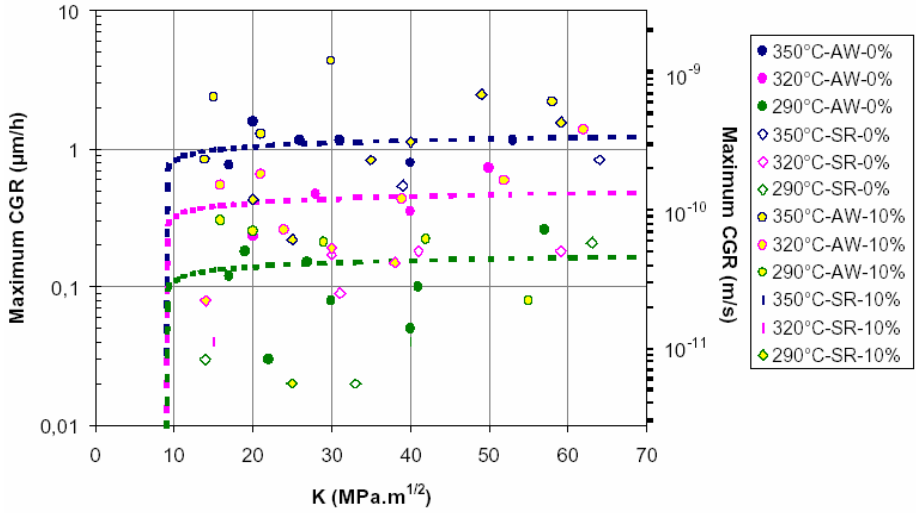

Figure 82. Influence of mechanical loading parameter (K) on the maximum crack growth rate of Alloy 182 (Valliant et al. 2002, Le Hong et al. 2001).

The influence of stress-relief heat treatment has been investigated by Le Hong et al. (2001). Stress-relief heat treatment is aimed at reducing the residual stresses after welding, but it can also have an effect on the crack growth susceptibility of the material. Crack growth rates of Alloy 182 in as-welded and stress-relieved conditions were compared at the same mechanical loading. Crack velocities were lower in the stress-relieved condition than in the as-welded condition by a factor of ~2. According to Le Hong et al. (2001) the stress-relief heat treatment can induce a relaxation of local residual stresses and a modification of the precipitation structure. A study investigating Alloy 182 welds manufactured by EDF, Studsvik and Westinghouse showed that the weld material and/or welding procedure can have a significant effect on crack growth behaviour, although the exact parameters could not be identified (NRC Current Event Notification Report 2005).

Crack growth rate tests organized by EPRI and performed by Westinghouse on Alloy 182 specimens in simulated PWR primary water at 325°C showed that the crack growth rate is 5 to 10 times higher along the dendrites than in the transverse direction. Pathania et al. (2002) suggested the following relation for the crack growth rate along the dendrites:

$$da/dt = 1.4 \times 10^{-11} \times (K_I - 9)^{1.16} \text{ m/s.} \quad (10)$$

Equation 10 indicates that the crack growth rate is strongly dependent on the stress intensity factor K, which is not in accordance with the data presented by Vaillant et al. (2002) and Le Hong et al. (2001).

The da/dt vs. $(K\text{-}K_{ISCC})^n$ dependencies presented above are based on the model developed by Scott and Combrade (2003). The model is based on the test results for

Alloy 600 steam generator tube materials and then modified for CRDM nozzles and other thick-wall components. The Scott model is based on PWSCC growth rate data obtained at Ohio State University. The data were developed at 330°C and include the effects of several different water chemistries. Only the data associated with the standard primary water chemistry of 2 ppm Li, 1200 ppm B, and pH = 7.3 were considered in developing the model. The equation fitted to this data set is:

$$da/dt = 2.8 \times 10^{-11} \times (K_I - 9)^{1.16} \text{ m/s.} \quad (11)$$

EPRI has released new disposition curves for Alloy 182 and Alloy 82, based on the screening of 261 data points from crack growth rate tests made in France, Sweden, Japan and USA (White et al. 2005). Due to a lack of data points at low K-levels, a conservative approach has been adopted, i.e., a zero K_{ISCC} value. The equations for the disposition curves for Alloy 182 and 82 are as follows:

$$da/dt \text{ (Alloy 182)} = 1.5 \times 10^{-12} \times K^{1.6} \text{ m/s.} \quad (12)$$

$$da/dt \text{ (Alloy 82)} = (1.5 \times 10^{-12}/2.6) \times K^{1.6} \text{ m/s.} \quad (13)$$

The disposition curve for Alloy 182 is also valid for Alloy 132. Jenssen et al. (2002) have reported results on crack growth rate tests on Alloy 182 in simulated PWR primary water. The screened data set with upper bound curves for the crack growth rate at 320°C are shown in Figure 83. Data measured at different temperatures were recalculated to 320°C using the Arrhenius equation. Activation energy Q used for the recalculation was 130 kJ/mol. Based on the results, they suggested different upper bound equations for K-levels above and below ~25 MPa√m, and additionally a slightly different N-bar:

$$N\text{-bar} = 0.13 \times (Nb + 2 \times Ti)/C. \quad (14)$$

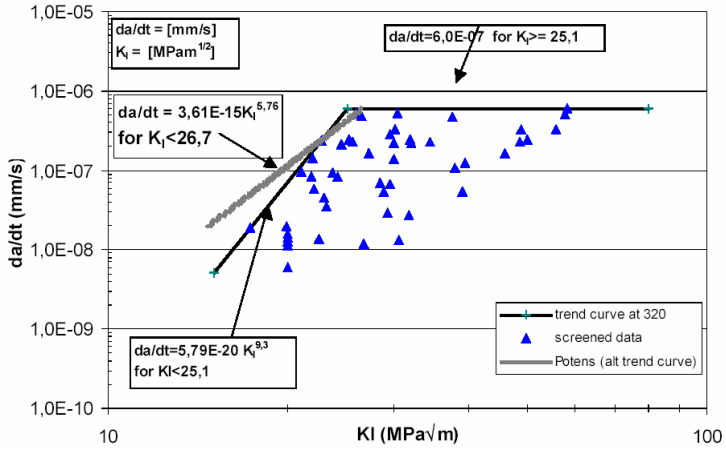

Figure 83. Screened data and bounding curves for Alloy 182 in PWR primary water at 320°C (Jenssen et al. 2002).

The different crack growth rate curves are summarised in Figure 84.

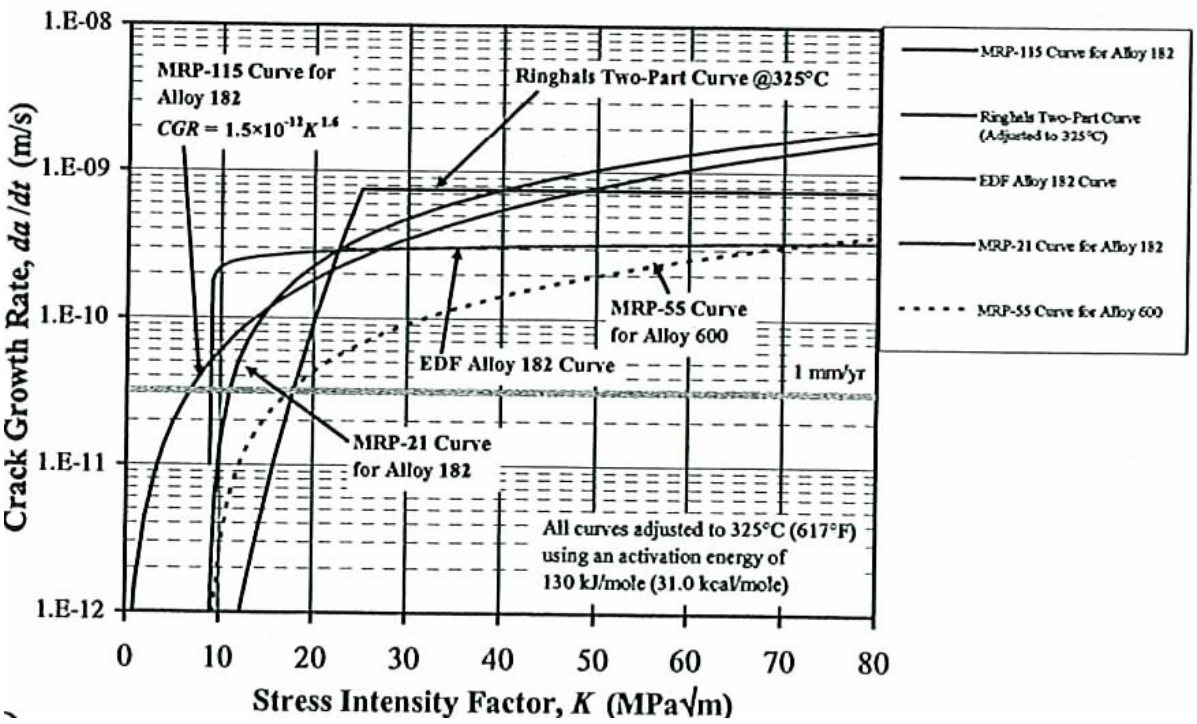

Figure 84. Different disposition curves for Alloy 182 and Alloy 600 in PWR environment (White et al. 2005).

Mills and Brown (2003) reported stress corrosion cracking (SCC) tests performed on seven Alloy 82H welds in 288 to 360°C water with 50 or 150 cc H_2/kg H_2O. Tests were conducted on longitudinally (T-L) and transversally (T-S) oriented (compared to the dendrite orientations) compact tension specimens under constant load conditions with periodic unloading/reloading cycles every 10 or 100 min, and with small amplitude ripple cycle. Crack growth rates exhibited an Arrhenius relationship with activation energy of 33 kcal/mol (138 kJ/mol). They observed that the SCC CGRs in the T-S direction tend to be about twice as high as those in the T-L direction. Examination of the fracture surfaces revealed that cracking first occurred along favourably oriented dendritic grain boundaries, which produced fingers of SCC. As local stress corrosion cracks grew and coalesced, the most resistant boundaries did not separate, which left unbroken ligaments in the wake of an advancing crack front. Because stresses are carried by these ligaments, local K_I values ahead of the intergranular fingers are diminished. Nevertheless, the intergranular fingers continue to extend, thereby indicating that the separation of the susceptible grain boundaries is relatively K-independent. Scatter factors for individual welds tested under constant-load conditions ranged from 2…5-times, while the scatter factor for all seven GTA welds was about an order of magnitude. Periodic unloading-reloading cycles tended to reduce data scatter: scatter factors were less than 2X in most of the cyclic tests. Periodic unloading appeared

to reduce crack incubation times, and so SCC consistently initiated shortly after specimens were loaded. Unloading-reloading cycles (R = 0.65) every 100 min did not affect CGRs, whereas unload-reload cycles every 10 min introduced a fatigue component that caused a small to modest acceleration in crack growth rates. Cyclic ripple loading with an R-value of 0.9 and a frequency of 1 cycle per min did not significantly accelerate the crack growth rate relative to the constant load SCC growth rate.

In Japan Alloy 132 has been used instead of Alloy 182. The difference between Alloys 182 and 132 is the lower hot cracking susceptibility of Alloy 132. According to Tsutsumi et al. (2003), no PWSCC CGR data for Alloy 132 have been reported. They investigated the PWSCC CGR of Alloy 132 in comparison with the literature data of Alloy 182, and evaluated the effect of loading condition on the PWSCC CGR of Alloy 132. SCC growth rate measurement tests in simulated PWR primary water on Alloys 132 and 82 weld metals were conducted at 325°C. The effects of the K value, periodic unloading interval and orientation of C(T) specimen on the crack growth rate were examined. The results are summarised in Table 12 and compared with literature data of Alloy 182 in Figure 85.

Tsutsumi et al. (2003) made the following conclusions and recommendations based on their study:

- PWSCC CGR of Alloy 132 weld metal was remarkably affected by K-value, from 20 to 35 MPa√m.
- The PWSCC CGR of Alloy 132 in this study was not larger than that of Alloy 182 literature data.
- The PWSCC CGR along the dendrites was about 3 times faster than that perpendicular to the dendrites.
- The periodic unloading method is not applicable for the PWSCC CGR measurements of nickel-base weld metals. The method is typically applied in order to maintain a straight crack front.
- The effect of periodic unloading on PWSCC CGR was observed. Periodic unloading is recommended to produce the interdendritic pre-crack, but constant loading is recommended for CGR measurement test with significantly long holding times to eliminate the influence of fatigue.

Table 12. Summary of Alloy 132 and 82 crack growth rate measurements of Tsutsumi et al. (2003).

Summary of Alloy 132 and 82 crack growth rate measurement test

Material	Environment	Specimen	Orientation	K (MPa√m)	Periodic unloading	Testing time (hrs)	CGR da/dt (m/s)	T.P. No.
Alloy 132	Simulated PWR primary water DO<5 ppb DH=30 cc/kg B: 1800 ppm Li: 3.5 ppm 325 °C	1/2TCT	TS	20	R=0.7, Holding time 9000 sec.	1000	<5.6E-12	MG7-1
					Constant load	200	Not grown	
		1/2TCT		35	R=0.7, Holding time 9000 sec.	950	2.4E-10	MG7-2
					Constant load	200	Not grown	
		1/2TCT	LS	20	R=0.7, Holding time 9000 sec.	1000	<5.6E-12	MG7 T-1
					Constant load	200	Not grown	
		1/2TCT		35	R=0.7, Holding time 9000 sec.	800	5.5E-10	MG7 T-2
					Constant load	200	Not grown	
		1/2TCT	LS	35	R=0.7, Holding time 9000 sec.	200	5.6E-11	132-2
				60	R=0.7, Holding time 9000 sec.	439	4.0E-10	132LS-1
		1/2TCT	TS	35	R=0.7, Holding time 9000 sec.	800	2.5E-10	MG7-5
					Constant load	650	1.1E-10	
		1/2TCT	LT	35	R=0.7, Holding time 1080 sec.	350	8.3E-11	MG7 L-1
					R=0.7, Holding time 9000 sec.	950	2.2E-11	
					Constant load	600	2.5E-11	
		1/2TCT		35	R=0.7, Holding time 360 sec.	800	8.3E-11	132-LT2
					R=0.7, Holding time 9000 sec.	300	2.8E-11	
Alloy 82		1/2TCT	LS	35	R=0.7, Holding time 9000 sec.	349	4.9E-12	82-3
		1/2TCT		35	R=0.7, Holding time 9000 sec.	400	3.3E-11	82-2
					Constant load	100	3.3E-11	

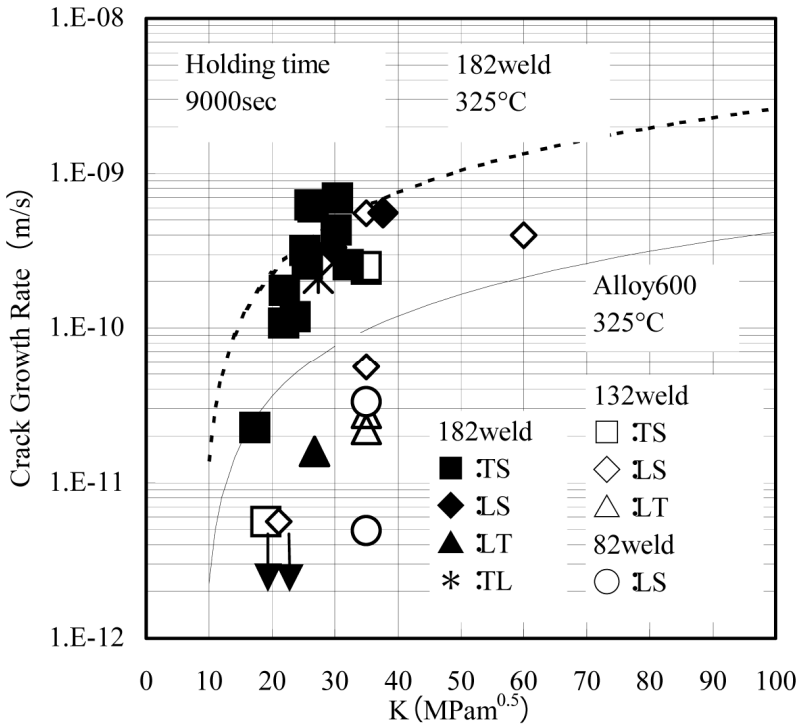

Figure 85. Comparison of crack growth rates between Alloys 132, 82 and 182 (Tsutsumi et al. 2003).

It is clear from the laboratory investigations, that the crack growth rate of nickel-base alloys is dependent on temperature. Vaillant et al. (2002) and Le Hong et al. (2001) suggested a mean activation energy of 130 kJ/mol for the whole available data, an example of which is shown in Figure 86. EDF uses an activation energy value of 125 kJ/mol (Boursier et al. 2004). Tests performed by CEA seem to provide a higher activation energy than those performed by ETH and EDF. Jenssen et al. (2002) also proposed an activation energy of 130 kJ/mol, based on the collected crack growth rate data for Alloy 182.

The amount of crack growth rate data for Alloy 52 or Alloy 52M is very scarce. A few tests were performed by Westinghouse in connection with the repair of the safe ends at Ringhals 3 and 4 using Alloy 52M. The tests were performed using 0.6 or 0.7T C(T) specimens at 340°C in simulated PWR environment, at stress intensities between 29.5 and 32.4 MPa√m. The specimens were removed in the T-L direction, although the T-S direction is considered to be more susceptible. No stress corrosion crack growth was obtained during the 2 700 h test time. (Jacko et al. 2003.)

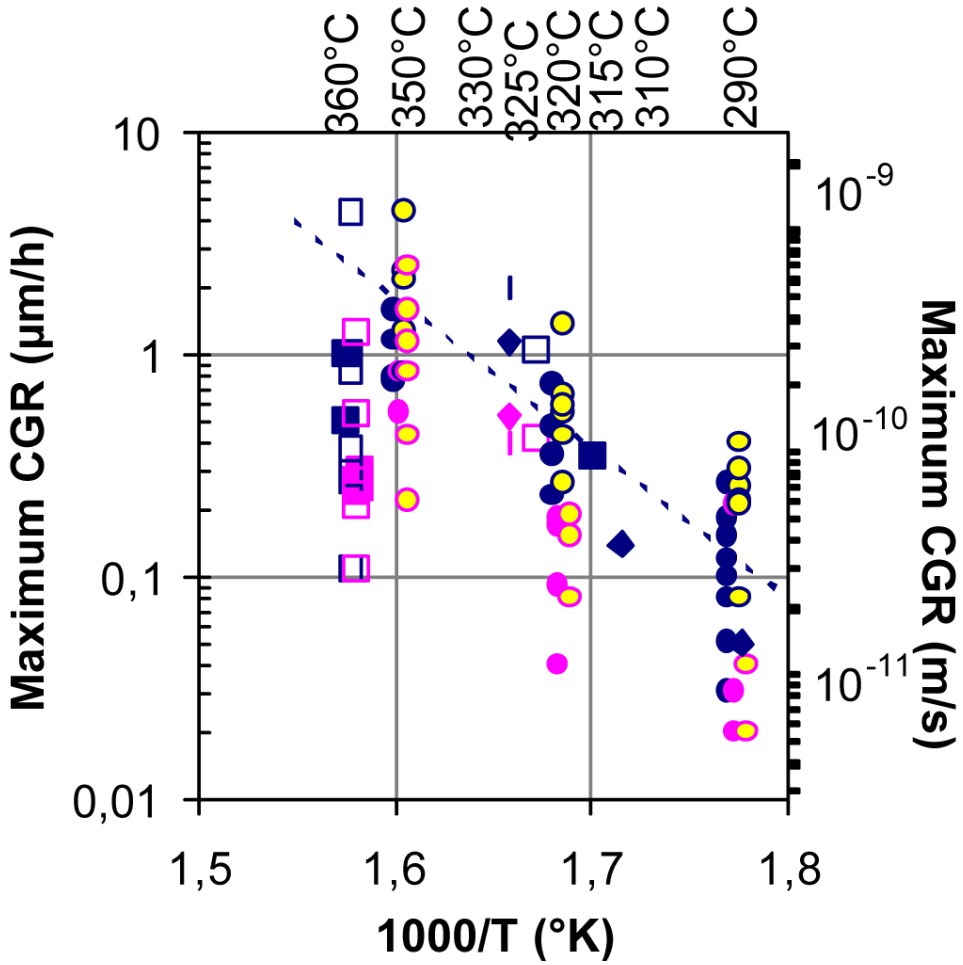

Figure 86. Effect of temperature on crack growth rate of Alloy 182 (K = 11-26 MPa √m) (NRC Current Event Notification Report 2005).

8.1.2 Initiation studies in PWR environment

Initiation studies on Alloy 182 and 82 indicated that Alloy 82 is 4–10 times more resistant to crack initiation in PWR primary water as compared to Alloy 182 (NRC Current Event Notification Report 2005).

Crack initiation using RUB-tests in simulated PWR primary water at 360°C on different nickel-base weld metals of Alloys 182, 82, 52 and 152 revealed crack initiation in Alloy 182 specimens after 500 h and in Alloy 82 in 2000–6500 h, but no crack initiation in the other alloys (Boursier et al. 2005). The investigation also included weldability studies using Varestraint and Gleeble testing. These tests revealed weldability differences between batches, the reason which is not fully known. A synthesis of laboratory test results on weld metals as a function of chromium content is shown in Figure 87 (Bousine et al. 1994). Results from investigations performed by Westinghouse on Alloy 52M before this alloy was used for the repair at the Ringhals NPP Unit 3, showed similar results, i.e., no cracking was observed in the doped steam testing of Alloy 52M after laboratory exposure correlating to 45 effective full power years (efpy), while SCC was observed in Alloy 182 weld metal specimens. Crack initiation occurred in Alloy 182 in 214 h, which is less than one fifth of the total exposure time for the Alloy 52M specimens (Bousine et al. 1994).

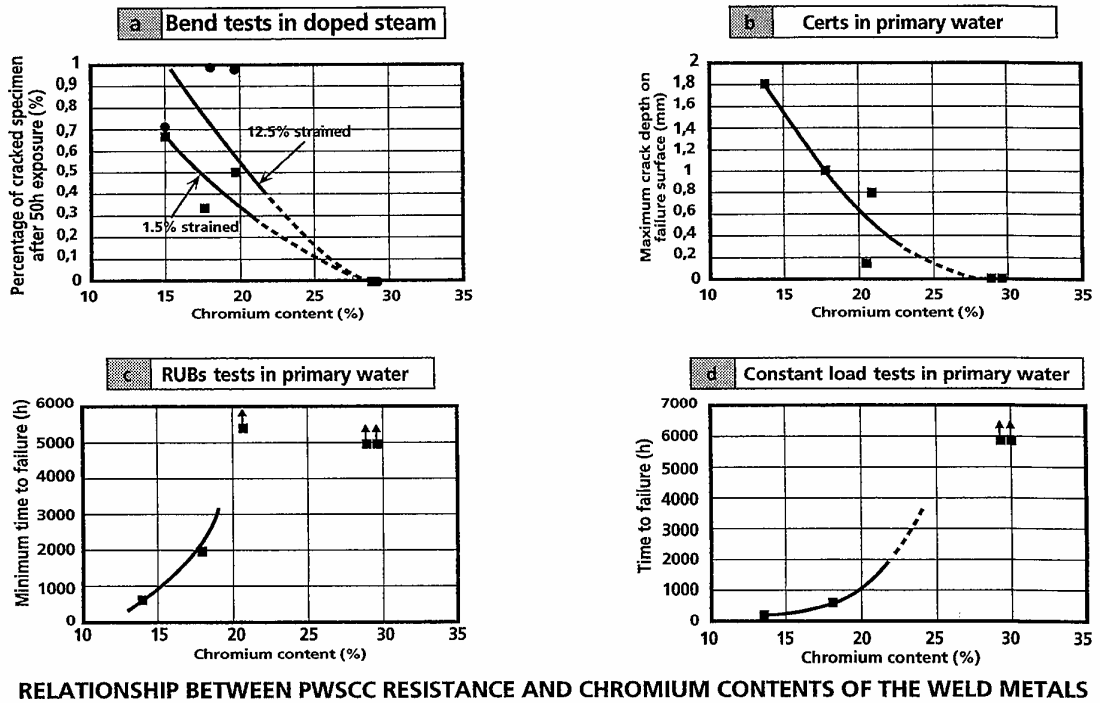

Figure 87. Synthesis of results from different tests in simulated PWR primary water on different weld metals and chromium contents (Bousine et al. 1994).

CERT tests (Psaila-Dombrowski et al. 1997) on Inconel 82 weld metal revealed an influence of strain rate on crack initiation, i.e., no cracking in simulated PWR primary water at the 'normal' strain rate of 10^{-6} s^{-1}, while cracking occurred at the very slow strain rate of 10^{-8} s^{-1}.

Amzallag et al. (2002) performed constant load tests on Ni-base weld metals in simulated PWR primary water on tensile specimens and internally pressurised capsules. According to Amzallag et al. (2002), Alloy 182 appears to be sensitive to primary water SCC (PWSCC) initiation only when the applied stresses are very high, Figure 88. The observed main trends for PWSCC initiation were:

- PWSCC is thermally activated. At temperatures between 330 and 360°C the activation energy is ~185 kJ/mol, which is the same as for Alloy 600. Constant load tests on tensile specimens in the stress range of 300 and 600 MPa indicate that the PWSCC threshold stress is close to 350 MPa (325°C). For Alloy 600 the threshold stress is close to 250 MPa (325°C). In both cases, the threshold stress exceeds the yield stress. In the case of Alloy 600, the failure time follows the relation: $1/t = B \times \sigma^4$.
- In the case of Alloy 182, the scatter of the data prevented the determination of a similar relation as for Alloy 600.
- Surface finish has an effect on the failure time in the constant load tests on tensile specimens. Constant load tests on Alloy 600 specimens with a cold-worked surface layer caused by lathe turning resulted in an order of magnitude lower failure times than tests on electrolytically polished specimens. The specimens were subjected to 2% tensile strain in the tests. The same tendency was observed on Alloy 182 specimens.
- High Si and C contents are detrimental. Comparison of the test results of Alloys 82 and 182 indicates that the increase in Cr content increases the time to cracking by a factor of ~5 (PWR primary water, 330°C).
- Post-weld heat treatment at 600°C is beneficial for Alloy 182, because it decreases the residual stresses. This is especially seen in the SCC susceptibility of high C% + high Si% Alloy 182. However, no effect of stress-relief heat treatment is seen on materials with lower SCC susceptibility.
- Susceptibility to SCC is minimized, when the principal stress axis is parallel to the solidification direction of the dendrites.

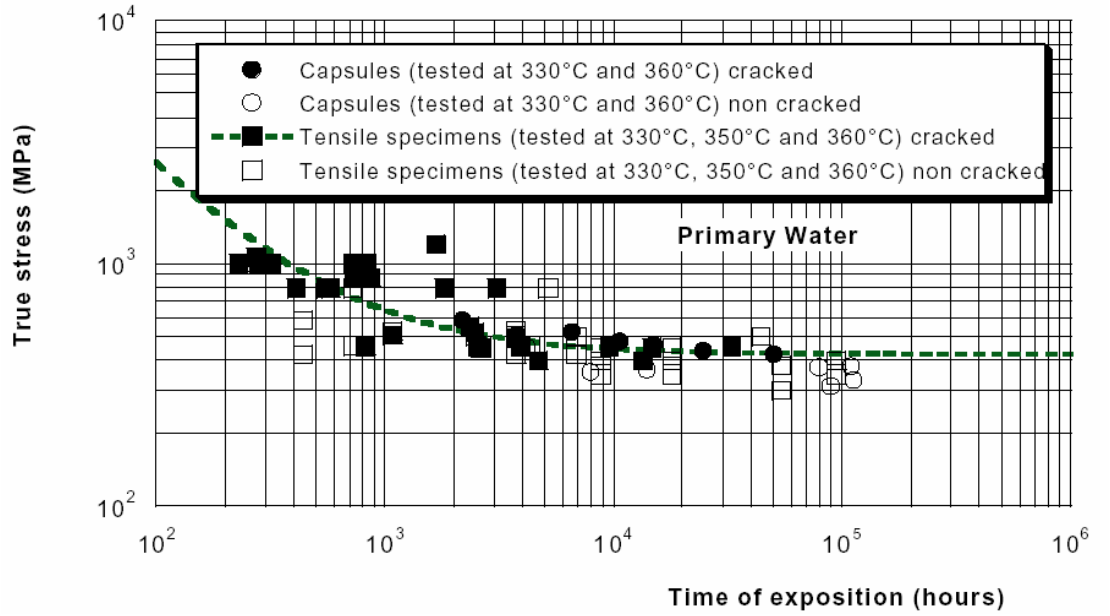

Figure 88. Time to failure of Alloy 182 in primary water in constant load tests on tensile specimens and pressurized capsules. The data points are normalized to the temperature of 325°C using activation energy of 185 kJ/mol (Amzallag et al. 2002).

According to Pathania et al. (2002), initiation tests on U-bend and C-ring specimens have revealed that Alloys 62, 82 and 182 with C ≥ 0.03 wt% (EN82H) are susceptible to PWSCC initiation in PWR primary water with very high pH (10–10.3). The failure rate of the high carbon Alloy 82 (EN82H) was lower than that of the low carbon Alloy 82. Thermal treatment at 607°C was beneficial, but did not eliminate PWSCC initiation. The test temperatures were 315, 338 and 360°C.

8.1.3 Low temperature crack propagation, LTCP

Low temperature crack propagation was observed in laboratory investigations performed in hydrogenated water (150 cc/kg) at temperatures below 150°C (Mills & Brown 1999). The fracture resistance (and tearing modulus) of nickel-base weld metals, Alloy 82 and Alloy 52, is drastically reduced (down to J_{IC} values < 5 kJ/m^2) compared to values obtained in air or high temperature water (Brown & Mills 2005, Young et al. 2005). Also the fracture mode changes from ductile to intergranular. Based on the investigations performed so far, the phenomenon is considered to be a form of hydrogen embrittlement occurring at temperatures lower than 150°C in hydrogenated water. A crack is considered to be a prerequisite for LTCP, and the loads needed to initiate cracking are rather high. However, based on the limited data existing so far, the risk for LTCP, e.g. during cool-down sequences in commercial PWRs cannot be omitted (Demma et al. 2005).

8.2 Laboratory investigations in BWR environment

According to the generally-accepted hypotheses on SCC in BWR environment, the basic cracking mechanism is the same for stainless steels and nickel-base alloys, i.e., they crack via the slip-dissolution mechanism (Andresen 1987, 1988, 1991, Andresen & Ford 1996, Horn et al. 2002). A susceptible material, a tensile stress and an oxidising environment enhance the cracking susceptibility. Cracking susceptibility for Alloy 182 is, thus, higher in normal water chemistry (NWC) as compared to hydrogen water chemistry (HWC) or noble metal chemistry, although cracking is not considered impossible in the latter two environments. Based on this mechanistic understanding, the BWR community has applied a significant amount of effort over the last two decades to quantify the cracking behaviour of Alloy 182 in both NWC and HWC environments. It has been necessary to provide data to support justifications for continued operation of cracked Alloy 182 dissimilar metal welds, as well as to provide new approaches for evaluating cracking in reactor internal components, if crack indications are found in future inspections.

Based on the experimental and field data and a screening process to limit data to relevant conditions, both NWC and HWC disposition lines for crack growth rate have been developed as part of the BWR-VIP activity. The data clearly substantiate significantly lower crack growth rates in HWC over those measured for the highly oxidizing NWC environment. However, it must be recognized that there is still some measurable crack growth over time even in an effective HWC environment that is supposed to mitigate the crack growth in BWRs.

The CGR of Alloy 182 in non-oxidising BWR-environment is considered to be slow, on the order of 3×10^{-9} mm/s. This is much slower than the CGRs typically measured in PWR primary water. The most important difference between BWR and PWR environments as concerns CGRs in Alloy 182, is the temperature, being about 50°C lower in BWR environment compared to that of PWRs. Assuming a similar behaviour of stainless steels and nickel-base alloys, 4–5 times higher CGRs are to be expected at 320ºC (PWR-typical outlet T) as compared to 288°C (BWR outlet T).

No published data was found in the studied literature for Ni-base weld metals Alloy 52, 152, 132 or 72 for relevant (i.e., low impurity) BWR conditions.

In order to reduce the corrosion potential, some power plants have taken hydrogen water chemistry (HWC) in use. The effect of corrosion potential on the crack growth rate of Alloy 182 is shown in Figure 89.

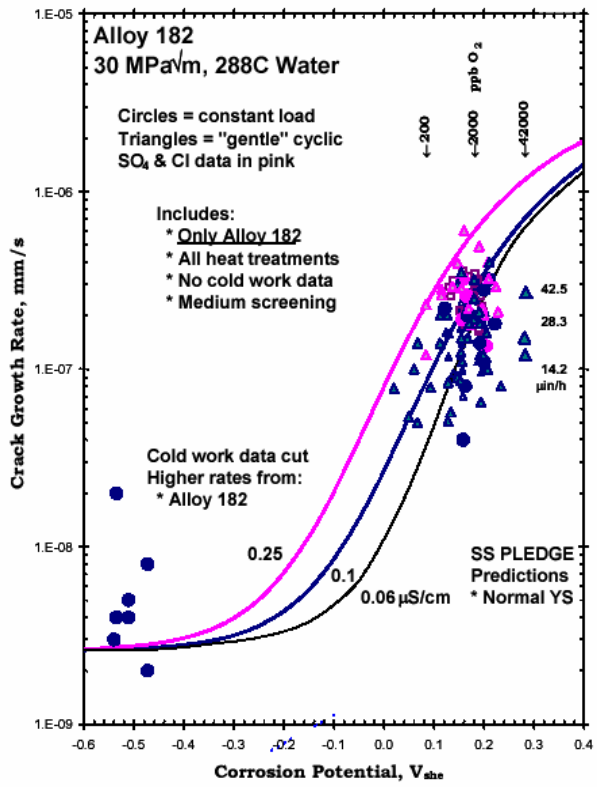

Figure 89. Measured crack growth rates for Alloy 182 as a function of corrosion potential in simulated high purity BWR water at 288°C (Horn et al. 2002).

Itow et al. (2003) evaluated the influence of the corrosion potential on SCC crack growth behaviour of Alloy 182 in the case of a deep crack. A 1T-C(T) specimen was machined from a 70 mm thick weld joint made of Alloy 600 and Alloy 182 weld metal. In order to simulate a deep surface crack encountered in actual plant components, a precrack more than 10 mm long was introduced into the specimen, and side covers were attached on the both side surfaces to prevent the dilution of the crack tip water chemistry. The crack growth tests were carried out under constant load at 288°C in simulated BWR water with normal and hydrogen water chemistries. The crack growth rate was suppressed by a factor of approximately 50 as the corrosion potential was decreased from 190 mV_{SHE} to –400 mV_{SHE} at K_I of approx. 60 MPa√m. The results are in line with those reported by Horn et al. (2002).

The effect of water impurities, especially sulphate ions, on stress corrosion crack initiation and propagation in Inconel 182 weld metal in BWR water has been investigated in many studies (Andresen 1987, Itow et al. 1997, Lidar 1995, Ljungberg & Stigenberg 1997, McCinn & Page 1988a, 1988b). In these references, sulphate ions were observed to have an accelerating effect on the crack growth rate. Initiation was also enhanced if the sulphate ion concentration was high enough to change the pH value from near neutral to acidic. However, the amounts of sulphate ion additions have

commonly been high, on the order of 1 ppm, and only a few results are available on the effects of small amounts, i.e., 30 ppb or less sulphate, comparable to possible ion exchange resin intrusion induced concentrations in a real BWR plant.

The presence of anionic impurities has been shown to enhance the crack growth rate in Inconel 182 weld metal even at low temperatures. The decrease of the corrosion potential, e.g., by hydrogen water chemistry, reduces the crack growth rate and also the detrimental effect of impurities. However, with increasing temperature, the crack growth rate can be significant even in de-aerated water, i.e., at low corrosion potentials, if the anion concentration is high (Andresen & Ford 1996, Ljungberg & Stigenberg 1997).

The critical sulphate ion level required to accelerate the crack growth depends on the flow conditions and the duration of the impurity transients. In tests conducted in Studsvik, two sulphate intrusions of short duration (<14 h) were needed before measurable acceleration in the crack growth rate was observed (Lidar 1995). On the other hand, the decrease in the crack growth rate after returning to the low impurity level in the bulk environment can be prolonged up to >100 h.

Toivonen et al. (2001) and Toivonen (2004) studied the effects of water chemistry impurity concentration on crack growth rate in Alloys 82 and 182. Stress corrosion crack growth rates of Alloy 182 and 82 weld metals in thermally aged (400°C/200 h) conditions were measured in simulated BWR conditions at 273°C. The time for the onset of accelerated crack growth due to impurity / conductivity transient was measured by adding sulphate as H_2SO_4 in the range of 10–100 ppb into de-mineralized feed water. The addition of 10 ppb sulphate increased the crack growth rate by an order of magnitude compared to pure water. Higher sulphate concentration did not increase the crack growth rate any further. Crack growth was monitored using the potential drop method during combined slow rising displacement / constant displacement tests on 10×10 mm^2 cross-section prefatigued SEN(B) specimens. In the tests an increase in the crack growth rate became visible in Alloy 182 within 25–45 h after sulphate was introduced into the water. The crack growth rate did not return to the level prevailing prior to the transient within hundreds of hours, even if the sulphate injection was finished. In Alloy 82 no crack growth was observed with any of the applied conditions. The measured crack growth rates of Alloy 182 are shown in Figure 90 as a function of K_J (i.e., J integral converted to K units).

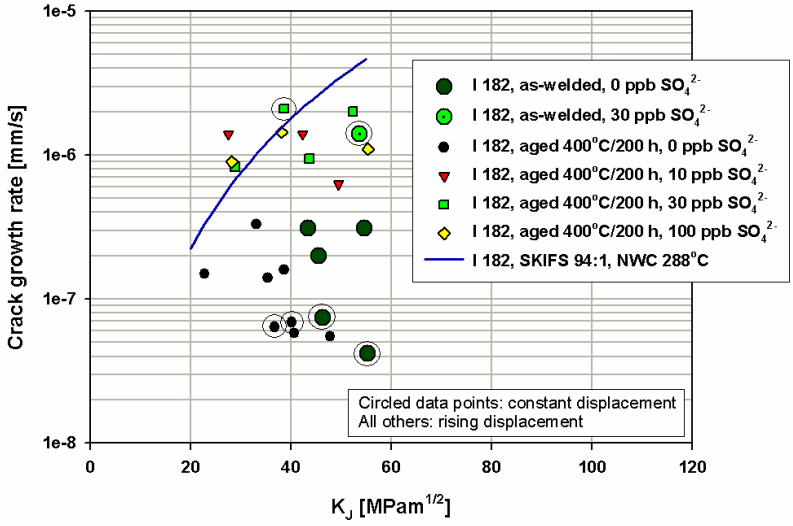

Figure 90. Crack growth rates in as-welded and in thermally aged (400°C/200 h) Inconel 182 weld metal as a function of K_J in simulated BWR water. T = 273°C, conductivity (outlet) = 0.1 – 0.9 µS/cm, dissolved O_2 (outlet) = 300 ppb, ECP = 50 – 150 mV_{SHE}. An old Swedish disposition line for the same material and for normal BWR water chemistry at 288°C is also shown (Toivonen 2004).

Although the corrosion potential affects the crack growth rates in Alloy 182, the crack growth rates are higher in typical PWR primary water than in BWR HWC. The difference, according to Horn et al. (2002) is related to the temperature difference between the plant types. The higher operating temperatures of PWRs (nearly 50°C difference) result in up to 10 times higher CGRs.

Sulphate has an accelerating effect on the crack growth rate in BWR water. Sulphates result from the ion exchangers, and enrich remarkably in the crack tip area, up to 100 times (Andresen & Ford 1996) or even more (MacDonald et al. 1997). Numerous investigations on this topic have been performed (Aaltonen et al. 2002, Gott 1995, Itow et al. 1997, Lidar 1995, Ljungberg et al. 1991, Ljungberg 1993, Ljungberg et al. 1993, Ljungberg et al. 1995, Ljungberg & Stigenberg 1997, McMinn & Page 1988a, 1988b, Mills et al. 2001), and the main results may be summarised as follows:

- There is a time delay (typically some tens of hours) between the sulphate intrusion and the increase in the crack growth rate.
- Sulphate ions concentrate in cracks in appreciable amounts in BWR NWC environment.
- After sulphate intrusions, higher crack growth rates are sustained for long periods, >>100 h, after the bulk environment is nominally clean.
- The CGR of Alloy 182 is higher than that of sensitised austenitic stainless steel of type AISI 304 in clean NWC environment.

- An acceleration factor of about 10 for sensitised AISI 304 stainless steel, and about 4…8 for heat-treated Alloy 182 has been reported at a sulphate ion concentration of 30 ppb, compared to the CGR in clean NWC.
- At high amounts of sulphate ions (about 100 ppb), the observed CGRs for sensitised stainless steel and Alloy 182 are similar.
- Crack initiation is largely independent of conductivity per se, but is affected by the pH, and initiation is enhanced at pH below neutral.

Kuniya et al. (2003) studied the effects of a crevice on SCC initiation in DNiCrFe-1J weld metal in BWR water with 8 ppm oxygen at 288°C. The composition of the weld metal Alloy 132 is shown in Table 13.

Table 13. Chemical composition of DNiCrFe-1J (wt.-%) (Kuniya et al. 2003).

C	Si	Mn	P	S	Ni	Cr	Fe	Nb
0.04	0.2	3.03	0.005	0.003	70.5	14.45	9.53	1.69

Kuniya et al. (2003) observed that an artificially formed crevice around tensile specimens under constant load conditions decreased the time to failure. The specimens were loaded to 410 MPa (yield stress was not reported, tensile stress was 597 MPa). The failure times were 7000–14 000 h under crevice conditions. Specimens tested under crevice-free conditions had not failed, when Kuniya et al. (2003) reported their results (i.e., up to 14 900 h) except for one specimen, which failed after 13 700 h loading time. The anion concentrations within the crevices are shown in Table 14. The autoclave inlet conductivity was 0.067 and outlet conductivity was 0.33 μS/cm, respectively.

Table 14. Measured anion concentrations within the crevices during the constant load tests on tensile specimens (Kuniya et al. 2003).

Cl^-	NO_3^{2-}	SO_4^{2-}
2100 ppb	430 ppb	7400 ppb

Saito et al. (1999) also reported initiation test results measured using tensile specimens with artificially formed crevice conditions around the gauge section of the specimens. They performed constant load tests with periodic unloading on Alloy 182 specimens in NWC and (partial) HWC conditions within the corrosion potential range of –100…+190 mV_{SHE}. The conductivity was controlled using either $NaNO_3$ (0.1 μS/cm) or Na_2SO_4 (0.3 μS/cm) addition. The applied stress was from 412 to 568 MPa. Based on the

results, Saito et al. (1999) concluded that partial HWC condition was effective in mitigating the SCC initiation in Alloy 182 in BWR water. Decreasing the corrosion potential from +190 mV_{SHE} to 0 mV_{SHE} improved the lifetime by a factor of 10. The failure time at +190 mV_{SHE}, 412 MPa and 0.3 μS/cm was 18 h.

Jenssen et al. (1999) tested bolt-loaded Alloy 600 and 182 C(T) specimens with U-notches (i.e., the specimens were not pre-cracked) in BWR NWC and HWC chemistries. The stress states of the notches were controlled using different U-notch radii under the same crack mouth opening displacements. The specimens were exposed to the test environments in two operating Swedish BWRs. In Alloy 182 specimens, the cracks initiated more easily in NWC than in HWC conditions. The first cracks initiated in Alloy 182 specimens during the first year of exposure to NWC conditions. After 5 years, cracks had initiated in 19 of the total number of 56 specimens. In HWC conditions, cracking was verified in 13 of the total number of 56 specimens installed. As could be expected, the initiation frequency was higher in the specimens having a small notch radius. The Alloy 600 specimens were less susceptible to crack initiation. In Alloy 600 specimens, no cracking was observed in HWC conditions and only one specimen out of 26 cracked in NWC conditions. An important issue is that in several specimens there were intergranular attack penetrations which had not actually developed into cracks. The intergranular attack penetrations did not have any apparent correlation with the notch radius. Jenssen et al. (1999) speculated that local chemical attack, with no relation to the stress state, on the grain or dendrite boundaries may act as initiation sites for stress corrosion cracking.

Jacko et al. (2003) reported an accelerated laboratory test series performed in an environment consisting of 400°C hydrogen containing steam doped with fluoride, chloride and sulphate anions. Comparison tests were performed using Alloy 600 and Alloy 182 weld metal. Alloy 52M welds, prepared to simulate the Ringhals 4 field repairs of the reactor vessel outlet nozzle, exhibited complete resistance to stress corrosion crack initiation for the laboratory exposure times exceeding 45 efpy (effective full power years) equivalent service time. Stress corrosion cracks initiated in Alloy 182 welds after exposure times less than one-fifth of the total exposure time of the Alloy 52M specimens. Crack initiation was also observed in specimens of Alloy 600 CRDM nozzle material in the doped steam environment.

The specimens were prepared as flat plates, and were bolt-loaded in specially designed four-point bending fixtures. The Alloy 52M weld specimens, as provided by Uddcomb, were 180 mm long × 40 mm wide × 9 mm thick plates, in which the welds were transverse to the long dimension.

Two strain/stress levels were tested. The lower level was 0.35% strain and the higher level was 1% strain. The lower level corresponds approximately to the strain at 0.2% offset yield strength of the material.

8.3 Cracking mechanisms

According to Scott and Combrade (2003) there is no general consensus on the mechanism of IGSCC or IDSCC of Ni-base alloys in PWR primary water. Several mechanistic models have been developed. Most of these hypotheses can be divided into two broad groups, those based on dissolution/oxidation of the crack tip and those based on the consequences of the associated evolution of hydrogen at the nearby cathode in the crack. Models based on hydrogen generally lack the ability to explain the cracking at high temperatures.

Slip-dissolution models have been successfully applied to predict IGSCC of sensitized or solution-annealed and cold-worked stainless steels and nickel-base alloys in the relatively oxidizing conditions of Boiling Water Reactors (BWR) and their extension to PWR conditions has been proposed. One difficulty with this approach seems to be the lack of a good correlation between the potential dependence of IGSCC of Alloy 600 (and Alloy 182) and the anodic current transients measured in fast straining or potential (cathodic to anodic) step experiments (Scott & Combrade 2003).

Laboratory investigations show that the susceptibility to environmentally assisted cracking in PWR primary water is a function of the chromium content of the material (Boursier et al. 2004, Bousine et al. 1994, Jenssen et al. 2001).

Nickel-base weld metals (Alloy 82 and Alloy 82H) can suffer from hydrogen assisted cracking at low-temperature water containing dissolved hydrogen (Pathania et al. 2002). The temperature range where this behaviour has been observed is 54–93°C. Initiation has not been detected, but the phenomenon can occur at location with pre-existing cracks. Alloy 52 (and wrought Alloy 690) is also susceptible to this type of cracking, but to a lesser extent than Alloy 82. The investigations performed and reported in the open literature so far have not been performed in simulated PWR-environment, but in water containing dissolved hydrogen. Investigations on the effect of dissolved lithium and boron on this low-temperature cracking phenomenon are planned.

8.4 Hydrogen embrittlement

Attanasio and Morton (2003) studied the oxide film properties and CGRs of EN82H in water at 338°C as a function of dissolved hydrogen content. They observed that there is a maximum in the crack growth rate at the dissolved hydrogen content of 8 cc/kg. The crack growth rate was 8 times higher at hydrogen content of 8 cc/kg than at 60 cc/kg. They attributed the crack growth rate maximum to the oxide layer transition from NiO to Ni, which takes place at a hydrogen content of 13.8 cc/kg at 338°C. The crack growth rate measurements were performed at an initial K_I value of 38.5 MPa√m. The crack growth rates are shown in Figure 91 as a function of hydrogen concentration.

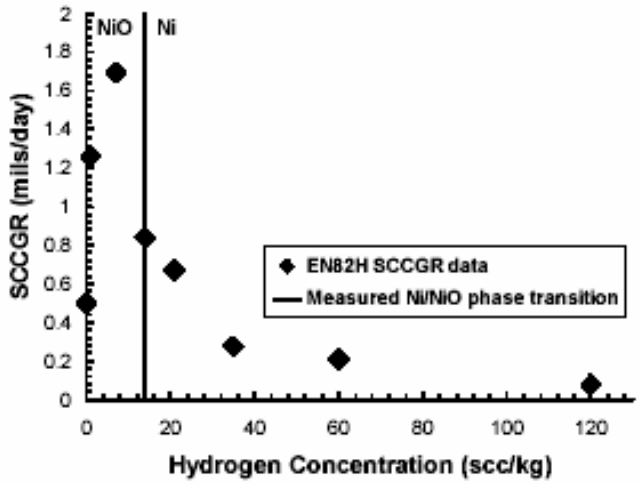

Figure 91. Stress corrosion crack growth rate of EN82H (high %C Alloy 82) as a function of dissolved hydrogen content in water at 338°C. The measured NiO-Ni transition is shown with the vertical line (13.8 cc/kg). (Attanasio & Morton 2003.)

According to Mills et al. (2001), as-fabricated EN82H welds are susceptible to low temperature embrittlement in 54°C hydrogenated water. Values of J_{Ic} in water are typically 90% to 99% lower than those in air due to a fracture mechanism transition from microvoid coalescence to hydrogen-induced intergranular fracture. Environmental J_{Ic} testing demonstrated that high temperature (1093°C) annealing and furnace cooling alleviates the material's susceptibility to hydrogen-induced intergranular cracking. To identify metallurgical and compositional features that are responsible for the material's environment-sensitive cracking behaviour, detailed characterization of the micro-structure and grain boundary chemistry for the as-fabricated and as-annealed materials was performed. Results from light optical microscopy, analytical electron microscopy, electron probe microanalysis, Auger electron spectroscopy and mechanical property characterization were used to provide insight into the observed low temperature embrittlement phenomenon. The key microstructural feature responsible for low temperature cracking in as-fabricated welds appeared to be fine niobium- and titanium-

rich carbonitrides that cover most of the grain boundaries. These precipitates are believed to be effective hydrogen traps that promote hydrogen-induced intergranular cracking. Dissolution of the fine carbonitrides during the anneal at 1093°C reduces grain boundary trapping sites, which accounts for the improved fracture resistance displayed by the annealed weld metal. The role of strength level in promoting the low temperature embrittlement was evaluated by cold rolling the annealed weld metal to increase its yield strength from 280 to 640 MPa. The annealed and cold-rolled weld metal exhibited high toughness in 54°C water and showed no evidence of hydrogen-induced intergranular cracking, thereby demonstrating that strength is not the primary cause of low temperature embrittlement. According to Mills and Brown (1999), Alloy 52 is also susceptible to hydrogen-assisted cracking in low temperature water containing H_2.

Pathania et al. (2002) summarised laboratory results and pointed out that interdendritic hydrogen-assisted crack growth has also been seen in Alloy 82 in addition to Alloy EN82H during rising load tests in low temperature (54–93^{o}C) water containing dissolved H_2.

According to Scott and Combrade (2003), several variants of hydrogen embrittlement mechanisms have been proposed, involving diffusion of hydrogen to and concentration at the crack tip followed by atomic scale decohesion or interactions with dislocations as in the Hydrogen-Enhanced Localised Plasticity (HELP) or Corrosion-Enhanced Plasticity (CEPM) models of hydrogen-induced fracture. With the possible exception of the CEPM, it is difficult to explain the observed decrease in the cracking susceptibility with increasing hydrogen partial pressure after the maximum observed at ~$E_{Ni/NiO}$. It is also to be noted that the grain boundary carbides enhance intergranular hydrogen embrittlement at lower temperatures, whereas they clearly improve resistance to IGSCC in the PWR primary water.

Smuk et al. (1999) studied the diffusivity of hydrogen and its interaction with dislocations in Inconel 600 and 690 alloys using internal friction measurements. Entalpy for the hydrogen diffusion jumps was found to be higher for Alloy 690 containing more Cr than that for Alloy 600. The enthalpies were 0.52 and 0.38 eV, respectively. The hydrogen-dislocation binding energies in deformed Alloys 600 and 690 were 0.24 and 0.16 eV. According to Smuk et al. (1999) hydrogen-enhanced localized plasticity (HELP) is possible only below 450 K (177^{o}C) in Alloy 600 and below 400 K (127^{o}C) in Alloy 690. This is consistent with the observed low temperature embrittlement of Ni-base weld metals.

8.5 References

Aaltonen, P., Bojinov, M., Helin, M., Kinnunen, P., Laitinen, T., Muttilainen, E., Mäkelä, K., Reinvall, A., Saario, T. & Toivonen, A. 2002. Facts and Views on the Role of Anionic Impurities, Crack Tip Chemistry and Oxide Films in Environmentally Assisted Cracking. VTT Research Notes 2148. Espoo: VTT. 68 p. + app. 21 p. http://virtual.vtt.fi/inf/pdf/tiedotteet/2002/T2148.pdf .

Amzallag, C., Boursier, J., Pages, C. & Gimond, C. 2002. Stress Corrosion Life Experience of 182 and 82 Welds in French PWRs. Proceedings of Fontevraud 5, Contribution of Material investigation to the Resolution of Problems Encountered in Pressurized Water Reactors. SFEN. Fontevraud, France, 23–27 September 2002. Pp. 69–80.

Andresen, P. 1987. Effect of Dissolved Oxygen, Solution Conductivity and Stress Intensity on the Interdendritic Stress Corrosion Cracking of Alloy 182 Weld Metal. Proceedings of Corrosion/87. San Francisco, California, USA, 9–13 March 1987. Paper No 85. 12 p.

Andresen, P. 1988. Observation and Prediction of the Effects of Water Chemistry and Mechanics on Environmentally Assisted Cracking of Inconels 182 Weld Metal and 600. Corrosion Science, Vol. 44, No. 6, June, pp. 376–385.

Andresen, P. 1991. Effect of Specific Anionic Impurities on Environmental Cracking of Austenitic Stainless Materials in 288°C Water. Proceedings of the International Symposium on Environmental Degradation of Materials in Nuclear Power Systems – Water Reactors. Monterey, California, 25–29 August 1991. Pp. 209–218.

Andresen, P. & Ford, P. 1996. Fundamental Quantification of Crack Advance for Life Prediction in Energy Systems. Proceedings of Corrosion/96 Research Topical Symposia. NACE International, Houston, TX 77084. Pp. 51–99.

Attanasio, S. & Morton, D. 2003. Measurement of the Nickel/Nickel Oxide Transition in Ni-Cr-Fe Alloys and Updated Data and Correlations to Quantify the Effect of Aqueous Hydrogen on Primary Water SCC. Proceedings of 11th International Conference of Environmental Degradation of Materials in Nuclear Systems – Water Reactors. Stevenson, WA, USA, 10–14 August 2003. CDROM.

Boursier, J., Valliant, F. & Yrieix, B. 2004. Weldability, Thermal Ageing and PWSCC Behaviour of Nickel Weld Metals Containing 15 to 30% Chromium. ASME/JSME Pressure Vessels and Piping Conference. San Diego, California, USA, 25–29 July 2004. Ed. T. Tahara. PVP Vol. 490. Pp. 109–121.

Boursier, J., Couvant, T., Valliant, F. & Yrieix, B. 2005. A Review of PWSCC, Weldability and Thermal Ageing of Nickel Weld Metals in PWR Primary Water. International PWSCC of Alloy 600 Conference and Exhibit Show. New Mexico, USA, 7–10 March 2005.

Bousine, D., Vaillaint, F., Vidal, P. & Gimond, C. 1994. PWSCC Resistance of Nickel-base Weld Metals with Various Chromium Contents. EPRI Workshop on PWSCC of Alloy 600 in PWRs. Tampa, Florida, USA, 15–17 November 1994. 14 p.

Brown, C. & Mills, W. 2005. Load Path Effects on the Fracture Toughness of Alloy 82H and 52 Welds in Low Temperature Water. Proceedings of the 12th International Conference on Environmental Degradation of Materials in Nuclear Power Systems – Water Reactors. Snowbird, Utah, USA, 15–19 August 2005. To be published.

Demma, A., McIlree, A. & Herrera, M. 2005. Low Temperature Crack Propagation Evaluation in Pressurized Water reactor Service. Proceedings of the 12th International Conference on Environmental Degradation of Materials in Nuclear Power Systems – Water Reactors. Snowbird, Utah, USA, 15–19 August 2005. To be published.

Gott, K. 1995. Using Material Research Results in New Regulations – The Swedish Approach. Proceeding of the 7th International Symposium on Environmental Degradation of Materials in Nuclear Power Systems – Water Reactors. Breckenridge, Colorado, 7–10 August 1995. NACE. Pp. 639–649.

Horn, R., Andresen, P. & Hickling, J. 2002. BWR Alloy 182 Stress Corrosion Cracking Experience. Proceedings of Fontevraud 5, Contribution of Material Investigation to the Resolution of Problems Encountered in Pressurized Water Reactors. SFEN. Fontevraud, France, 23–27 September 2002. Pp. 55–67.

Itow, M., Abe, Y., Sakamoto, H., Hida, S., Takamori, K. & Suzuki, S. 1997. The Effect of Corrosion Potential on Alloy 182 Crack Growth Rate in High Temperature Water. Proceedings of the 8th International Symposium on Environmental Degradation of Materials in Nuclear Power Systems – Water Reactors. Amelia Island Plantation, Florida, 10–14 August 1997. Pp. 712–719.

Itow, M., Kikuchi, M. & Tanaka, N. 2003. The Influence of Corrosion Potential on SCC Growth Behavior of a Deep Crack in Alloy 182 in Simulated BWR Environment. Proceedings of 11th International Conference of Environmental Degradation of Materials in Nuclear Systems – Water Reactors. Stevenson, WA, USA, 10–14 August 2003. CDROM.

Jenssen, A., Stigenberg, M. & Ljungberg, L. 1999. Initiation of Stress Corrosion Cracking in Alloys 600 and 182. Proceedings of the 9th International Conference on Environmental Degradation of Materials in Nuclear Power Systems – Water Reactors. Newport Beach, CA, USA, 1–5 August 1999. Pp. 331–337.

Jenssen, A., Norrgård, K., Lagerström, J., Embring, G. & Tice, D. R. 2001. Assessment of Cracking in Dissimilar Metal Welds. Proceedings of the 10th International Conference on Environmental Degradation of Materials in Nuclear Power Systems – Water Reactors. Lake Tahoe, Nevada, USA, 5–9 August 2001. CDROM.

Jenssen, A., Norrgård, K., Jansson, C., Lagerstöm, J., Embring, G. & Efsing P. 2002. Structural Assessment of Defected Nozzle to Safe End Welds in Ringhals 3 and 4. Proceedings of Fontevraud 5, Contribution of Material Investigation to the Resolution of Problems Encountered in Pressurized Water Reactors. SFEN. Fontevraud, France, 23–27 September, 2002. Pp. 43–54.

Jacko, R., Gold, R. & Kroes, A. 2003. Accelerated Corrosion Testing of Alloy 52M and Alloy 182 Weldments. Proceedings of 11th International Conference of Environmental Degradation of Materials in Nuclear Systems – Water Reactors. Stevenson, WA, 10–14 August 2003. CDROM.

Kilian, R. 2005. Personal communication.

Kuniya, J., Yamamoto, M., Namatame, S. & Suzuki, S. 2003. Effects of Crevice Environment on the SCC Initiation of Alloy 600 and Nickel Base Weld Metal in High Temperature Oxygenated Water. Proceedings of 11th International Conference of Environmental Degradation of Materials in Nuclear Systems – Water Reactors. Stevenson, WA, USA, 10–14 August 2003. NACE. CDROM.

Le Hong, S., Boursier, J., Amzallag, C. & Daret, J. 2001. Measurements of Stress Corrosion Cracking Growth Rates in Weld Alloy 182 in Primary Water of PWR. Proceedings of the 10th International Conference on Environmental Degradation of Materials in Nuclear Power Systems – Water Reactors. Lake Tahoe, Nevada, USA, 5–9 August 2001. CDROM.

Lidar, P. 1995. Influence of Sulphate Transients on Crack Growth in Type 304 Stainless Steels in Water at 288°C. Proceedings of the 7th International Symposium on Environmental Degradation of Materials in Nuclear Power Systems – Water Reactors. Breckenridge, Colorado, USA, 7–10 August 1995. NACE. Pp. 597–607.

Ljungberg, L., Cubicciotti, D. & Trolle, M. 1991. Crack Propagation in Alloys 600 and 182 in Simulated BWR Environment. Proceedings of the 5th International Symposium on Environmental Degradation of Materials in Nuclear Power Systems – Water Reactors. Monterey, California, 25–29 August 1991. Pp. 226–235.

Ljungberg, L. 1993. Stress Corrosion Cracking of Alloys 600 & 182 in BWRs. Interim ABB Report, Volume 1, November. Research Project 2293-1.

Ljungberg, L., Örtnäs, A., Ståhle, P. & Nelson, L. 1993. Stress Corrosion Cracking Initiation in Alloys 600 and 182. Proceedings of the 6th International Symposium on Environmental Degradation of Materials in Nuclear Power Systems – Water Reactors. San Diego, California, USA, 1–5 August 1993. Pp. 379–384.

Ljungberg, L., Stiegenberg, M., Gott, K., Morin, U., Nelson, L., Bengtsson, B. & Jansson, C. 1995. Propagation of Stress Corrosion Cracking in Weld Structures in Nickel-base Alloy 182. Proceedings of International Symposium of Plant Aging and Life Predictions of Corrodible Structures. Sapporo, Japan, 15–18 May. Pp. 911–920.

Ljungberg, L. & Stigenberg, M. 1997. Stress Corrosion Cracking Propagation in Low-strength Nickel-base Alloys in Simulated BWR Environment. Proceedings of the 8th International Symposium on Environmental Degradation of Materials in Nuclear Power Systems – Water Reactors. Amelia Island Plantation, Florida, 10–14 August 1997. Pp. 704–711.

MacDonald, D. 1997. Clarification of Issues Raised by P.-L. Andresen and F. P. Ford in their Response to 'On the Modelling of Stress Corrosion Cracking of Iron and Nickel-Base Alloys in High Temperature Envrionments'. Corrosion Science 39 (1997). Pp. 1487–1490.

McMinn, A. & Page, R. 1988a. Stress Corrosion Cracking of Inconel Alloys and Weldments in High Temperature Water – The Effect of Sulfuric Acid Addition. Corrosion, Vol. 44, No. 4, April, pp. 239–247.

McMinn, A. & Page, R. 1988b. Stress Corrosion Cracking Resistance of Alloys 600 and 690 and Compatible Weld Metals in BWRs. EPRI Project 1566-1. Final Report EPRI NP-5882M, July.

Mills, W., Brown, C. & Burke, M. 2001. Effect of Microstructure on Low Temperature Cracking Behavior of EN82H Welds. Proceedings of the 10th International Conference on Environmental Degradation of Materials in Nuclear Power Systems – Water Reactors. Lake Tahoe, Nevada, USA, 5–9 August 2001. CDROM.

Mills, W. & Brown, C. 1999. Fracture Behavior of Nickel-base Alloys in Water. Proceedings of the 9th International Conference on Environmental Degradation of Materials in Nuclear Power Systems – Water Reactors. Newport Beach, CA, USA, 1–5 August 1999. Pp. 167–174.

Mills, W. & Brown, C. 2003. Stress Corrosion Crack Growth Rates for Alloy 82H Welds in High Temperature Water. Proceedings of 11th International Conference of Environmental Degradation of Materials in Nuclear Systems – Water Reactors. Stevenson, WA, USA, 10–14 August 2003. NACE. CDROM.

NRC Current Event Notification Report for March 16, 2005. http://www.nrc.gov/reading-rm/doc-collections/event-status/event/en.html.

Pathania, R., McIlree, A. & Hickling, J. 2002. Overview of Primary Cracking in Alloys 182/82 in PWRs. Proceedings of Fontevraud 5, Contribution of Material Investigation to the Resolution of Problems Encountered in Pressurized Water Reactors. SFEN. Fontevraud, France, 23–27 September 2002. Pp. 13–27.

Psaila-Dombrowski, M., Wade, C., Sarver, J., Van der Sluys, W. & Doherty, P. 1997. Evaluation of Weld Metals 82, 152, 52 and Alloy 690 Stress Corrosion Cracking and Corrosion Fatigue Susceptibility. Proceedings of the 8th International Symposium on Environmental Degradation of Materials in Nuclear Systems – Water Reactors. Florida, USA, 10–14 August 1997. Pp. 412–421.

Rao, G., Jacko, R. & McIlree, A. 2002. An Assessment of the CRDM Alloy 600 Reactor Vessel Head Penetration PWSCC Remedial Techniques. Proceedings of Fontevraud 5, Contribution of Material Investigation to the Resolution of Problems Encountered in Pressurized Water Reactors. SFEN. Fontevraud, France, 23–27 September 2002. Pp. 93–105.

Saito, N., Tanaka, S. & Sakamoto, H. 1999. Effect of Corrosion Potential on the SCC Initiation Lifetime of Alloy 182 Weld Metal. Proceedings of the 9th International Conference on Environmental Degradation of Materials in Nuclear Power Systems – Water Reactors. Newport Beach, CA, USA, 1–5 August 1999. Pp. 493–500.

Scott, P. & Combrade, P. 2003. On the Mechanism of Stress Corrosion Crack Initiation and Growth in Alloy 600 Exposed to PWR Primary Water. Proceedings of 11th International Conference of Environmental Degradation of Materials in Nuclear Systems – Water Reactors. Stevenson, WA, USA, 10–14 August 2003. NACE. CDROM.

Smuk, S., Hänninen, H., Jagodzinski, Y., Tarasenko, O. & Aaltonen, P. 1999. Comparison of Hydrogen Effects on Alloy 600 and 690. Proceedings of the 9th International Conference on Environmental Degradation of Materials in Nuclear Power Systems – Water Reactors. Newport Beach, CA, USA, 1–5 August 1999. Pp. 59–68.

Toivonen, A., Aaltonen, P., Taivalaho, L., Moilanen, P. & Muttilainen, E. 2001. Effects of Water Chemistry Transients on Crack Growth Rate of Nickel-base Weld Metals. Proceedings of the 10th International Conference on Environmental Degradation of Materials in Nuclear Power Systems – Water Reactors. Lake Tahoe, Nevada, USA, 5–9 August 2001. CDROM.

Toivonen, A. 2004. Stress Corrosion Crack Growth Rate Measurement in High Temperature Water using Small Precracked Bend Specimens. VTT Publications 531. Espoo: VTT Technical Research Centre of Finland. 206 p. + app. 9 p. http://virtual.vtt.fi/inf/pdf/publications/2004/P531.pdf.

Tsutsumi, K., Kanasaki, H., Yoshimoto, K., Nomura, Y., Asada S. & Yonezawa, T. 2003. SCC Growth Rate of Nickel-base Alloy 132 Weld Metal in PWR Primary Water. Proceedings of 11th International Conference of Environmental Degradation of Materials in Nuclear Systems – Water Reactors. Stevenson, WA, USA, 10–14 August 2003. CDROM.

Valliant, F., Moulart, P., Boursier, J. M., Amzallag, C. & Daret, J. 2002. Crack Growth Rates in Thick Materials of Alloy 600 and Weld Metals of Alloy 182 in Laboratory Primary Water. Comparison with Field Experience. Proceedings of Fontevraud 5, Contribution of Material Investigation to the Resolution of Problems Encountered in Pressurized Water Reactors. SFEN. Fontevraud, France, 23–27 September 2002. Pp. 107–116.

White, G., Hickling, J. & Harrington, C. 2005. MRP Development of Crack Growth Rate Disposition Curves for Primary Water Stress Corrosion Cracking (PWSCC) of Thick-Section Alloy 600 Components and Alloy 82, 182 and 132 Weldments. 2005 International PWSCC of Alloy 600 Conference and Exhibit Show. Hyatt Regency Tamaya Resort, New Mexico, USA, 7–10 March 2005.

Young, B., McIlree, A. & King, P. 2005. Reduction in Toughness Results for Weld Metal 182 in a PWR Primary Water Environment with Varying Dissolved Hydrogen, Lithium Hydroxide and Boric Acid Concentrations. 12th International Conference on Environmental Degradation of Materials in Nuclear Power Systems – Water Reactors. Snowbird, Utah, USA, 15–19 August 2005. To be published.

9. Experimental issues

Experimental factors in the determination of crack growth rates for the safety analysis purposes of nuclear power plants have been of interest lately, mainly because of the large scatter in the experimental data, even when the test environments and materials have been nominally the same. Andresen and Ford (1996) have listed possible issues that should be closely considered when crack growth rate measurements are performed:

- Control and monitoring of water chemistry (water purity and dissolved gases), especially related to the static autoclaves.
- Fluctuations in temperature, including potentially large contributions from low temperature exposure when preloaded specimens are heated and cooled and from poor high temperature stability.
- Fluctuations in load, including U-bend and C-ring specimens that undergo >50% stress relaxation, and ~ 2 Hz oscillations from high pressure pumps with missing or improperly installed pulse dampeners (or poorly performing pressure regulators) which allow the water pressure fluctuations to be transmitted via the loading linkage (load ratios, R <0.9 are possible). Similarly, solid Teflon sliding seals can produce large and uneven friction on the loading pull rod.
- Improper recording or interpretation of factors like outlet solution conductivity in tests in BWR water (the outlet is much more representative of the specimen conditions than the inlet, and knowledge of the specific ionic contributions is important), and sensitisation [standard EPR (electrochemical potentiokinetic repassivation) tests provide a poor measure of the minimum Cr level at the grain boundary, so that very high EPR values can occur with only moderate Cr depletion, while quite low EPR values are measured with deep but narrow Cr depletion].
- Problems with reference electrode accuracy, drift, placement, stray currents (e.g., from poor insulation of dc potential drop leads), etc., which can cause very large fluctuations (>1000 mV) and differences (>300 mV) in reported corrosion potential under identical conditions.
- Fatigue precracking and fully transitioning to SCC, including producing a fully intergranular (IG) or interdendritic (ID) morphology along the entire crack front, and plastic zone characteristics that closely match those of a crack grown under only SCC conditions. (IG/ID SCC is the relevant morphology in most austenitic materials – ferritic steels often exhibit transgranular SCC, but still require transitioning after air fatigue precracking). The idea that SCC should develop easily from a transgranular fatigue precrack produced in air, at a different temperature, and under ΔK, K_{max}, and frequency conditions that bear little or no resemblance to SCC is

often a serious error. There are only a few instances where SCC in the plant components nucleates from a transgranular fatigue crack.

- Managing crack front unevenness and interpreting crack length vs. time data is difficult. Because most laboratory crack depth measurement techniques are biased by uncracked ligaments (the crack appears much shorter than its average depth), SCC artificially appears to slow down as unevenness develops, and to accelerate as unevenness diminishes. While there is no debating that unevenness is a characteristic of SCC in most plant components, performing a controlled experiment in which crack length is accurately measured, and the stress/strain fields/stress intensity factor can be well characterized at the crack tip, requires that the crack front unevenness is minimized.

Stress corrosion cracking in Ni-base weld metals is interdendritic, and uneven crack propagation is especially common. The accuracy of the commonly-used Potential Drop (PD) crack length measurement method is sensitive to this unevenness.

Stress corrosion cracks and hot cracks are, however, very difficult to distinguish from each other, as both are interdendritic in nature. Based on extensive investigations (Boursier et al. 1999), a methodology has been presented by which SCC and hot cracks can be distinguished from each others. Based on Varestraint test results, Boursier et al. (1999) determined a few fractographic criteria by which hot cracks and SCC cracks can be differentiated. Hot cracks are relatively smooth, the grain boundaries are not visible, have perfectly demarcated (delimited) grain boundaries and do not show secondary cracking. There is also a difference in the appearance of precipitates on the fracture surface. In the case of hot cracks, the precipitates are typically flower shaped (due to free solidification) while the precipitates are embedded in the matrix in the case of SCC cracks. Furthermore, the fracture surface of hot cracks in Alloy 182 revealed systematically higher amounts of niobium, manganese and even silicon as compared to SCC fracture surfaces.

9.1 References

Andresen, P. & Ford, P. 1996. Fundamental Quantification of Crack Advance for Life Prediction in Energy Systems. Proceedings of Corrosion/96 Research Topical Symposia. NACE International, Houston, TX 77084. Pp. 51–99.

Boursier, J., Cleurennex, M., Rouillon, Y., Arnoldi, F. & Buisine, D. 1999. Differentiation between Hot Cracking and Stress Corrosion Cracking in PWR Primary Water of Alloy 182 Weld Metal. Proceedings of Eurocorr ’99. Long Term Prediction and Modelling of Corrosion. ECF Event No. 266. Nice, France, 12–16 September 2004. 11 p. CDROM.

10. Corrosion and thermal fatigue

According to IAEA-TECDOC-1361, the dissimilar metal welds in the PWR reactor coolant system piping represent geometrical and metallurgical discontinuities, which are probable locations for high stress and strain concentrations. The stress and strain concentrations may result in reduced fatigue resistance. The welds also represent locations for fabrication defects and inclusions.

The detrimental properties of the discontinuity across the weld depend on the type of the used filler metal. In general, the filler metals are nickel-base alloys or stainless steels. According to IAEA-TECDOC-1361, stainless steel based filler metals have a slightly more detrimental influence on fatigue life of the dissimilar metal welds than Ni-base filler metals. If Type 309 stainless steel butter layer is welded to the PWR pressure vessel nozzles before heat treatment, carbides decompose and carbon migrates across the metallurgical discontinuity from the ferritic pressure vessel steel into the stainless steel layer during post-weld heat treatment.

The driving force for the carbon migration is the carbon concentration difference between the ferritic pressure vessel steel and stainless steel weld metal. The carbon migration from the ferritic pressure vessel steel results in a narrow carbon-depleted zone in the heat-affected zone. The carbon-depleted zone has a lower yield stress compared to the unchanged ferritic steel. Next to the carbon depleted zone is a hard zone with carbide precipitates in the stainless steel butter. These adjacent zones represent a considerable yield stress gradient across a narrow region. The differences in the mechanical properties across this region may localize the strains in certain conditions. An example showing the carbon distribution across a dissimilar metal weld boundary is shown in Figure 92.

Because thermal expansion coefficients of ferritic pressure vessel and austenitic stainless steels are different (about 20–30% higher for austenitic stainless steel than for ferritic pressure vessel steel, see Table 11), heat-up and cool-down cycles result in cyclic thermal stresses in the dissimilar metal welds. The induced thermal stresses along with the changes in the mechanical properties resulting from carbon migration are possible issues that shorten the fatigue life of a dissimilar metal weld consisting of stainless steel as weld metal.

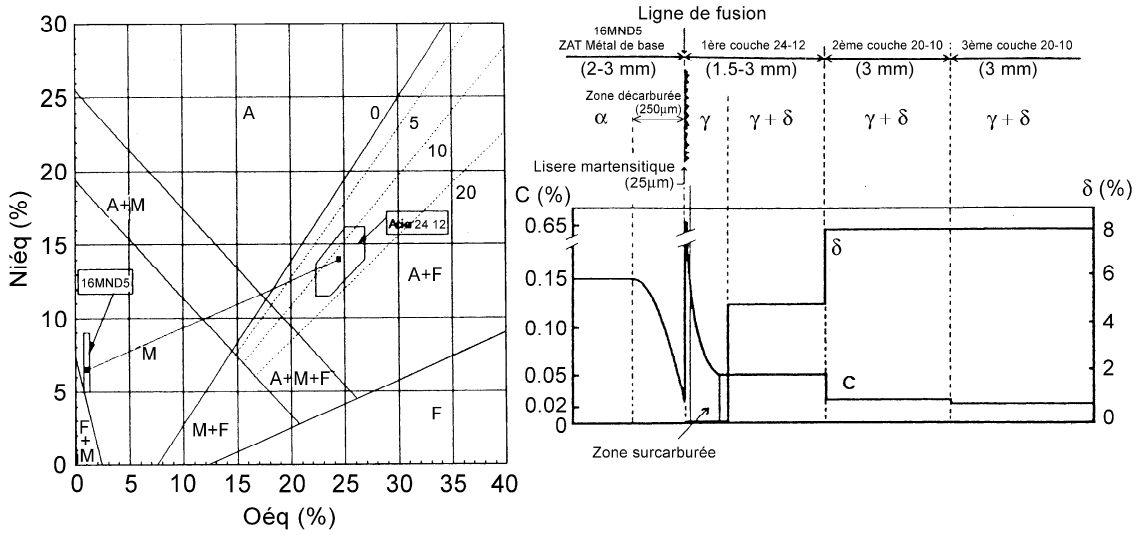

Figure 92. Schaeffler diagram and carbon distribution for the dissimilar metal weld between the stainless steel spray line and the low-alloy steel (A508-3) pressurizer nozzle (Cattant et al. 1994).

According to IAEA-TECDOC-1361, Ni-base weld metals in dissimilar metal welds have a less pronounced effect on the fatigue life. Carbon migration speed in Ni-base weld metals is lower than in stainless steel weld metals. Also, the differences in the thermal expansion coefficients between Ni-base weld metals and ferritic pressure vessel steels are smaller than between stainless and pressure vessel steels. However, the mismatch in thermal expansion coefficients between the Ni-base weld metals and the stainless steel piping remain significant.

Ni-base weld metals can not, however, be considered resistant to corrosion or thermal fatigue. Although the authors of this work did not find any field failure cases of dissimilar metal welds with Ni-base alloys directly caused by mechanical or thermal fatigue from literature, fatigue enhanced crack growth rates have been reported in several papers, e.g. Mills and Brown (2003) and Tsutsumi et al. (2003).

10.1 Other failure mechanisms

Intergranular attack (IGA) was found at Zorita NPP, Spain, in a CRDM penetration nozzle of a Westinghouse design PWR. The IGA was associated with the weld between the inner surface of the reactor closure head and the CRDM penetration. This IGA was attributed to locally high sulphate concentration resulting from two de-mineralizer resin ingress events. This damage mechanism differs from the more commonly observed mechanisms, because sulphate cracking can occur in regions that are not subject to significant stresses (NRC 1997). This was a rare incident related to dissimilar metal welds. However, IGA may operate as an initiation site for stress corrosion or fatigue cracking.

According to Wood et al. (1998) DMW failures have been a common problem in the boiler reheater and superheater sections of fossil-fired plants. The failed DMWs include welds in superheater outlet connections with Inconel 132 and 182 weld metals. Operating temperatures of these failed DMWs were 565°C and pressures 143 bar and 142 bar, respectively. The service times were 144 000 and 145 000 h. The joints showed microvoid formation and interfacial cracking in association with the interfacial carbides at the weld fusion line. In the case of the failure of the DMW welded using Inconel 132, microcracking resembling creep failure occurred away from the weld fusion line (i.e., in AISI 304 tube) as well as interfacial cracking took place. However, these temperatures are not encountered in the light water reactors, and thus creep can not be considered as a probable primary failure mechanism.

Creep has been studied also in temperatures relevant to the light water reactor environments, although the aim has been in the modelling of stress corrosion cracking mechanisms (Angeliu 2000, Vaillant et al. 1999, Yi et al. 1999). For example, Angeliu (2000) measured the creep rates of stainless steels and nickel-base alloys by testing compact tension specimens in air at 288^{o}C. The aim of the tests was to benchmark the different materials with respect to the role of crack tip creep strain rate in stress corrosion cracking. He observed that the primary and steady state creep rates were higher in austenitic stainless steels than in Inconel alloys. Based on the results, Angeliu (2000) stated that the austenitic stainless steels can be expected to be more susceptible to intergranular stress corrosion cracking than Ni-base alloys.

10.2 References

Angeliu, T. M. 2000. Characterizing the Creep Behavior of Austenitic Alloys Relevant to the Crack Tip Strain Rate and BWR SCC. Proceedings of Corrosion/00, NACE. Paper No. 185. 15 p.

Cattant, F., de Bouvier, O., Economou, J., Teissier, A. & Yriex, B. 1994. “Examens et Études Métallurgiques de Liaisons, Bimétalliques de Circuit Primaire Principal”, Contribution des expertises sur matériaux à la résolution des problèmes rencontrés dans les réacteurs à eau pressurisée, Colloque International Fontevraud III, Fontevraud, France, Septembre 1994.

IAEA-TECDOC-1361. 2003. Assessment and Management of Ageing of Major Nuclear Power Plant Components Important to Safety; Primary Piping in PWRs. http://www.pub.iaea.org/MTCD/publications/PDF/te_1361_web.pdf. 242 p.

Mills, W. J. & Brown, C. M. 2003. Stress Corrosion Crack Growth Rates for Alloy 82H Welds in High Temperature Water. 11th Inf. Conf. Environmental Degradation of Materials in Nuclear Systems, Stevenson, WA, 10–14 August 2003. 15 p.

NRC. 1997. Degradation of Control Rod Drive Mechanism Nozzle and Other Vessel Head Penetrations. NRC GENERIC LETTER 97-01. http://www.nrc.gov/reading-rm/doc-collections/gen-comm/gen-letters/1997/gl97001.html.

Tsutsumi, K., Kanasaki, H., Yoshimoto, K., Nomura, Y., Asada, S. & Yonezawa, T. 2003. SCC Growth Rate of Nickel Based Alloy 132 Weld Metal in PWR Primary Water. 11th Int. Conf. Environmental Degradation of Materials in Nuclear Systems, Stevenson, WA, 10–14 August 2003. 11 p.

Vaillant, F., Mithieux, J.-D., de Bouvier, O., Vancon, D., Zacharie, G., Brechet, Y. & Louchet, F. 1999. Influence of Chromium Content and Microstructure on Creep and PWSCC Resistance of Nickel Base Alloys. Proceedings of the 9th International Conference on Environmental Degradation of Materials in Nuclear Power Systems – Water Reactors. Newport Beach, CA, USA, 1–5 August 1999. Pp. 251–260.

Wood, G. R., Khoury, J. M. & King, J. P. 1998. Recent Experience in Dissimilar Metal Weld Failures. A DB Riley Technical Publication RST-148.

Yi, Y., Was, G., Cookson, J., Fish, J., Attanasio, S., Krasodomski, H. & Wilkening, W. 1999. Creep of Nickel Base Alloys in High Temperature Water. Proceedings of the 9th International Conference on Environmental Degradation of Materials in Nuclear Power Systems – Water Reactors. Newport Beach, CA, USA, 1–5 August 1999. Pp. 269–276.

11. NDE inspection

In this section the main principles of the NDE inspection of dissimilar metal welds are discussed and it is described how the qualification should be carried out to get best possible results concerning inspection of the butt welds, vessel head penetrations and RPV head wastage.

EPRI has initiated the Materials Reliability Program (MRP), which is divided in three parts, Figure 93. The inspection committee gives input to the safety assessment committee on the NDE capabilities and results from inspections, proper inspection frequencies, and acceptance criteria. The committee can be addressed with NDE questions, possible alternative NDE techniques in development, leak detection capabilities and qualification items as well as risk informed inspection potentials. The inspection committee evaluates, e.g., the possible boric acid walk-down adequacy, helps in mock-ups for the inspections and follows lessons learned in the USA and abroad. The main inspections focussed on in the MRP program are:

- CRDM penetrations
- butt weld inspections
- inspections of other Alloy 600/82/182 locations.

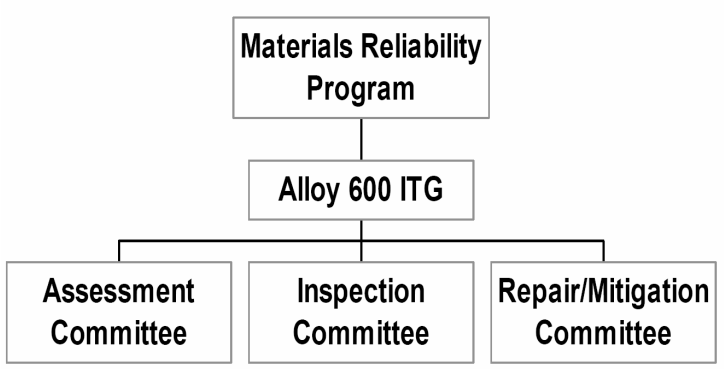

Figure 93. Division of the materials reliability program in different committees (Alley 2002).

The inspection committee cooperates with organisations such as MPR, EPRI, PDI, NEI, NRC and ASME. As a result, the committee is able to demonstrate the inspection technologies, monitor the experience, give guidance for inspections and keep the data base of the results.

The NESC-3 blind round-robin inspection trials were developed in the project ADIMEW partly funded by European Commission. The objective of ADIMEW was to quantify the accuracy of the structural integrity assessment procedure for defect-

containing, Austenitic Dissimilar Metal Welds. In order to disseminate the results from ADIMEW further and to provide additional input contribution on an in-kind basis, it was decided to incorporate it under the existing NESC network. The ADIMEW project did not foresee any inspection programme, and it was therefore decided that NESC-3 will launch its own blind Round-Robin Trials (RRT). The ADIMEW project was investigating a large-scale component with an austenitic (E308L) dissimilar metal weld. During the development of the NESC-3 RRT a number of defects were found in Inconel 182 dissimilar metal welds (e.g., V.C. Summer, USA; Ringhals, Sweden; Biblis, Germany). It was decided within NESC-3 to manufacture a mock-up containing 2 different types of dissimilar metal welds – austenitic 308L and Inconel 182, see Figure 94 and Figure 95 (Eriksen et al. 2004). The RRT gives guidance on detectability of the ultrasonic techniques usable for dissimilar metal welds as well as on the sizing techniques.

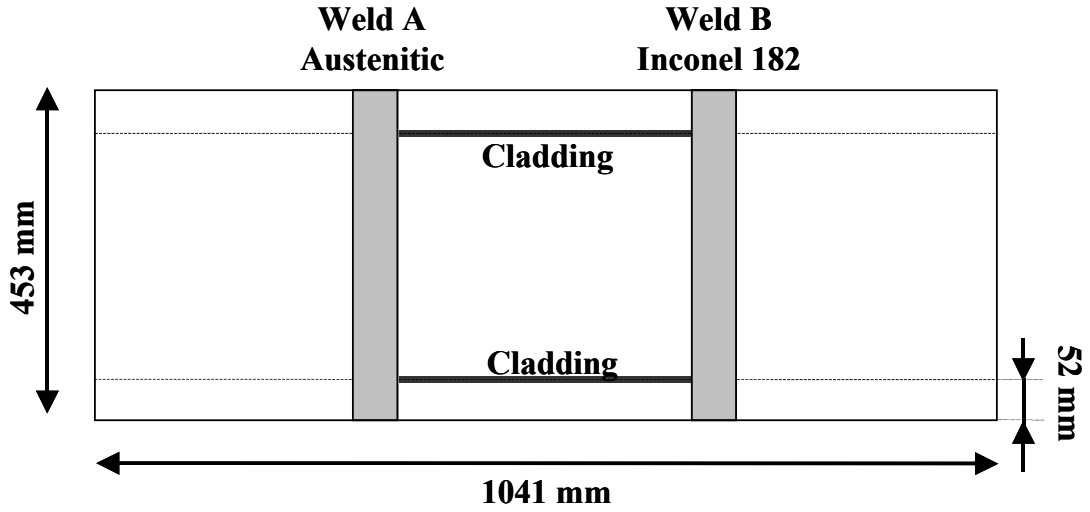

Figure 94. NESC-3 blind test block for dissimilar metal weld RRT (Eriksen et al. 2004).

	Weld A (Austenitic)	Weld B (INCONEL)
# 1: Ferritic	SA508	SA508
# 2: Austenitic	304L	304L
# 3: Buttering	A309L + A308L	INCONEL 182
# 4: Weld	E308L	INCONEL 182
# 5: Cladding	309L	309L

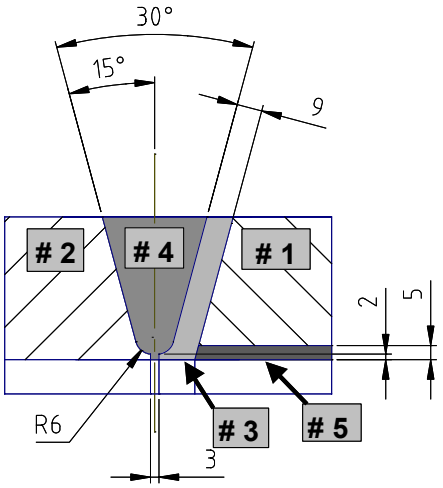

Figure 95. Materials used in the welds of different manufacturing techniques "A" and "B" (Eriksen et al. 2004).

The teams made full volumetric inspections of the two welds. The input data for the expected defect types were the following (Eriksen et al. 2004):

Circumferential defects:

- outer surface breaking defects (weld A only), see Figure 96
- embedded defects
- inner surface breaking defects.

Axial defects:

- inner surface breaking defects (weld B only).

The detection target for both welds was 5 × 10 mm and the sizing target was ±3 mm for through-wall sizing (Figure 97) and +10/-5 mm for length sizing (Figure 98).

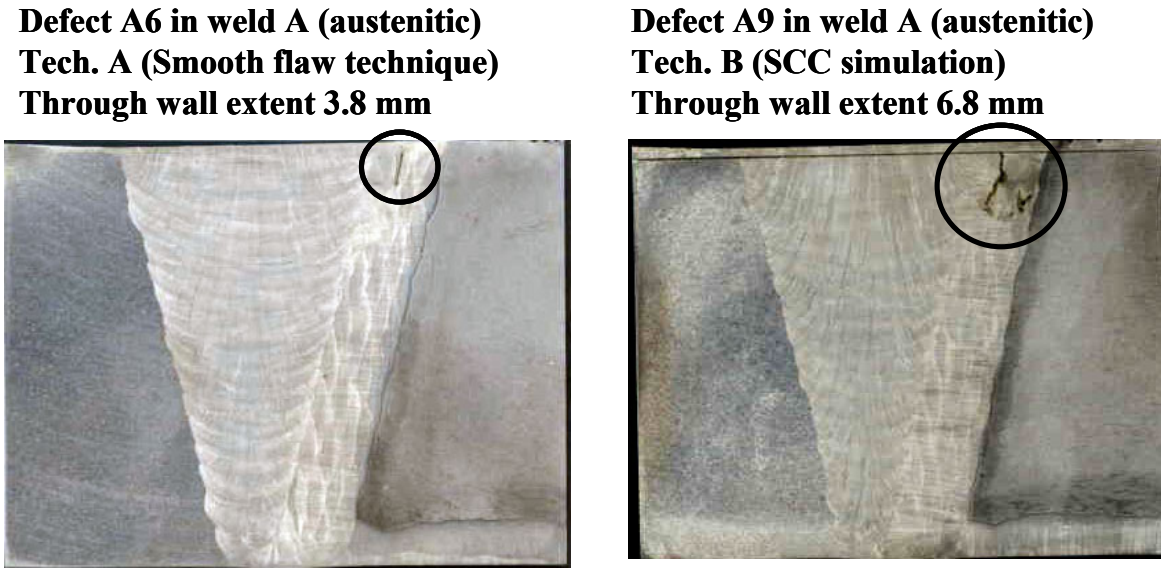

Figure 96. Examples of defects manufactured by techniques "A" and "B" after destructive examination (Eriksen et al. 2004).

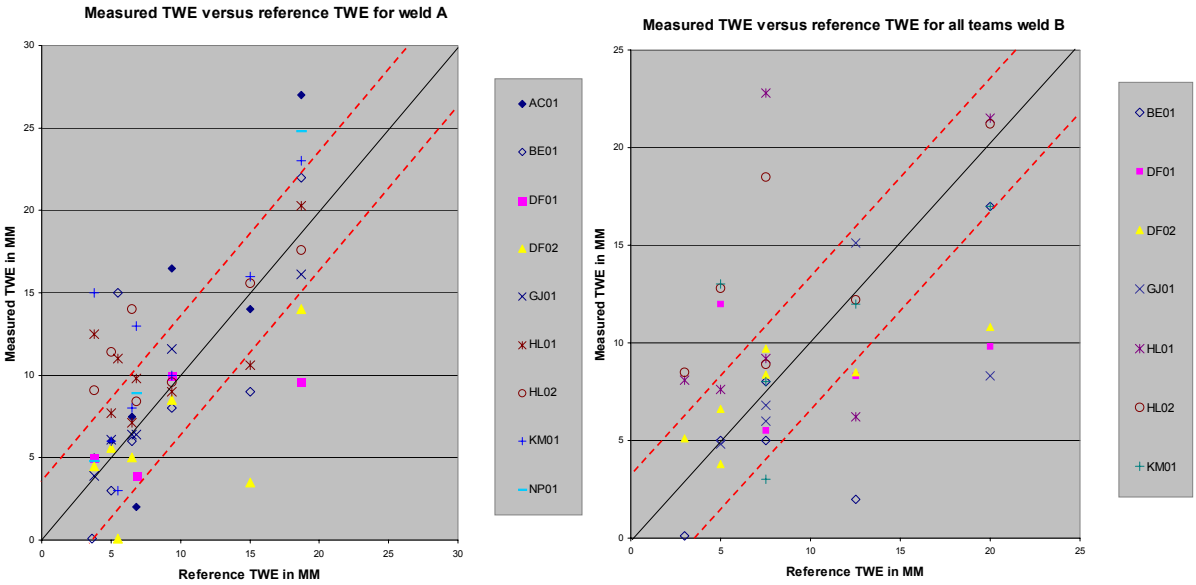

Figure 97. Examples of the inspection results of through-wall sizing for defects manufactured by techniques "A" and "B" (Eriksen et al. 2004).

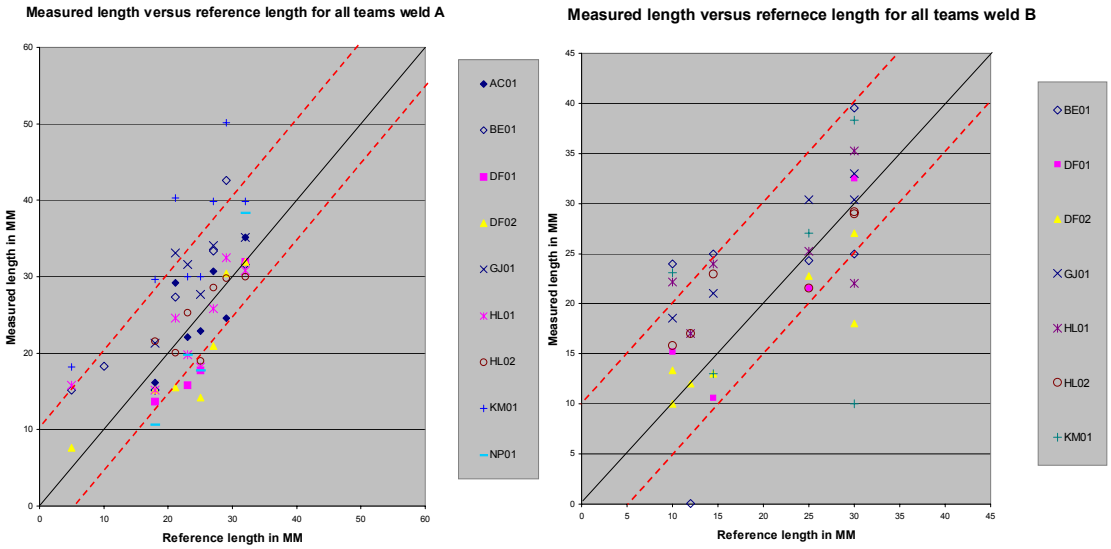

Figure 98. Examples of the inspection results of length sizing for defects manufactured by techniques "A" and "B" (Eriksen et al. 2004).

Several other activities in the field of dissimilar metal weld inspection and materials research have been activated because of the cracking events in the dissimilar metal welds around the world, e.g. Figure 99.

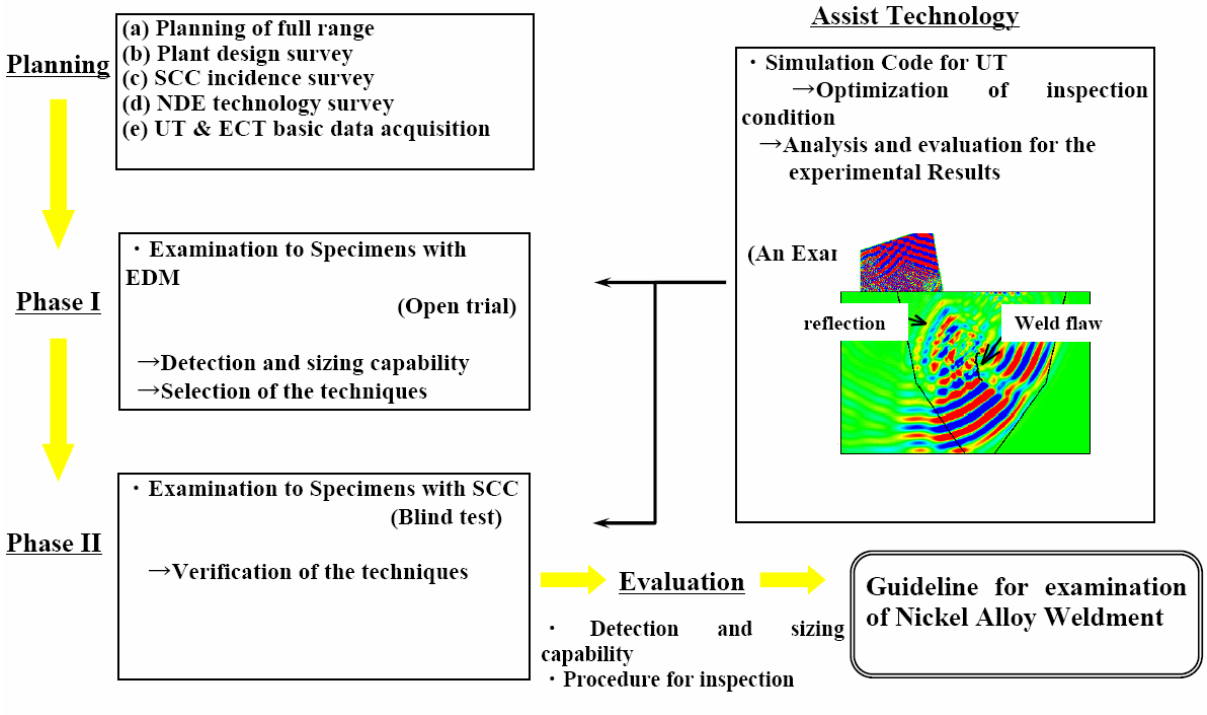

Figure 99. Programme for Inconel alloy weld inspection in Japan (JNES 2004).

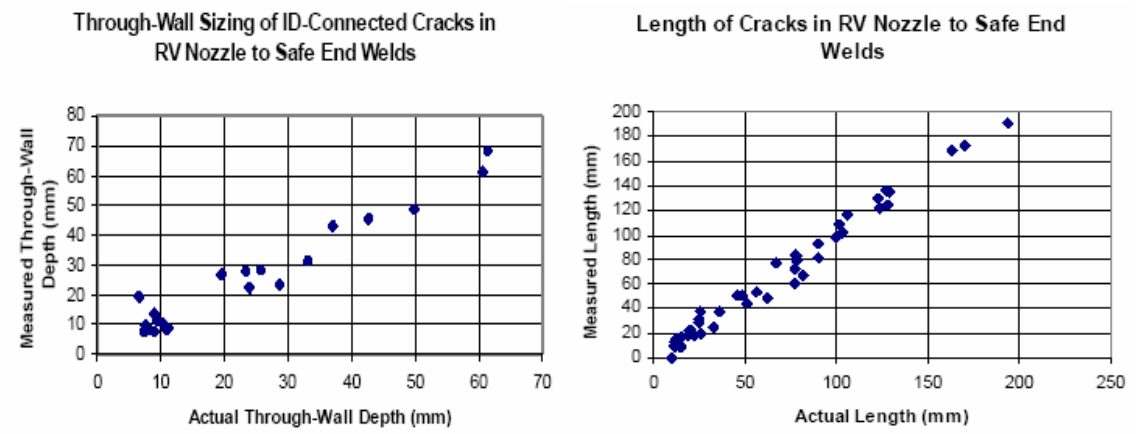

Figure 100. Defect sizing of a vendor from a qualification block for DMW inspection (Lareau & Adamonis 2004).

DMW inspections have shown problems in detection and sizing around the world, which can be clearly noticed in the qualifications carried out by EPRI. This was also noticed in NESC-3 RRT. There is a need to develop improved inspection techniques for this type of welds, for defects in both circumferential and axial directions. The best possible techniques and qualified personnel are needed to do the inspections, to combine techniques, to improve qualification efforts and modify the available software to a more flexible industrial direction. Future improvements in Phased array technique development can possibly provide this technological level. In Figure 100 is shown the

qualification results from open trial (Lareau & Adamonis 2004). The result is excellent, but sometimes the distribution and stress state of the real cracks can be different in the qualification test blocks than the real components. This causes huge difficulties in inspections on site.

11.1 NDE inspection technique requirements

The ASME XI code sets requirements for non-destructive testing. In the primary piping system the dissimilar metal welds are sometimes called bi-metallic or tri-metallic welds. Dissimilar metal welds are defined in Section XI as (IAEA 2003):

- carbon or low-alloy steel to high-alloy steel welds
- carbon or low-alloy steel to high-nickel alloy welds
- high-alloy steel to high-nickel alloy welds.

In the in-service inspection, the examination requirements for Class 1 piping welds are generally categorized in Table IWB-2500-1 (ASME XI, 2000) as Examination Category B-J, "Pressure Retaining Welds in Piping". During ISI, examination is required for 25% of all the butt and socket welds in the Class 1 piping, which includes volumetric and/or surface examination. In accordance with examination category B-J, Note (1), the examination sample shall include all dissimilar metal welds, which are not covered under category B-F.

In the ASME XI (2000), the other category of piping welds included in IWB are the dissimilar metal welds of examination category B-F. In the 2004 Addenda of Section XI, Examination Category B-F was reorganized to "Pressure Retaining Dissimilar Metal Welds in Vessel Nozzles". This category includes several types of dissimilar metal nozzle-to-safe end butt welds such as:

- reactor vessel nozzle to safe end butt welds
- pressurizer nozzle to safe end butt welds
- steam generator nozzle to safe end butt welds
- generally Class 1 components that are exempt from examination are piping systems NPS 1 and smaller.

NPS1 means a nominal pipe size of 1 in., excluding the welds already classified as Examination Category B-F welds. For volumetric and surface examination purposes, the adjacent base metal extends half of the nominal wall thickness of the weld. To this category also belong Class 1 heat exchangers, except all piping welds in heat exchangers from this category, to eliminate redundancy in the Code. Under examination

category B-F, 100% of the dissimilar metal welds to vessel nozzles are examined. The examination requirements are similar to those of examination category B-J; that is, volumetric of the inner 1/3 volume and/or surface examination of the external surface, depending on size (normal procedure in ASME XI). The requirements for welds in CRD housing are shown in examination category B-O.

In addition to the normal inspection problems that exist for each of the individual materials contained in the weld joint, the combination of materials further complicates ultrasonic examination due to differences in acoustic properties (i.e., velocity, attenuation) of the materials. The large, often columnar grain structure typical for austenitic welds leads to anisotropic acoustic properties and the size and arrangement of the grains, along with the differences in the elastic properties of the materials cause (IAEA 2003):

- scattering
- mode conversions
- beam distortions
- velocity variations that vary with position and scanning direction.

These variations in material properties decrease examination reliability through attenuation or redirection of the sound beam that interferes with crack detectability and characterization of both cracks and the real geometry of the weld.

In the French RCC-M in MC2700 are described the special requirements for ultrasonic testing of the Inconel welds for manufacturing and for in-service inspection in RSE-M, where for instance safe ends to pressure vessel welds should be inspected from inside with ultrasonic or gamma radiography described in section A and B in parts 3000 and 4000 (RCC-M 2000, RSE-M 1990).

An example of a typical inspection programme used for carbon steel piping is that performed in Germany. Siemens performed ultrasonic inspection of the cladding from the outside surface (Figure 101, IAEA 2003) on the total component surface to inspect disbonding of the cladding and to detect postulated underclad cracks in production test coupons, which were taken directly from the straight clad pipe or clad elbow as follows:

- chemical analysis of chips taken from the skin of the cladding of production test coupons for dilution control of the welding process
- radiographic and ultrasonic testing of the butt welds
- dye penetrant testing of the cladding
- magnetic particle testing of the ferritic weld surface.

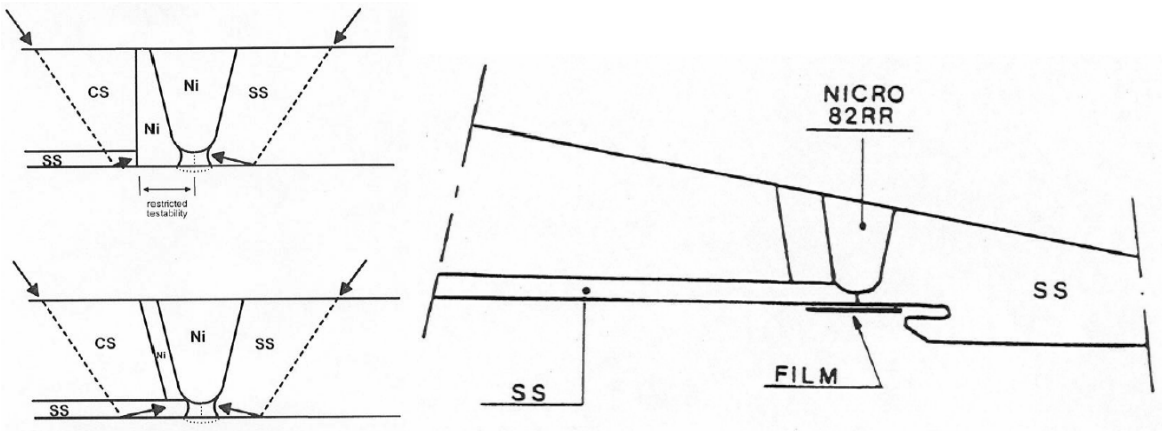

Figure 101. Ultrasonic and radiographic inspection procedure for a dissimilar metal weld in Germany (IAEA 2003).

Ultrasonic examination of the piping welds is addressed in the Mandatory Appendix III of ASME Section XI. The criteria used in Appendix III regarding detection of flaws are based on comparison of the reflected amplitude from a flaw to that of a reference reflector, typically a notch. The 1985 Addenda of the 1983 Edition reduced the recording level such that flaw indications exceeding 20% of the calibrated reference level had to be recorded and investigated. The reference level is determined by the reflected amplitude from the calibration notches (side-drilled holes are also used in some situations), which decreases as metal path distance increases. The resulting curve is called distance-amplitude correction or DAC curve. This amplitude-based inspection has already been shown to be unreliable. Normally most reliable, for instance, in PISC trials, were procedures, which considered all indications to the noise level. Defect detection amplitude-based method is usable, but in sizing this type analysis is not any more reliable.

There has been a lack of defect sizing guidelines in ASME Section XI. It has been proven in many occasions that amplitude-based sizing is not as reliable as other techniques such as mode-conversion techniques, ultrasonic diffraction based sizing or creeping wave analysis. Flaw sizing guidelines are currently being prepared for ASME Section XI (IAEA 2003). The dB-drop method is effective in determining the crack length, but it has been shown to be an ineffective method for determining the depth of planar reflectors such as cracks. As demonstrated by the PISC 2 trials, and shown in Figure 102, time-based sizing methods (i.e., crack-tip diffraction techniques) using time-of-flight to determine crack depth are far superior to the amplitude-based sizing methods. The amplitude-based methods tend to undersize flaws, especially the deeper ones, as indicated by the flat response shown in Figure 102, while measurements made with the time-based methods (i.e., crack-tip diffraction techniques) correlate well with the actual flaw depth. These crack-tip methods tend to be superior compared to the amplitude-based method, but in cases where the cracks are in Inconel welds in an axial or circumferential direction, the crack tip signals are very difficult to detect. In some cases, perhaps with longitudinal

wave mode the tip signals can be detected or the crack face can be revealed from the surrounding materials. For instance, the mode-conversion technique can be useful in these cases. The geometrical and ultrasonic limitations have to be recognised.

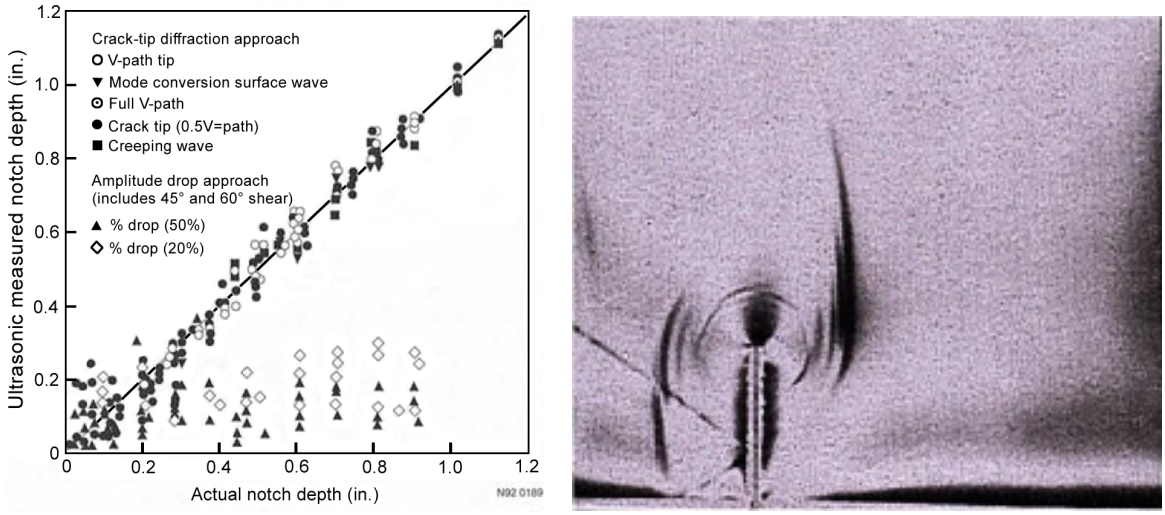

a) *b)*

Figure 102. Assessment of UT flaw sizing techniques showing the poor performance of the amplitude-based sizing techniques compared to crack-tip diffraction techniques (a) and ultrasonic diffraction from a slit (b) (IAEA 2003, Silk 1977).

In the materials such as Inconel nozzle welds, the material will cause strong attenuation and scattering of the ultrasonic waves. In this kind of materials the diffraction methods are only partly usable, because the tip diffraction echoes are in most cases hardly detectable in the weld volume.

The inspection approach is based on the use of longitudinal waves because of smaller attenuation compared to shear waves. This attenuation was compared by Matthies et al. (1986), who showed that actually the longitudinal and shear waves attenuate similarly at the same wave length. Normally the velocities of the longitudinal waves are about 2 times larger compared to those of shear waves, and the wave lengths are similarly double at the same frequency. The difference is the skewing of the ultrasonic beam in the weld. The longitudinal waves have smaller skewing in Inconel welds than shear waves. These facts lead to use of longitudinal wave modes in Inconel weld inspection. The resolution limit is a compromise, which comes from the attenuation of the ultrasonic waves in the weld material. To use as high a frequency as possible is the normal decision for the best resolution, but lower frequencies make it easier to detect a defect, because the spreading function of the beam is affected by the frequency. The smaller frequency leads to the higher spreading and to easier detection. To improve detection at a certain depth, focussed transmitter-receiver probes can be used for detection. By using shear waves one must use lower frequencies. To optimise the detection it is better to use lower frequency shear waves (0.5 MHz to 2 MHz). By using

composite probes the signal is shorter and frequency spectrum correspondingly larger. This also improves signal transmission in highly attenuating materials, and reduces noise from the grain boundaries.

By proper angle selection mode-conversion signals can be generated in both directions for detection of axial and circumferential defects. The mode-conversion signals are sensitive to the crack-type reflectors (planar reflectors). To optimise detection and sizing in Inconel weld inspection, TR-longitudinal probes must be used for detection and sizing purposes. Low frequency shear waves can be used for detection of corner reflections both in axial and circumferential directions, and TR-shear wave probes improve near field detection. To optimise crack detection in the circumferential direction, the secondary creeping-wave technique can be used. To optimise these techniques requires certain ultrasonic probes for each material and geometry combination at several focus depths. This can be achieved by using Phased array probes, but the special characteristics of the Phased array probes have to be considered. Crack tip signals can be detected reliably in austenitic base materials in front of the weld or in ferritic base materials but in the Inconel buttering or in the Inconel weld this is especially difficult or impossible. Thus, the defect sizing must be carried out by the before mentioned techniques.

There is also the possibility to use special techniques such as acoustic holography or SAFT techniques to improve the sizing capability, depending on the defect location.

The requirements for the inspection techniques are the very important facts when the inspection techniques are considered. Figure 103 shows a comparison between ASME code requirements and Swedish authority requirements for nozzle butt weld inspection. As can be seen that the Swedish requirements are more strict than the ASME code requirements.

Appendix VIII Supplement 10	SKIFS 20-00:1 Qualification
• Minimum size flaw for detection - 10% of thickness and greater*	• Target flaws for detection - 6mm high x 18mm long ID crack, 12mm high x 50mm long embedded planar flaw, 9mm high x 40mm long OD crack*
• Planar flaws oriented axial and circumferential; primarily ID connected	• Flaws oriented axial and circumferential
• 100% detection rate is required for procedure qualification	• 100% through-wall coverage
• Approximately 70 - 80% detection rate with 13 - 19% false call rate is required for equipment and personnel qualification*	• Flaw characterization of planar and volumetric flaws, surface and embedded
• Length sizing tolerance – ± 19mm*	• 100% detection rate required 100% detection rate with ≤ 20% false call rate for personnel qualification*
• Depth sizing tolerance - ± 3.2mm	• Length sizing tolerance - ± 13.9mm (ID crack), ± 19.2mm (OD crack), ± 20mm (embedded planar), based on target flaw sizes*
	• Depth sizing tolerance - ± 2.3mm (ID crack), ± 3.0mm (OD crack), ± 3.5mm (embedded planar), based on target flaw sizes*

Figure 103. Requirements for dissimilar metal weld UT inspection compared between ASME Section XI and Swedish authority requirements (Lareau & Adamonis 2004).

11.2 Inspection of CRDM penetration assemblies and BMIs

The first defect in RPV head penetration was detected in the Bugey plant. Between 1992–2000 a lot of inspections and repairs were carried out around the world. The following NDT-techniques have been used for vessel head penetration inspections: visual inspection, rotating UT, blade UT, penetrant testing, photothermal crack detection and ET.

For Inconel base materials and dissimilar metal welds visual inspections are made in the USA according to NRC requirements from October 2002 for vessel head penetrations (NRC Bulletin, 3rd July 2001). The plants can be divided in three categories, see Table 15 (EPRI 2002):

- low susceptibility plant (<10 EDY)
- moderate susceptibility plant (10–18 EDY)
- high susceptibility plant (>18 EDY).

The category according to Effective Degradation Year (EDY) is connected to non-detection of through-wall cracks and leak. The visual inspections are applicable to RPV heads, which are accessible from the upper surface, and RPV heads with closely conformed rigid insulation. Figure 104 and Figure 105 (Hiser 2002) show vessel head penetration constructions and boric acid deposits and corrosion on the vessel head.

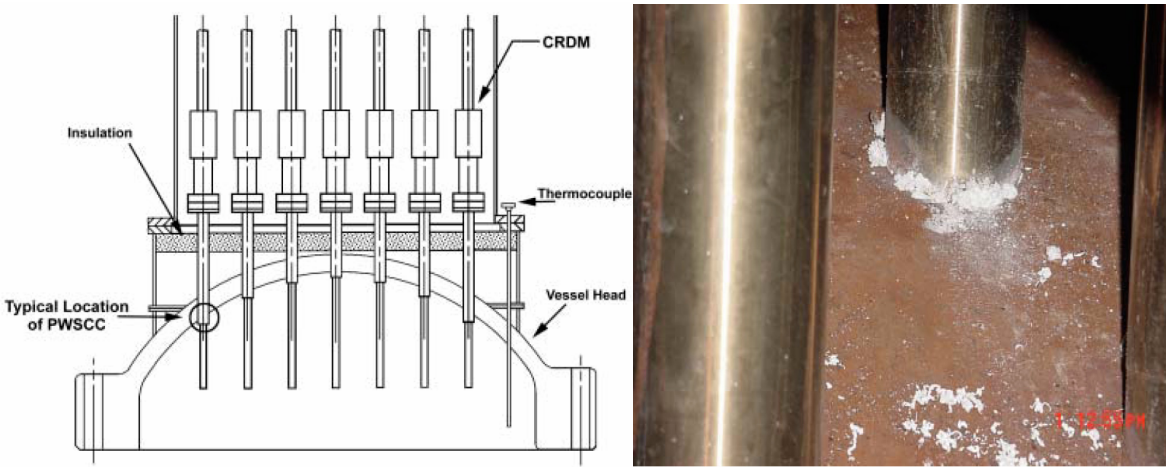

Figure 104. Typical reactor vessel head and boric acid deposit on the vessel head penetration (Hiser 2002).

Table 15. Recommend programs for vessel head penetration wastage inspection (EPRI 2002). Initial inspection is followed each 3rd RFO by 100% non-visual inspection in moderate plants and high susceptibility plants and in low susceptibility plants it is an alternative.

Inspection program	BMV	Non-visual NDT	Suppl. visual NDT
Low susceptibility	100% VHP each 10 EDY	VHP 100% each 10th EDY + J-groove weld	each 2nd RFO where not BMV or non-visual NDT
Moderate susceptibility	100% VHP 1st RFO and after each 2nd (<5th) EDY	VHP 100% 1st RFO and each 4th (<10th) EDY + J-groove weld	each 2nd RFO where not BMV or non-visual NDT
High susceptibility	100 % VHP at each RFO	VHP 100% 1st RFO and each 4th (<6th) EDY + J-groove weld	each 2nd RFO where not BMV or non-visual NDT

RFO = Refuel Outage, VHP = Vessel Head Penetration, EDY = Effective Degradation Year.

Plants where PWSCC is not detected are categorised according to NRC in three categories (Hiser 2002):

- high susceptibility plants to PWSCC (<5 EFPY [Effective Full Power Year] from the ONS3 condition)
- moderate susceptibility plants to PWSCC (from 5 to 30 EFPY of ONS3)
- low susceptibility plants.

In the USA all plants are in these categories. There are 7 high susceptibility plants and an additional 5 plants have already identified PWSCC. 32 moderate susceptibility plants have been identified. There is a total of 25 plants where no PWSCC is expected during their whole life time.

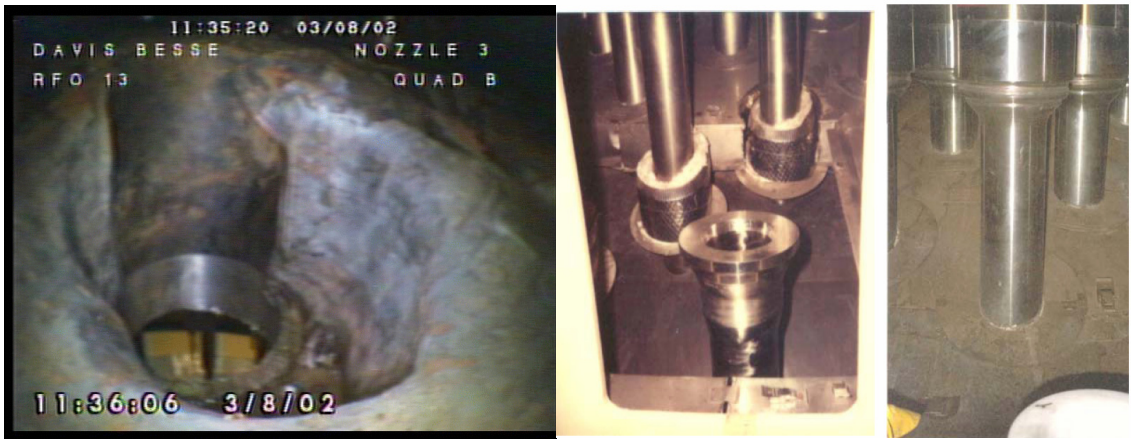

Figure 105. Corrosion cavity in Davis-Besse nozzle (left). Isolations cause some disturbance for visual inspections of vessel head penetrations (right) and in some cases they must be removed destructively (Hiser 2002).

The NRC approach to inspections of CRDM penetration assemblies and BMIs is the following:

- For high susceptibility plants of qualified visual examination (or UT/ET) is recommended, followed by UT for flaw sizing in nozzles not cleared by visual inspection. Qualified visual examination needs plant-specific demonstration that VHP nozzle cracks will lead to deposits on the RPV head. Demonstration of inspections so that they are not restricted by insulations, pre-existing deposits or other impediments is required.

- For moderate susceptibility plants effective visual inspection is required for RPV head surface, and UT for nozzle ID and ET for nozzle ID and J-groove weld inspect-tion are recommended. Effective visual inspection shall not be restricted by insulation, pre-existing deposits or other impediments.

- For low susceptibility plants only inspections according to Guideline 88-05 for boric acid deposits or bare metal visual inspection (BMV) are recommended.

11.2.1 Visual inspection

Visual inspection types are:

- Bare Metal Visual (BMV) inspection, in which the entire intersection of the RPV and each penetration must be visually inspected to approximately 1 in. distance of the adjacent bare surface of the upper head.

- Supplemental Visual (SV) inspection, which can be a direct remote visual examina-tion carried out according to plant's 88-05 General Visual Inspection programme.

The visual inspection is mainly carried out in order to find evidence of a significant boric acid accumulation that can be associated with an incipient wastage.

According to Cumblidge et al. (2004), visual testing using a 20/20 vision camera is capable of:

- detecting cracks with a Crack Opening Displacement (COD) of 10 μm on a perfect surface, Figure 106
- resolving features as small as 75 μm in size
- increasing minimum detectable and resolvable sizes in the presence of visual "noise".

Video and digital cameras generally have a lower resolving power than the human eye:

- Video cameras require higher magnifications than the naked eye to achieve the same resolution.
- Cameras have more difficulty with lighting situations and for low contrast between the target and the background.

A digital camera collects and stores the image using a matrix of pixels. The detected contrast level between the target and the background depends on the actual contrast and the number of pixels that encompass the target. If the indication is smaller than one pixel, it will loose contrast and become distorted in appearance, Figure 107 (Cumblidge et al. 2004).

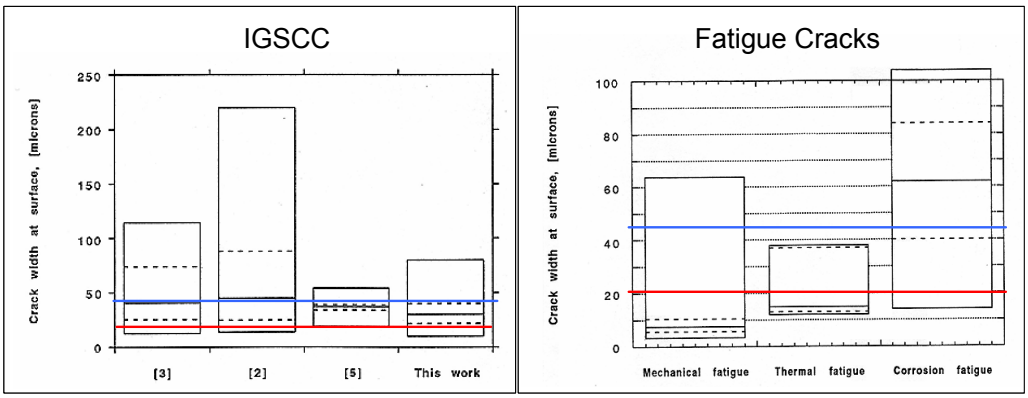

Figure 106. COD effect on the detection of different types of cracks. If COD is less compared to the red line, then the detection is very difficult. If COD is larger than the blue line, the detection is easy (Cumblidge et al. 2004).

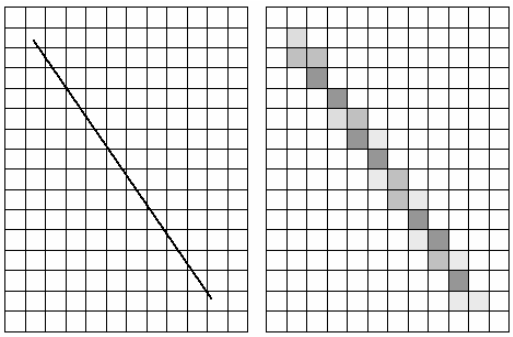

Figure 107. Digitised image resolution depends on the pixel size of the image (Cumblidge et al. 2004).

Reliable visual testing depends on:

- visual acuity of the system
- size of indications
- contrast between indication and surface
- scanning speed
- surface conditions
- light level
- lighting angle
- many human factors.

At the moment visual testing is less reliable than the non-visual testing methods. This is the reason for planning of a round robin for visual testing in the USA. This is reached with a reliable testing procedure and an optimized visual technique as well as with qualified personnel, as in the case of ultrasonic testing.

11.2.2 Ultrasonic inspection techniques

In ultrasonic testing of vessel head penetration assemblies it is possible to use normal shear wave probes using 45°, 60°–70° angle probes or mode-conversion probes for circumferential defect detection. These techniques are applicable for base material inspection as well as TOFD technique or TRL 70°. 0°-longitudinal probe can be used for contour measurement as well as in the weld areas for defect detection. The probe types used in the vessel head penetration inspections are shown in Figure 108 and data visualisations from measurement of cracked and non-cracked vessel head penetration are shown in Figure 109. Rotating probes are used for ID and OD axial and circumferential crack detection and characterization in the nozzle wall and detection of leak path in the interference fit. There are two types of blade probes: circumferential probe (axial beam direction) and axial probe (circumferential beam direction). Circumferential probe is used for initial inspection, optimised defect detection and characterization. This probe also has good performance in axial and off-axis defect detection. Axial probe is optimised for axial defect detection and characterisation. Both blade type probes are also used for detection of leak path in the interference fit. Ultrasonic inspection techniques depend strongly on the vessel head penetration geometry: in cases where ultrasonic inspection can be carried out from inside tube almost every technique is applicable using rotating UT-probes. In these cases TOFD technique is preferred. In the case where blade probes are used, TOFD probes are also preferred. In the case where vessel head penetration must be inspected from outside, 60°–70° TRL probes can be used.

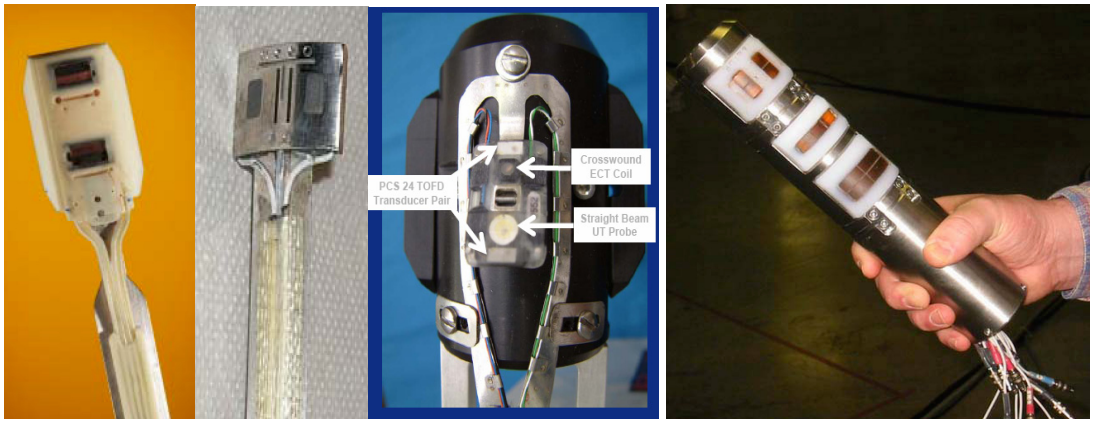

Figure 108. UT techniques of head penetrations; blade probes for axial and circumferential defect detection and rotating UT-probe for both types of defect detection (Schalder et al. 2002, Cazorla 2002, Lareau 2002, Hacker 2002).

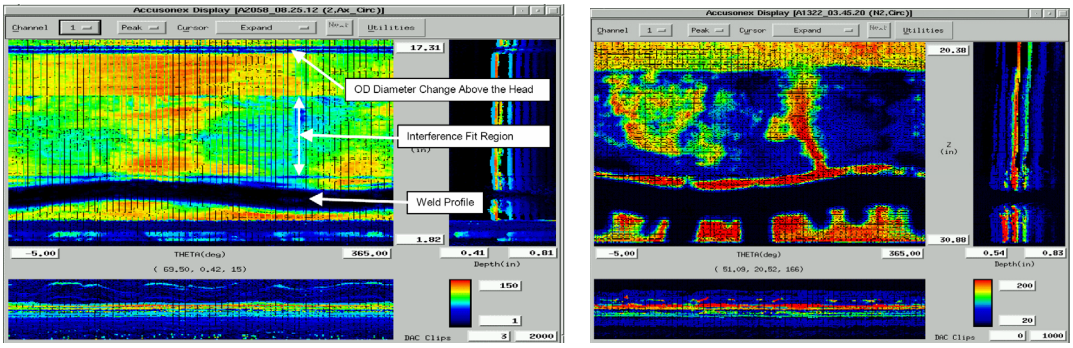

Figure 109. a) Typical leak path without cracking. b) Typical leak path with nozzle cracking (Hacker 2002).

TOFD is one of the main inspection techniques for the vessel head penetration assemblies, Figure 110, and it differs from normal ultrasonic analysis. Some technical items like probe, frequency and focus depth selection and analysis of results are important for the TOFD inspection. Analysis of the time of flight signal is described in the standards ENV-583-6 and prCEN/TS 14751. Normally the TOFD probes have a wide beam opening in order to cover the whole inspection volume. In the frequency selection compromises always have to be made. The frequency of the probe must be as high as possible in order to get maximised resolution in the wall-thickness direction. The frequency spectrum of the probe should be at least 75% in 6 dB limits. The pulse length should not exceed 2 wave lengths (10% limits). TOFD technique is not well suited for small surface defects on the same side as the probes. In analysing TOFD signals the detected indications are classified as surface breaking or internal defects by using the following properties of echoes:

- disturbancies in lateral wave or in back-wall reflection
- indication between lateral wave and back-wall reflection
- the phase of the signal compared to lateral wave and back-wall echo phase
- changes between back-wall reflection and mode-conversion part of the back-wall reflection.

The phase of the crack upper tip is in the same phase as the back-wall reflection, the phase of the lower tip is in the same phase as the lateral wave. The echo height, phase and location and form of the indication include the information for analysing the signals.

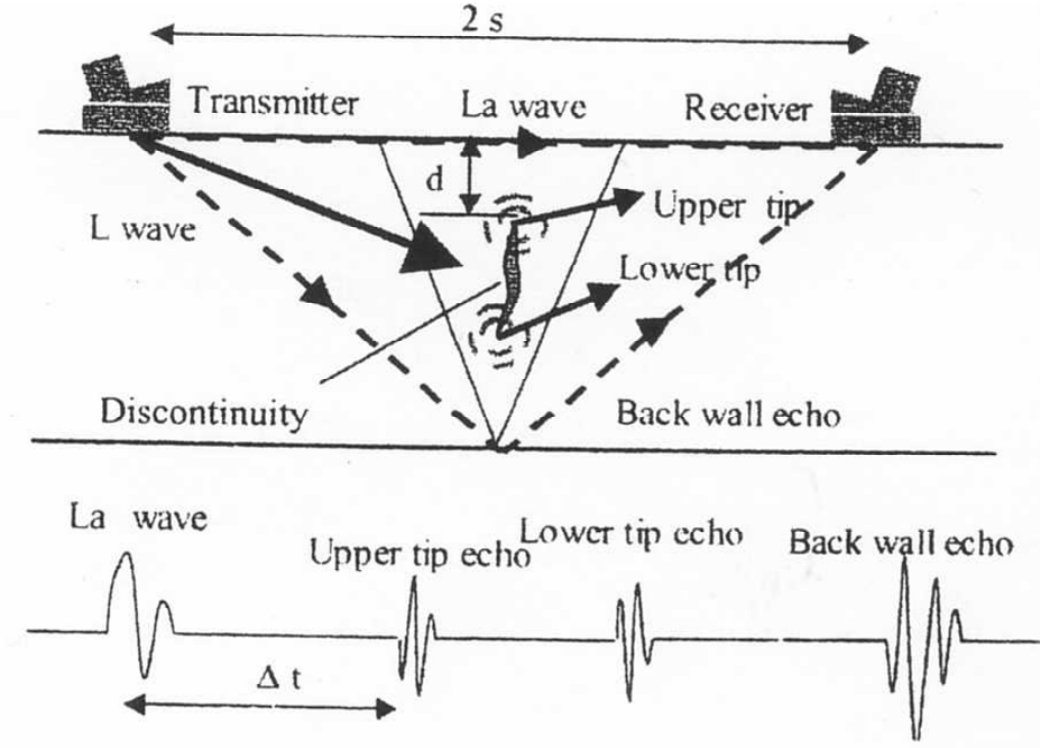

Figure 110. Principle of the TOFD technique (Lareau & Adamonis 2004).

11.2.3 Eddy current inspection techniques

According to the NRC, a failure in the J-groove weld can be the reason for nozzle cracking. Weld and nozzle cracks permit the primary water to penetrate into the CRDM annulus, where the boric acid solution will be oxygenated, leading to crevice corrosion. Eddy current inspection was studied with the following frequencies: 800, 600, 400 and 75 kHz. Different types of coils were tried and the best signal-to-noise ratio was obtained with a cross wound coil (+ -point-coil). Eddy current testing can be used for detection and ultrasonic testing for sizing. In the outside inspection the targets are axial or circumferential defects in the base material and in the weld zone, above and below the weld. Normal pancake or plus point coils are used in rotating probes. In rotating

probes the surface coil is mechanically rotated in the circumference direction. These coils have until recently been the main analysis technique for suspicious indications measured with the bobbing coils. The plus point coil is an improved version of the pancake coil. By using plus point coils, detection of cracks in both axial and circumferential directions of the tube are possible. Array coil development brings also improvement in EC testing of the J-groove weld. Figure 111 shows defects detected in EC testing. The array coil has to be flexible in order to adapt to the changing surface conditions. A calibration array coil with the EPRI PWSCC mock-up gives a response from even the smallest defect. The plus-point coil does not show in the visualisation the response from all defects, Figure 112. The flexible array coil seems to be more accurate in characterising the defects.

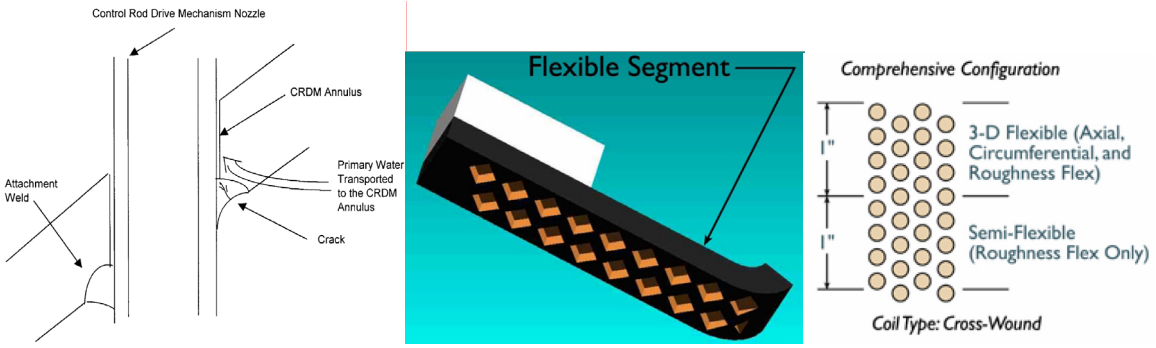

Figure 111. Defect location in J-Groove welds for ET inspection and flexible array coil for J-groove weld inspection (Lara et al. 2002).

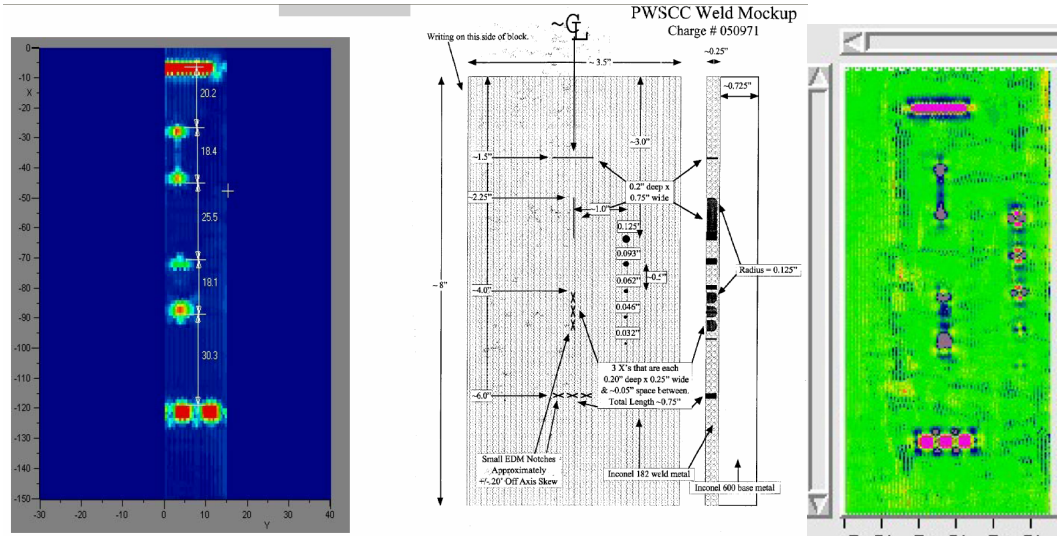

Figure 112. Plus-point coil and array coil demonstration for EPRI PWSCC weld mock-up (Cazorla 2002, Lara et al. 2002).

11.2.4 Other inspection techniques

In some cases mechanised dye penetrant testing is used for crack detection in vessel head penetrations, Figure 113 (Lareau 2005a). According to Lareau (2005b) photothermal inspections have also been carried out for crack detection in vessel head penetrations.

Figure 113. Dye penetrant testing of the vessel head penetration (Lareau 2005a).

In photothermal inspection a focussed laser beam scans and heats the surface to be inspected from point to point. The thermal sum image of all heated points is formed. This image corresponds to the thermal characteristics of the object on the surface and near surface volume. In photothermal inspection the in-phase information and amplitude can be stored. The measurement system is easy to move. One of these kinds of system is called Aladdin, Figure 114 (Siemens 1989). The characteristics of the system are the power 350 mW, wavelength 1064 nm and modulation frequency from 1 Hz–5 kHz. The surface area to be measured is 25 mm^2. The system is easy to handle and almost all kinds of materials can be tested. It can be used for surface breaking crack detection.

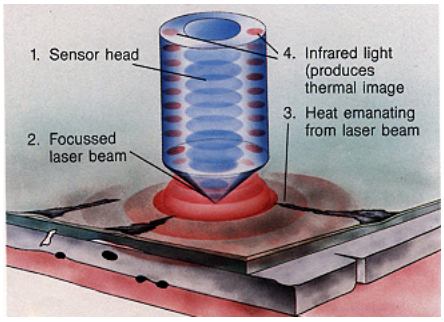

Figure 114. Photothermal inspection principle for detection of surface breaking cracks (Siemens 1989).

11.3 Inspection of RPV dissimilar metal weld nozzles

Inspections of dissimilar metal welds are mainly concentrated on the following aspects (Ammirato 2002, 2004):

- the weld type and quality
- the thickness of the component and weld
- inspection side – inner / outer / ferrite side / austenite side
- ultrasonic attenuation and scattering properties of the weld material
- in thick components the detectability and resolution suffer from the attenuation and lead to the use of lower frequencies.

In some cases the outer surface can vary quite a lot geometrically, Figure 115 and Figure 116, and sometimes the actual site has differed from the design drawings. The inspection personnel have to deal with these circumstances, which occasionally lead to a decreased result in detection and sizing. This is one of the main reasons for the required qualifications in inspections.

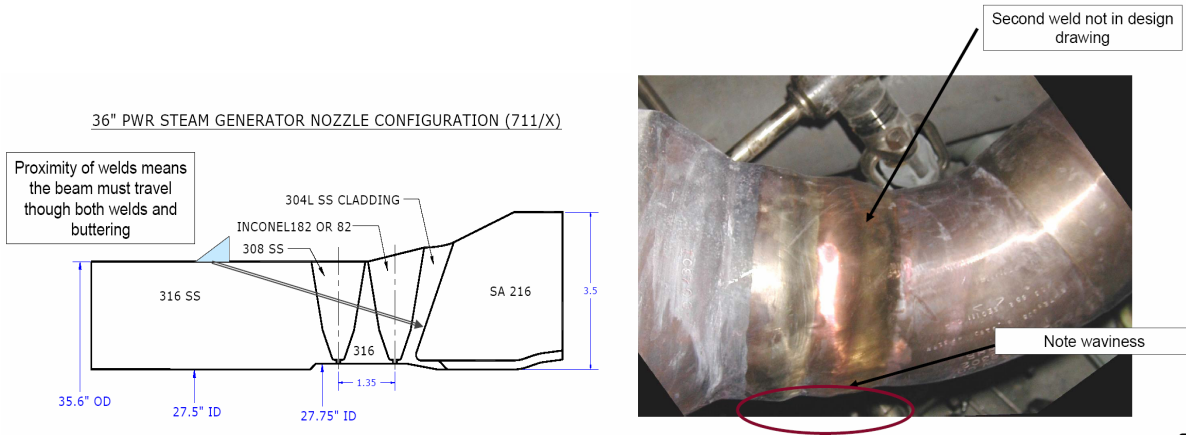

Figure 115. Difficult geometries as well as waviness of the inspection object can cause large deviations in detection and sizing results (Ammirato 2002, 2004).

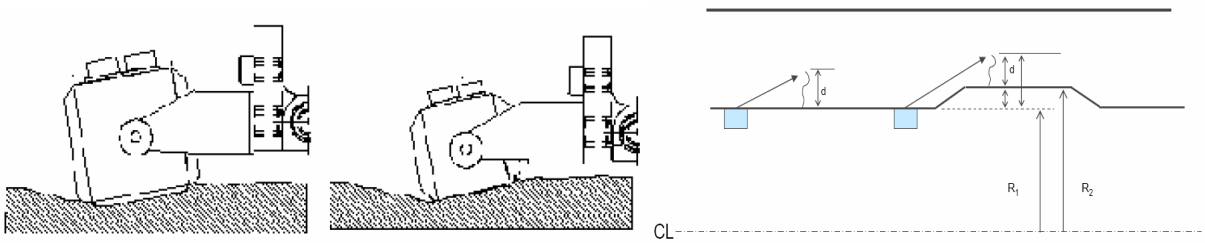

Figure 116. Irregular surface makes inspection difficult to carry out without loosing good coupling. In ID inspection the contour information helps in sizing and this information has not always been available. This must be improved in the future (Ammirato 2002, 2004).

11.3.1 Ultrasonic inspection techniques

Improvements in search unit technology have moved far beyond the 45° shear wave approach described by the code. As discussed briefly in previous sections, manufacturers now build numerous types of search units incorporating different wave modes (shear, longitudinal and mode-conversion probes), angles, and configurations (single, dual element, tandem, Phased array), all designed to enhance sensitivity to crack detection. Supplementing code techniques with these enhanced inspection techniques and using a proactive approach to examining components is far more effective than the code described techniques alone.

An inspection approach developed for IGSCC inspection that can be effective for the inspection of thermal fatigue cracks is the use of "ID creeping waves (secondary creeping wave)" and related mode-conversion techniques to detect and size cracks. This family of techniques has gained wide acceptance in the nuclear industry because of the high sensitivity to inside diameter (ID) connected flaws.

Crack-tip diffraction techniques depend on time measurement of the signal that is emitted from the crack tip. When an ultrasonic wave impinges upon a crack, the sound energy is reflected in a specular fashion from the crack face (no surface roughness), forms texture reflections from the rough flaw surface, and is diffracted at the end or tip of the crack. This diffracted energy acts as a point source and radiates in all directions, and thus, can be detected using a backscatter approach (i.e., transmitter and receiver are on the same side of the crack) or a forward scattering approach (transmitter and receiver are on the opposite sides of the crack). Using the transducer angle and sonic velocity in the material (both known quantities), the distance to the crack tip and the crack depth are easily calculated. It is worth noting that there are numerous approaches for sizing of cracks based on the ultrasonic diffraction. These techniques often have high resolution to maximize signal separation, and come in a variety of configurations to optimize the tip response for the applicable condition (i.e., depth in material, weld configuration). These include single element backscatter techniques such as "PATT" (Pulse Arrival Time Technique) or "PET" (Peak Echo Technique) and "SPOT" (Satellite Pulse Observation Technique) and dual element approaches using tandem and side-by-side arrangements. Double element techniques are often preferable, because they can be modified to focus energy at various depths, and they tend to have better signal-to-noise ratio due to the separate transmitter and receiver.

11.3.1.1 Shear wave techniques

Inconel and austenitic steel welds cause ultrasonic attenuation and beam distortion, especially with shear waves. In spite of this, these techniques can be used for corner

reflection detection. The best possible angle is of course 45° to find ID defects. In some cases the geometry of the weld crown prevents the ultrasonic beam from reaching the ID surface properly. In these cases we need larger angles, if possible (55°). The lower frequency has lower spreading property as well as larger penetration depth. Shear waves can be used to detect a possible crack tip in front of the weld. In the weld, the crack tip detection is not reliable. Suitable frequencies for the corner reflection are from 1 to 2 MHz and crack tip detection from 2 to 5 MHz. For detection of lack of fusion in the interface between weld and base material, angles between 55°–70° can be used, depending on the geometry. For the detection of near-probe defects, TRT probes can be used. This type of probe has been used very seldom. These probes are dual crystal probes, divided into the transmitter crystal and receiver crystal. This type of probe has a focussing range, which must be considered in inspection. As already said, the inspection depth according to ASME is 1/3 of the wall thickness, and thus the main interest is ID defect detection. But of course in the welds, a lot of manufacturing type of defects are present, which have not been registered during the acceptance inspection, and if a crack is larger than the in-service inspection depth, all possible techniques should be used to characterise the defect.

11.3.1.2 Longitudinal wave techniques

A longitudinal wave attenuates less compared to a shear wave of the same frequency. According to Matthies et al. (1986), if we use the wavelength as the criterion, both wave modes attenuate similarly. The beam distortion is anyhow less compared to the shear waves, and this is the main property that can be used in Inconel metal weld inspection. By using TRL probes we can achieve better results in the Inconel weld metal inspection, Figure 117.

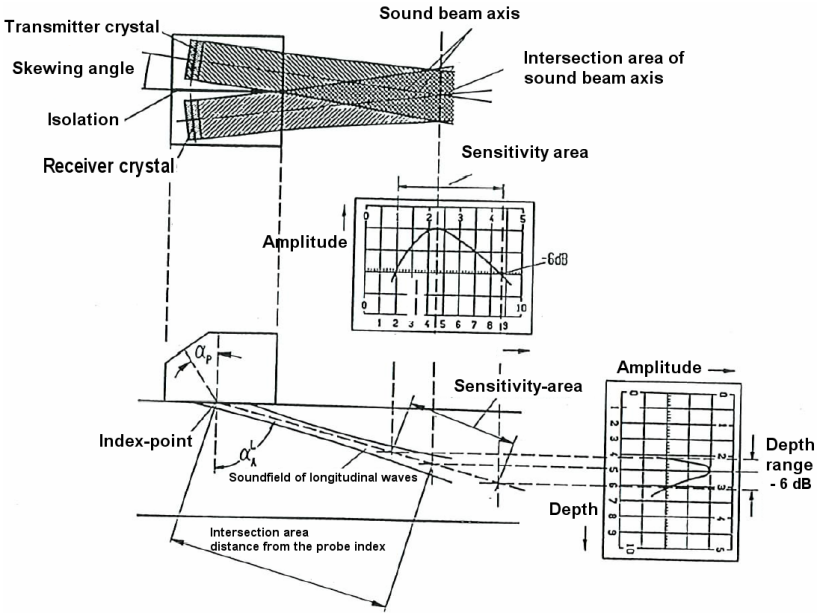

Figure 117. TRL probe sound field characteristics as a function of the distance from the probe.

The characteristics of the TRL probe are the following:

- Optimised sensitivity (maximum signal-to-noise ratio) is located in the intersection area of the sound beams of both crystals (–6 dB range, see Figure 117).
- The angle of the probe decreases with increasing depth.
- No near field present enables inspection also near the probe, which is not possible with the single crystal probes.

Longitudinal waves offer a better possibility to detect crack tip signals even in welds, but this also depends on the depth-to-wavelength ratio. The penetration depths with the longitudinal wave modes in Inconel welds are better compared to the shear waves. Thus, the weld volume inspection should be carried out mainly with longitudinal waves. This type of probe needs to have several focus depths in the inspection volume, and they are both expensive and the inspection speed is slow. The frequency range should be from 500 kHz–5 MHz, depending on the supposed defect distance from the probe as well as the material and weld effect on the longitudinal wave propagation.

11.3.1.3 Mode-conversion techniques

The mode-conversion probe sends direct longitudinal waves (L) at a 70° angle, and at the same time direct shear waves (S) at about 30°, Figure 118 (IAEA 2003). The head wave generates a primary creeping wave (C_f) on the outer surface. It also sends an indirect shear wave (S_i) at an angle of 31°, which converts in the inner surface to the secondary creeping wave (C_b). In the inner surface the shear wave mode converts to an indirect longitudinal wave (L_i). The main components of this probe in in-service inspection are the use of the creeping wave C_b and mode-converted indirect longitudinal wave. In Figure 119 is seen the behaviour of those wave types in a notch case in a 20 mm thick austenitic steel sample, in which there are notches at 1 mm, 2 mm, 5 mm and 9.5 mm depths. The creeping wave is detecting these notches clearly, but has no effect on the defect depth. On the other hand, the indirect longitudinal wave is very sensitive to defect depth until 50% of the wall thickness. This means that in the case of smaller defects the sizing can be carried out with this wave mode comparing to creeping wave signal. Creeping wave is not so sensitive to notch tilt or skew. The frequency used should be from 1.5 MHz to 2 MHz.

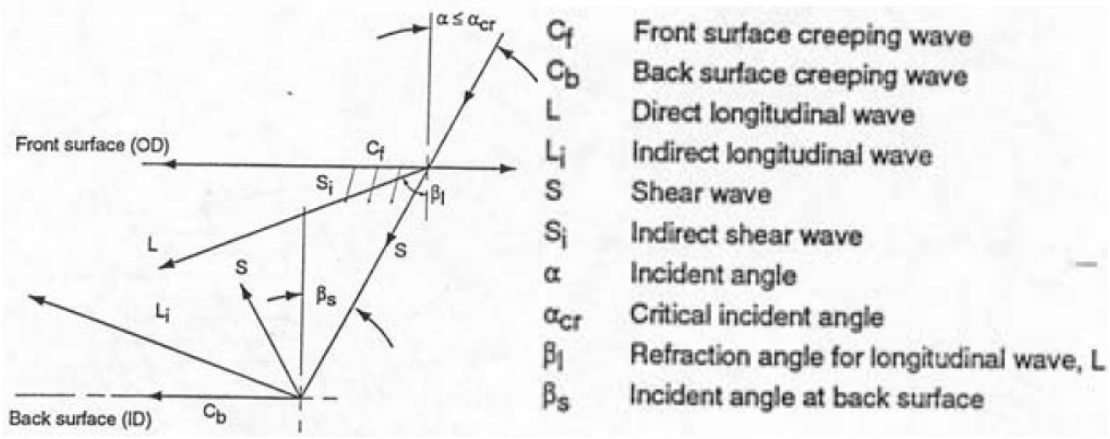

Figure 118. Mode-conversion technique principle (IAEA 2003).

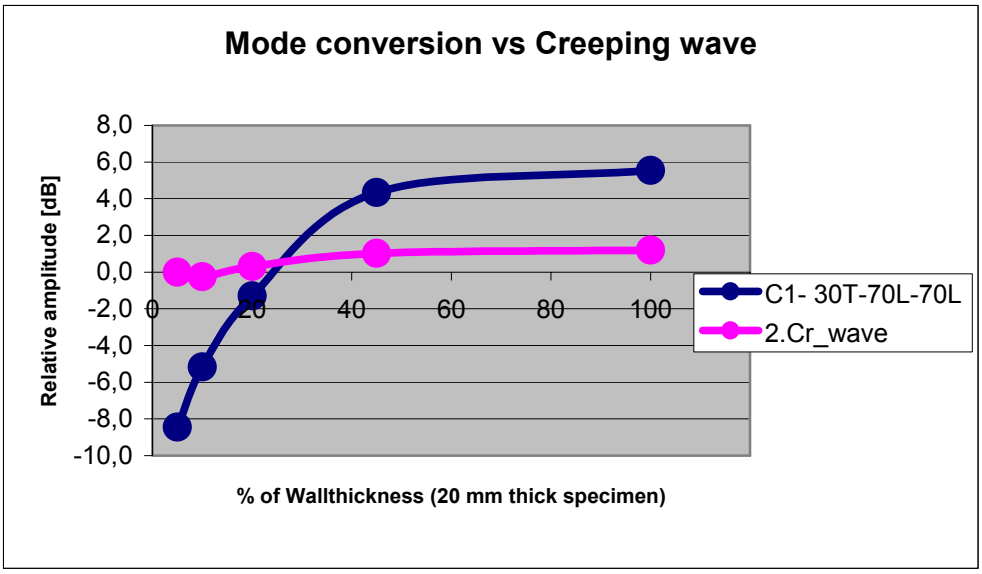

Figure 119. Secondary creeping wave (Cr_wave) behaviour comparison to indirect longitudinal wave mode also called mode-conversion component (C1) in 20 mm thick austenitic material.

11.3.1.4 SAFT

Back propagation of elastic waves in synthetic aperture focussing technique (SAFT) is applicable to a wide range of ferritic and austenitic materials and is used for testing of pipes, turbines, plates, vessels or pump housings. The improvement of signal-to-noise-ratio (SNR) is one of the main advantages, which is considered in the theoretical background of SAFT. SAFT-reconstruction is valid in the far field (Fraunhofer Region). This technique is mainly used for one crystal probes.

Important elements in practical SAFT measurements are the following: the aperture for measurement can be calculated from a simple equation:

$$L = 2\frac{\lambda}{D_R * \cos\beta} S, \tag{15}$$

where L [mm] is the aperture of measurement, λ [mm] is the wavelength of sound beam emitted by the probe, S [mm] is sound path, D_R [mm] is the crystal diameter and β [°] is the angle of incidence of the probe.

The resolution of the reconstruction is D/2, half of the crystal size of the probe. This is at the same time an advantage and also a disadvantage. With the small element size the near field is close to the probe and opening angle is large. Even though the resolution of small crystals is good, the power of ultrasonic signals is low. To increase the power especially with long sound paths, larger crystals are necessary. Thus, the resolution is decreased. It is possible to increase the power by using as wide crystals as possible. Of course, the near field must be between the probe and defect. The axial resolution is equal to the pulse length and is not related to the size of the aperture.

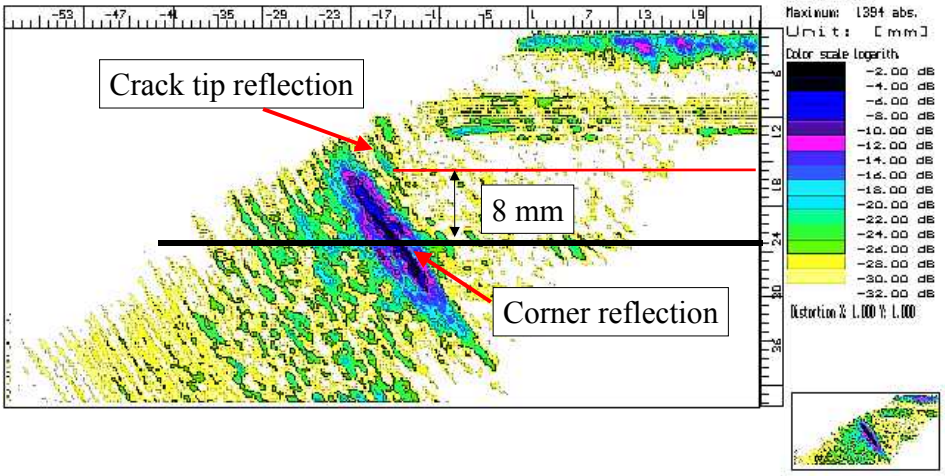

Figure 120. SAFT reconstruction for an IGSCC crack in front of an austenitic weld.

SAFT is a useful tool to determine whether a defect is planar or volumetric. Strong evidence of a planar defect is the appearance of tip reflection echo(s). Especially, in the case of large cracks the crack face can be seen in the SAFT reconstruction.

Five different sizing techniques are generally used. In the following they are presented in the order of their field of application. Sizing of cracks is based on tip reflection. Subsurface cracks are sized by measuring the vertical distance between the positions of tip echoes. Surface cracks are sized by measuring the position of crack tip or by determining the vertical distance between the corner and tip echoes. In Figure 120 a corner reflection from a real IGSCC crack is shown. The size of this crack is about 5–7 mm, depending on the spot, where measurement is taking place.

Figure 121 shows data from inspections carried out by VTT, data from Erhard et al. (1998) and data from the NESC trial. All measurements have been compared destructively. It can be seen that the error of the SAFT measurement is normally less than 2 mm from the real value. In the three cases the error is 3 mm or more.

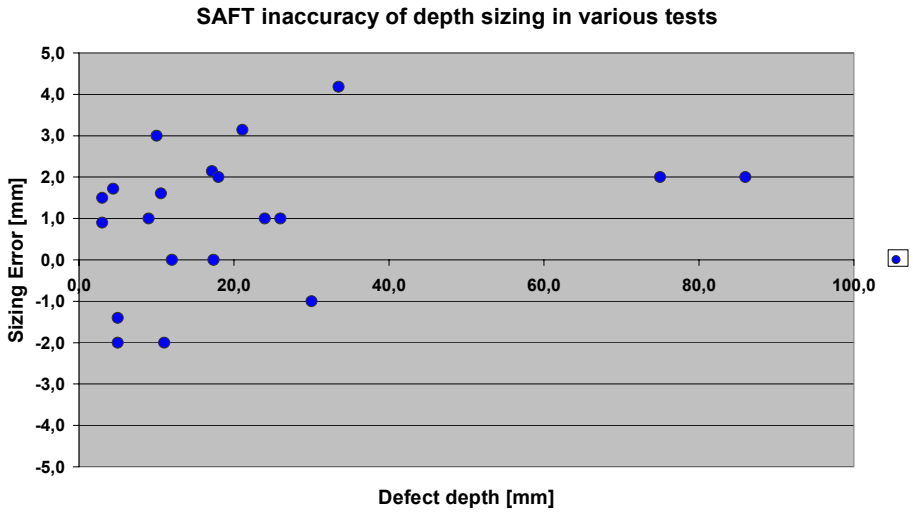

Figure 121. Sizing error using SAFT measurement with different defect sizes.

These values are only giving a tendency noticed in sizing performance with SAFT method. The accuracy is depending on many factors and not only the physical resolution of the method is decisive. Coupling, ultrasonic probe, sizing technique, human factors etc. also affect the accuracy.

11.3.1.5 Acoustic holography

In acoustic holography, coherent treatment of A-scans results in acoustic images with high resolution. The special algorithm of combination of images obtained using both longitudinal and shear waves provides the increase of signal/structure-noise ratio by testing type 2 welded joints. The obtained two-mode holographic images (B, C, and D images) were used for determination of the defect sizes and final assessment of the weld quality.

The highly resolved austenitic and Inconel weld ultrasonic images appear after the holographic treatment of A-scans. The holographic treatment increases the ratio of a useful signal-to-noise in comparison with the review of data approximately at 6 dB. The additional increasing of this ratio (not less than 6 dB) is reached by joining of the images obtained with the longitudinal and shear waves. In this case the special algorithm of two-mode testing is used. Therefore the signal-to-noise ratio at expert holographic testing is not less than 12 dB in comparison with the testing by known methods. The two-mode holographic images (B-, C- and D-projections) are used for flaw sizing and weld quality estimation. In Figure 122 indications measured in NESC III RRT are shown.

The essence of acoustic holography is that the weld is tested by the pulses of different frequencies, received echo signals are compared by time of reception and amplitude; the signals with equal time of reception and amplitude exceeding a determined level of cut-off are selected. In the case of optimal choice of frequency band and angle of ray incidence the multi-frequency method increases the signal-to-structure noise ratio by 6–12 dB. In the multi-frequency method both longitudinal and shear wave modes can be used for inspection, by automatic and manual testing. However, the analog devices developed more than ten years ago do not provide the required resolution and sensitivity.

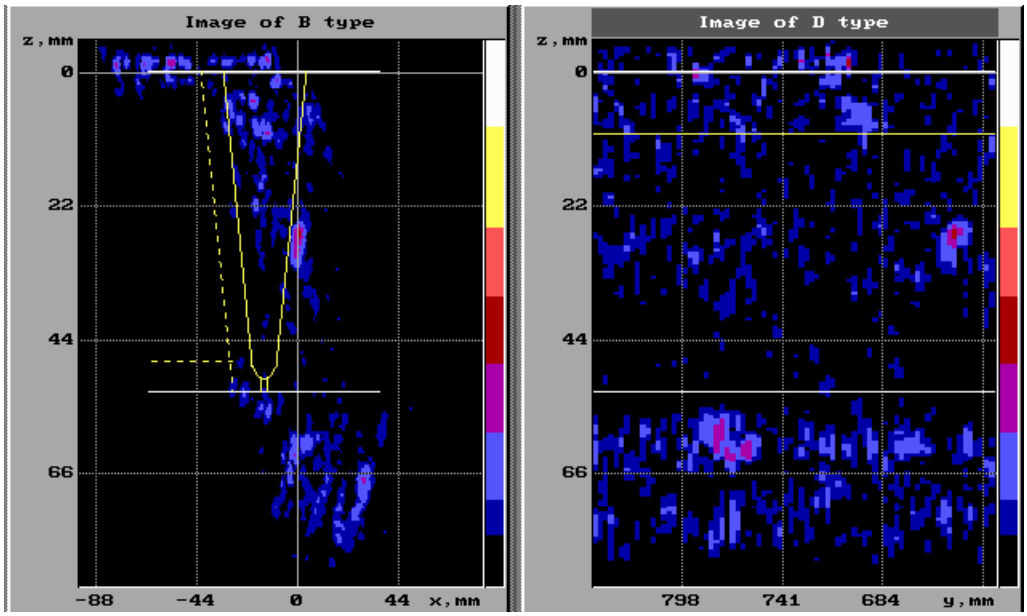

Figure 122. Acoustic holography reconstruction B- and D-scan images for defects in an Inconel weld.

The relation of the useful signals from notches to the mean level of structure noise is increased on average by 6 dB when testing by Augur system using the same probes and holographic method. The possibility of notch detection using shear waves is much better than in the case of longitudinal ones. The latter wave type cannot detect notches of 1 mm in height. One should note that conventional criterion of defect detection on noise background: +6 dB can be lowered to +3 dB in the case of testing by holographic method. The relation A/A_n hardly achieves the newly introduced criterion of 3 dB, when testing by holographic method using shear waves reflected from bottom surface. It means that one cannot select using color scale notch images from chaotically placed spots corresponding to ultrasound dispersion on structure heterogeneities. The additional increase of A/A_n ratio (SNR) was achieved, when holography and multi-frequency methods were applied together. Augur system realizes it through combination of images that correspond to two frequencies (1.65 and 2.5 MHz) using the following algorithm (Grebennikov et al. 2002 a & b):

$$A(x,y,z)=\begin{cases}\dfrac{A_1(x,y,z)+A_2(x,y,z)}{2},\ldots A_1(x,y,z)\geq A_{10}\wedge A_2(x,y,z)\geq A_{20}\\ 0,\ldots\ldots\ldots\ldots\ldots\ldots\ldots\ldots A_1(x,y,z)<A_{10}\vee A_2(x,y,z)<A_{20}\end{cases} \quad (16)$$

A_{10} = n%·max A_1 (x, y, z) A_{20} = n%·max A2 (x,y,z)

After application of this operation the increase of SNR comparing with holography method is 5–6 dB for testing using shear waves and direct beam and 2–3 dB for longitudinal waves. By the shear wave testing using the beam reflected from the bottom surface, the maximal increase of SNR is ~5 dB (angle of incidence –60º). Use of the two-frequency method in combination with holographic one enabled successful detection of all notches (and notch of 1 mm height, too). One should note that the resolution of the holographic method, when testing by longitudinal waves is about 2 times worse than one by shear waves (2–2.5 mm comparing to 1–1.5 mm). To confirm this, one should compare images of notches measured by different wave types. At the notch images measured by shear waves, it differs from longitudinal waves. The method gives possibility for exact measurement of defect depth. Moreover, the diffracted signals are present in the reflected beam data. This important information is used in data interpretation.

The comparison of results of the measurements of signal-to-noise ratio at shear and longitudinal waves confirms that the plate type defects are much better detected using shear waves than longitudinal ones. On the contrary, the volume type defects are better detected with longitudinal waves than shear waves. In this connection it is reasonable to test using simultaneously two types of waves: longitudinal and shear waves (two-mode testing). If the images are combined according to the above described algorithm (1), increase of noise-independence of testing due to both difference in spatial frequencies of two types of waves and the difference in nature of dispersion of elastic waves of different types is achieved (Grebennikov et al. 2002 a & b). The image of austenitic steel weld can be produced through combination of longitudinal and shear wave images with rejection level of 10%. The signals connected with structure noises are not present in the combined images.

11.3.1.6 Phased array techniques

In the Phased array technique, the acoustic beam is steered by using electronic delays between different elements of the probe. These delays are used both in transmission and reception modes, Figure 123 (Delaide et al. 2000). By help of these delays the angle of incidence can be varied in certain range as well also the focus depth, Figure 124 (Delaide et al. 2000). The optimised angle for the inspection can be selected with one probe even if the circumstances vary a little bit. It has to be remembered that by the optimised angle probe signal-to-noise ratio is always better as compared to Phased array

probe, Figure 125. Phased array is on the other hand always more flexible and can be more easy to adjust to varying geometrical changes.

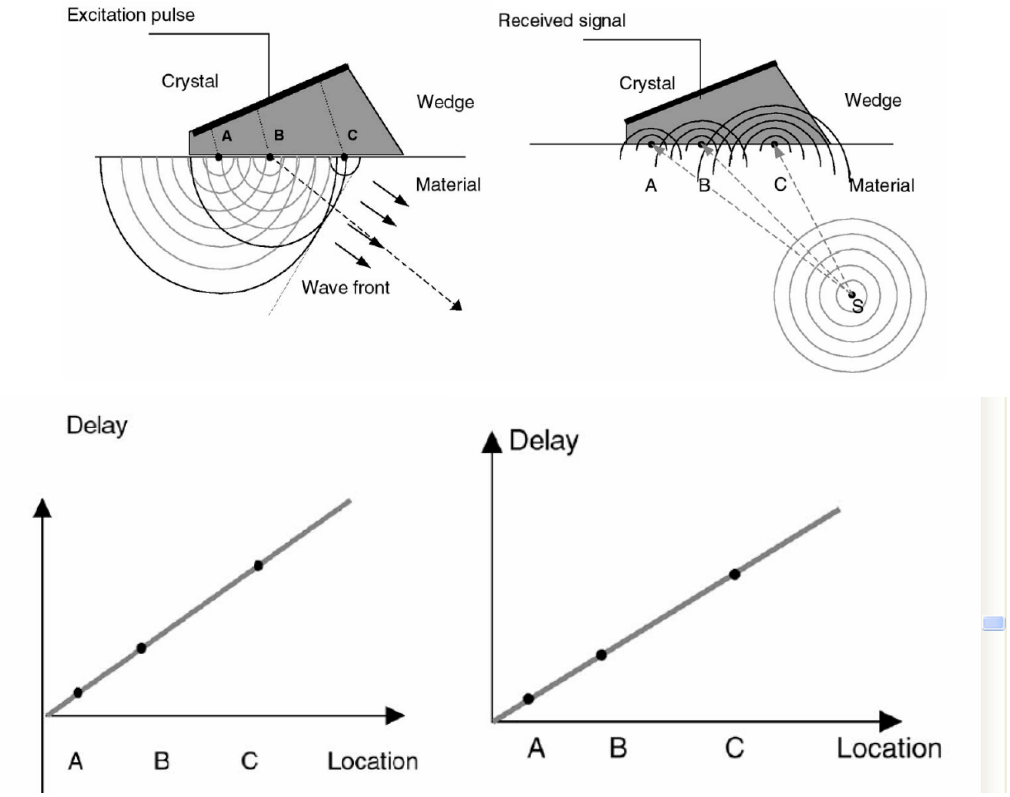

Figure 123. Principle of transmitting and receiving signals of Phased array probe (Delaide et al. 2000).

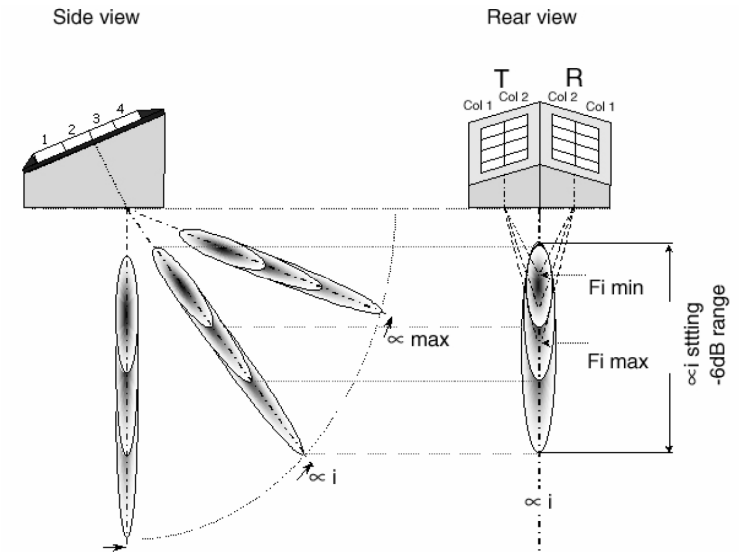

Figure 124. Angle variation and focus depth variation for linear Phased array technique (Delaide et al. 2000).

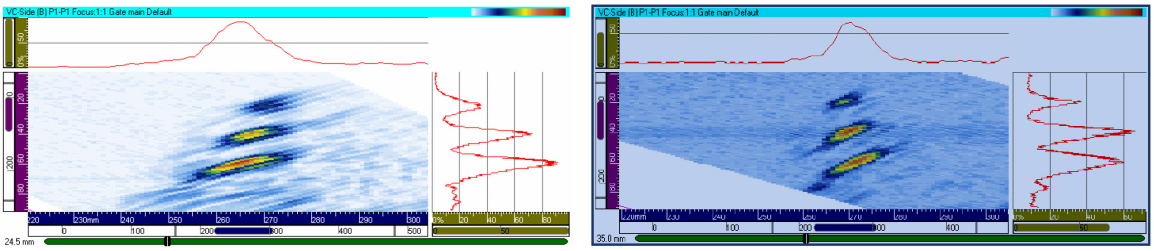

a) *b)*

Figure 125. Defects in cast austenitic steel inspected with focussed TRL probe (a) and Phased array TRL probe (b) (Delaide et al. 2000).

11.3.2 Inspection using electromagnetic Phased array transducer – EMAT

With EMAT, horizontally polarized shear waves (SH) can be generated, which have two advantages over longitudinal and vertically polarized shear waves (SV) (IAEA 2003, Neumann et al. 1995):

- Shear waves offer better sensitivity to defects due to the corner effect.
- SH are less influenced by weld and metallurgical features than SV waves, which tend to be easily redirected by grain structure.
- EMAT techniques require no liquid couplant, since the ultrasonic sound waves are produced in the metal electromagnetically.

This approach is especially useful for dissimilar metal welds and austenitic stainless steel materials, where attenuation and beam redirection are problems and sensitivity to small flaws is critical.

11.3.3 Phased array inspection of circumferential defects

For inspection of circumferential defects, linear Phased array can be constructed so that probe produces ±15° skew in sonification angle. This covers all the angles that should also be carried out in manual inspection. This is the lack in normal ultrasonic inspection compared to the manual inspection. Normally defects can be a little skewed, and are not so clearly detectable without skewing the probe. This method has been qualified by EPRI for austenitic steel piping inspections.

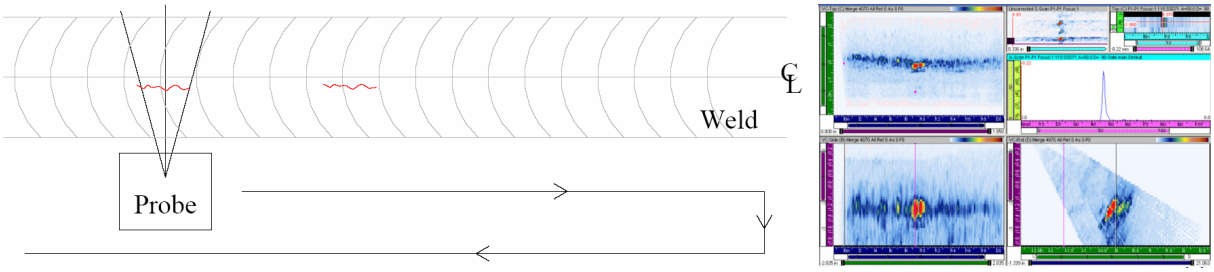

Figure 126. Ultrasonic Phased array inspection of dissimilar metal weld by changing skewing angle to detect circumferential defects (Landrum et al. 2002).

Sizing is the biggest difficulty in qualification. Accurate sizing is very important, especially for circumferential defects, Figure 126. The accepted RMS error for sizing qualification by EPRI is 3.2 mm according to ASME XI.

11.3.4 Phased array inspection of axial defects

If the weld crown is not ground, the inspection of the axial defects must be carried out outside the weld crown area. This causes problems to detect axial defects and by using Phased array property for varying the skewing angle, the improved detection can be achieved. In Figure 127 the principle of Phased array inspection for a weld having a crown is shown.

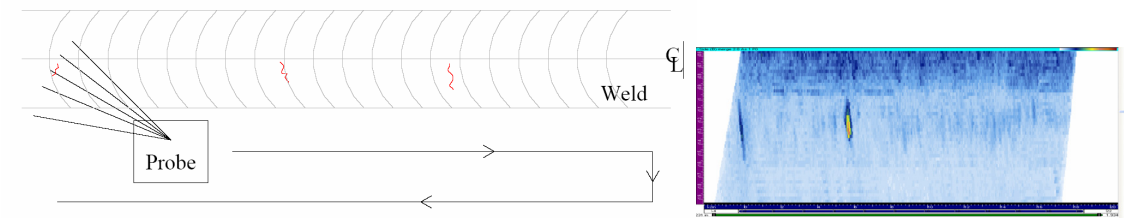

Figure 127. Ultrasonic Phased array inspection of dissimilar metal weld by changing the skewing angle to detect axial defects (Landrum et al. 2002).

BAM (Federal Research Institute for Materials in Germany) made some trials for axial defect detection in dissimilar metal weld inspection. The used mock-up is shown in Figure 128 (Munikoti 2004) and visulisation in Figure 129. In the weld there are 4 axial notches of the dimensions showed in Table 16. The longest defect, but lowest in depth, was not detected. The weld geometry caused scattering of the ultrasonic waves. In the middle of the weld the highest defects were detected. Thus, the interface between the weld and the base material lowers the reflected amplitude from the defects. The length of the calibration defect for axial defect detection must be carefully chosen.

Table 16. BAM mock-up for dissimilar weld inspection according to KTA (Munikoti et al. 2004).

Defect No.	Length × Height	Location	Detection	Defect type
1	26 mm × 2 mm	buttering-weld-base material	not detected	axial notch
2	20 mm × 2 mm	cladding-buttering-weld	not detected	axial notch
3	10 mm × 5 mm	weld mainly	detected	axial notch
4	10 mm × 8 mm	weld mainly	detected	axial notch

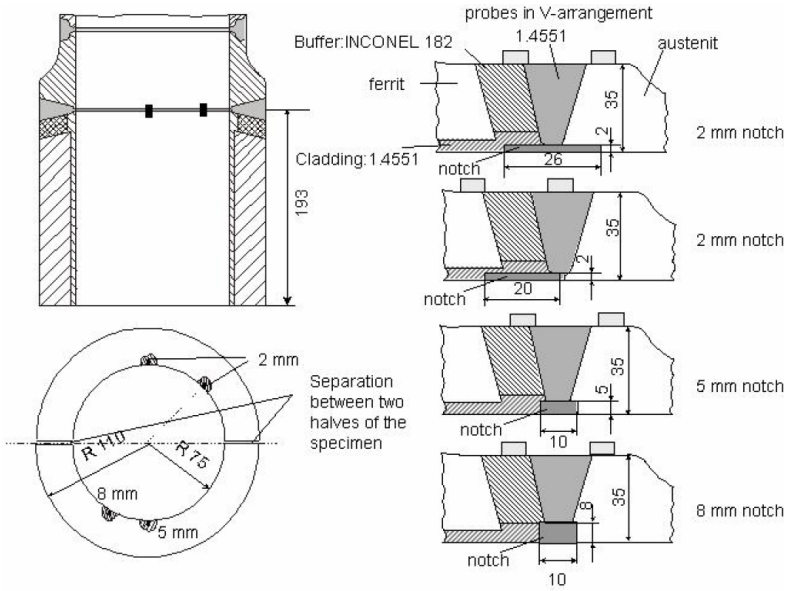

Figure 128. Experimental for measuring axial notches in dissimilar metal weld (Munikoti et al. 2004).

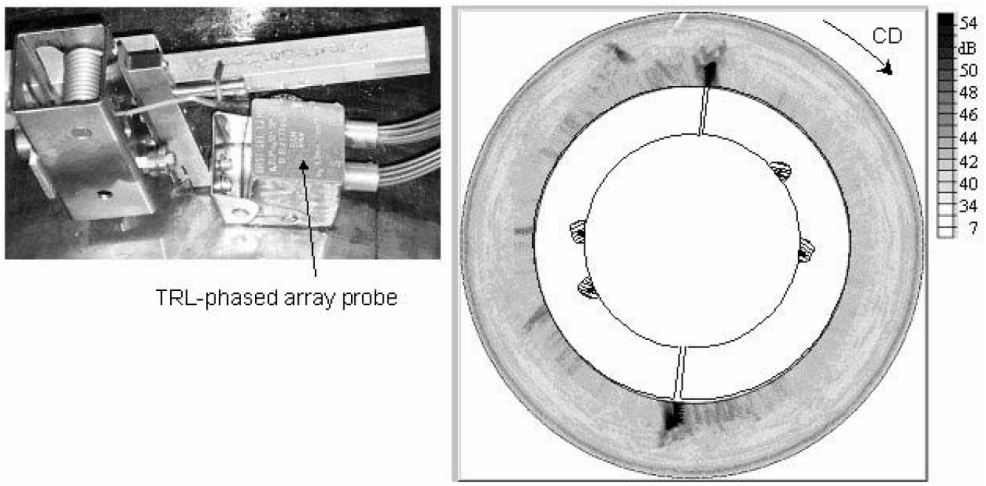

Figure 129. The used TRL Phased array probe and the visualisation of the measured data (Munikoti et al. 2004).

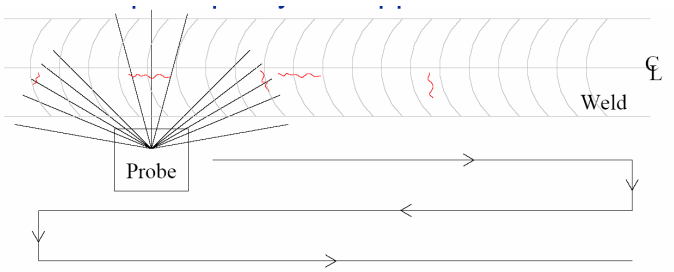

Figure 130. Ultrasonic Phased array developments for both axial and circumferential defect detection (Landrum et al. 2002).

EPRI had a goal to qualify the technique shown in Figure 130. This has not yet been qualified successfully for piping inspection. There have been some occasions where axial cracks (V.C. Summer, USA; Ringhals, Sweden; Biblis, Germany; Tsugura Unit 2, Japan; DMW in Pressuriser) have been present in components. More attention has to be paid to inspections for detection of axial defects. Some cracks in the circumferential directions have also been detected, such as safe-end to pipe weld in Oconee 2 (USA), where the crack extended 360° circumferentially at the inside surface and about 77° circumferentially on the outer surface. These defects have been simulated in various qualification blocks as shown in Figure 131 and Figure 132, which belong to EPRI as demonstration mock-up for dissimilar metal weld inspection.

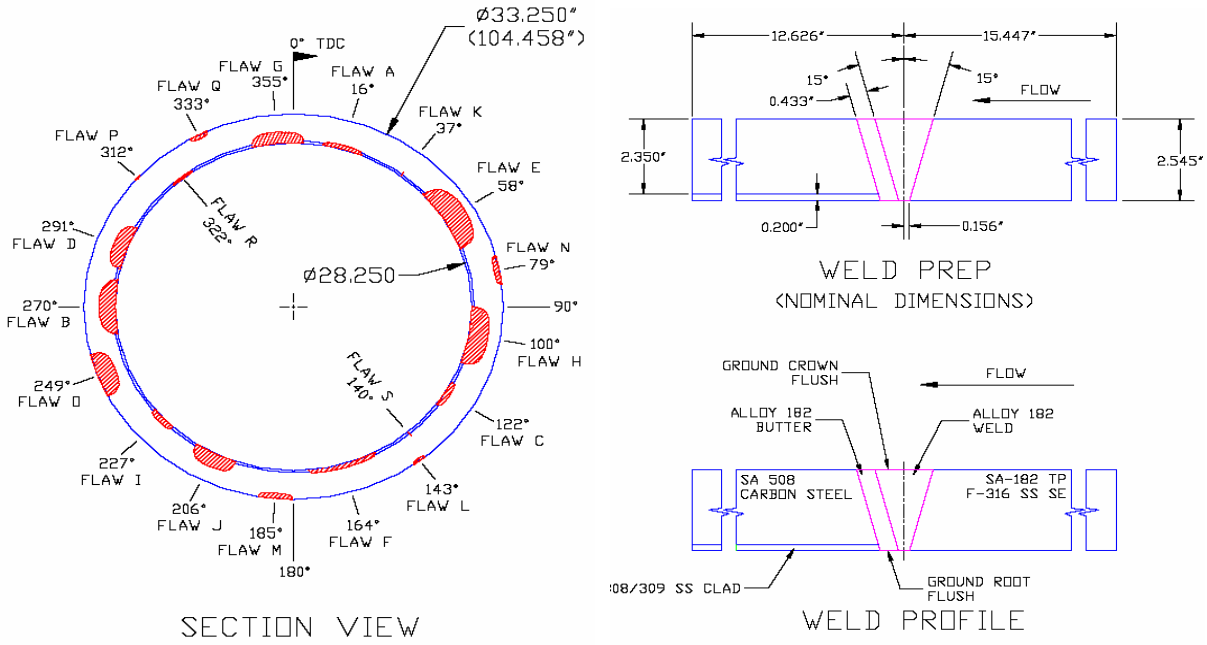

Figure 131. EPRI mock-up for dissimilar metal weld inspection (Alley 2002).

This mock-up was used to evaluate capability of the vendors in inspection. The V.C. Summer flaw was compared to deep flaws in EPRI mock-up and the response and signal-to-noise ratio were similar, but V.C. Summer flaw had somewhat lower

amplitudes. The mock-up also contains thermal fatigue cracks, which are used to qualify inspections, for instance in Sweden.

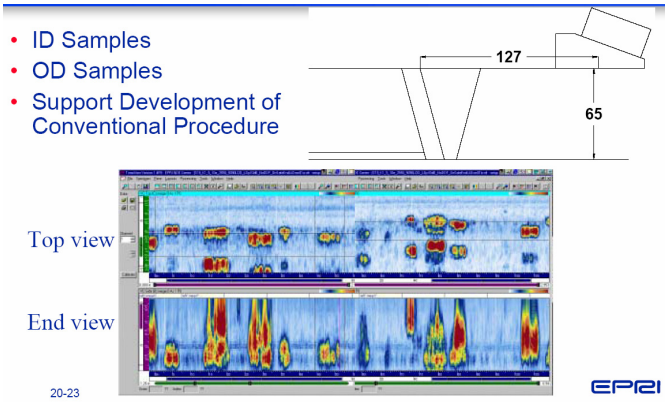

Figure 132. Results of ultrasonic inspection for EPRI mock-up of dissimilar metal weld inspection (Landrum et al. 2002).

11.3.5 Sizing with Phased array

Sizing with the Phased array probe does not differ from sizing with conventional single crystal probe. The techniques which can be used in sizing are amplitude-based methods such as –6dB or similar, crack tip detection, mode-conversion technique, sizing using multiple maximum. Of course, crack-tip detection is especially difficult in weld metal areas and in most cases it is not possible to detect crack-tip signals. The stress state in the fracture surface especially clearly affects the crack tip detection. The corner echo can also disappear, if compressive stresses on the ID surface are sufficiently large.

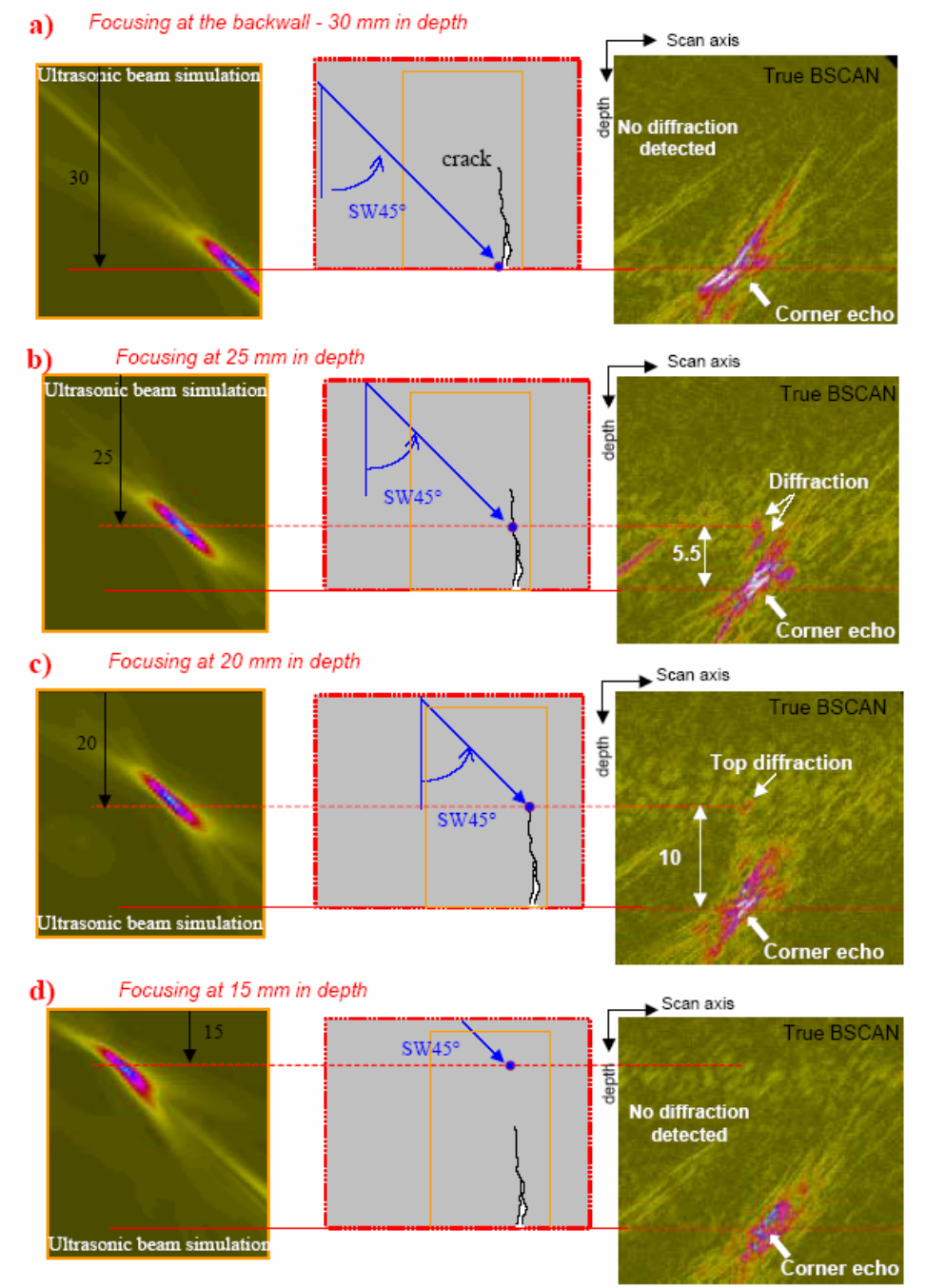

Figure 133. Effect of the different focussing depths using Phased array probes for evaluation of a crack (Dupond et al. 2004).

Because of the flexibility of the Phased array probe it is possible to change the focus depth and the signal-to-noise ratio in the focus area. This is normal behaviour in focussed sound fields, as is seen in Figure 133, that the crack tip signals will be clearly detectable with proper focussing depth. This means that, after having found a defect, the software should include a routine, which enables more accurate inspection in the defected area with varying focus depths using a Phased array technique. As we can see

from Figure 133 (Dupond et al. 2004), the focussing depths from 20 to 25 mm provide the best information from the crack. This kind of inspection needs very flexible and easy to use software, which also improves the defect characterising potential with Phased array probes.

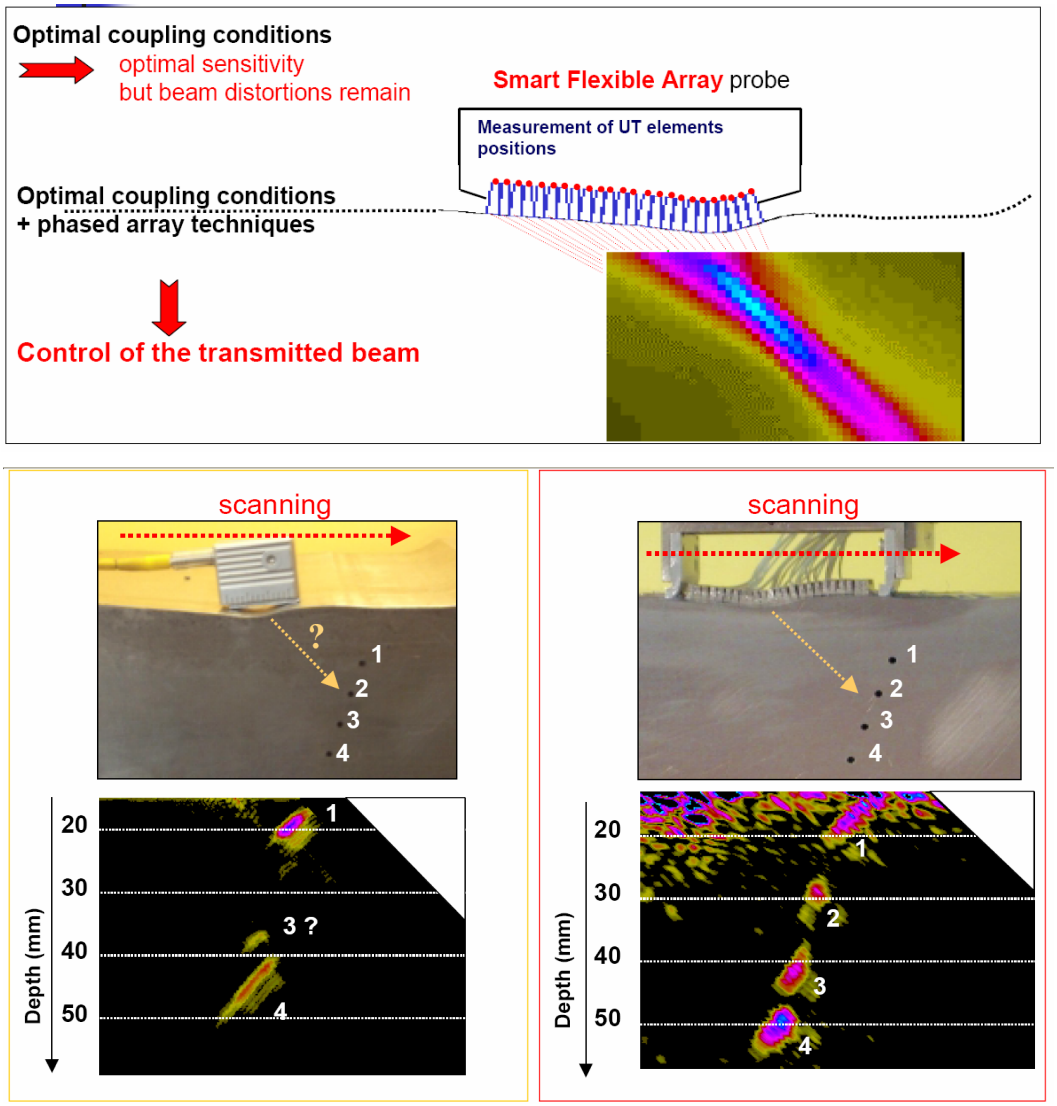

Figure 134. Flexiple ultrasonic Phased array adjustable for various surface conditions compared to conventional probe on an irregular surface with corresponding measured signals (Landrum et al. 2002).

Very important for inspection are the coupling conditions. If the surface is irregular, the defects cannot be detected and the sizing capability decreases. There are some possibilities to improve reflected signals coming from the defect in that case. One possibility is to reduce the probe contact area. Other way to approach is to produce flexible Phased arrays, which can adapt the probe to changes of the surface contour. These changes can be measured and simultaneously calculated in order to rectify the resulting sound field in the material. The sound field can be corrected using optimised

algorithm and inspection can be carried out. There is a lot of input to develop this technique for normal Phased array inspections. Especially, for the curved area of piping some Phased array probes have already been built and tested to meet the difficult contact requirements, Figure 134 (Landrum et al. 2002).

11.4 Qualification procedure for inspection

Appendix VIII qualifications due to the inadequacies of Section XI examination procedures for detecting and sizing of IGSCC, qualification of inspection personnel and procedures was mandated in NRC Generic Letter 88-01 to ensure that effective examinations are performed (Hacker 2002). Similarly, publication of Mandatory Appendix VIII, "Performance Demonstrations for Ultrasonic Examination Systems" was intended to improve the effectiveness and reliability of UT, in general. Appendix VIII, published already in the 1989 Addenda of ASME Section XI, provides requirements for the performance demonstration of ultrasonic examination personnel, procedures, and equipment used to detect and size flaws (IAEA 2003).

The intent of Appendix VIII is to establish a minimum level of skill and effectiveness for ultrasonic inspection systems. It will be a requirement for the in-service inspection of piping welds, vessels, vessel nozzles, and bolts and studs. Although the implementation schedule is still uncertain, the US industry is in the process of preparing the necessary mock-ups for the performance demonstrations. In order to minimize the number of samples needed and eliminate the need for site-specific qualifications, test blocks are being prepared to cover a range of pipe sizes and thicknesses rather than one block for each specific size.

Appendix VIII does not dictate any specific ultrasonic testing methods. Rather, it is meant to encourage industry to develop and use reliable techniques and procedures. Appendix VIII currently addresses piping welds, vessel welds, vessel base metal-to-clad interface, vessel nozzle welds and inside radius sections, and bolts and studs. As specified by the 1989 Addenda, performance demonstrations will be performed on mock-ups with weld preparation, geometry, and access conditions representing those encountered during in-service inspection. The blocks must also contain a certain number of realistic defects to confirm inspection technique reliability. For wrought austenitic piping welds, all flaws must be cracks with at least 75% of the defects being either thermal fatigue or IGSCC cracks. For ferritic piping welds, all flaws must be cracks with at least 75% of the defects being either mechanical or thermal fatigue cracks (IAEA 2003).

Requirements for dissimilar metal welds and cast stainless steel are in the course of preparation and will appear in a future edition or addenda of the ASME code. A new standard is in preparation for austenitic and dissimilar metal weld inspection (CEN 2003). Similar approach as in ASME code is presented in the French RSEM code, with two types of performance demonstration and qualification: one generic (for all general applications) and one specific (for focused applications). An enhanced technique with potential for detection and sizing of cracks in piping systems is the time-of-flight diffraction (TOFD) method, which has been used effectively to size cracks in control rod drive penetrations. TOFD is a forward scattering crack-tip diffraction method that employs opposing elements as shown in Figure 110. As shown in Figure 110 (IAEA 2003), two signals are present in the absence of a crack, a direct lateral wave signal and a back-wall reflection signal from the ID surface. Diffraction occurs when the incoming sound beam impinges upon a finite planar reflector such as a crack. The diffracted sound energy from the crack-tip acts as a point source and radiates a sound wave to the receiving transducer. The time of arrival of this signal can then be used to pinpoint the tip of the crack and determine the crack depth. Figure 110 illustrates such a diffracted signal produced by the tip of a crack; note the presence of a back-wall reflection signal and the absence of a lateral wave signal. A through-wall signal would of course eliminate all signals as shown in Figure 110. This approach provides a means of both sizing and verifying the extent of the crack, but could be hindered by weld geometry on the OD and ID surfaces (i.e., weld crown or weld root) that can cause a loss of transducer contact and/or the loss of the back-wall signal or the lateral wave signal for reasons other than the presence of a crack. TOFD-techniques were estimated critically according to Erhard et al. (1998) because of large under-sizing in comparison between SAFT- and TOFD-techniques made in Germany. A powerful ultrasonic inspection approach is the use of Phased-array technology that has been employed successfully in a number of applications including feed water nozzles, and for detection of IGSCC. This Phased-array approach is getting more applications in nuclear field as shown, e.g. by Japanese applications for Phased-array inspections (Matsura 2002). Especially, matrix Phased-array development has been started for real application in the field inspections (Matsura 2002). A Phased-array transducer consists of multiple elements that can be controlled under certain limits. It is conceivable that this approach can eliminate the need for performing the surface examination on the OD surface. However, reliability will be inadequate in many cases depending on the crack depth, orientation, and surface conditions. It is recommended to use those beam patterns, which have been shown to be adequate according to the qualifications or calibration specimen. The pulse sequence can be controlled to alter the inclination angle or focus the beam. In a Phased-array technique the beam can be focused electronically to the area of interest and has been used to enhance examination of PWR feed-water pipe-to-nozzle welds. This technique reduces beam spread and allows the beam to focus on the crack opening to enhance detection, or focus on the crack tip to improve sizing accuracy. It is clear that Phased-

array technique will be major technical solution for the future. A technique using a divergent transducer with computer focusing is the synthetic aperture focusing technique SAFT. Similarly as acoustic multi-frequency holography, it provides also similar information as Phased-array technology. The last mentioned techniques will survive maybe as a part of special software when extra accuracy is needed in detection or sizing. In Phased-array technology all the conventional techniques will be used as before. It is just easier to adapt new techniques with the Phased-array probes. This sets still high requirements for the qualification because in each qualification the setup of the equipment must be similar or has to be verified by modelling. In conventional probes the setup is always the same after calibration. In Phased-array this cannot be verified so easily. In the following chapters the Finnish qualification procedure will be handled, which is at the moment mainly used for ultrasonic qualifications.

11.4.1 Qualification dossier

After completed qualification the licensee delivers the qualification dossier to radiation safety regulator organisation STUK for approval. The documents included in the qualification dossier are:

- qualification input information
- qualification procedure
- technical justification
- description of test pieces and practical trials
- inspection procedure
- qualification assessment report
- qualification certificates
- documents from the actions and decision making of the qualification body such as: minutes of the meetings, surveillance and assessment reports of testing trials
- separate statements, evidences and research reports linked to the qualification
- calibration and inspection reports and data from practical trials
- authority decisions concerning the qualification.

The description of the test pieces is usually included fully or partly in the qualification procedure, Table 17. Also, the plan for practical trials is presented in the qualification procedure and reporting of these trials takes place in the assessment report.

Table 17. Qualification dossier procedure in Finnish qualifications.

Function	Authority	Licensee	Vendor	QB	Qualification organisation
Input information	H	R	H	H, C	
Qualification procedure	H	H	H	R	
Technical justification	H	H	R	H, C	
Description of open trial test pieces		H (R)	H(R)	H, C	H
Description of blind trial test pieces				H, C	R
Open trial document made by QB	H	H	H	R	H
Blind trial document made by QB		H		R	H
Inspection procedure	H	H	R	H	H
Evidence			R	C	
Modelling			R	C	
Calibration documents for open and blind trial carried out by vendor			R	H	H
Data files for open trials			R	H, C	H
Data files for blind trial			R*	C	H
Inspection report from open trial		H	R	H, C	H
Inspection report from blind trial			R*	C	H
Qualification certificates		H	(H)	C	R
Qualification acceptance	R	H			

H, Holder of the document or test specimen
C, Check or control of the realised events
R, Responsible
R*, Responsible from the measurement but not titled to keep the results
(H), can also hold these documents.

11.4.2 Qualification blocks

There are three types of test blocks:

- test block for laboratory tests
- open trial test blocks
- blind trial test blocks.

Test blocks for the laboratory tests are normally held by the vendor, and in some cases also the licensee. Open test blocks are provided by the licensee and all documentation is carried out by the licensee.

The responsibility to provide the test blocks for the qualification is by the licensee. Licensee or the qualification organisation stores the test blocks. The documentation of the open trial test blocks is responsibility of the licensee and that of the blind test blocks the qualification organisation. All the data from the open trial test blocks can be given to all participants of the open trials. The open trial test blocks are used mainly to qualify the inspection procedure and the blind test blocks for qualification of the personnel. The qualification body must always accept all used test blocks for the qualification. The acceptability of the test blocks depends on the defect comparability and location to the real conditions of similar components. The qualification test block will be designed according to the input data and on the bases of the technical justification taking into consideration:

- material
- geometry of the object (weld/base material)
- dimensions and weight
- defect (types and sizes compared to input data)
- number of defects and their distribution.

All the defects shall be distributed so that they do not shadow each other. All the accurate data from the test blocks shall be stored.

11.4.3 Qualification trials

There are three types of tests:

- laboratory test
- open trial
- blind trial.

The laboratory tests are carried out by the vendor. This information is used for the technical justification and also for the development of the inspection procedure. The open trials are the examination tests supervised by the qualification organisation. The open trial will demonstrate the performance of the inspection method or one part of it and its performance with open test blocks, the defect data of which is available for all parties taking part in the qualification. In the blind test the inspection method performance can be checked or qualified by the inspection personnel. In the blind test

the defects are not available to the vendor. In the open and blind trials the exact protocol from all the necessary events in the examination are documented.

The vendor must make the report from all these different types of tests and all data must be available to verify its traceability. The qualification body documents all events and makes reports and stores all data linked to blind tests and supervises blind test blocks during the whole blind test. After the blind test, all the data must be turned over to the qualification body. The qualification organisation will keep the register and data from these trials.

11.4.4 Personnel qualification

The requirement for a normal ultrasonic inspector is a basic qualification according to EN-473 level II, and for defect detection or defect sizing a supplementary qualification according to the new Finnish Nuclear Guidelines YVL 3.8. is needed. For the personnel, the supplementary qualification must always be performed through the blind test in Finland.

In mechanised ultrasonic inspection the art of work is divided into 4 categories, Table 18: helping personnel, operator, inspector, and analyser. The helping personnel does not require any qualification, but the vendor has to train and show that the personnel has sufficient training to carry out the task. The helping personnel is typically mounting scanner or driving the eddy current probe. The operator adjusts according to inspection procedure the NDT equipment and carries out data acquisition and uses mechanised equipment. The operator must have a proper qualification, EN-473 level I or higher level, and a verified training to use the equipment. He has to know and understand the inspection procedure. The inspector requirement is level II according EN-473 or higher and supplementary qualification according YVL 3.8 inspector has to be able to distinguish between geometrical or metallurgical indications and defects and locate the indication. Analyser must be level II or higher and has to have a supplementary YVL 3.8 qualification. Analyser has to be able to locate, size and characterise defects.

The false call rate is normally described in the input data as well the POD 80% depth. In the depth sizing the RSM value shall not exceed the value 3.2 mm according to ASME XI. Also the grading units are similarly divided and the depth distribution in the qualification examination is recommended in the ASME XI performance demonstration part.

Table 18. Requirements for personnel qualification for mechanised and/or manual inspection of dissimilar metal welds in Finnish qualifications (according ENIQ recommendations).

Category	Verified Training Equipment	EN 473 Qualification Blind test	YVL 3.8 Qualification Blind test			Knowledge about (Controlled by the Qualification Body)	
	Training Certificate	Written and Practical Examination	Written Examination	Defect detection	Defect sizing	Inspection procedure	Technical Justification
Helping Personnel	X						
Operator	X	Level I or higher				X	
Inspector	X	Level II or higher	X	X		X	X
Analyzer	X	Level II or higher	X	X	X	X	X
Manual Inspector		Level II or higher	X	X		X	X
Manual Analyzer		Level II or higher	X	X	X	X	X

11.5 References

Alley, T. 2002. MRP Alloy 600 Butt Weld Inspection. 6th EPRI Piping & Bolting Inspection Conference. Point Clear, Alabama, USA, 30 July – 1 August 2002. 19 p.

Ammirato, F. 2002. Opening Presentation. 6th EPRI Piping and Bolting Inspection Conference. Point Clear, Alabama, USA, 30 July – 1 August 2002. 11 p.

Ammirato, F. 2004. 2nd Meeting of the International Cooperative Research Project on NDE for PWSCC in Ni-Base and Dissimilar Metal Welds. Washington, USA, 5–6 May, 2004. 36 p.

ASME XI. 2000. Rules for Inservice Inspection of Nuclear Power Plant Components. ASME, New York, 1 July 2000.

Cazorla, F. 2002. Inspections of RPV Head Penetrations. 6th EPRI Piping and Bolting Inspection Conference. Point Clear, Alabama, USA, 30 July – 1 August 2002. 46 p.

CEN. 2003. ISO/DIS 22825:2003. Draft prEN ISO 22825. Nondestructive Testing of Welds – Ultrasonic Method – Testing of Welds in Austenitic Steels and Nickel Based Alloys. 14 p.

Cumblidge, S., Anderson, M. & Doctor, S. 2004. An Assessment of Remote Visual Testing in the Nuclear Industry. 4th International Conference in Relation to Structural Integrity for Nuclear and Pressurised Components, 6–8 December 2004. 18 p.

Delaide, M. 2000. Paper presented at G. Maes and D. Verspeelt, "Design and Application of Low-frequency Twin Side-by-side Phased Array Transducers for Improved, UT Capability on Cast Stainless Steel Components". Second International Conference on NDE in Relation to Structural Integrity for Nuclear and Pressurized Components, New Orleans, USA, 24–26 May 2000. 24 p.

Dupond, O., Poidevin, C. & De Nathan, N. 2004. Advanced Phased Array Transducer for Detection of Closed Crack Tip Diffraction. 4th International Conference in Relation to Structural Integrity for Nuclear and Pressurised Components, 6–8 December 2004. 10 p.

EPRI. 2002. Future for Alloy 600 Inspections, Mitigations? 6th EPRI Piping and Bolting Inspection Conference, 30 July – 1 August 2002. 35 p.

Erhard, A., Schulz, E., Brekow, G., Wüstenberg, H. & Kreier, P. 1998. Critical Assessment to the TOFD Approach for Ultrasonic Weld Inspection. Proceedings of the 7th ECNDT European Conference on Non-destructive Testing. Copenhagen, Denmark, 26–29 May 1998. Pp. 1236–1242.

Eriksen, B., Eriksson, A., Houghton, R., Iacono, I. & Pitkänen, J. 2004. NDT Inspection Results Obtained in the NESC-III Blind Round Robin Trials on Austenitic and Inconel 182 Dissimilar Metal Welds. 4th International Conference in Relation to Structural Integrity for Nuclear and Pressurised Components, 6–8 December 2004. 6 p.

Grebennikov, V., Badalyan, V., Grebennikov, D. & Vopilkine, A. 2002a. Comparative Analysis of the Ways to Increase Signal to Noise Ratio at NDT-Inspections of Austenitic Welds. World Conference on NDT, Rome, Italy. 9 p.

Grebennikov, V., Grebennikov, D., Krylov, V. & Vopilkine, A. 2002b. Ultrasonic Two-mode Testing of Austenitic Welded Joints of Vacuum Vessel of Thermonuclear Reactor ITER. 8th ECNDT, Barcelona, Spain. 12 p.

Hacker, K. 2002. Ultrasonic Examination of Reactor Vessel Head Penetrations. 6th EPRI Piping and Bolting Inspection Conference. Point Clear, Alabama, USA, 30 July – 1 August 2002. 25 p.

Hiser, A. 2002. Regulatory Activities Related to Circumferential Cracking Reactor Pressure Vessel Head Penetration Nozzles and Reactor Vessel Head Degradation. US Nuclear Regulatory Commission Office of Nuclear Reactor Regulation. 6th EPRI Piping and Bolting Inspection Conference, 30 July – 1 August 2002. 22 p.

IAEA. 2003. Assessment and Management of Ageing of Major Nuclear Power Plant Components Important to Safety – Primary Piping in PWRs. IAEA-TECDOC-1361, July. 242 p.

JNES. 2004. NDE Programs at JNES. PINC-Meeting at NRC. Washington, USA, May 2004. 23 p.

Landrum, J., Dennis, M., Selby, G. & Macdonald, D. 2002. Appendix VIII Qualification of Phased Array for Piping. 6th EPRI Piping and Bolting Inspection Conference. Point Clear, Alabama, USA, 30 July – 1 August 2002. 29 p.

Lara, P., Samso, R. & Bureau, J. F. 2002. Reactor Vessel Head Penetration J-Groove Weld Examination with Eddy Current Array. 6th EPRI Piping and Bolting Inspection Conference. Point Clear, Alabama, USA, 30 July – 1 August 2002.

Lareau, J. P. 2002. CRDM NDE Review. Westinghouse Experience. 6th EPRI Piping and Bolting Inspection Conference. Point Clear, Alabama, USA, 30 July – 1 August 2002. 17 p.

Lareau, J. P. 2005a. Thermal Imaging for the Detection of PWSCC in Alloy 82/182 Welds. 2005 International PWSCC Alloy 600 Conference and Exhibit Show. Tamaya Resort, New Mexico, USA, 7–10 March 2005. 9 p.

Lareau, J. P. 2005b. Experience in Reactor Head Nozzle and J-Welds Inspections. 2005 International PWSCC Alloy 600 Conference and Exhibit Show. Tamaya Resort, New Mexico, USA 7–10 March 2005. 10 p.

Lareau, J. P. & Adamonis, D. C. 2004. Inspection Technology for PWSCC. PINC-Meeting at NRC. Washington, USA, May 2004. 23 p.

Matsura, T. 2002. Study on Applications of Phased Array UT Technique to Nuclear Power Plants. 6th EPRI Piping and Bolting Inspection Conference, 30 July – 1 August 2002. 21 p.

Matthies, K., Neuman E. & Mrasek, H. 1986. Ultraschallprüfung von Komponenten und Anlagen bei Temperaturen bis 250°C. 12. MPA-Seminar, Stuttgart Germany, October. 25 p.

Munikoti, V., Brekow, G., Tessaro, U. & Erhard, A. 2004. Ultrasonic Inspection for Transverse Defects in Dissimilar Weld: Theoretical and Experimental Results. Materials Evaluation. 17 p.

Neumann, E., Hirsekorn, S., Schmid, R., Hübschen G. & Just., T. 1995. Ultraschall-prüfung von austenitischen Plattierung, Mischnähten und austenitischen Schweißnähten. Kontakt und Studium, Bd. 377. 341 p.

RCC-M. 2000. Design and Construction Rules for Mechanical Components of PWR Nuclear Islands. Edition June.

RSE-M. 1990. Inservice Inspection Rules for Mechanical Components of PWR Nuclear Islands. Edition July.

Schalder, D., Cole. B., Gebetsberger, K. & Myers, P. 2002. Inspection and Repair Techniques Addressing Reactor Vessel Head Penetration Degradation in the U. S. 6th EPRI Piping and Bolting Inspection Conference. Point Clear, Alabama, USA, 30 July – 1 August 2002. 32 p.

Silk, M. G. 1977. Sizing Crack Like Defects by Ultrasonic Means. Research Techniques in Non-Destructive Testing. Vol. III. Ed. R. S. Sharpe. Pp. 51–98.

Siemens. 1989. The Aladin, Thermomicroscope. Brochure. 6 p.

12. Summary

This study is part of the national Dissimilar Metal Welding project, where the main objective was to first review the field experience related to the Ni-base materials and components where degradation has occurred in the light water reactor (LWR) systems. The operating experience of major nuclear power plant (NPP) pressure boundary components has recently shown that dissimilar metal weld joints can jeopardize the plant availability and safety because of increased incidences of environment-assisted cracking (EAC, PWSCC) of Alloy 600 and corresponding weld metals (Alloys 182/82). Nickel-base weld metals are used throughout the LWRs to join the low alloy steel pressure vessel and pressure vessel nozzles to wrought Ni-base alloy and austenitic stainless steel components. Alloy 690 and associated weld metals (Alloys 152/52) are widely used for repair and replacement of the affected thick-section components in PWRs, while in BWRs Alloy 82 is considered to be the best choice. The selection of new materials relies mainly on excellent laboratory results and short-term service experience. The long-term behavior of these materials and their performance in the plant has still to be demonstrated.

Weldability of the studied Ni-base materials is evaluated based on the results obtained with weld metals of different chromium contents. The susceptibility to hot cracking is examined based on the number of different types of tests allowing ranking of the materials. The mechanistic understanding of the hot cracking behavior of Ni-base weld metals is still largely missing and careful metallurgical studies of the solidification mechanisms are needed.

The PWSCC susceptibility in the reactor primary water is strongly affected by the Cr-level of the Ni-base weld metals and is also based on the metallurgical properties of the nickel-base alloys. The microstructure and microchemistry in the multi-pass Ni-base alloy welds is very different than in the wrought and recrystallized Ni-base materials, but the details of the EAC susceptibility and mechanisms are still open, especially related to the possible role of hydrogen in the cracking mechanism. Additionally, the thermal ageing experience of various Ni-base weld metals is discussed, but the results are scarce at present. Weld residual stresses and their role in PWSCC as well as surface stress improvement techniques for PWSCC mitigation are reviewed and are considered to play very important role in cracking susceptibility. Especially, the weld repairs seem to be important in local increase of the stress levels. The EAC susceptibility of Ni-base alloys in both PWR and BWR conditions are considered from the different temperature, oxidant level, H_2 level and water purity points of view, and common dependencies have been observed in both PWR and BWR conditions.

Finally the application, improvements and qualification of NDE for Ni-base weld locations are evaluated concerning the probes, techniques and scanning devices. The need for representative mock-ups for technique development and qualification is realized. The technical basis for development of inspection requirements for dissimilar metal welds and efforts to qualify inspection procedures and personnel are also emphasized.

Maintaining the structural integrity of the NPP and oil refinery main components throughout the service life, in spite of the several possible ageing mechanisms related to the dissimilar metal welds, is essential for plant safety and availability. To achieve this objective, better understanding related to the various damage mechanisms is needed, together with the qualified methods for degradation analysis and assessment.

Acknowledgements

The project ERIPARI (dissimilar metal welds), launched in 2004, deals with dissimilar metal weld issues in nuclear power and oil refinery industry. The three-year project is funded by Tekes, TVO, Fortum Nuclear Service, Metso, Fortum Oil & Gas and VTT, which is gratefully acknowledged. The objectives of the project are to develop reliable methods to measure and evaluate the manufacturing, properties and performance of new dissimilar metal welds. A main objective is also to understand the aging of Ni-base weld metals and the failure causes of dissimilar metal welds in nuclear power plants and to develop non-destructive examination techniques for them. This report is a part of the project and is the literature survey on the manufacturing of dissimilar metal welds and their field experience in nuclear power plants and oil refineries.

Published by

Series title, number and report code of publication

VTT Research Notes 2347
VTT–TIED–2347

Author(s)

Hänninen, Hannu, Aaltonen, Pertti, Brederholm, Anssi, Ehrnstén, Ulla, Gripenberg, Hans, Toivonen, Aki, Pitkänen Jorma & Virkkunen, Iikka

Title

Dissimilar metal weld joints and their performance in nuclear power plant and oil refinery conditions

Abstract

The operating experience of major nuclear power plant (NPP) pressure boundary components has recently shown that dissimilar metal weld joints can jeopardize the plant availability and safety because of increased incidences of environment-assisted cracking (EAC, PWSCC) of Alloy 600 and corresponding weld metals (Alloys 182/82). Alloy 690 and associated weld metals (Alloys 152/52) are widely used for repair and replacement of the affected thick-section components. The selection of new materials relies mainly on excellent laboratory results and short-term service experience. The long-term behavior of these materials and their performance in the plant has still to be demonstrated.

Weldability of the studied nickel-base materials is evaluated based on the results obtained with weld metals of different chromium contents. The susceptibility to hot cracking is examined as well as the PWSCC susceptibility in the reactor primary water based on the metallurgical properties of the nickel-base alloys. The microstructure and microchemistry in the multi-pass nickel-base alloy welds is very different than in the wrought and recrystallized nickel-base materials. Additionally, the thermal ageing experience of various nickel-base weld metals is discussed. Weld residual stresses and their role in PWSCC as well as surface stress improvement techniques for PWSCC mitigation are also reviewed.

Finally the application, improvements and qualification of NDE for nickel-base weld locations are evaluated concerning the probes, techniques and scanning devices. The need for representative mock-ups for technique development and qualification is discussed. The technical basis for development of inspection requirements for dissimilar metal welds and efforts to qualify inspection procedures and personnel are also emphasized.

Maintaining the structural integrity of the NPP and oil refinery main components throughout the service life in spite of the several possible ageing mechanisms related to the dissimilar metal welds is essential for plant safety and availability.

Keywords

nuclear power plants, refineries, steel structures, welded joints, dissimilar metals, welding, Ni-base alloys, residual stress, environment-assisted cracking, hot cracking, non-destructive testing

ISBN

951–38–6805–2 (soft back ed.)
951–38–6806–0 (URL: http://www.vtt.fi/publications/index.jsp)

Series title and ISSN

VTT Tiedotteita – Research Notes
1235–0605 (soft back edition)
1455–0865 (URL: http://www.vtt.fi/publications/index.jsp)

Project number

631

Date	Language	Pages	Price
June 2006	English	208 p.	E

Name of project

ERIPARI

Commissioned by

Tekes, TVO, Fortum Nuclear Service, Metso, Fortum Oil & Gas, VTT

Contact

VTT Technical Research Centre of Finland
Otakaari 3 A, P.O. Box 1000, FI-02044 VTT, Finland
Phone internat. +358 20 722 111
Fax +358 20 722 6390

Sold by

VTT Technical Research Centre of Finland
P. O. Box 1000, FI-02044 VTT, Finland
Phone internat. +358 20 722 4404
Fax +358 20 722 4374

The operating experience of major nuclear power plant pressure boundary components has recently shown that dissimilar metal weld (DMW) joints can jeopardize the plant availability and safety because of increased incidences of environment-assisted cracking (EAC, PWSCC) of Alloy 600 and corresponding weld metals (Alloys 182/82). Alloy 690 and associated weld metals (Alloys 152/52) are widely used for repair and replacement of the affected thick-section components. Weldability of the Ni-base materials is evaluated based on the results obtained with weld metals of different Cr-contents. The susceptibility to hot cracking is examined as well as the PWSCC susceptibility in the reactor primary water based on the metallurgical properties of the Ni-base alloys. Weld residual stresses and their role in PWSCC as well as surface stress improvement techniques for PWSCC mitigation are reviewed. Finally the application, improvements and qualification of NDE for Ni-base weld locations are evaluated concerning the probes, techniques and scanning devices. The need for representative mock-ups for technique development and qualification is discussed. The technical basis for development of inspection requirements for DMWs and efforts to qualify inspection procedures and personnel are also emphasized.

Tätä julkaisua myy

VTT
PL 1000
02044 VTT
Puh. 020 722 4404
Faksi 020 722 4374

Denna publikation säljs av

VTT
PB 1000
02044 VTT
Tel. 020 722 4404
Fax 020 722 4374

This publication is available from

VTT
P.O. Box 1000
FI-02044 VTT, Finland
Phone internat. + 358 20 722 4404
Fax + 358 20 722 4374

ISBN 951–38–6805–2 (soft back ed.)
ISSN 1235–0605 (soft back ed.)

ISBN 951–38–6806–0 (URL: http://www.vtt.fi/inf/pdf/)
ISSN 1455–0865 (URL: http://www.vtt.fi/inf/pdf/)